HUMBOLDT-UNIVERSITÄT ZU BERLIN

HUMBOLDT-UNIVERSITÄT ZU BERLIN

DOCTORAL THESIS

Post-transcriptional mechanisms contributing to RNA and protein localization: study of local translation and alternative 3′UTRs in induced neurons

Dissertation
zur Erlangung des akademischen Grades Doctor of Philosophy(Ph.D.)
im Fach Biologie eingereicht an der
Lebenswissenschaftlichen Fakultät der Humboldt-Universität zu Berlin

von MSc Camilla CIOLLI MATTIOLI
(https://doi.org/10.18452/20702)

Präsidentin der Humboldt-Universität zu Berlin
Prof. Dr.-Ing. Dr. Sabine Kunst
Dekan der Lebenswissenschaftlichen Fakultät der Humboldt-Universität zu Berlin
Prof. Dr. Bernhard Grimm

Tag der mündlichten Prüfung:
01.11.2019

Gutachter/innen:
(i) Uwe Ohler
(ii) Florian Heyd
(iii) Sutapa Chakrabarti

Abstract

MSc Camilla CIOLLI MATTIOLI

Post-transcriptional mechanisms contributing to RNA and protein localization: study of local translation and alternative 3′UTRs in induced neurons

Keywords: ribosome profiling, neurons, local translation, alternative 3′UTRs, MOV10, *Cdc42*

Asymmetric distribution of mRNA and proteins inside a cell defines polarity, which allow tight regulation of gene expression in space and time. In this thesis I investigated how asymmetric distribution characterizes the somatic and neuritic compartments of in induced neurons, in terms of transcriptome and translatome. Spatial ribosome profiling analysis revealed that half of the local proteome is defined by mRNA localization and local translation. These, are processes accomplished by the synergistic activity of *trans*- and *cis*-acting elements. I focused on MOV10 as *trans*-acting element, and on alternative 3′UTRs as *cis*-elements, to investigate their role in asymmetry. MOV10 is an RNA helicase which participates to many aspects of RNA metabolism. With RIP and PAR-CLIP I showed that MOV10 targets are localized to the neurites, consistently with MOV10-neuritic localization, and that MOV10 might be involved in translational repression. Indeed, among MOV10 protein interactors, I identified several proteins involved in translational repression, i.e. AGO2, FMR1, and TRIM71. On the side of *cis*-elements, I performed mapping of alternative 3′UTRs. This analysis identified several genes expressing differentially localized 3′UTR isoforms. In particular, I focused on *Cdc42*. I showed that the two isoforms of *Cdc42* are differentially localized at mRNA level, and that the 3′UTR is the driver of mRNA and protein localization. Moreover, I identified several RBPs that might be involved in *Cdc42* localization. This analysis points to usage of alternative 3′UTR isoforms as a novel mechanism to provide for differential localization of functionally diverse alternative protein isoforms.

Schlüsselwörter: ribosomale Profilanalyse, lokalen Translation, alternative 3'UTRs, Neuronen, MOV10, *Cdc42*.

Die asymmetrische Verteilung von mRNA und Proteinen innerhalb einer Zelle definiert die Polarität. Dies ermöglicht eine strikte Regulierung der Genexpression in Raum und Zeit. Ich habe in dieser Arbeit untersucht, wie das Soma und die Neuriten in induzierten Neuronen sich hinsichtlich ihres Transkriptoms und Translatoms unterscheiden. Eine räumliche ribosomale Profilanalyse ergab, dass die Hälfte des lokalen Proteoms durch die mRNA-Lokalisierung und der lokalen Translation definiert wird. Dies sind Prozesse, die durch die synergistische Aktivität von *trans*- und *cis*-agierenden Elementen durchgeführt werden. In dieser Arbeit konzentrierte ich mich auf MOV10 als *trans*-agierendes Element und die alternativen 3′UTRs als cis-agierende Elemente, um ihre Rolle in der Asymmetrie zu untersuchen. MOV10 ist eine RNA-Helikase, welche an vielen Aspekten des RNA-Metabolismus beteiligt ist. Mit den Methoden RIP und PAR-CLIP konnte ich zeigen, dass sowohl MOV10-Ziele als auch MOV10 selbst in den Neuriten lokalisiert sind. Aušerdem ist MOV10 möglicherweise an der translationalen Repression mitinvolviert. In der Tat konnte ich unter den MOV10-Protein-Interaktoren mehrere Proteine identifizieren, welche an der translationalen Repression beteiligt sind, wie z.Bsp. AGO2, FMR1, und TRIM71. Für die Identifizierung der *cis*-agierenden Elemente führte ich das "Mapping" von alternativen 3′UTRs durch. Diese Analyse zeigte mehrere Gene, die differentiell lokalisierte 3′UTR-Isoformen exprimieren. Insbesondere habe ich mich auf *Cdc42* konzentriert. Ich konnte beweisen, dass die beiden Isoformen von *Cdc42* auf mRNA-Ebene unterschiedlich lokalisiert sind und dass die 3′UTR der entscheidende Faktor für die mRNA- und Proteinlokalisierung ist. Darüber hinaus habe ich mehrere RBPs identifiziert, die an der *Cdc42*-Lokalisierung beteiligt sind. Diese Analyse zeigt, dass für die differenzierte Lokalisierung von funktional unterschiedlichen alternativen Protein-Isoformen die Verwendung von alternativen 3′UTR Isoformen als neu-entdeckter Mechanismus eine entscheidende Rolle spielt.

Declaration of Authorship

I, MSc Camilla CIOLLI MATTIOLI, declare that this thesis titled, "Post-transcriptional mechanisms contributing to RNA and protein localization: study of local translation and alternative 3′UTRs in induced neurons" and the work presented in it are my own. I confirm that:

- This work was done wholly or mainly while in candidature for a research degree at this University.
- Where any part of this thesis has previously been submitted for a degree or any other qualification at this University or any other institution, this has been clearly stated.
- Where I have consulted the published work of others, this is always clearly attributed.
- Where I have quoted from the work of others, the source is always given. With the exception of such quotations, this thesis is entirely my own work.
- I have acknowledged all main sources of help.
- Where the thesis is based on work done by myself jointly with others, I have made clear exactly what was done by others and what I have contributed myself.

Signed:

_____

Date:

_____

Preface

Each figure in this thesis is labelled with the contributions from colleagues. Immunostaining of iNs on the filter was performed by Alessandra Zappulo (Chekulaeva group, MDC-BIMSB). Primary neurons were isolated by Mandy Terne (Birchmeier group, MDC). Data analysis of RNA-seq was performed by Vedran Franke (Akalin group, MDC-BIMSB bioinformatics platform). Data analysis of Ribo-seq was performed by Lorenzo Calviello (Ohler group, MDC-BIMSB) and Vedran Franke (Akalin group, MDC-BIMSB bioinformatics platform). Data analysis of RIP and PAR-CLIP was performed by Vedran Franke (Akalin group, MDC-BIMSB bioinformatics platform). MOV10-KO cell line was generated by David van den Bruck (Chekulaeva group, MDC-BIMSB). Data analysis of 3′end-seq was performed by Aviv Rom (Ulitsky group, Weizmann Institute of Science) and Vedran Franke (Akalin group, MDC-BIMSB bioinformatics platform). RT-qPCR for *Kif1b* and *Mtap4* was performed by Gerard Arrey (Chekulaeva group, MDC-BIMSB). RNA-seq data was generated by David van den Bruck (Chekulaeva group, MDC-BIMSB). Spatial LC-MS/MS data was generated by Alessandra Zappulo (Chekulaeva group, MDC-BIMSB) and analyzed by Koshi Imami (Selbach group, MDC-BIMSB). Spatial QuanCAT and pSILAC data was generated by David van den Bruck (Chekulaeva group, MDC-BIMSB) and analyzed by Koshi Imami and Erik McShane (Selbach group, MDC-BIMSB). Nicolai von Kügelgen performed comparison of transcriptome published datasets. Parts of this thesis were published in "RNA localization is a key determinant of neurite-enriched proteome" (Zappulo*, Van Den Bruck*, Ciolli Mattioli*, Franke* et al., 2017) and in "Alternative 3′ UTRs direct localization of functionally diverse protein isoforms in neuronal compartments" (Ciolli Mattioli et al., 2018).

"Usually the object of the search is found in another or different realm, which may be located very far away horizontally or at a great vertical height or depth."

Italo Calvino

Acknowledgements

I acknowledge my supervisor.

To the members of my committee, Uwe and Markus, I would like to express my sincere gratitude for their interest in the project, and their helpful suggestions throughout the years.

I would like to thank all the collaborators, in particular Vedran and Koshi, for their precious work, including the greek grill and ouzo.

I would like to thank the people met in the labs where I worked. The LPVM (and evergreen), where I started. "Il cubo" and Silvo, whom I admire the most for his playful passion for science. Haus 89 in Buch and the first generation of lab mates, Ale, David, Larissa, Marta, the core unit of the lab. And the second generation, Guli, Sam, Nicolai and Sayaka, for the - very windy - trip to Copenhagen. And the passengers, Debby, Olivier, Rutger and Gerard, for the salmon hugs, the mushroom picking, dungeons and dragons.

Special mention goes to Inga, Alessandra and Ivano (patience you must have my young Padawan), Elena and Gin, Francesca and Denjo, who spent time reading and correcting my thesis. The translator Miguelito (ma Miguel non c'era!). Antonio and his pirates' illustrations. And Giulia (and the night of the living dead animals), LoLudo, Eleonora and the memorable Christmas's gremlins and all my friends for sharing this moment with me.

Finally - and most importantly - to all the adventures, perros, and cuccioli de perros! And to the friends (abete and pino) - the space fauna! - and family from San Casciano (V.P.).

Contents

List of Figures

List of Tables

List of Abbreviations

4sU	**4**-thio**U**ridine
A-site	**A**minoacyl-site
AHA	L-**A**zido**H**omo**A**lanine
AID	**A**uxin-**I**nduced **D**egron
ALE	**A**lternative **L**ast **E**xon
APA	**A**lternative **P**oly**A**denylation
ARE	**A**U-**R**ich **E**lement
CDE	**C**onstitutive **D**ecay **Element**
CDS	**C**o**D**ing **S**equence
CMV	**C**yto**M**egalo**V**irus
CPE	**C**itoplasmic **P**olyadenylation **E**lement
DAPI	4′,6-**D**i**A**midino-2-**P**henyl**I**ndole
DIV	**D**ay *In Vitro*
DTT	**D**i**T**hio**T**hreitol
EBs	**E**mbryoid **B**odie**s**
ESC	**E**mbryonic **S**tem **C**ell
FDR	**F**alse **D**iscovery **R**ate
FISH	**F**luorescence ***I**n **S**itu* **H**ybridization
FXS	**F**ragile **X** **S**yndrome
GAP	**G**TPase **A**ctivating **P**rotein
GDI	**G**uanine nucleotide **D**issociation **I**nhibitor
gDNA	**g**enomic **DNA**
GEF	**G**uanine **E**xchange **F**actor
HITS-CLIP	**HI**gh-**T**hroughput **S**equencing of RNA isolated by **C**ross**L**inking **I**mmuno**P**recipitation
hnRNP	**h**eterogeneous **n**uclear **R**ibo**N**ucleo**P**rotein
IDR	**I**ntrinsically **D**isordered **R**egion
iNs	**i**nduced **N**euron**s**
IF	**I**mmuno**F**luorescence
IPTG	**I**so**P**ropyl β-D-1-**T**hio**G**alactopyranoside
kb	**k**ilo**b**ase
KD	**K**nock-**D**own
LB	**L**uria **B**roth
LTP	**L**ong-**T**erm **P**otentiation
LC-MS/MS	**L**iquid **C**hromatography-tandem **M**ass **S**pectrometry
MCP	**M**S2 **C**oat **P**rotein
mESC	**m**ouse **E**mbryonic **S**tem **C**ell
miRNA	**mi**cro**RNA**
mRNA	**m**essenger **RNA**
mRNP	**m**essenger **R**ibo**N**ucleoprotein **P**article
NF	**N**euro**F**ilament

NGS	**N**ext **G**eneration **S**equencing
NLS	**N**uclear **L**ocalization **S**ignal
nm	**n**ano**m**eter
NMD	**N**onsense-**M**ediated mRNA **D**ecay
OD	**O**ptical **D**ensity
ON	**O**ver **N**ight
ORF	**O**pen **R**eading **F**rame
P-site	**P**eptidyl-site
pA	**p**oly(**A**) site
PAK	**p**21-**A**ctivated **K**inase
PAP	**P**oly(**A**) **P**olymerase
PAR	**PAR**titioning-defective
PAR-CLIP	**P**hoto**A**ctivatable **R**ibonucleoside-enhanced **C**ross**L**inking and **I**mmuno**P**recipitation
PARP	**P**eri**A**xoplasmic **R**ibosomal **P**laque
PAS	**P**oly**A**denylation **S**ignal
PEI	**P**oly**E**thylen**I**mine
PFA	**P**ara**F**orm**A**ldehyde
PPC	**P**P7 **C**oat **P**rotein
PPI	**P**rotein-**P**rotein **I**nteraction
PSD	**P**ost**S**ynaptic **D**ensity
pre-mRNA	**RNA**-**I**nduced **S**ilencing **C**omplex
puro-PLA	**puro**mycin-**P**roximity **L**igation **A**ssay
RER	**R**ough **E**ndoplasmatic **R**eticulum
RISC	**R**NA-**I**nduced **S**ilencing **C**omplex
RBP	**R**NA **B**inding **P**rotein
RGC	**R**etinal **G**anglion **C**ell
RNAi	*RNA* **i**nterference
ROS	**R**eactive **O**xygen **S**pecies
RPF	**R**ibosome **P**rotected **F**ootprint
RRM	**R**NA **R**ecognition **M**otif
RT	**R**oom **T**emperature
RT-qPCR	**q**uantitative **R**everse **T**ranscription **P**olymerase **C**hain **R**eaction
SER	**S**mooth **E**ndoplasmatic **R**eticulum
sfGFP	**s**uper **f**older **G**reen **F**luorescent **P**rotein
shRNA	**s**hort **h**airpin **RNA**
SILAC	**S**table **I**sotope **L**abeling with **A**mino acids in **C**ell culture
smFISH	**s**ingle **m**olecule **FISH**
snRNP	**s**mall **n**uclear **R**ibo**N**ucleo**P**rotein
SRP	**S**ignal **R**ecognition **P**article
TE	**T**ranslation **E**fficiency
tRNA	**t**ransfer **RNA**
uORF	**u**pstream **O**pen **R**eading **F**rame
UTR	**U**n**T**ranslated **R**egion
WASP	**W**iskott-**A**ldrich **S**yndrome **P**rotein

To pasta, cooked with love…

1 Introduction

1.1 Right where it belongs: biological functions of RNA localization and means of localization

The spatial organization of messenger RNAs (mRNAs) in subcellular compartments of a cell guarantees an exquisite temporal and spatial control of gene expression, providing the basis for cell polarization. The functional and structural asymmetries that arise from mRNA localization and local translation underlie several important processes, which span from:

(i) embryo development, where gradients of different maternal mRNAs define the patterning of the cell (Johnston and Nüsslein-Volhard, 1992);

(ii) to cell migration in fibroblast, where RNA transport and local translation in protrusions is crucial for motility (Liao et al., 2015);

(iii) to establishment of dendrites and axons identity and several other processes in neurons (outlined in chapter 1.1.1).

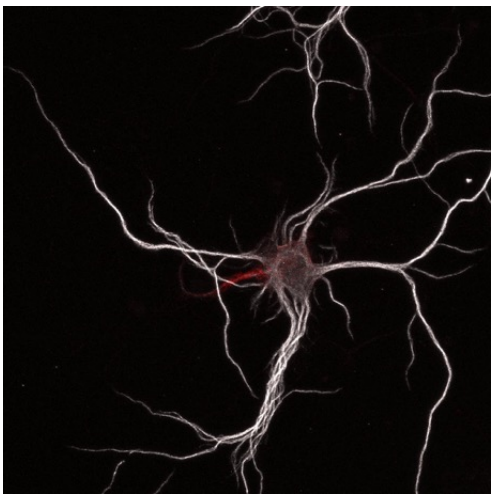

FIGURE 1.1: **Neuron morphology.** Cortical neuron at DIV21, stained with MAP2 (white) for dendrites, and AnkG (red) for the initial segment of the axon.

1.1.1 Roles of RNA localization and local translation in the neuron perspective

In neurons, cell polarization is particularly relevant, as these cells are characterized by a very unique morphology (Fig. 1.1). In fact, the somatic cell body of neuronal cells can be hundreds of microns away from both the dendritic terminals and axon tip. In the human body, the biggest distance is represented by the axon of the sciatic nerve, which measures up to a meter (Fletcher and Theriot, 2004). Moreover, axons and dendrites can be considered as semi-autonomous structures, performing very different functions from each other, and from the cell body. These features make this class of specialized cells particularly interesting for the study of cell asymmetry in terms of spatial organization and distribution of mRNAs and proteins. In the following sub-chapters I will explore in more details some of the known examples where RNA localization and local translation have a great functional significance in the context of neurons.

Neuronal polarity

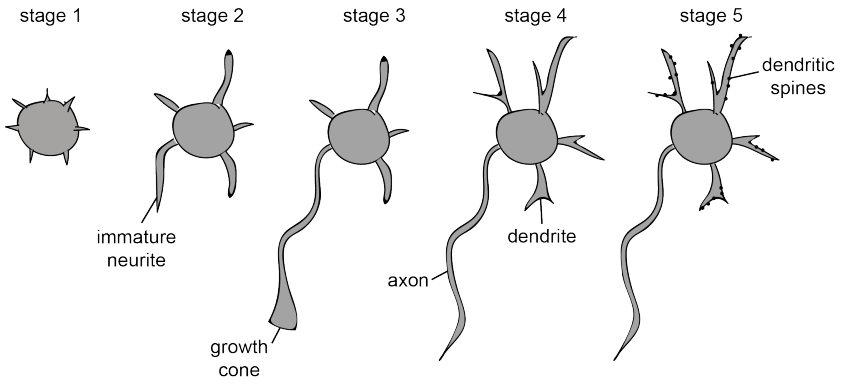

FIGURE 1.2: **Stages of neuronal morphology during polarization.** At stage 1, the immature neuron forms small protrusions, which develop into several immature neurites at stage 2. At stage 3, one neurite starts growing faster than the others, establishing polarity. At stage 4, dendrites developed from the rest of the neurites acquire their typical characteristics. At stage 5, synaptic contacts are formed through dendritic spines and axon terminals.

A mature neuron is characterized by two molecularly and functionally distinct compartments that extend from the cell body: a single axon responsible of transmitting signals, and multiple shorter dendrites doing the opposite job of receiving signals. Before these two structures are specified, neurons form several thin filopodia, which eventually will become immature neurites, also

called minor processes (Fig. 1.2 stage 2). Immature neurites are morphologically equal, and undergo several rounds of random growth and retraction, until one of them takes over and starts extending rapidly, becoming an axon, in three stages that have been described as protrusion, engorgement and consolidation (stages 3 to 5 in Fig. 1.2) (Dotti, Sullivan, and Banker, 1988, Dent and Gertler, 2003). The remaining neurites will then develop in functional dendrites during stage 4 and 5.

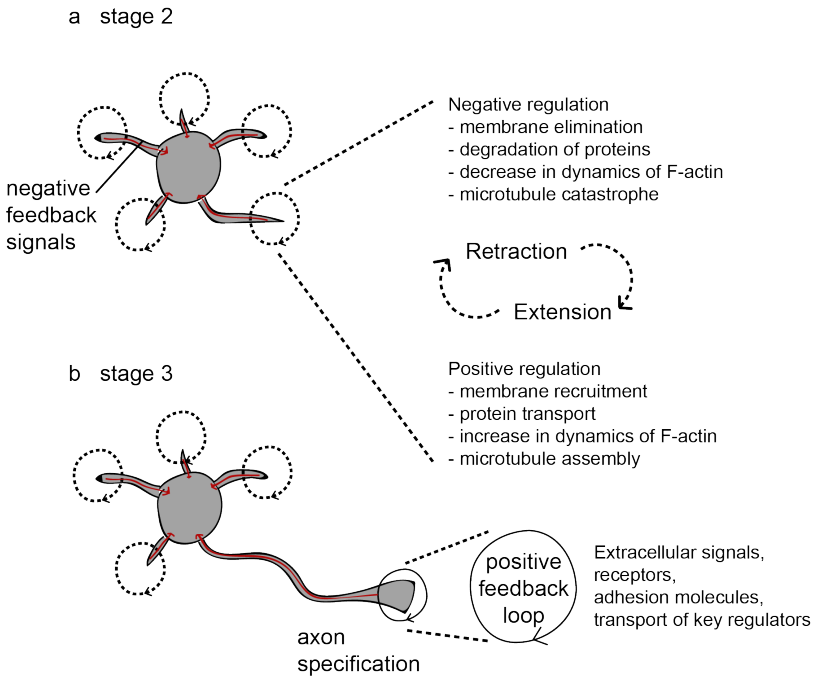

FIGURE 1.3: **Axon specification in neuronal polarization.** a| At stage 2, random extension and retraction characterize the immature neurites. The extension is driven by cytoskeletal rearrangements which involve actin dynamics and microtubule formation, and by local recruitment/concentration of signalling molecules and vesicles increasing the plasma membrane. This positive regulation is counteracted by other signalling molecules (such as GTPase-activating proteins and phosphatases) inducing microtubule catastrophe (retraction), decrease in actin dynamics and in vesicles fusion. b| When the positive signals overcome the negative ones, one neurite elongates rapidly becoming the future axon, and the establishment of a positive feedback loop sustains continuous elongation.

At the molecular level, this asymmetric growth is influenced by signalling molecules acting at the level of cytoskeletal rearrangements and protein trafficking. When the balance between growth regulators is lost in one of the immature neurites, and the positive regulators take over, an axon is born (Fig. 1.3) (Lowery and Vactor, 2009). This process underlies the importance of localization at onset of neuronal polarization, where the factors involved in axonal specification are asymmetrically localized in the axon-to-be (table 1.1).

TABLE 1.1: List of localized factors involved in establishment of neuronal polarity

Protein	**Function**	**Subcellular localization**	**Ref**
PI3K	kinase	Activated at the tip of future axon (stages 2,3)	Shi, Jan, and Jan, 2003
R-RAS	small GTPase	Single neurite (stage 2); axon (stage 3)	Oinuma, Katoh, and Negishi, 2007
RAP1B	small GTPase	Tip of single minor process (stage 2); tip of axon (stage 3)	Schwamborn and Püschel, 2004
CDC42	small GTPase	Tip of single minor process (stage 2); tip of axon (stage 3)	Schwamborn and Püschel, 2004
AKT	mediates the signals of growth factors	Tips of minor processes (stage 2); tip of axon (stage 3)	Yan, Guo, and Wang, 2006
GSK3β	glycogen synthesis	Tips of all neurites (stage 2); tip of axon (stage 3); pGSK3β: tip of axon (stage 3); cell body	Jiang et al., 2005
PAR3	involved in asymmetric cell division and cell polarization	Tips of minor processes (stage 2); tip of axon (stage 3)	Shi, Jan, and Jan, 2003
PAR6	involved in asymmetric cell division and cell polarization	Tip of axon (stage 3)	Shi, Jan, and Jan, 2003
MARK2	microtubule affinity-regulating kinase	All neurites, or tip of longest neurite (stage 2); tip of axon (stage 3)	Yu et al., 2006
CRMP2	mediator in semaphorin 3A signalling; cargo receptor	Diffuse (stage 2); distal part of axon (stage 3)	Kimura et al., 2005, Inagaki et al., 2001

Axonal growth and pathfinding

Axonal growth is driven by asymmetric distribution of guidance cues, which allows growth cones to navigate by making directional turns. Four different families of guidance cues influence this process: netrins, ephrins, slits and semaphorins. They act as attractive or repulsive external polarized signals which the growth cone follows or avoids (Fig. 1.4).

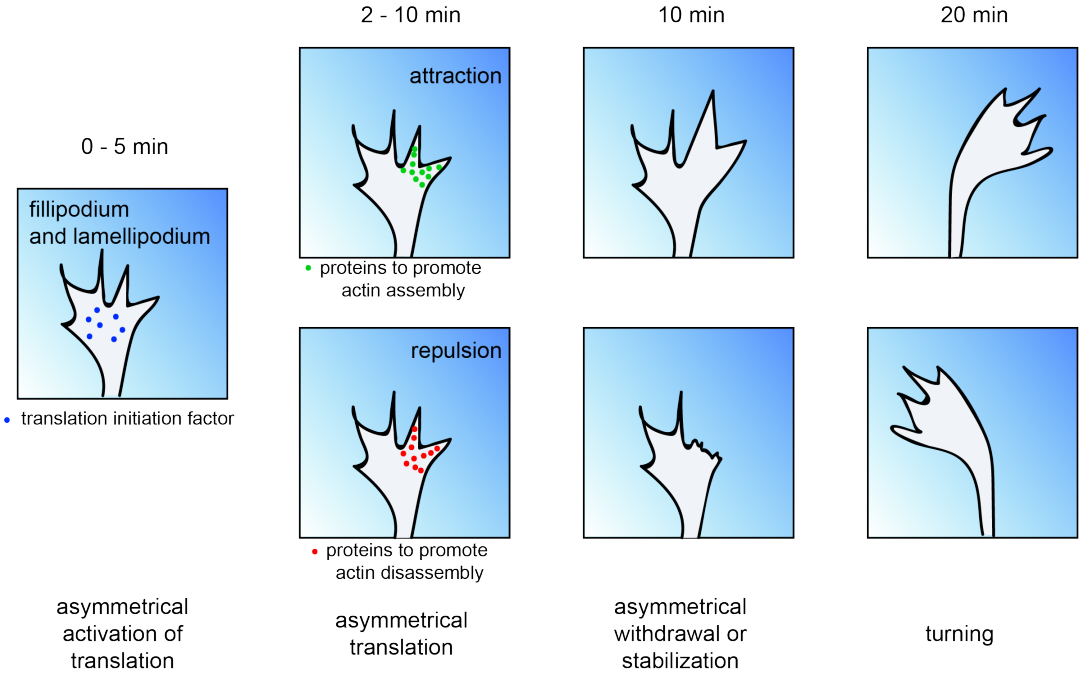

FIGURE 1.4: **Cue-guided asymmetrical synthesis of cytoskeletal proteins.** An attractive cue induces the synthesis of proteins that promote actin assembly (green dots), resulting in turning of the growth cone towards the stimulus; on the other hand a repulsive cue induces the synthesis of proteins that promote actin disassembly (red dots), resulting in the growth cone turning in the opposite direction.

The decision of the axon is carried out through the accumulation of an internal factor, for example *β-actin* mRNA, whose transport and translation are rapidly induced by Netrin-1 or brain-derived neurotropic factor (BDNF) gradients, resulting in the axon turning towards them (Leung et al., 2006, Yao et al., 2006). Examples of repulsive cues are given by SLIT2, which induces the translation of Cofilin-1, an actin depolymerizing factor (Piper et al., 2006), or SEMA3A, which increases RhoA synthesis, determining growth cone collapse (Wu et al., 2005). Translation initiation underlies the response to cues, and is dependent on the eukaryotic initiation factor 4E (eIF4E), which binds the 5′ cap of mRNAs. Phosphorylation of eIF-4E binding protein (eIF-4EBP) via MAP kinases (MAPKs) and via the mammalian target of rapamycin (mTOR), induced by SEMA3A and Netrin-1, releases eIF4E which in turn can recruit

the rest of the translation initiation complex and initiates translation (Lin and Holt, 2007).

Another interesting example of precise spatio-temporal regulation critical for axonal pathfinding is given by the combination of expression of different *Robo3* isoforms and nonsense-mediated mRNA decay (NMD) local regulation (see also chapter 1.1.2).

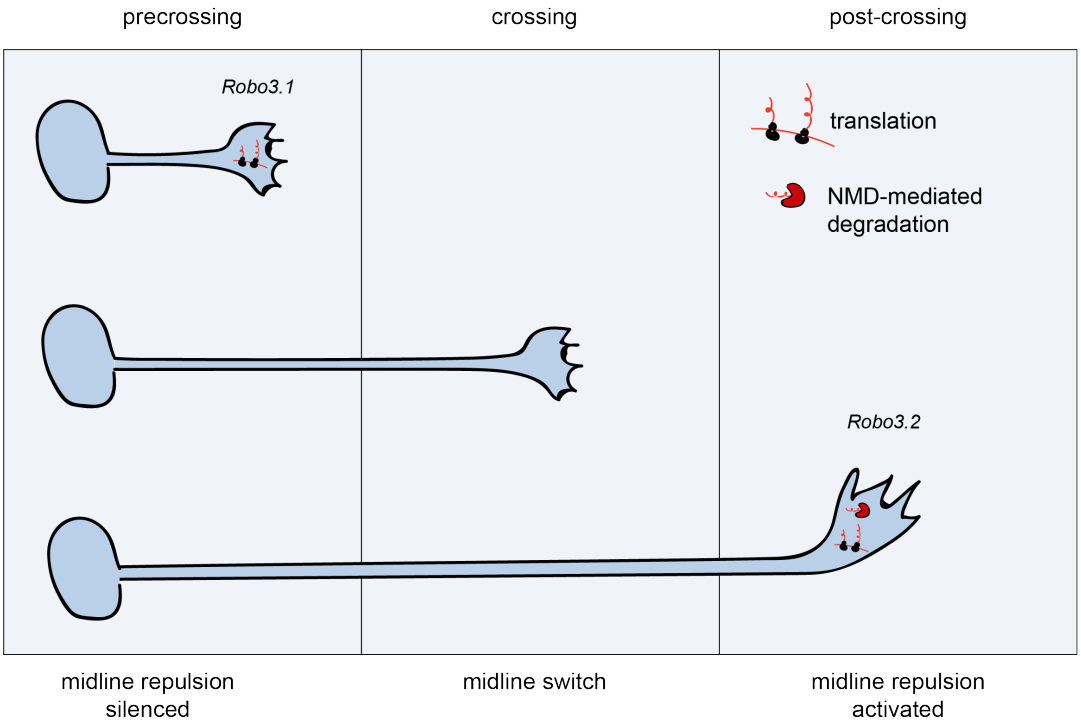

FIGURE 1.5: **NMD local regulation of axon pathfinding.** While crossing the spinal cord midline, *Robo3.2* translation is induced by signal cues released from the floor plate. ROBO3.2 protein levels are tightly controlled by NMD, in such a way that the limited amounts of ROBO3.2 allows for proper lateral positioning of the axons.

Through the NMD surveillance system, transcripts containing a premature stop codon are targeted for degradation (Hoek et al., 2019, Doma and Parker, 2007, Lejeune and Maquat, 2005). The feature that characterizes a NMD-target is the presence of a exon-junction complex, downstream of a ribosome positioned at the stop codon. The exon-junction complex is composed of proteins involved in splicing, which after the splicing reaction remain bound at the junction between each exon. Usually exon-junction complexes are found upstream of the stop codon, and are removed during the first rounds of translation (Dostie and Dreyfuss, 2002, Ishigaki et al., 2001). However, in the case of a mutation leading to a premature stop codon, some exon-junction complexes might be found after the stop codon, eventually leading to mRNA degradation (Chang, Imam, and Wilkinson, 2007, Maquat, 2004).

In the spinal cord, during commissural axon guidance, axons are first attracted to the ventral midline, and once crossed, they become repulsed. These events are guided by unknown cues released by specialized glia cells located in the midline (also called floor plate) (Long et al., 2004), and by alternative splicing of *Robo3*, which determines the switch from attraction to repulsion. The expression of *Robo3* isoforms is spatially regulated in relation to the midline: *Robo3.1* is expressed while the axon grows towards the midline, and once the midline is reached and crossed, signals coming from the floor plate induce the translation of the axon-localized *Robo3.2* isoform. Expression of *Robo3.2* is tightly regulated: *Robo3.2* is a target of NMD, which allows to control for protein levels in postcrossing axons. In fact, when NMD pathway is deficient, the too elevated levels of ROBO3.2 determine an over-repulsion from the midline, whilst upon normal conditions, NMD-dependent control of *Robo3.2* levels allows the axons to position properly in a lateral fashion during ascension in the spinal cord (Colak et al., 2013) (Fig. 1.5).

Axonal arbor architecture and connectivity

The branching complexity of an arbor is a critical determinant of neural circuit assembly, as it defines the number and the extent of post-synaptic partners for a neuron (Ruthazer, 2006). Many axon branch regulators are the same guidance cues that trigger translation in axons, such as Netrin-1, BDNF, SEMA3G and SLIT2 (Kalil and Dent, 2014), hinting to a link between local protein synthesis and axonal arbor architecture. Evidence supporting this hyoithesis comes from *Drosophila* (Pan et al., 2004) and *Danio rerio* (Tucker, Richards, and Lardelli, 2006), where downregulation of a negative translational regulator - the RBP Fragile X mental retardation protein (FMRP) - was associated with an increase of axonal branching. However, the downregulation of FMRP was not compartment specific but across the whole cell, therefore the direct link between local translation and axonal branching was still missing. Recently, in a live-imaging study in axons of *Xenopus laevis*'s visual system (Wong et al., 2017), the role of local protein synthesis in axonal arbor architecture was finally shown. Wong and colleagues observed that the sites where new branches emerge are characterized by the docking of RNA granules, and those same RNA granules invade a new stabilized branch (Wong et al., 2017). Moreover, they observed that newly synthesized β-actin colocalizes with the docked RNA granules, and arbor disruption was achieved by inhibition of axonal translation of β-actin, demonstrating that local protein synthesis is necessary for the complex architecture of the axonal arbor (Wong et al., 2017). Additional evidences were given by Shigeoka and colleagues, in a study where translation of mRNAs associated with branching was shown

in vivo in axon terminals of mouse retinal ganglion cell (RGC) (Shigeoka et al., 2018).

Dendrite morphology

Dendritic spine size has been shown to be regulated locally by the activity of a microRNA (miRNA) (see also chapter 1.1.2). miRNAs are small non-coding RNA involved in post-transcriptional regulation of gene expression. They function as guides, by pairing with partially complementary sites present in the 3′UTR of their target mRNAs, and recruiting a complex of proteins which causes translational repression, mRNA deadenylation and decay (Fabian and Sonenberg, 2012).

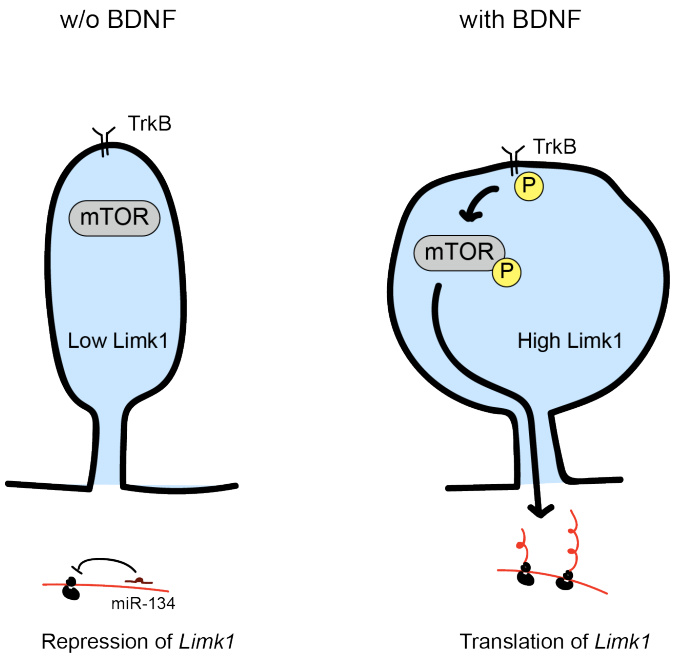

FIGURE 1.6: **miR-134-mediated regulation of dendritic spine development.** miR-134 is involved in tranlsational repression of *Limk1* during its transport to the synapses. Upon synaptic stimulation, BDNF activates the TrkB/mTOR signalling pathway, resulting in miR-134 release of repression and *Limk1* translation activation, which eventually results in spine growth.

miR-134 was found to be specifically expressed in brain, and localized to the synapto-dendritic compartment in rat hyppocampal neurons (Schratt et al., 2006). It functions as repressor of *Limk1*: it was speculated that miR-134 binds to *Limk1* during its transport to the dendritic spines, and it maintains it in a dormant state by recruiting the silencing complex, as long as synaptic activity is absent. The translational repression of *Limk1* mediated by miR-134 determines a decrease in the dendritic spine volumes, phenotype that was

rescued by expressing a mutant of *Limk1* lacking the seed region for miR-134 (Schratt et al., 2006). Upon synaptic stimulation, the TrkB/mTOR signalling pathway is stimulated by BDNF, and miR-134 repression is relieved, leading to enhanced translation of *Limk1* and spine growth (Fig. 1.6), which hereupon might contribute to synaptic development (Schratt et al., 2006).

Synapse formation

Synaptogenesis occurs between appropriate pre- and post-synaptic partners, and it is initiated by cell-cell contacts. A secreted neuropeptide, sensorin, was shown to regulate presynaptic growth and synapse stabilization between sensory and motor neurons in *Aplysia* (Hu, 2004). Its mRNA localizes to distal neurites (Brunet et al., 1991), and its local translation in response to synapse formation signals is essential for synapse growth and maintenance (Lyles, Zhao, and Martin, 2006).
Another example is *Snap25*, which encodes for a protein responsible of synaptic vesicles fusion to the plasma membrane. Its axonal translation was shown to be upregulated and required in the assembly of presynaptic terminals (Batista, Martínez, and Hengst, 2017).

Plasticity and memory formation

"...it is possible that synthesis of specific proteins is the essential physical phenomenon paralleling memory, fantasy, and intuition. This hypothesis is supported by the fact that protein synthesis occurs in strongly stimulated neurons and that cells are able to 'learn' to synthesize new specific proteins..." (Monné, 1948).

It was already postulated 70 years ago, that synthesis of new proteins might be crucial for the establishment of long-term memories in brain. Since then, many studies acquired more evidence supporting this idea, specifically through the use of translation inhibitors (Huang et al., 1996, Davis and Squire, 1984), and the field proceeded further in giving local translation a particular hot spot in this process (Steward, 2007). The functional significance of dendritic protein synthesis on behaviour was shown by Steward and colleagues, were they focused on the Ca^{2+}/calmodulin-dependent protein kinase II alpha (CaMKIIα) (Steward, 2007), already known to be highly expressed in dendrites, with a potential role in plasticity (Burgin et al., 1990). In this study, the localization of *CaMKIIα* mRNA to dendrites was specifically disrupted through mutagenesis of the 3′UTR (Mayford et al., 2002), which produced a dramatic reduction of CaMKIIα in postsynaptic density (PSD). This perturbation resulted

in a reduction in late-phase long-term potentiation (LTP), which consists in a cellular measure of memory formation, and it also led to impairments in spatial memory, contextual fear conditioning and object recognition memory, demonstrating that local translation contributes to synaptic and behavioural plasticity.

1.1.2 Spatial and temporal control of RNA localization and local translation: the importance of the untranslated region

All the processes mentioned above (chapter 1.1) are characterized by a precise spatial regulation of mRNA localization, which overcomes entropy to maintain asymmetry. How is this asymmetry achieved?
mRNA conveys genetic information from DNA to the ribosomes: it encodes for a message which is read and translated into proteins by the ribosomes. Additionally to the coding sequence, it contains two untranslated regions (UTRs), at the 5′ and 3′ ends, which are responsible for different aspects of post-transcriptional regulation, with the 5′ mainly involved in translation regulation, and the 3′ in various stages of RNA metabolism, including nuclear export, localization in the cytoplasm, trafficking to specific intracellular compartments, translational control, mRNA stability and protein-protein interactions (PPIs). The complexity of post-transcriptional regulation mediated by the 3′UTR can be explained describing its "anatomy": the 3′UTR contains the so called *zip*-codes or *cis*-elements, which are very heterogeneous sequences in size (from few nucleotides to > 1 kb) and structure, that can serve as docking point for the binding of specific *trans*-acting elements, namely RNA binding proteins (RBPs), which in turn can act at all the levels of post-transcriptional regulation just mentioned. The messenger ribonucleoprotein particle (mRNP) which forms upon binding of RBPs to the mRNA, generates already in the nucleus after transcription: the processing of premature mRNA (pre-mRNA), involving splicing and polyadenylation, allows the deposition of RBPs onto the transcript, which ultimately will determine its cytoplasmic migration and fate. Once in the cytoplasm, depending on the mRNP's additional factors that might be gained or lost, the mRNA will either freely diffuse, or be actively transported along the cytoskeleton by motor proteins, or be protected from degradation, or anchored to a compartmentalized domain, or a combination of those. In the following subchapters, the different means by which mRNAs get localized and locally translated are described, and in the following table (table 1.2) a selection of mRNAs, RBPs, and types of transport discussed later in the text are introduced.

mRNA	RBPs	Localization element	Type of movement	Cell type/organism and subcellular destination	Significance
Vg1	40LoVe, hnRNP I, Vg1RBP/ Vera, Kinesin-1, Kinesin-2	VM1 or E2 (3′UTR)	kinesin-directed transport	*Xenopus* oocyte: vegetal pole	embryonic development
bicoid	Staufen	stem loop IV/V and domain III (3′UTR)	dynein-directed transport	*Drosophila* oocyte: anterior pole	embryonic patterning
oskar	Y14, Staufen, hnRNP A/B	EJC (5′ and 3′UTR)	diffuse and kinesin-directed transport	*Drosophila* oocyte: posterior pole	germ line differentiation
ASH1	She2p	E1, E2A, E2B, E3 (ORF and 3′UTR)	myosin-directed transport	yeast: distal bud tip	mating type switching
nanos	multiple	3′UTR	selective degradation, diffuse and trap	*Drosophila* oocyte: posterior pole	embryonic patterning
CaMKIIα	Staufen, hnRNP U, PSF, FMRP	G-quadruplex (3′UTR)	directed, oscillatory	mammalian cells: neurons dendrite	memory formation
β-actin	ZBP1, ZBP2	5′-CGGAC-19nt-C/A-CA-C/U-3′ (3′UTR)	active transport, diffuse and capture	somatic cell periphery, neuron dendrite, axonal growth cones	directed mobility, axon guidance, dendrite arborisation
Arc	multiple	3′UTR	bidirectional transport	mammalian cells: neurons dendrites	synaptic plasticity

TABLE 1.2: Examples of localized mRNAs

Polarized export from the nucleus

In 1985 it was hypothesized that directed nucleocytoplasmic transport could be a way to localize transcript in the cytoplasm ("gene gating" hypothesis, Blobel, 1985). There is not much evidence supporting this idea, apart from one study in *Chlamydomonas reinhardtii*, a biflagellated single-cell algae (Colón-Ramos et al., 2003). The algae is characterized by cellular asymmetry, where the flagella are localized at the anterior pole, and the chloroplast at the posterior pole of the cell, with the nucleus nested in-between. Colón-Ramos and colleagues observed asymmetric distribution of nuclear pore complexes towards the posterior pole, especially in response to deflagellation (both flagella removed) (Colón-Ramos et al., 2003). Concomitantly, they also observed an accumulation of *β-tubulin* at the posterior cytoplasmic region adjacent to the nuclear area enriched in nuclear pore complexes (Colón-Ramos et al., 2003). Based on this results, they suggested that transcript localization in the cytoplasm can be affected by nuclear architecture.

Cytoplasmic transport via motor proteins

Motor	**Speed *in vivo***	**Speed *in vitro***	**Function**
Conventional kinesins	1.8	0.84	anterograde axonal transport
Nkin	0.8	1.8	secretory vesicle transport
Unc104/KIF	0.69	1.2	transport of synaptic vesicle precursors and mitochondria
Fla10/KinII	2	0.4	transport in axons
Dyneins	1.1	1.25	retrograde axonal transport
Myosin II	6	8	fast skeletal muscle
Myosin II	0.2	0.25	smooth muscle contraction
Myosin V	0.2	0.35	vesicle transport

TABLE 1.3: Motor proteins speed in μm^2/sec. From Howard, 2002.

mRNAs can travel at different speed and different directions (uni- or bidirectional) along different types of cytoskeletal tracks (microtubules or actin filaments). These properties are specified by the nature and number of active molecular motors recruited to a target mRNA (Bullock, 2004, Gagnon and Mowry, 2011, Marchand, Gaspar, and Ephrussi, 2012). Kinesins, dyneins, and myosins constitute the three families of motor proteins, and they work

by hydrolyzing ATP in order to change conformation and move along the cytoskeleton. Active transport of cargos through motor proteins is faster than diffusion, where diffusion of mRNA stands around 0.1 - 0.4 μm^2 per second (Park et al., 2014), however, it vastly varies depending on the motor at issue (see table 1.3).

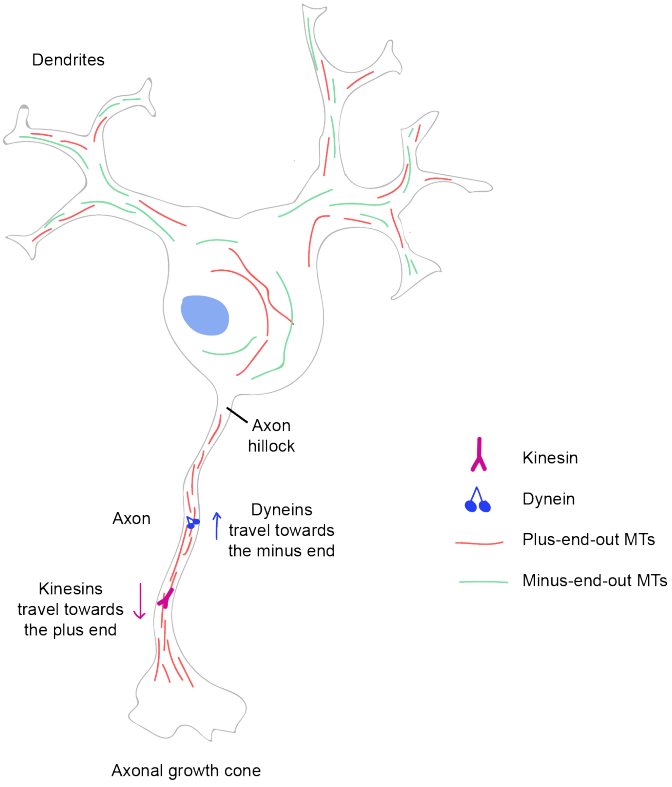

FIGURE 1.7: **Motor proteins transport along the microtubules**. Microtubule orientation is mixed in dendrites and directional in axons (plus end towards the tip of the axon). Kinesins travel towards the plus end, on the contrary dyneins travel across the minus end.

Kinesins usually transport cellular cargos to the plus ends of microtubules, while dyneins to the minus ends, in a context where the microtubule orientation is uniform in axon (with the plus end facing the tip), and mixed in dendrites (with the plus end facing the cell body or the dendritic tip) (Fig. 1.7, panel b).

Kinesin-1 is a tetrameric protein complex, composed of two identical heavy chains (KHC) and two light chains (KLC). The KHC motor domain is responsible for ATP hydrolysis and binding to microtubules (Yang, Laymon, and Goldstein, 1989), while the KLC for cargo binding (Hirokawa et al., 1989).

One well-characterized example of kinesin-mediated transport is represented by *Vg1* mRNA during oogenesis in *Xenopus*, where *Vg1* is required at the vegetal pole of the oocyte for correct patterning (Birsoy, 2006). Kinesin-1 and Kinesin-2 were shown to be responsible for the correct localization by

an interference experiment where depletion of either Kinesin-1 or -2 abolished *Vg1* vegetal localization, suggesting that both motors are required for successful mRNA transport (Messitt et al., 2008).

Dyneins are divided into two subclasses: axonemal dyneins and cytoplasmic dyneins. Axonemal dyneins are involved in coordinating the beating of flagella and cilia, while cytoplasmic dyneins are responsible for cargo transport to the minus end of microtubules. This latter group consists of a multi-protein complex made of a catalytic homodimeric heavy chain and additional non-catalytic subunits, among which the dynactin complex, that affects dynein subcellular localization, processivity and adapt dynein to cargo (Schroer, 2013).
In the *Drosophila* oocyte, dynein-mediated transport is responsible for *bicoid* localization to the anterior pole: delocalization of *bicoid* mRNA derives from disruption of dynein function, pointing to the fact that dynein continuously transport *bicoid* to the minus end of microtubules (Weil, Forrest, and Gavis, 2006).
Another example in *Drosophila* is given by *oskar* mRNA, where both dyneins and kinesins are necessary at different step of *oskar*'s travels across the oocyte. The first step of the trip, which consists in entering the oocyte from the nurse cells, is accomplished by dyneins. Two adaptor proteins, Egl and BicD, mediate the interaction between the dyneins and *oskar*, by binding to its 3′UTR (Dienstbier et al., 2009). Once in the oocyte, the adaptor protein Tropomyosin1-I/C can bind another *cis*-element in *oskar* 3′UTR, and mediate the transfer to Kinesin-1, which takes over the rest of the trip to the posterior pole (Gáspár et al., 2017, Zimyanin et al., 2008). The function of Oskar protein at the posterior pole is linked to *nanos* gradient formation that is required for proper embryo patterning (Martin and Ephrussi, 2009).

The myosin superfamily of motor proteins contains twenty structurally and functionally distinct classes. Most are characterized by an N-terminal domain responsible of actin-binding and ATP hydrolysis, a neck domain required for light chain attachment, and a C-terminal tail for cargo binding. They travel along actin filaments, which make most of the architecture at the synapses.
In *Saccharomyces cerevisiae*, Myo4p class V myosin motor is responsible for *ASH1* mRNA localization. *ASH1* encodes for a transcription factor that blocks the expression of HO endonuclease, and by doing so, it represses mating type switching in the daughter cell (Gonsalvez, Urbinati, and Long, 2005). *ASH1* localization is required to be restricted to the yeast budding tip, and this is accomplished by the binding of She2p, an RBP that binds the *cis*-elements

present on *ASH1* mRNA and allows the recruitment of the complex She3p-Myo4p (Bohl, 2000). The so-formed motor-containing mRNP can travel along the actin cytoskeleton to the daughter cell (Gonsalvez, Urbinati, and Long, 2005).

Diffusion and entrapment model

mRNA can diffuse and localize by a trapping mechanism, where previously localized anchors ensure mRNA docking. One particular instance in which mRNA travels by diffusion is during oogenesis and germ plasm deposition in *Drosophila*, when functional microtubules are missing because of cytoskeletal rearrangements. In fact, assembly of germ plasm occurs in two phases. During mid-oogenesis, nurse cells provide the oocyte with maternal mRNAs, among which *oskar*, that is deposited at the posterior pole via dyneins and kinesins (see above). There, *oskar* is translated and can recruit other germ plasm proteins. The transition towards the late phase of oogenesis is characterized by the apoptosis of the nurse cells and the "nurse cell dumping", which consists in the deposition of the nurse cells' content into the oocyte. During this process, the microtubule cytoskeleton reorganizes into cortical bundles. This is when *nanos* gets localized, and since the architecture of the cytoskeleton doesn't support long-range transport, localization of *nanos* occurs via diffusion and entrapment by association with germ plasm proteins previously localized (Forrest and Gavis, 2003, Sinsimer et al., 2011).
Diffusion and entrapment has also been shown in the *Xenopus levis* oocyte, for *Xcat2* and *Xdaz1* mRNAs, where they diffuse and associate to a structure called mitochondrial cloud. The mitochondrial cloud then moves towards the vegetal pole, where these mRNAs are destined (Chang, 2004).

Temporal and spatial degradation

mRNA transcripts can be temporally and locally regulated by degradation, through the activity of localized miRNAs or via nonsense-mediated mRNA decay (NMD).

In the context of temporal regulation of gene-expression, miR-430 plays a critical role during maternal-to-zygotic transition in zebrafish. In early development, maternal mRNAs cover gene expression requirements. At the onset of zygotic transcription, the high expression of miR-430 leads to the required clearance of maternal mRNAs (Giraldez et al., 2006).
In the context of spatial regulation, dendrites and synapses have been shown

to be enriched with a set of miRNAs (Kosik, 2006). One of the most abundant dendritic miRNAs is miR-26a, responsible of inhibition of *Map2* translation, involved in microtubule assembly (Kye et al., 2007). Another example is the brain-specific miR-134, involved in synaptodendritic degradation in neurons. By repressing the translation of *Limk1*, it negatively regulates dendritic spine morphogenesis in cultured hippocampal neurons, during the absence of synaptic activity (Schratt et al., 2006) (see also chapter 1.1.1).
In *Drosophila*, *Hsp83* is locally regulated by silencing: in early fertilized eggs, *Hsp83* mRNA is distributed throughout the egg, but at later stages is restricted to the posteriorly localized germ plasm (Ding et al., 1993). When the silencing machinery is absent, this specific spatial distribution is lost, however still remains unclear how this selective spatial degradation is accomplished (Semotok et al., 2005).

Interestingly, miRNAs maturation - a process that starts in the nucleus and ends in the cytoplasm - was suggested to also happen at the synapses, where pre-miRNAs were found (Bicker et al., 2013). This was recently shown to be indeed the case. Sambandan and colleagues showed that pre-miR-181a, highly expressed in hippocampus, can undergo maturation at the synapses upon local stimulation of neural activity, resulting in a local reduction of CaMKIIα protein synthesis (Sambandan et al., 2017).

Aside miRNA silencing, spatial degradation can be accomplished by NMD. Colak and colleagues were the first to identify NMD components (UPF1, UPF2 and SMG1) in axons (Colak et al., 2013). In the context of commissural axon guidance in the spinal cord (see also chapter 1.1.1), they attribute to NMD a key function for the local regulation of *Robo3.2* translation in the growth cones (Colak et al., 2013). *Robo3* gene produces several isoforms, among which *Robo3.2* that retains an intron, resulting in a premature stop codon upstream of an exon-junction complex, consequently making it target of NMD (Black and Zipursky, 2008). *Robo3.2* isoform is transported to the axon, and only when the axon crosses the midline its translation is activated thanks to unknown guidance cues coming from the plate floor (Long et al., 2004). Its activation leads to a lateral turn of the axon, which will starts growing in diagonal trajectories (Chen et al., 2008). Tight control of ROBO3.2 levels through NMD has been shown to be fundamental for the correct positioning of the axon in relation to the spinal cord midline.

Local translation

One of the mechanisms which controls protein abundance is translation (Schwanhüusser et al., 2011): its spatial regulation allows the synthesis of proteins with precise timing (upon certain stimuli) and at specific subcellular location (Besse and Ephrussi, 2008, Buxbaum, Haimovich, and Singer, 2015, Holt and Schuman, 2013).
The discovery of ribosomes in dendritic spines and in axonal growth cones dates back to structural studies from the '70-90s (Tennyson, 1970, Zelená, 1972, Bunge, 1973, Steward and Levy, 1982, Martin, Fritz, and Giuditta, 1989, Pannese and Ledda, 1991), accompanied by metabolic labelling experiments that proved these compartments as able to *de novo* synthesize proteins (Feig and Lipton, 1993, Giuditta, Dettbarn, and Brzin, 1968, Koenig, 1967, Torre and Steward, 1992).

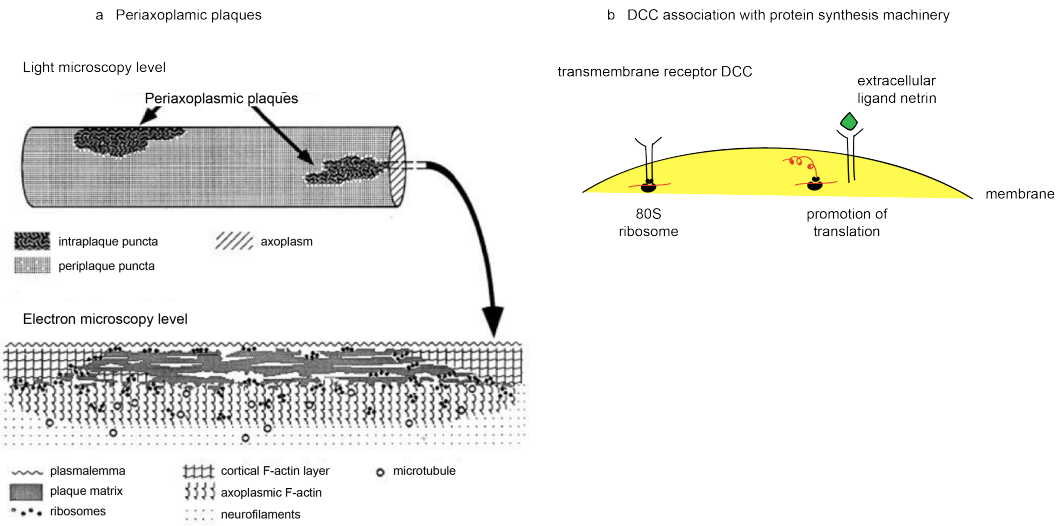

FIGURE 1.8: **Plasmamembrane association of ribosomes.** a | Periaxoplasmic plaque model at the light microscopy level, and the electron microscopy level (90° rotation). From Koenig and Martin, 1996. b | The transmembrane receptor DCC associates with the translation initiation machinery. When the receptor and its ligand Netrin come in contact, the translation machinery is released from DCC and translation is induced.

In axons of mature myelinated neurons though, the detection of ribosomes has been more challenging. In this case, ribosomes have been shown to cluster to discrete domains, distributed at random intervals close to the plasmamembrane, denominated periaxoplasmic ribosomal plaques (PARPs) (Fig. 1.8, panel a) (Koenig and Martin, 1996, Koenig et al., 2000). These domains have been shown to contain Myosin Va and Kinesin II, suggesting an involvement of the microtubule-dependent transport machinery to deliver mRNPs

(Sotelo-Silveira et al., 2004).

An additional finding supporting the idea of ribosomes localized nearby the plasmamembrane has been proposed in the broader context of stimuli-dependent translational regulation: it was shown that in axons and dendrites, ribosomes can associate with Deleted in colorectal cancer (DCC), a well-characterized transmembrane receptor involved in axon growth and found in dendrites (Keino-Masu et al., 1996, Fazeli et al., 1997). The association DCC-ribosome can induce translation upon reception of the external positive signal Netrin (Fig. 1.8, panel b) (Tcherkezian et al., 2010), a well-characterized axonal positive guidance cue (Campbell and Holt, 2001).

Moreover, myelinated axons have also been shown to be receivers of polyribosomes from Schwann cells, glia cells with several important roles in the development and maintenance of the peripheral nervous system. With a simple and elegant experiment, where the ribosomes of Schwann cells only were tagged with eGFP, it was observed the presence of fluorescent ribosomes in the axons, proving the directional uptake from glia cells to neurons, process upregulated in injured and regenerating axons (Court et al., 2008, Court et al., 2011).
Finally, ribosomes have also been detected in variably sized mRNPs inside axons of rat sciatic nerve (Kun et al., 2007).

Intuitively, local translation is finely linked to mRNA localization: mRNA, once localized, needs to be translated. In order to achieve this type of regulation, it is generally believed that mRNA travels in a translational repressed state, followed by activation once the final destination is reached (Doyle and Kiebler, 2011). Regarding this point, contrasting evidence comes from two independent papers (Wu et al., 2016, Wang et al., 2016), where it was shown that mRNA carrying either *β-actin* or *Arc* 3′UTR undergoes active transport in dendrites once translation has already started. Nonetheless, translational repressors have been identified, and showed to inhibit translation at the initiation stage, by directly binding RNA regulatory sequences and taking part in the mRNP (Besse and Ephrussi, 2008). For instance, in *Drosophila* embryos it was shown that localized translation can be achieved by overall translational repression everywhere in the embryo but on the site where the protein is required. Specifically, this latter mechanism has been shown for *nanos*, whose localized translation contributes to the formation of a gradient crucial for embryo patterning. The correct gradient formation is obtained by the combination of *nanos* translational repression in the bulk of the embryo and translational activation at posterior pole. Repression of translation is mediated by Smaug protein, which binds to the 3′UTR of *nanos* and recruits the deadenylation complex CCR4-NOT, leading to deadenylation and consequent mRNA

decay (Zaessinger, Busseau, and Simonelig, 2006). At the posterior pole, this mechanism is prevented thanks to Oskar binding to *nanos* 3′UTR, which precludes CCR4-NOT Smaug-mediated recruitment (Zaessinger, Busseau, and Simonelig, 2006), leading to localized translation activation.

Apart from few characterized examples, it is not so clear how transcripts that are repressed during transport, get activated for translation upon arrival. Phosphorylation acting as a molecular switch gives one explanation: phosphorylation of translational repressors can decrease the affinity for their targets, resulting in relief from translational blockage. One example of this type of regulation is given by FMRP, an RBP switching from translational repressor to activator of the dendritically localized *Dlg4*, depending on the phosphorylation status. When phosphorylated it appears to promote the formation of the RNA-induced silencing complex (RISC)-miRNA, an inhibitory complex repressing translation, whilst upon FMRP dephosphorylation, the RISC complex is released resulting in translation activation (Muddashetty et al., 2011). The cytoplasmic polyadenylation element binding protein (CPEB) is also a translational repressor regulated by phosphorylation. CPEB binds to cytoplasmic polyadenylation elements (cpes) present in the 3′UTR of several dendritically localized transcripts, inhibiting their translation (Richter, 2007). CPEB phosphorylation is induced upon LTP induction and is mediated by the kinase Aurora A, which eventually leads to the polyadenylation and promotion of translation of several mRNAs, among which *CaMKIIα* (Wu et al., 1998, Huang et al., 2002, Udagawa et al., 2012). Zipcode-binding protein-1 (ZBP1) is another example: the unphosphorylated form of this RBP is responsible for the synaptic localization of *β-actin* mRNA in neurons, in a translationally-repressed form. Phosphorylation of ZBP1, mediated by a synaptic-restricted Src kinase, diminishes its binding affinity to its target, leading to *β-actin* translation activation (Hüttelmaier et al., 2005).
However, it is still unclear how the mRNA being translated is retained within the compartment where it is localized. For *β-actin* in migrating fibroblast, it was reported that increased translation correlated with dwell times, eventually determining cell polarity and motility (Park et al., 2012). Some evidence supports the role of elongation factor 1α (EF1α) in anchoring mRNA to formins (proteins associated with the fast-growing ends of actin filaments) and the leading edge actin cytoskeleton (Liu et al., 2002). Consistently, mRNA maintenance at the leading edge of fibroblast was previously shown to depend on actin cytoskeleton (Sundell and Singer, 1991). Otherwise, it has also been suggested that RNP size might influence RNA retention depending on the the cytoplasmic microenvironment (Yamagishi et al., 2009).

In neurons local translation is particularly important, as delineated in chapter 1.1.1. It regulates remodeling of synaptic connections, playing a role in learning and memory (Bramham and Wells, 2007). Moreover, upon initiation of LTP, an increase in the number of polysomes in dendritic spines is observed (Ostroff et al., 2002).
However, the translation machinery and the post-translational factors involved in protein processing are not equal everywhere: a feature which distinguishes dendrites and axons, is the presence or lack of rough endoplasmatic reticulum (RER) and Golgi outposts. Axons host smooth endoplasmatic reticulum (SER) only, which is delivered through vesicles via myosin-based transport (Tsukita and Ishikawa, 1976, Tsukita and Ishikawa, 1979, Langford, 1999, Tabb et al., 1998). Because of this difference, one would think that secreted and membrane proteins, which require RER- and Golgi-processing, would not be synthesized in axons. However, this is not the case, and both invertebrates and vertebrates have been shown to be able to traffic axonal synthesized proteins into secretory pathways, even if they appear to lack morphologically recognizable RER or Golgi apparatuses. Some examples are a G-coupled receptor in anucleated *Lymnea* axons (Spencer et al., 2000), κ-opioid receptor in rodent sensory axons (Bi et al., 2006, Tsai, 2006), guidance receptor EPHA2 in developing vertebrate neurons (Brittis, Lu, and Flanagan, 2002). Moreover, some ER and Golgi proteins have been detected in axons, such as signal recognition particle (SRP) and TRAPα, providing more evidence for the ability of axons to locally synthesize and process secreted and membrane proteins (Krijnse-Locker et al., 1995, Weclewicz, Svensson, and Kristensson, 1998, Willis, 2005, Merianda et al., 2009).

Additionally, because neurons are such a peculiar class of polarized cells, there is a special interest in understanding whether there might be a specific intracellular localization for “specialized” ribosomes" (Xue and Barna, 2012). Specialized ribosomes are ribosomes which either differ in composition from the canonical ones or have a specialized activity, conferring regulatory control in gene expression (Slavov et al., 2015, Shi et al., 2017, Kondrashov et al., 2011). Supporting the idea of the presence of specialized ribosomes in subcellular compartments of neurons was the observation that a specific subset of mRNAs encoding for ribosomal proteins is enriched in neurites, up to tenfold (Moroz et al., 2006). It was hypothesized that thanks to the presence of newly synthesized ribosomal proteins in the distal parts of the neurons, the subset of ribosomes present in the neurites might be distinct from the cell body pool.
This implies a mechanism of ribosome assembly at the neurites, which has recently been proven by the Holt lab (Shigeoka et al., 2018). The authors

show that incorporation of axonally synthesized ribosomal proteins happens *in situ* (axons), in a nucleolus-independent fashion. Moreover, a *cis*-element (YYYYTTYC) was found in the 5′UTR of most of the ribosome protein-coding mRNAs, upstream of the initiation codon, which can be bound by Netrin-1 to form a loop-structure motif inducing axonal translation (Shigeoka et al., 2018).

Interestingly, proteins synthesized locally seem to be structurally and functionally diverse from transported proteins (Weatheritt, Gibson, and Babu, 2014). They often contain intrinsically disordered regions (IDRs) which might promote protein-protein interactions (PPIs). IDRs are polypeptide segments lacking a stable tertiary structure, providing more flexibility and wider surface available for interaction. SHANK1, a member of the postsynaptic density complex, is one of such examples of locally synthesized proteins, characterized by extensive disordered regions (Böckers et al., 2004). Moreover, IDRs of locally synthesized proteins are enriched in linear motifs, consisting of 3-5 residues essential for mediating physical interactions, found next to post-translational modification sites in a range of 5 residues distance (Weatheritt, Gibson, and Babu, 2014). These sites, when in the vicinity of linear motifs, have been shown to act as switches resulting in modulation of protein on/off states (Van Roey, Gibson, and Davey, 2012, Van Roey et al., 2013, Honnappa et al., 2009).

Translation: some facts and numbers (*excursus*) Translation occurs at a speed of $\sim$ 5 aa / sec, with initiation occurring every $\sim$ 30 seconds (Morisaki et al., 2016, Wang et al., 2016, Yan et al., 2016, Wu et al., 2016, Ingolia, Lareau, and Weissman, 2011). Polysomes mainly act independently - translating one mRNA - with an average of 10 - 25 ribosomes per mRNA, and 1 ribosome every 200 - 900 nucleotides. A small fraction ($\sim$ 5%) can be found where two distinct mRNAs are translated simultaneously (Morisaki et al., 2016). In terms of mobility, they show stationary, sub-diffusive and diffusive motion, with occasional directed motion (less than 0.1% of the polysomes) (Wang et al., 2016). The diffusion coefficient changes depending on the proteins being translated and on the cell type. As expected, cytosolic proteins display a higher diffusion coefficient (0.021 or 0.006 $\mu m^2/s$ in HeLa or neurons, respectively) compared to secreted and transmembrane proteins (0.0015 $\mu m^2/s$ in HeLa), since the latter associate with the ER (Wang et al., 2016). In neurons, translation displays a "bursting" behaviour in dendrites, with $\sim$ 20 - 30 proteins synthesized per burst, and the numbers of translated mRNAs decrease as a function of distance to the soma ($\sim$ 40% in proximal dendrites within 30

μm from the soma, $\sim$ 10% in distal dendrites within 100 μm from the soma) (Wu et al., 2016). When the mRNA being translated carries a 3′UTR with localization *cis*-elements (e.g. *Arc* 3′UTR), polysomes move with a direct motion in a bidirectional fashion, both anterograde and retrograde, with a speed of $\sim$ 1 - 3 μm / sec (Wang et al., 2016).

1.2 Mechanisms regulating the 3′UTR identity: alternative polyadenylation and splicing

As previously mentioned (chapter 1.1.2), the 3′UTR region of mRNA is critical for its regulation in terms of stability, translation and localization. Interestingly, genes can encode for mRNA isoforms which differ exactly in this particular region. The power of encoding for multiple isoforms that change in the "add-ons" present in the 3′UTR gives the cells more versatility and control, providing a tool to finely tune expression in space (localization) and time (stability and translation). It is noteworthy that the complexity in terms of 3′UTR length and isoforms number increased during evolution: more complex organisms are characterized by longer 3′UTRs (tenfold increase from yeast to human) and by genes encoding multiple isoforms with alternative 3′UTRs, which in addition are longer compared to the 3′UTR of genes encoding for a single transcript (Mayr, 2017). Depending on the stringency of the cut-off to call an isoform as such, it has been calculated that 51 to 79% (low or high stringency) of human genes encode for multiple isoforms, with an average of 4 isoforms per gene (Hoque et al., 2013, Derti et al., 2012, Tian et al., 2005). Interestingly, genes encoding for single isoforms are usually associated with classical "housekeeping" functions such as ribosome biogenesis, translation, energy metabolism, whilst multi-UTRs genes are associated with regulatory functions such as transcription factors, kinases, phosphatases, RBPs (Lianoglou et al., 2013). It has been suggested that genes encoding for multiple 3′UTR isoforms use post-transcriptional regulation and changes in the isoforms ratio as an alternative mechanism to transcription, to control for protein levels (Lianoglou et al., 2013).

One of the main mechanisms contributing to 3′UTR specification is a alternative polyadenylation (APA). Polyadenylation is a co-transcriptional mechanism which involves endonucleolitic cleavage of the pre-mRNA to add an untemplated poly(A) tail at the end of an mRNA, a synthesis reaction carried out by a poly(A) polymerase (PAP). This is part of the maturation process of nearly all eukaryotic mRNAs (with the exception of replication-dependent histone transcripts). Importantly, alternative poly(A) sites (pAs) can be present

on the pre-mRNA, and depending on the pAs choice, different isoforms can be generated via alternative polyadenylation. The sequence context affects the site of cleavage (Fu and Ares, 2014, Millevoi and Vagner, 2009): *cis*-elements important for pA choice are located upstream and downstream of the pA (Fig. 1.9, panel a).

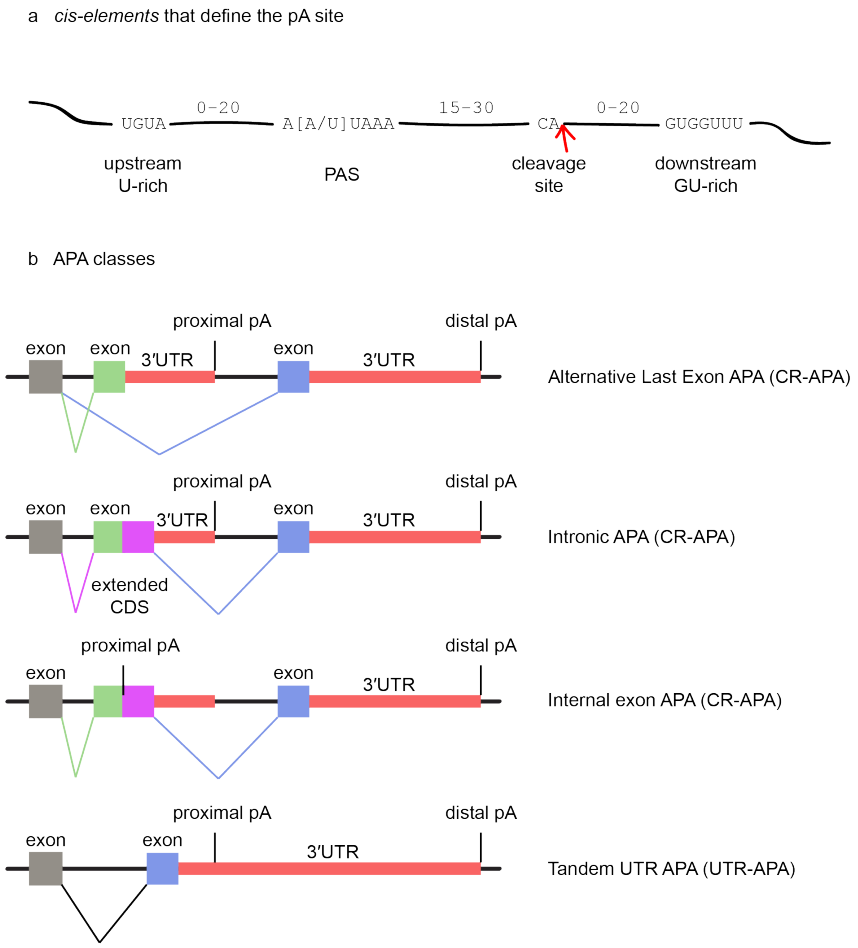

FIGURE 1.9: **Alternative polyadenylation: sequence context and classes.** a | Features present on the pre-mRNA for binding of the polyadenylation machinery. The red arrow points to the cleavage site where the poly(A) tail is added. PAS stands for polyadenylation signal. b | Depending on where the polyadenylation occurs, several isoforms can be generated, classified in CR-APA if the isoforms differ in the coding sequence, or UTR-APA if the isoforms differ in the 3′UTR.

Among the common upstream elements, we find A[A/U]UAAA hexamer (also known as polyadenylation signal - PAS), U-rich elements and U[G/A]UA elements. Interestingly, while the canonical PAS sequence is conserved in genes encoding for one transcript only, the less-conserved variants (more than ten variants have been reported) occur frequently in genes encoding for multiple isoforms (Beaudoing et al., 2000, Tian et al., 2005). Among the downstream elements we find U-rich and G-rich elements. Immediately 5′ of

the cleavage site, a CA or UA dinucleotide is often present (Li and Du, 2013). Depending on the combination of upstream and downstream elements, the strength of the pA site changes, affecting alternative polyadenylation. This can lead to a global regulation when the concentration of polyadenylation factors changes, impacting important biological processes.
For example, global regulation of APA is typical in specific tissues, like brain, ovary and testis. Brain is characterized by a shift towards distal pA sites (producing longer 3′UTRs), while testis and ovary are characterized by the usage of proximal pA sites (shorter 3′UTRs) (Miura et al., 2013, Wang et al., 2008, Smibert et al., 2012, Li and Du, 2013, Liu et al., 2007, Ulitsky et al., 2012). For testis, it was suggested the involvement of specific polyadenylation specific factors in the specification of the polyadenylation pattern (MacDonald and McMahon, 2010, Dass et al., 2002). In fact, testis' isoforms are characterized by less-conserved variants of the PAS hexamer, as well as unique upstream and downstream elements. Moreover, shortening of the 3′UTRs has also been reported during spermatogenesis (Li et al., 2016). Alternative polyadenylation also occurs in mouse development. Ji and colleagues showed that during embryonic development progression, mouse genes tend to express transcripts with longer 3′UTRs (Ji et al., 2009). On the other hand, during proliferation in the context of T lymphocytes activation, Sandberg et al. reported a reduction in 3′UTR length (Sandberg et al., 2008). Cellular transformation and carcinogenesis are also characterized by a change in the polyadenylation profile, but in this case both lengthening and shortening are involved (Mayr and Bartel, 2009, Singh et al., 2009, Lin et al., 2012, Xia et al., 2014, Fu et al., 2011).

Depending on where polyadenylation occurs, different classes of events can be defined (Fig. 1.9, panel b). Polyadenylation can occur in internal introns/exons, generating different protein isoforms (coding region (CR)-APA), or in the 3′UTR, generating isoforms differing in the 3′UTR region (UTR-APA). I will specifically talk about alternative last exon events belonging to the CR-APA class, and tandem UTRs belonging to the UTR-APA class, as these are the cases presented in chapter 4.4.1.

1.2.1 CR-APA

The alternative use of intronic pA sites gives rise to protein isoforms. This mechanism is splicing-dependent and it is known as alternative last exon usage (ALE). Through ALE, two isoforms are produced, differing in the 3′ terminal exon, meaning in the last bit of the coding sequence and in the

3′UTR. The choice of which terminal exon to include is mediated by splicing factors and the polyadenylation machinery. The pre-mRNA is bound by both the spliceosomal and the polyadenylation components, on a set of conserved *cis*-elements. In addition to the core signals, other features located within $\sim$ 300 nucleotides from the splice sites of the pre-mRNA are important for alternative splicing regulation, making up the "splicing code" (Wang and Burge, 2008). These features are bound by specific RBPs that regulate alternative splicing, usually in a cell-type-specific or developmental-stage-specific manner (Zhang, Lee, and Tian, 2005, Calarco, Zhen, and Blencowe, 2011, Kalsotra and Cooper, 2011). For example, during neuron activation, a shift towards proximal ALEs is observed (Flavell et al., 2008). NOVA, RBFOX, PTBP, nELAVL, nSR100 and MBNL2 are among the RBPs that are specifically expressed or enriched in neurons, which contribute to exon choice (Fig. 1.10, panel a) (Raj and Blencowe, 2015). They can work together or compete for exon exclusion or inclusion (Fig. 1.10, panel b). For instance, NOVA was shown to bind to clusters of YCAY. Depending on where the clusters are located, if downstream or within/upstream of the target exon, inclusion and exclusion are promoted, respectively (Ule et al., 2006).
Alternative splicing has been linked to localization in neurites, in the particular case of ALE events. Taliaferro and colleagues identified distal ALE isoforms preferentially localized in the neurites of a neuroblastoma cell line and implicated muscleblind-like (Mbnl) family of splicing factors in their localization (Taliaferro et al., 2016).

Interestingly, dysregulation of alternative splicing/polyadenylation can lead to disease, for example in the case of *Cyclin D1*. The protein encoded by this gene regulates the progression through G1-S phase, and the loss of controlled cell-cycle progression is a critical event in tumorigenesis. *Cyclin D1* encodes for two major isoforms, full-length *D1a* and *D1b*. *D1b* is cleaved at a pA site within intron 4, and skips the exon 5, which is included in *D1a* isoform. Several cancer types show high expression of *D1b* isoform, moreover the protein encoded by this isoform is constitutively nuclear, leading to increased transforming capability (Lu, Gladden, and Diehl, 2003, Solomon et al., 2003). The mutation associated to an increase in expression of *D1b* has been linked to a G870A polymorphism in exon 4, which might impair the recognition of the splicing machinery ultimately leading to the usage of intron 4 pA site (Solomon et al., 2003, Comstock et al., 2009, Betticher et al., 1995).

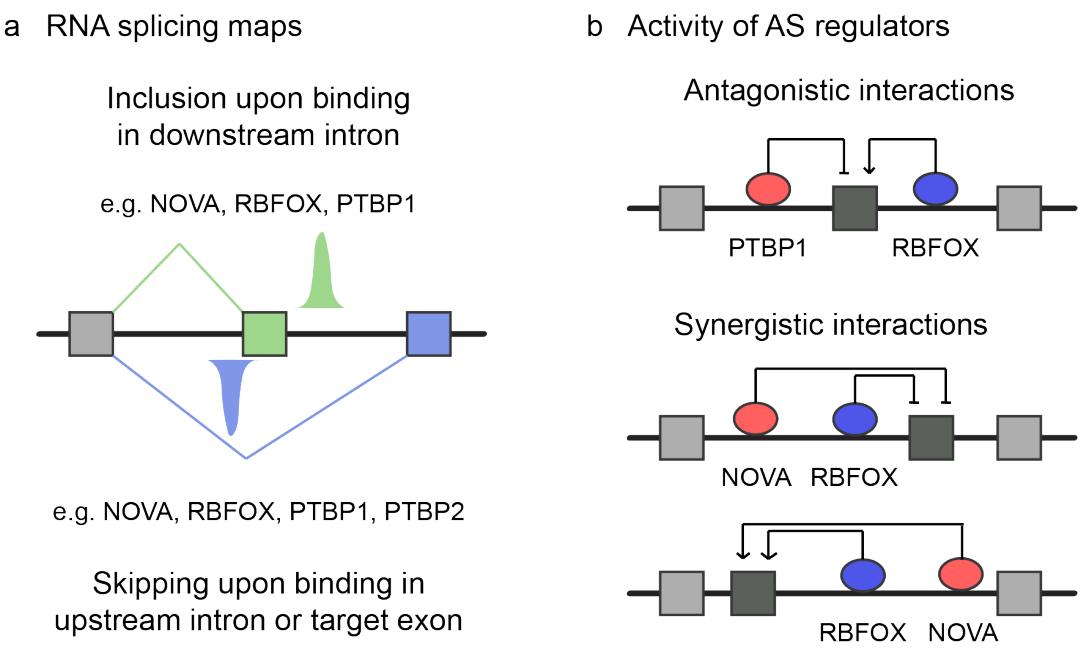

FIGURE 1.10: **Alternative splicing regulators.** a | Alternative splicing factors regulate exon skipping or inclusion by binding in the downstream or upstream intron. b | Splicing factors can collaborate for the same purpose in synergistic interaction, or antagonize each other.

1.2.2 UTR-APA

UTR-APA gives rise to mRNA isoforms with significantly different 3′UTR lengths (tandem UTRs): the median lengths of mouse 3′UTRs differ about seven-fold, with 249 nt for the short and 1773 nt for the long isoform, respectively (Hoque et al., 2013). Since the difference between the isoforms is not in sequence but in length, the longer 3′UTR fully contains the shorter. The common intuition that arises from this similarity is that any RBP that binds the shorter isoform, can also bind the longer one. However, this intuition is only based on the sequence in terms of nucleotides, without considering secondary and tertiary structures that can be completely distinct between the short and the long isoforms, with the consequence of exposing different binding sites for different RBPs. *Bdnf* and *CaMK4* are examples of tandem 3′UTRs where their isoforms localize to different subcellular compartments. In the case of *Bdnf*, the isoform carrying the long 3′UTR was shown to localize to dendrites, where it affects pruning and dendritic spine enlargement (An et al., 2008). *CaMK4* expresses two tandem UTR isoforms that differ for 10 kb in their 3′UTRs. The short isoform is associated with nuclear functions, whilst the long one was shown to localize to axons of dorsal root ganglion (Harrison et al., 2014). Additional examples are given by *BDNF* (An et al., 2008), *Ranbp1* (Yudin et al., 2008), *Impa1* (Andreassi et al., 2010), *MKK7* (Feltrin et al.,

2012) and *KPNB1* (Perry et al., 2012), where the long isoform localizes to the neurites.

In the context of miRNA regulation, UTR-APA is particularly interesting as it has been shown that if the target site is located near the end of the 3′UTR, miRNA targeting is more efficient (Bartel, 2009). A shortening in 3′UTR length by APA could results in more efficient degradation of a certain subset of mRNAs that are targeted by a specific miRNA. This type of regulation has been shown to be important during cell proliferation (Hoffman et al., 2016): the shortening of the 3′UTRs of anti-proliferation mRNAs improves their targeting by miRNAs resulting in promotion of cell proliferation.

Also for UTR-APA, failure in correct polyadenylation can lead to various diseases, for example to IPEX (immune dysfunction, polyendocrinopathy, X-linked), a disease characterized by dysfunction of regulatory T cells which leads to autoimmunity. This pathology is caused by a SNP mutation in the PAS (AAUAAA to AAUGAA) of *Foxp3*, which encodes for a transcription factor. This mutation affects the strength of the canonical pA site, leading to the use of the next downstream signal. The inclusion of additional 5.1 kb sequence in the 3′UTR affects mRNA stability, determining a decrease in FOXP3 protein, which ultimately leads to disease onset (Rosenwasser, 2001).

1.3 *Trans*-functions of 3′UTRs

1.3.1 3′UTRs can mediated protein-protein interactions

3′UTRs can also facilitate PPIs during the translation process, by bringing in close proximity the nascent polypeptide which the mRNA encodes for, with potential protein interaction partners loaded on the 3′UTR itself. This vicinity allowed by the 3′UTR might increase the proteins' association rates compared to free diffusion, therefore contributing to PPIs. It has been recently shown for *Cd47* isoforms, that the 3′UTR of the long isoform determines protein localization independently of mRNA localization (Berkovits and Mayr, 2015). APA of *Cd47* produces tandem 3′UTR isoform, identical in coding and 3′UTR sequence, but different in 3′UTR length. The long isoform possesses binding sites for HuR, which in turn recruits SET protein. SET, while *Cd47* is being translated, can bind to CD47 cytoplasmic domains. SET interaction with RAC1 determines the surface localization of CD47, whilst the short isoform, which doesn't allow HuR binding, produces the intracellular version of the protein. The same findings were shown for additional plasma membrane proteins, such as CD44, Integrin α1, and BAFF receptor

(Berkovits and Mayr, 2015). Additionally, the Mayr lab also found that the 3′UTR-dependent interaction of SET with membrane proteins was promoted by a newly-defined subcellular domain called TIGER (Ma and Mayr, 2018). This domain is formed by the association of RNA granules to ER, where the RNA granules are composed of TIS11B, an RBP binding to AU-rich elements of membrane protein-encoding mRNAs. The TIGER domain has distinct biophysical and biochemical features compared to the cytoplasm, and allows the establishment of PPIs that would not form otherwise.
Birc3 is another example where the isoform carrying the long 3′UTR only is involved in 3′UTR-dependent PPIs (Lee and Mayr, 2019). This isoform is upregulated in malignant B cells, and involved in chronic lymphocytic leukemia. Lee and colleagues showed that BIRC3 encoded from the long 3′UTR recruits IQGAP1 and RALA to CXCR4. This allows the regulation of surface levels of the CXCR4 receptor, which mediates B cell migration, ultimately increasing chronic lymphocytic leukemia cell survival (Lee and Mayr, 2019).
Another example of 3′UTR-mediated PPIs has been shown in yeast, for membrane proteins. When translation occurs for membrane proteins-encoding transcripts, the signal recognition particle (SRP) is responsible for translocating the translating ribosomes to the endoplasmatic reticulum (ER), to release the newly synthesized protein into the ER lumen. Previously, it was believed that SRP recruitment to the ribosome was mediated by the recognition of the exposed N-terminal hydrophobic signal sequence consequent to mRNA translation. The SRP-bound ribosome would then halt translation and migrate to the surface of the ER before restarting translation. This model is still valid for a minority of membrane proteins, whilst for the majority a different mechanism has been characterized, where the 3′UTR is the critical factor responsible for SRP recruitment. It has been shown that the 3′UTRs of genes encoding for membrane proteins determine the association of the SRP to the ribosome before the translation of the signal sequence has occurred, that is, before the exposition of the polypeptide chain encoding the signal sequence (Chartron, Hunt, and Frydman, 2016).

1.3.2 Post-transcriptional cleavage and 3′UTRs as independent functional units

Additionally to their established role in *cis* regulation, 3′UTRs can also exist as distinct functional RNAs, suggesting that they might possess additional biological functions as non-coding RNAs. They arise not as new products of transcription, but rather by post-transcriptional processing (Mercer et al., 2011), therefore lacking a 5′ cap which should render them very unstable

and lead to rapid degradation. However, CAGE-library analysis revealed the existence of several 3′UTRs containing 5′ caps (Mercer et al., 2011). *De novo* cytoplasmic capping has indeed been observed in mouse and human cell lines (Mukherjee, Bakthavachalu, and Schoenberg, 2014, Otsuka, Kedersha, and Schoenberg, 2009). Moreover, 3′UTR fragments are protected at the 3′ end by the poly(A) tail, and might be protected at the 5′ too, by strong structural elements like pseudoknot (Chapman et al., 2014), or by the binding of an RBP, or when XRN1 levels (5′-3′ exonuclease) are low (Schoenberg, 2011). Some examples of functional 3′UTRs exist for *troponin I*, *tropomyosin*, *α-cardiac actin*, *ribonucleotide reductase*, *DM protein kinase* and *prohibitin*, which have been shown to be involved in regulation of cell proliferation and differentiation, independently of their protein counterparts (Fan et al., 1996, Rastinejad et al., 1993, Rastinejad and Blau, 1993, Jupe et al., 1996, Amack, Paguio, and Mahadevan, 1999). Another example is provided by *oskar* in *Drosophila*: its 3′UTR is sufficient to rescue an oogenesis defect which occurs in *oskar*-null mutants, suggesting that the 3′UTR might function as a scaffold to recruit Staufen protein from the nurse cells to the oocyte (accumulation required for proper oogenesis) (Jenny, 2006). Another study reported unbalanced expression of CDSs and their cognate 3′UTRs in neurons and other tissues, where the ratio between 3′UTR and CDS for certain genes appeared to be non-random, characterizing distinct spatial patterns and gradients, and certain cell types and developmental stages, and suggested that 3′UTRs might have a negative regulatory function on protein expression (Kocabas et al., 2015).

Interestingly, a couple of recent studies have reported post-transcriptional cleavage of 3′UTRs in naive mouse T cells, B cells and brain (Malka et al., 2017), and in axons of sympathetic neurons (Andreassi et al., 2019). Malka and colleagues showed that mRNAs can be cleaved post-transcriptionally at APA sites, generating two fragments, one containing the CDS and a shortened 3′UTR, and one consisting of an uncapped 3′UTR tail (Malka et al., 2017). The finding showing post-transcriptional cleavage at proximal APA sites is also supported by another *in vitro* study, where by using reporters containing a wt or a mutated version of a proximal APA site, cleavage occurred only in the case of the wt reporter upon incubation with cell lysate (Jenal et al., 2012). So far, these were descriptive studies, reporting the phenomenon of post-transcriptional cleavage but leaving the mechanism elusive. Andreassi and colleagues after observing the same event in axons of sympathetic neurons, aimed at addressing the mechanistic question of how the cleavage is accomplished (Andreassi et al., 2019). Previous observations already pointed to AGO2 (the only member of the argonaute proteins with endonucleolitic activity) as a possible driver of such 3′UTR endonucleolytic

products (Karginov et al., 2010). Andreassi et al. took a step forward postulating that a complex formed by HuD, PABPC4 and AGO2, mediates the cleavage of transcripts in the vicinity of the proximal APA site, where a stem-loop structure is formed (Andreassi et al., 2019).
Specifically for aged brain, a different type of cleaving mechanism has been proposed by Sudmant and colleagues, where they suggest that ribosomes entering the 3′UTR and the No-Go decay pathway play a role in the biogenesis of 3′UTR fragments (Sudmant et al., 2018). Oxidative stress - typical of aged brain - is the factor involved in the generation of 3′UTR fragments: reactive oxygen species (ROS) impair the activity of the ribosome recycling factor ABCE1 (its activity depends on 2 iron-sulfur clusters). This leads to the accumulation of ribosomes in the 3′UTR and eventually to the cleavage of the mRNA upstream the stop codon, according to the No-Go decay pathway. This mechanism produces stable fragments protected from exonucleases at the 5′ end by the stalled ribosome, and at the 3′ end by the poly(A) tail.
Several questions still remain to be answered: how are shortened transcripts re-adenylated after cleavage? What is the regulatory function of such an event? Do the 3′UTR tails have an additional function?

1.4 Experimental techniques to study RNA localization and local translation

A selection of methods useful to investigate mRNA distribution and dynamics are discussed in the following chapter (table 1.4).

1.4.1 Imaging-based methods

Among the imaging-based methods, we find *in situ* (FISH and puro-PLA) and *in vivo* (TRICK and SINAPS) techniques for imaging of fixed or live cells, respectively.

Fluorescence *in situ* hybridization and its evolution

Fluorescence *in situ* hybridization (FISH) is a technique which allows the visualization of mRNA molecules at the subcellular level in fixed samples, via probing with fluorescent oligos and by using widefield fluorescence microscopy. With the occurence of single molecule FISH (smFISH) (Femino et al., 1998, Raj et al., 2008), this technique became quantitative: the visualization of individual transcripts as diffraction-limited spots is enabled by the use

	Sample	Target	Spatial resolution	Throughput	Readout
smFISH	Fixed cells and tissue	RNA	Subcellular	Low to medium	Microscopy
seqFISH	Fixed cells and tissue	RNA	Subcellular	Medium to High	Microscopy
SPOTs	Purified RNA	RNA	Bulk	High	Microscopy
Puro-PLA	Fixed cells and tissue	Protein	Subcellular	Low	Microscopy
TRICK	Live cells	RNA and protein	Subcellular	Low	Microscopy
SINAPS	Live cells	RNA and protein	Subcellular	Low	Microscopy
Ribo-seq	Purified RNA	RNA	Bulk	High	RNA-seq
Proximity-specific Ribo-seq	Purified RNA	RNA	Subcellular	High	RNA-seq
Axon-TRAP	Purified RNA	RNA	Subcellular	High	RNA-seq
pSILAC	Lysate	Proteins	Bulk	Medium to High	Mass-spectrometry
QuaNCAT	Lysate	Proteins	Bulk	Medium to High	Mass-spectrometry

TABLE 1.4: Current methods for spatially resolved transcriptomics and other omics measurements

of a minimum of 20 DNA probes complementary to the target RNA, labelled with fluorescent dyes. Recently, because of some photophysical shortcoming of organic dyes, quantum dots have been optimized in order to allow their use in FISH: they provide exceptional photostability and more robust transcript quantification thanks to enhanced brightness, particularly significant for 3D biological specimen where acquisition of a full z-stack might take up to tens of seconds (Liu et al., 2018). Moreover, they allow a broader level of multiplexing, as they are characterized by a greater multispectral tenability compared to organic dyes.

Moreover, multiplexing is possible by a method called seqFISH, based on sequential barcoding (Lubeck et al., 2014). In this approach, in each round of hybridization, the previous probes are removed by DNAse digestion, freeing the previously assigned color channels. With this method, with as little as four dyes and 8 rounds of hybridization the whole cell transcriptome can be visualized (4^8 = 65,536, seven rounds are not sufficient: 4^7 = 16,384).

An interesting development of seqFISH is RNA sequential probing of targets

(SPOTs) (Eng et al., 2017). This technique is an *in vitro* method used to assess the transcriptome, overcoming some flaws of seqFISH in terms of optical crowding, but losing the *in situ* spatial information as it is based on capturing the transcripts onto an oligo(dT) surface. Using a 12 pseudo-colors scheme, it is possible to cover the whole transcriptome with four rounds of barcoding (12^4 = 20,736 genes). Compared to the standard cDNA-based RNA-seq, this method gives a direct measurement of mRNA abundance.
However, recent advances in next generation sequencing (NGS) Nanopore technology also allow the direct sequencing of RNA (Garalde et al., 2018, Keller et al., 2018), avoiding cDNA and PCR amplification, reducing the biases in RNA quantitation.

Puro-PLA

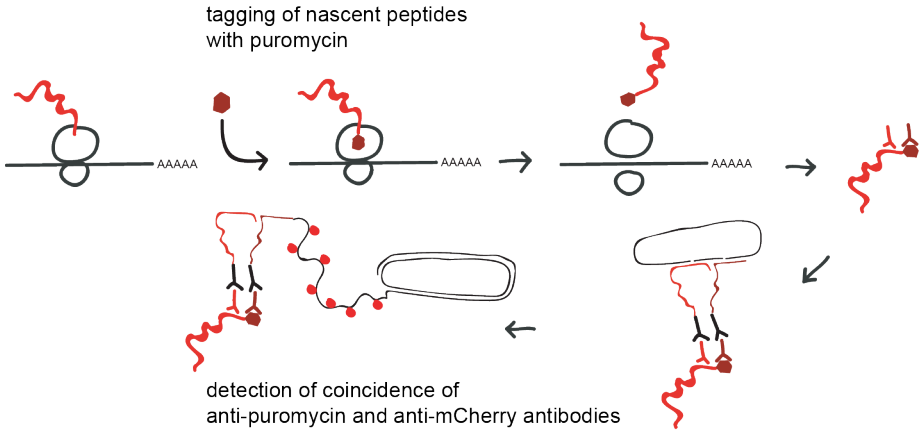

FIGURE 1.11: **Scheme of puro-PLA technique.** PURO-PLA detects *de novo* synthesized proteins. Puromycin is used to tag newly synthesized proteins. One antibody against puromycin and one against the protein of interest are used at the same time. Signal for local synthesis is detected after rolling-circle amplification, only if the two antobodies occur in close proximity.

Puromycin-proximity ligation assay (puro-PLA) is a microscopy technique which allows visualization of local translation through the combination of puromycin treatment, proximity-ligation and rolling-circle amplification (Tom Dieck et al., 2015). Puromycin tags nascent peptides as it is incorporated into the nascent polypeptide chains due to its structural analogy with the aminoacylated 3′end of transfer RNAs (tRNAs), causing the formation of a puromycylated nascent chain and premature chain release. Two antibodies are used at the same time, one against puromycin and one against the protein of interest. The secondary antibodies are coupled to different oligonucleotide probes, and only when they occur in close proximity, a linker can hybridize

to both for rolling circle amplification, which ultimately allows signal detection (Fig. 1.11).

Recently, doubts have arisen regarding the application of this technique for the study of protein-protein interactions (Aslemarz, Lasko, and Fagotto, 2018). The maximal distance that is allowed for the proximity-ligation reaction to occur is 40 nm, below the limit of optical resolution and therefore meaningless to study co-localization. By testing characterized antigens which should result in positive or negative interactions, the authors show that false positives occur, causing erroneous interpretation of the results, and the use of controls only help to establish the specificity of the antibodies.

Real-time imaging of translation

Two different techniques can achieve real-time imaging of translation of single mRNA molecules. They are both based on dual labelling of the mRNA and the nascent polypeptide chain, but the output of the double signal has opposite meanings: in one case it stands for the OFF, and in the other for the ON state of translation. Additionally, a recent developed technique from the Tanenbaum's lab allows to study translation heterogeneity by dual labelling of the nascent polypeptide chain, where one color is used to measure canonical translation and the other color for an alternative pathway (frame-shifting events, uORF, read-through events) (Boersma et al., 2019). Details below.

Dual labelling for OFF state TRICK stands for translating RNA imaging by coat protein knock-off. It is a technique based on displacement of RNA binding protein by translating ribosomes (Halstead et al., 2015). This method requires tagging of the mRNA of interest with PP7 and MS2 stem-loops, in the coding region and in the 3′UTR respectively. These two regions are targeted for binding and dual labelling with site-specific RNA binding proteins fused to fluorescent proteins: PP7 coat protein (PCP) fused to GFP and MS2 coat protein (MCP) fused to RFP. Detection of green and red fluorescent signals is achieved when PP7-GFP and MCP-RFP can both bind an mRNA molecule meaning that translation is off, whilst upon translation activation PCP-GFP is displaced, resulting in red-only fluorescence signal for translated mRNAs.

Dual labelling for ON state Four different methods were developed concomitantly, which rely on the same principle of dual labelling of mRNA and nascent polypeptide, and differ on the labels that are used to tag the CDS

or the 3′UTR (Fig. 1.12) (Wu et al., 2016, Morisaki et al., 2016, Wang et al., 2016, Yan et al., 2016). The mRNA of interest is tagged both in the coding sequence and in the 3′UTR. Flag tag or a SunTag epitope are employed to tag the coding region, for translation visualization with anti-Flag or single-chain variable fragment (scFV) conjugated to a fluorescent tag. The SunTag epitope consists of a tandem array (24 copies) of short V4 peptides (Tanenbaum et al., 2014), that can be bound by (up to 24 copies of) scFV, which in turn is fused to super folder green fluorescence protein (sfGFP) to allow imaging. MS2 or PP7 stem-loops are used to tag the 3′UTR region, for mRNA visualization with MCP or PCP fused to a fluorescent tag.

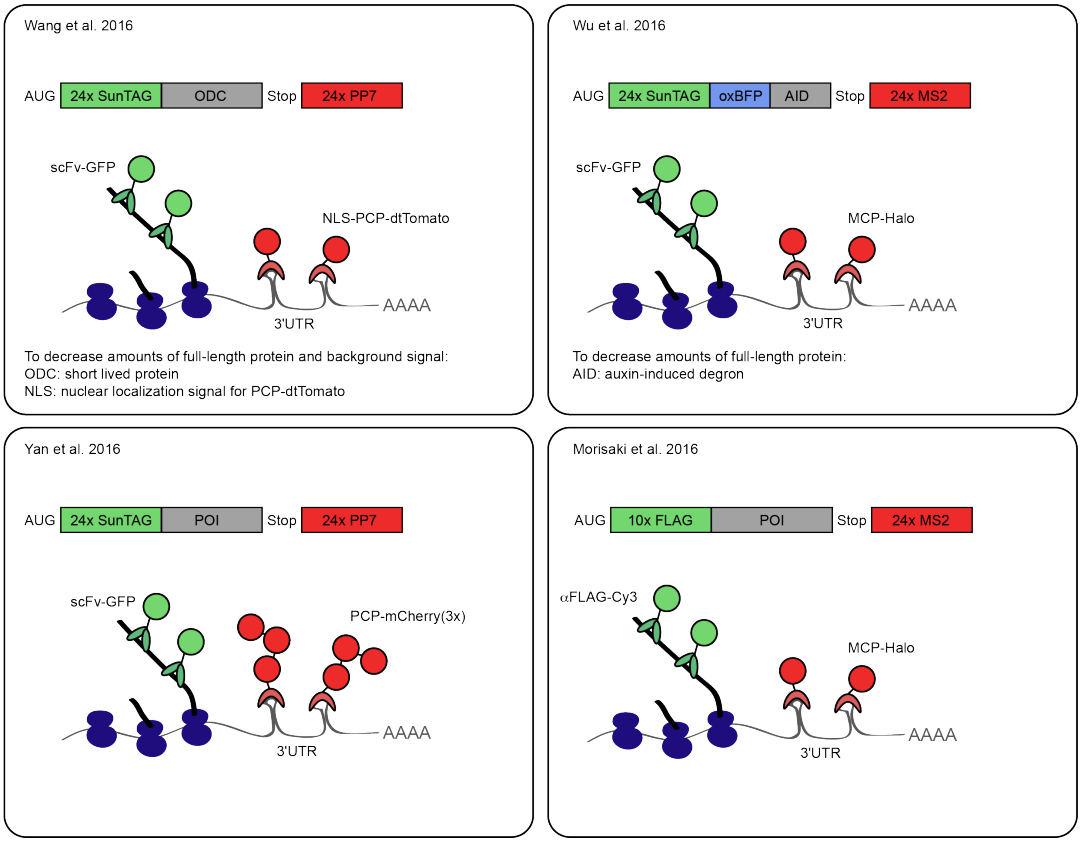

FIGURE 1.12: ***In vivo* dual labelling for ON translational state.** The ON state of translation is visualized *in vivo* through the dual labelling of a reporter. For fluorescent detection, the nascent polypeptide is bound by the SunTag or by αFLAG-Cy3. Moreover the 3′UTR region of the reporter contains PP7 or MS2 repeats, which allow PCP or MCP binding and visualization through the fused fluorescent tag.

In two of these papers, extra care is taken for background removal. The full-length protein, which would accumulate with translation and give rise to background signal, is removed with different approaches: Wu and colleagues chose auxin-induced degron (AID) (Wu et al., 2016) and Wang and colleagues ornithine decarboxylase (ODC) (short lived protein) as C-terminal

fusions of the reporter (Wang et al., 2016), in order to facilitate degradation once translation is completed. Wang et al. also implemented the use of nuclear localization signal (NLS) for tdTomato-PCP in order to restrict the unbound reporter to the nucleus and therefore reduce the background (Wang et al., 2016).

Dual labelling for translation heterogeneity Boersma and colleagues employ a system where two fluorescent labelling tags, MoonTag and SunTag, are combined in different designs in order to visualize translation heterogeneity (Fig. 1.13) (Boersma et al., 2019). For instance, to capture readthrough events the reporter is built so that the first ORF encodes for the MoonTag, and the SunTag follows after the stop codon. In this way readthrough events are captured. Otherwise, in a different design aimed at visualizing translational start sites, they mash the MoonTag and the SunTag in what they call the MashTag reporter, where the coding sequences of the two tags are out of frame between each other. Depending on the frame used for translation, therefore on the start site, either one or another reporter will be translated (2 out of 3 frames can be visualized).

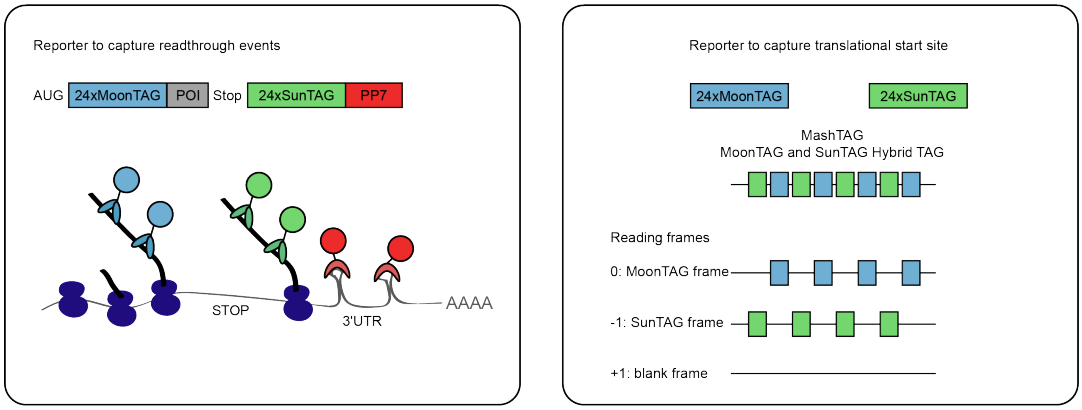

FIGURE 1.13: ***In vivo* dual labelling for translational heterogeneity.** Different designs allow to visualize translational heterogeneity. Readthrough events are visualized by combining the two tags, and separating them by a stop codon. Translational start sites are visualized by combining the two tags in different frames.

With this sophisticated system, Boersma and colleagues showed that, strikingly, start site selections appears more heterogeneous than expected (Boersma et al., 2019). However the biological reason explaining the heterogeneity in start site selection still remains open.

1.4.2 NGS-based and high-throughput methods

High-throughput methods are required for detection of the whole translatome. The study of translation can be approached on the side of mRNA or proteins. Translated mRNAs can be analyzed with ribosome profiling or via ribosome-pulldown coupled to RNA-seq, while newly synthesized proteins can be labelled and analyzed with pSILAC and QuaNCAT (description below).

Ribosome profiling and its proximity-specific flavour

Ribosome profiling is a technique which allows to quantitatively characterize the translational landscape by sequencing of ribosome protected footprints (RPFs). An RNase is used to digest the unprotected RNA, the so-generated RPFs are size-selected through a gel, and then converted in a library for deep sequencing. RPFs are typically 27 - 29 nt long and reflect the movement of the ribosome along the transcript, providing a measurement for active translation.

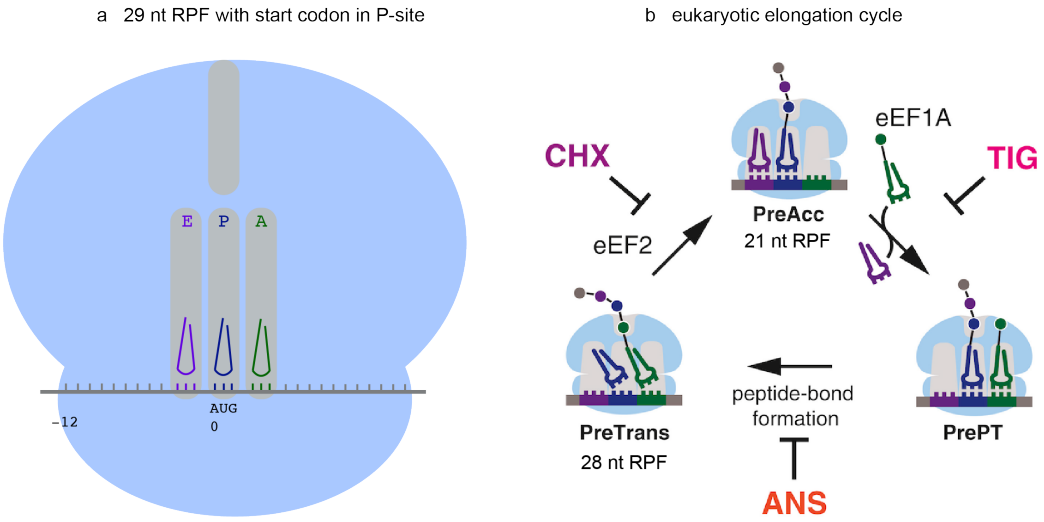

FIGURE 1.14: **Ribosome footprints, and their length according to the ribosome functional state.** a | 29 nt RPF with start codon in P-site. b | With the use of several translation inhibitors (cycloheximide CHX, anisomycin ANS, tigecycline TIG), different ribosomal conformations were mapped to different RFPs' length: 21 nt RPFs derive from ribosomes in a pre-accomodation state (PreAcc) with the A site open, or from ribosomes in a pre-petide bond formation (PrePT) (because tRNA is lost from PrePT in the lysate), whilst 28 nt RPFs derive from ribosomes in a pre-translocation state (PreTrans). From Wu et al., 2019.

Recent studies have shown that aside the canonical 27 - 29 nt RPFs (Fig. 1.14, panel a), other conditions or conformations of the ribosome give rise to other

informative footprints (16, 21, 40 - 65 nt) (Guydosh and Green, 2014, Lareau et al., 2014). RPFs 16 nt in length are observed when ribosomes stall at the 3′ termini of partially degraded RNAs; longer 40 - 65 nt RPFs are observed in correspondence of stalled polyribosomes; 21 nt RPFs have been assigned to translocating ribosomes. Specifically, thanks to a combinatorial use of different elongation inhibitors (cycloheximide, anisomicyn, and tigecycline), it was shown that short 20 - 22 or classical 27 - 29 RPFs correspond to ribosomes with open or occupied ribosomal A sites, respectively (Wu et al., 2019) (Fig. 1.14, panel b).

During each cycle of peptide elongation, the ribosome takes a 3-nucleotide step along its mRNA (codon-by-codon movement). This physical process creates triplet periodicity (or sub-codon phasing) in ribosome profiling data (Calviello et al., 2016), which becomes visible when the reads are mapped to their P-site offsets (where the P-site offset is the distance from the 5′ or 3′ end of a RPF to the P-site of the ribosome that generated the footprint). This is one of the most peculiar and remarkable features of ribosome profiling data. Additionally, this technique allows the identification of upstream open reading frame (uORF) outside the main canonical coding sequence (CDS) (Calviello et al., 2016, Ingolia, Lareau, and Weissman, 2011), together with read-through events and rare instances such as ribosomal frameshifting (Ketteler, 2012). Ribosome profiling has also been adapted in order to gain spatial resolution (Jan, Williams, and Weissman, 2014). In this case, ribosomes are tagged with an AVI-moiety which makes them substrate for biotinylation. Then, in order to gain spatial resolution, the biotin ligase (BirA) enzyme is fused to a protein which provides localization. After the biotin pulse, only the biotinylated ribosomes are pulled down to proceed with the protocol. The combination of this purification strategy with ribosome profiling allows to obtain the translatome of messengers that are being translated at subcellular sites of interest. So far, this technique has only been used to study ER- and mitochondria-associated translatome, by fusing BirA to SEC61β, a member of the translocon, and to OM45, a major constituent of the mitochondrial outer membrane (Jan, Williams, and Weissman, 2014).

Axon-TRAP

In order to achieve selective HA-tagging of ribosomes in retinal ganglion cells (RGCs), Shigeoka and colleagues crossed the RiboTag knockin mouse line (Sanz et al., 2009) with a Pax6-alpha-Cre mouse (Marquardt et al., 2001), which allows to transiently express Cre in neuronal progenitors in the peripheral retinal premordium (Shigeoka et al., 2018). This system determines

the Cre-mediated recombination switch of the RiboTag allele, which encoded a HA-tagged *Rpl22* component of the 60S ribosomal subinit, in RGCs only. Dissection then allows the separation of the whole eyes from the superior colliculus, containing the retinal axons only (Fig. 1.15).

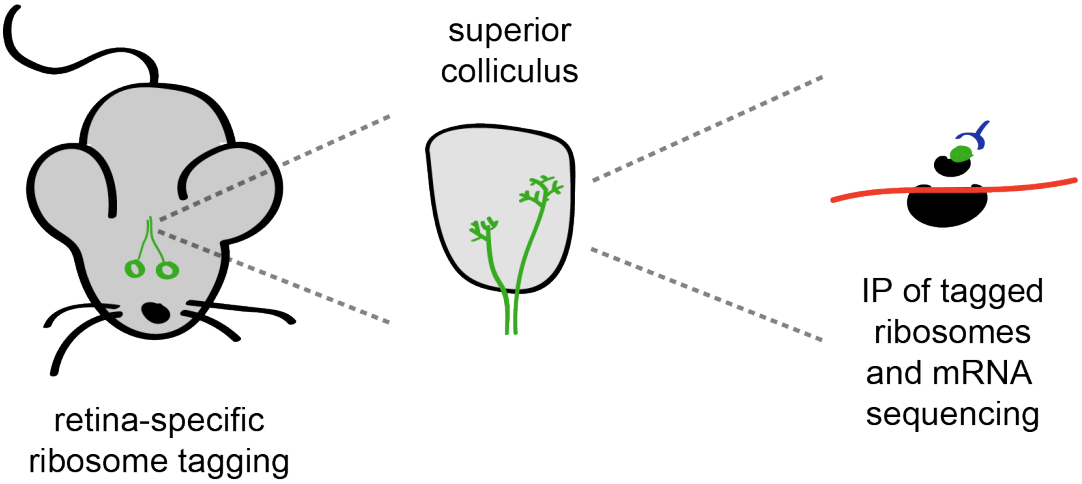

FIGURE 1.15: **Scheme of axon-TRAP.** Two mouse lines are crossed in order to HA-tag ribosomes in RGCs. After dissection, HA-pulldown and RNA-seq, the axonal ribosome-bound mRNAs are identified.

Proteomics-based methods

stable isotope labeling with amino acids in cell culture (SILAC) is a mass spectrometry-based approach that detects differences in protein abundance between samples using non-radioactive isotopic labeling (Ong et al., 2002) (Ong et al., 2002). Cells are metabolically labelled with heavy (H) or light (L) stable isotope versions of essential amino acids, resulting in proteins owning a different mass depending on the media. These two populations can be combined and analyzed together by mass-spectrometry. Due to the difference in mass, pairs of chemically identical peptides can be distinguished. The ratio of H/L peptides indicate the protein turnover rate, which is influenced by both synthesis and degradation. Therefore SILAC can't be used to measure translation rates. On the other hand, pSILAC (pulsed SILAC) allows to acquire the translational rate parameter (Schwanhäusser et al., 2009) (Fig. 1.16), by removing the degradation parameter. This is accomplished by using a "pulse" of labelling: cells are in light medium, and are pulsed in either medium (M) or heavy (H) media for a short time. In this period, newly synthesized proteins will be labelled with M of H amino acids, while pre-existing proteins will remain in the light form.

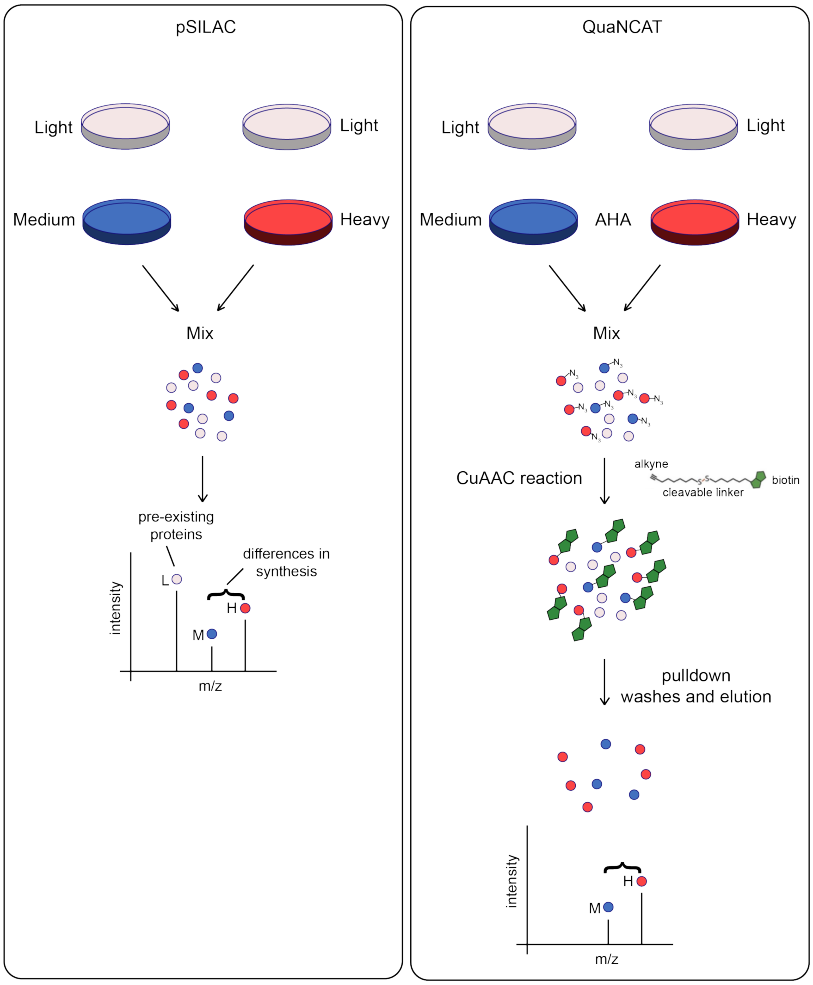

FIGURE 1.16: **Scheme of pSILAC and QuaNCAT.** In pSILAC, cells cultivated in light medium, are transferred to M or H media for a short period of time. After the pulse, cells are mixed to proceed for mass-spectrometry analysis. The H/M ratio represents differences in translation rates. In QuaNCAT, cells cultivated in light medium, are transferred to M or H media supplemented with AHA for a short pulse. After the pulse, cells are mixed together and by click-chemistry, a biotin tag is added to the newly synthesized proteins. After streptavidin-biotin pulldown, newly synthesized proteins are eluted and subjected to mass-spectrometry analysis.

Thanks to this implementation, this method is independent of differences in protein stability. In fact, pre-existing proteins are not taken into account, and therefore their degradation will not affect the analysis. Degradation will also affect newly synthesized proteins to a certain extent, but this degradation should occur at the same level for both the M and the H forms, without affecting the H/M ratio. The limitation of pSILAC is that a pulse of few hours will only label a small fraction of a proteins. BONCAT (bioorthogonal non-canonical amino-acid tagging) overcomes this limitation by using a click-chemistry trick, which uses L-azidohomoalanine (L-AHA) labelling (Dieterich et al., 2007). L-AHA is a methionine analog, containing an azido moiety that can be used for click-chemistry. In the presence of a Cu(I)-catalyzed azide-alkyne cycloaddition (CuAAC) catalyst, the azide group reacts with an alkyne carrying a biotin tag. This allows specific pulldown of newly synthesized proteins carrying the biotin tag. However, biotin-labelling might be not homogeneous for all proteins, due to the CuAAC reaction, which is site- and protein-dependent (van Kasteren et al., 2007, Kasteren et al., 2007). Moreover, the use of label-free mass-spectrometry based quantitation is not accurate. By combining pSILAC and BONCAT, QuaNCAT outperforms the two techniques by exploiting the strengths and being devoid of the drawbacks (Howden et al., 2013) (Fig. 1.16).

2 Aims

2.1 Aims

As illustrated in the introduction, neurons are a very interesting class of highly polarized cells, particularly attractive for the study of cell asymmetry in terms of spatial organization and distribution of mRNAs and proteins. Many fundamental processes where gene expression is spatially and temporally controlled, such as neuronal polarity, axonal growth, axonal arbor architecture, dendrite morphology, plasticity and memory formation, are in fact ruled by mRNA and protein localization.

Consequently, understanding how local functions are regulated and at which extent is crucial to understand how neurons work.

Cellular asymmetric distribution is regulated by a combination of processes, spanning from mRNA localization, local translation, and local degradation. If the topic of mRNA localization in neurons has been covered extensively (Cajigas et al., 2012, Gumy et al., 2011, Taylor et al., 2009, Minis et al., 2014, Taliaferro et al., 2016, Rotem et al., 2017, Briese et al., 2015, Tushev et al., 2018), several are the questions that remain to be answered. For instance:

(i) how much local translation contributes to the local proteome identity?

(ii) what are the factors regulating mRNA localization and local translation? And in particular:

(iii) which *trans*-acting factors and *cis*-elements are important for local RNA metabolism?

The present work was conceived with these questions in mind. Specifically, I used a Ascl1-induced neuronal cell line (Ascl1-iNs) from which I could isolate, collect, and individually analyze two cellular compartments: soma and neurites.

To identify the local translatome, at first I established a modified protocol for ribosome profiling, to tailor it to small input samples. Then, I applied this protocol to the subcellular compartments of Ascl-iNs.

Moreover, I aimed at identifying the key players participating in mRNA localization and local translation. The regulation of such processes, is achieved by the synergistic activity of *trans*- and *cis*-acting elements, where the latter are elements present in the 3′UTR of mRNAs, which serve as docking points for *trans*-acting elements, namely RNA binding proteins (RBPs), important regulators of mRNA metabolism.

I explored both aspects: I investigated the function of the *trans*-acting element MOV10, an RBP enriched in the neuritic compartment of Ascl-iNs, and in parallel I investigated whether isoforms differing in the 3′UTR would localize to different subcellular compartments.

3 Materials and Methods

3.1 Materials

3.1.1 Cell culture reagents and media

Cell culture reagents and media (tables 3.1, 3.2).

3.1.2 List of oligos

Primer pairs used in RT-qPCR (table 3.3).

3.1.3 List of plasmids

All the plasmids used or generated in this study and their sequences are available at Sigma or Addgene (table 3.4).

3.1.4 List of antibodies

List of antibodies used in western blot, IF, or puro-PLA (table 3.5).

3.1.5 List of reagents.

List of reagents and enzymes used in this thesis (table 3.6).

3.1.6 List of consumables

List of consumables (table 3.7).

3.1.7 List of equipment

List of devices used in this thesis (table 3.8).

TABLE 3.1: Cell culture reagents

Name	Manufacturer	Catalog N
Advanced DMEM/F12	Life Technologies GmbH	12634028
B27 serum-free supplement 50x, liquid	Life Technologies (Carlsbad, CA, USA)	17502048
DPBS without Ca and Mg	PAN Biotech (Aidenbach, Germany)	P04-36500
Dulbecco's Modified Eagle Medium (D-MEM)	Life Technologies (Carlsbad, CA, USA)	61965059
Fetal bovine serum	Life Technologies (Carlsbad, CA, USA)	10270-106
Fetal bovine serum embryonic stem cell	Life Technologies (Carlsbad, CA, USA)	10828028
Knockout DMEM	Life Technologies (Carlsbad, CA, USA)	10829018
KnockOut Serum Replacement	Life Technologies (Carlsbad, CA, USA)	10828028
MEM Non-Essential Amino Acids Solution, 100X	Sigma-Aldrich (Steinheim, Germany)	M7145-100ML
N2 supplement 100x, liquid	Life Technologies (Carlsbad, CA, USA)	17504044
Neurobasal(R) Medium (1X), liquid	Life Technologies (Carlsbad, CA, USA)	21103049
Nucleosides	Merck (Darmstadt, Germany)	ES008D
Opti-MEM I reduced serum Medium	Life Technologies (Carlsbad, CA, USA)	31985062
Recombinant mouse LIF	Amsbio (Abingdon, UK)	AMS-263-100
TrypLE Express (1X) Phenol red	Thermo Fisher scientific GmbH (Waltham, MA, USA)	12605028
SILAC Advanced DMEM/F-12 Flex Media	Life Technologies (Carlsbad, CA, USA)	A2494301

TABLE 3.2: Media's recipies

Medium	Composition
2i	50% Advanced DMEM/F12, 50% Neurobasal(R), 1x N2 supplement, 1x B27 supplement, 1 mM L-Glutamine, 0.1 mM 2-mercaptoethanol, 103 U/ml LIF, 3 μM CHIR99021, 1 μM PD03259901
mESC	Knockout DMEM, 14% fetal bovine serum embryonic stem cell, 0.1 mM 2-mercaptoethanol, 1 mM L-Glutamine, 1x MEM non-essential amino acid, 1x nucleosides, 103 U/ml LIF
AK	50% Advanced DMEM/F12, 50% neurobasal, 10% knockout serum replacement, 1 mM L-Glutamine, 0.1 mM 2-mercaptoethanol
Monolayer	Advanced DMEM/F12, 1x B27 supplement, 1x N2 supplement, 3 μg/ml doxycycline

TABLE 3.3: Primer pairs for RT-qPCR

Gene name	Oligo sequence	PrimerbankID
Thyn1	CCCTAAATGGTCGATGGTGGA	
	TTTGTGGGCTTGGTGATAGGT	
Gapdh	TGACCTCAACTACATGGTCTACA	126012538c2
	CTTCCCATTCTCGGCCTTG	
rRNA	AAACGGCTACCACATCCAAG	
	CCTCCAATGGATCCTCGTTA	
Rbfox3	ATCGTAGAGGGACGGAAAATTGA	26347765a1
	GTTCCCAGGCTTCTTATTGGTC	
Slc18a2	ATGCTGCTCACCGTCGTAG	270483858c1
	GGCAGTCTGGATTTCCGTAGT	
Tubb3	TAGACCCCAGCGGCAACTAT	12963615a1
	GTTCCAGGTTCCAAGTCCACC	
Sox2	CACAACTCGGAGATCAGCAA	
	TGTAATCCGGGTGTTCCTTC	
Mapkapk2	TTCCCCCAGTTCCACGTCA	1089896a1
	GCAGCACCTTCCCGTTGAT	
Kif1c	GGAGCCTCCGTGAAAGTTG	23821040a1
	CCGAAGTATGCGACCAGTAAGA	
Tagln	CCAACAAGGGTCCATCCTACG	291045204c1
	ATCTGGGCGGCCTACATCA	
Col3a1	CTGTAACATGGAAACTGGGGAAA	20380522a1
	CCATAGCTGAACTGAAAACCACC	
Syn1	AGCTCAACAAATCCCAGTCTCT	18606446a1
	CGGATGGTCTCAGCTTTCAC	
Gria2	TTCTCCTGTTTTATGGGGACTGA	29387225a1
	CTACCCGAAATGCACTGTATTCT	
Grin1	ATGCACCTGCTGACATTCG	26331234a1
	TATTGGCCTGGTTTACTGCCT	
Homer	ACCGTGTTCGGTTTGGGATTC	3834611a1
	GGAAGACGGGGTTTCACACC	
CamkII	ATGTCCGAGATCCTACCCTACG	12851286a1
	AGCGAAGAAGGAGTTGGTGTC	
Neurl1	ACTATCCACGACTCCATCGGG	15420883a1
	AGGATCTGGGAGCCCTTAGTG	
Dok6	AGCTAGGGATATTCAGACGATGC	85677490c2
	GTGCAGTTCAGTTACCTTGTGA	
Jph3	TTGACGATGGAGGGTCCTACT	10181142a1
	GTGCCTTGGTACGTGTTGC	
Psd95	TGAGATCAGTCATAGCAGCTACT	6681195a1
	CTTCCTCCCCTAGCAGGTCC	
Rassf3	AGAAGGAAACGCACAATTACCTC	118129986c1
	AGCTTGTCTGTAACGGCTGAA	
St3gal6	GGGGAACAAATGGCTATTGGT	118130739c1
	AGGGCAACGGAAAATTATTGGT	
Myo1d	GAGAAAGGACGCATCTACACATT	118026910c1
	TCGACAGTGTCCCTCCCATAG	
Dsg2	CGTGGTTGAAGGCATTCATTTC	22779879a1
	TAGCTGCTTGACCAGTGTCTT	
Dusp9	CCTGTGTGAAACCAGCTTCAG	32567764c1
	CAGCTCAAGGTGTCACGGTC	
Fam129a	AAGCAGACAACATTTGAAGCCC	11528504a1
	ATCACCAGCTTACTCAGGACC	
Nrk	GACCTGGGAGTTGGAGGGA	7305327a1
	CATAAGTACCAAGACCAATGGCT	
Slco2a1	TGAAGCGTTTTGTTTTCCCTCT	15217193a1
	CGGGTGTGGAACATCCCATAA	
Tgm2	GACAATGTGGAGGAGGGATCT	6678329a1
	CTCTAGGCTGAGACGGTACAG	
Vangl1	GATACCGAATCCACGTATTCTGG	29164511a1
	TCTGCCATCTTTATTCCTTGGTG	
Stra6	GAGTCCCAGGCATCTGAGAAT	242332596c1
	CCAGGAACGACAGTGAAGCC	
Cdc42-ENSMUST00000030417.9	AAGGCTGTCAAGTATGTGGAG	
	GAATATACAGCACTTCCTTTTGGG	
Cdc42-ENSMUST00000051477.12	AAGGCTGTCAAGTATGTGGAG	
	GCTCTGGAGATGCGTTCATAG	
Kif1b-ENSMUST00000060537.12	CTGCTAGCCCTTTAAGACTCG	
	AAACTCCTAGACAAACGCTCC	
Kif1b-ENSMUST00000030806.5	AGAAAGATCCCAATGAGCGAG	
	GGTCATCTACATCGGTTCCAC	
Mtap4-ENSMUST00000169851.7	CCTGACTTCCACCTGAATGAC	
	TTAAACTTCCCTGACCAACTCC	
Mtap4-ENSMUST00000035055.14	CCCCAAAGAAACAGAGACAAC	
	AGAGTGAAACCATGCCCTTG	
Calm1-long	CAGGCTTGTCTGTAACCTCTT	
	GCATCATCTACCCAGCTTCTAC	
Calm1-all	AAATTGTCAGCAGCCAGTTTAC	
	GGGCTGTGTCTCAGAGTTTAG	
Ascl1-long	TATGCAGCTACTGTCCAAACG	
	GGGAAGGCAATGGTAGAAACT	
Ascl1-all	TTCTCCGGTCTCGTCCTACTC	
	CCAGTTGGTAAAGTCCAGCAG	
Ascl1-long	AGTTTGGATAGAAAGCATGGAGA	
	GCAGTATTCGCATATTCACATCAA	
Ascl1-all	TGGATGATGTCTCTTATCCCTTATC	
	CCTGAGCAGGAAGGAACTAAA	

TABLE 3.4: Plasmids generated in this thesis

Plasmid name	Promoter	Addgene or Sigma N	Application
pBS_cdc42E6-boxB	T3	118609	IVT
pBS_cdc42E7-boxB	T3	118612	IVT
S2F-IMCg_doxy-CMV_mChe-Cdc42E7	TetOn CMV	118614	Transfer plasmid
S2F-IMCg_doxy-CMV_mChe-Cdc42E7-E6_3′UTR	TetOn CMV	118615	Transfer plasmid
pLenti_Syn_mChe-Cdc42E7	synapsin I	118620	Transfer plasmid
pLenti_Syn_mChe-Cdc42E7-E6_3′UTR	synapsin I	118622	Transfer plasmid
pLKO.1-puro_ctrl	U6	SHC001	Transfer plasmid
pLKO.1-puro_shQki	U6	SHCLND-NM_006775	Transfer plasmid
pLKO.1-puro_shPtbp2_a	U6	SHCLND-NM_021190	Transfer plasmid
pLKO.1-puro_shPtbp2_b	U6	SHCLND-NM_019550	Transfer plasmid

TABLE 3.5: List of antibodies

Name	Host	Manufacturer	Catalog N	Dilution
GFAP	rabbit	Dako	Z0334	1:1,000
H3F3a	rabbit	Abcam	ab1791	1:5,000
Homer	rabbit	Synaptic System	160003	1:1,000
IgG	rabbit	Thermo Scientific	31462	1:500
MAP2	chicken	Novusbio	NB300213	1:1,000
MAP2	guinea pig	Synaptic Systems	188004	1:200
mCherry	rabbit	Abcam	ab167453	1:500
NF	chicken	Biolegend	822601	1:10,000
Puromycin	mouse	Kerafast	3RH11	1:2,000
Tuj1/TUBB3	rabbit	Sigma	T2200	1:5,000
Alexa Fluor 488	chicken	ThermoFisher	A11039	1:10,000
Alexa Fluor 488	mouse	ThermoFisher	A11034	1:10,000
Alexa Fluor 568	rabbit	ThermoFisher	A10042	1:10,000
Alexa Fluor 568	chicken	ThermoFisher	A11019	1:10,000
Alexa Fluor 647	guinea pig	ThermoFisher	A21450	1:10,000
IgG HRP conjugate	mouse	Abcam	ab99632	1:5,000
IgG HRP conjugate	rabbit	Abcam	ab99697	1:5,000

TABLE 3.6: List of reagents

Name	Manufacturer	Catalog N
10x Phosphate Buffered Saline	BioRad (Hercules, CA, USA)	1610780
2-Mercaptoethanol	Sigma-Aldrich (Steinheim, Germany)	M6250-100ML
2-Propanol molecular biology grade	Millipore (Burlington, MA, USA)	M1096341000
20,000x SYBR Gold	Invitrogen (Carlsbad, CA, USA)	S11494
3 M NaOAc pH 5.5 RNase-free	Invitrogen (Carlsbad, CA, USA)	AM9740
40% Acrylamide/Bis Solution, 19:1	BioRad (Hercules, CA, USA)	161-0144
Acetic Acid	AppliChem GmbH (Darmstadt, Germany)	A3686,1000
Acrylamide/Bisacrylamide Solution 37.5:1 (40% w/v)	Serva (Heidelberg, Germany)	79-06-1
Adenosine 5′-Triphosphate 10 mM	NEB (Ipswich, MA, USA)	B0756A
Agarose Standard	Carl Roth (Karlsruhe, Germany)	3810.4
Agencourt AMPure XP, 60 mL	Beckman Coulter GmbH (Brea, CA, USA)	A63881
Agencourt RNAClean XP, 40 mL	Beckman Coulter GmbH (Brea, CA, USA)	A63987
Ammonium Acetate 5 M	Thermo Fisher scientific GmbH (Waltham, MA, USA)	AM9071
Ammonium Persulfate	BioRad (Hercules, CA, USA)	1610700
Ampicillin Sodium Salt	Carl Roth (Karlsruhe, Germany)	HP62.2
BD Matrigel GFR-RED Phenolfrei	Thermo Fisher scientific GmbH (Waltham, MA, USA)	15585729
Bio-Rad Protein Assay Dye Reagent Concentrate	BioRad (Hercules, CA, USA)	500-0006
Catalase	Sigma-Aldrich (Steinheim, Germany)	C3155
Chloroform	Sigma-Aldrich (Steinheim, Germany)	288306-100ML
CoverGrip Coverslip Sealant	Biotium (Fremont, CA, USA)	23005
Cycloheximide	Cell signaling Technology (Danvers, MA, USA)	877-616-CELL (2355)
D(+)-Saccharose molecular grade	AppliChem GmbH (Darmstadt, Germany)	A2211
Diethyl pyrocarbonate	Sigma-Aldrich (Steinheim, Germany)	D5758
DMSO, Cell culture grade	Genaxxon Bioscience (Ulm, Germany)	M6323.0250
DNase I	Ambion (Austin, TX, USA)	AM2222
dNTP Mix, 10mM each	Thermo Fisher scientific GmbH (Waltham, MA, USA)	11853933
Doxycycline monohydrate	Sigma-Aldrich (Steinheim, Germany)	D1822
EDTA	Merck (Darmstadt, Germany)	6381-92-6
ERCC RNA spike-in	Cell signaling Technology (Danvers, MA, USA)	4456740
Ethidium bromide solution 1%	Carl Roth (Karlsruhe, Germany)	2218.1
FastAP Thermosensitive Alkaline Phosphatase	Thermo Fisher scientific GmbH (Waltham, MA, USA)	EF0651
Formaldehyde, 16%, methanol free 20x10ml	Polysciences Europe GmbH (Hirschberg, Germany)	2637557
Formamide	Sigma-Aldrich (Steinheim, Germany)	F9037-100ML
GeneRuler 1 kb Plus DNA Ladder	Life Technologies (Carlsbad, CA, USA)	SMF-1082-5-BS
Gibson assembly master mix	NEB (Ipswich, MA, USA)	E2611S
Glucose oxidase	Sigma-Aldrich (Steinheim, Germany)	G0543
Glutathione-Sepharose 4B	GE Healthcare (Chicago, IL, USA)	17075601
Glycerol	Sigma-Aldrich (Steinheim, Germany)	G5516-500ML
GlycoBlue Coprecipitant (15 mg/mL)	Life Technologies (Carlsbad, CA, USA)	AM9516
GSK-3 inhibitor	Merck (Darmstadt, Germany)	361559-5MG
jetPrime Transfection Reagent	Polyplus (Strasbourg, France)	13-114-15
L-Glutamine, 200 ml Sterile filtered	Sigma-Aldrich (Steinheim, Germany)	G7513-100ML
Laminin	Sigma-Aldrich (Steinheim, Germany)	L2020-1MG
Lenti-X Concentrator	Takara (Kusatsu, Japan)	PT4421-2
Low Molecular Weight DNA Ladder	NEB (Ipswich, MA, USA)	N3233 L
Methanol	Carl Roth (Karlsruhe, Germany)	8388.1
Micrococcal Nuclease	Thermo Fisher scientific GmbH (Waltham, MA, USA)	88216
MicroSpin S-400 HR Columns	GE Healthcare (Chicago, IL, USA)	27514001
Millicell 6-well insert	Millipore (Billerica, MA, USA)	PISP30R48
Mini-PROTEAN TBE Gels, 5%, 30 microliters	Bio-Rad Laboratories GmbH	456-5013
Non-denaturing 5% polyacrylamide TBE gel 12 wells	BioRad (Hercules, CA, USA)	456-5013
Non-fat skimmed milk powder	AppliChem GmbH (Darmstadt, Germany)	A0830,1000
Novex TBE-urea sample buffer (2X)	Invitrogen (Carlsbad, CA, USA)	LC6876
NuPAGE Novex 4-12% Bis-Tris Protein Gels, 1.0 mm, 10 well-10 gels	Life Technologies (Carlsbad, CA, USA)	NP0321BOX
O'RangeRuler 10 bp DNA Ladder	Thermo Fisher scientific GmbH (Waltham, MA, USA)	SM1313
PageRuler Plus Prestained Protein Ladder	Thermo Fisher scientific GmbH (Waltham, MA, USA)	26619
Paraformaldehyde	Sigma-Aldrich (Steinheim, Germany)	158127-500G
PBS pH 7.2	PAN-Biotech (Aidenbach, Germany)	P04-36500
Pefabloc	Biophoretics (Sparks, NV, USA)	30827-99-7
Penicillin/Streptomycin 10.000 E/10.000	Biochrom (Berlin, Germany)	A 2213
peqGOLD TriFast 100 ml DNA/RNA/Protein	VWR Internat. GmbH (Peqlab)	30-2110
Phenol/Chloroform 25:24:1	Merck (Darmstadt, Germany)	516726-1SET
Phusion High-Fidelity DNA Polymerase	Thermo Fisher scientific GmbH (Waltham, MA, USA)	F-530L
Poly-D-Lysine hybromide	Sigma-Aldrich (Steinheim, Germany)	P6407-5MG
Poly-L-Ornithine Hydrobromide	VWR (Radnor, PA, USA)	114-15
prolong Gold Antifade Mounting with DAPI 10mL	Life Technologies (Carlsbad, CA, USA)	P36931
Prolong-Gold with DAPI	Cell Signaling (Danver, MA, USA)	8961S
Proteinase K, recombinant	Sigma-Aldrich (Steinheim, Germany)	3115836001
Random hexamers	Thermo Fisher scientific GmbH (Waltham, MA, USA)	N8080127
RNase OUT	Life Technologies (Carlsbad, CA, USA)	10777019
RNase-free water	Thermo Fisher scientific GmbH (Waltham, MA, USA)	AM9938
RNaseI 100 U/μl	Thermo Fisher scientific GmbH (Waltham, MA, USA)	AM2294
RQ1 RNase-free DNase	Promega (Fitchburg, WI, USA)	M6101
Sodium Chloride	Promega (Fitchburg, WI, USA)	H5271
Sodium Deoxycholate	Sigma-Aldrich (Steinheim, Germany)	D6750-100G
Sodium Dodcyl Sulfate	Serva (Heidelberg, Germany)	151-21-3
SpinX column with 0.45 μM pore size	Costar (Washington, DC, USA)	CLS6162
Superscript II	Thermo Fisher scientific GmbH (Waltham, MA, USA)	18064014
Superscript III	Thermo Fisher scientific GmbH (Waltham, MA, USA)	18080093
System buffer	National diagnostic (Charlotte, NC, USA)	EC835
System concentrate	National diagnostic (Charlotte, NC, USA)	EC830
System diluent	National diagnostic (Charlotte, NC, USA)	EC840
T3 megascript in vitro transcription kit	Thermo Fisher scientific GmbH (Waltham, MA, USA)	AM1338
T4 DNA Ligase	Thermo Fisher scientific GmbH (Waltham, MA, USA)	EL0014
T4 polynucleotide kinase	Thermo Fisher scientific GmbH (Waltham, MA, USA)	EK0031
T4 RNA ligase, truncated K227Q	NEB (Ipswich, MA, USA)	M0351L
TEMED	Thermo Fisher scientific GmbH (Waltham, MA, USA)	17919
Trifast	VWR (Radnor, PA, USA)	30-2010
Trifast-FL	VWR (Radnor, PA, USA)	732-3314
Tris Hydrochloride	Carl Roth (Karlsruhe, Germany)	9090.3
Tris(hydroxymethyl)aminomethane molecular biology grade	Serva (Heidelberg, Germany)	37186.04
Triton X-100 molecular biology grade	Sigma-Aldrich (Steinheim, Germany)	T8787-100ML
Trizima base	Sigma-Aldrich (Steinheim, Germany)	T1503-1KG
Trypan Blue Solution 0.4%	Thermo Fisher scientific GmbH (Waltham, MA, USA)	15250061
Turbo DNase 2 U/ćl	Invitrogen (Carlsbad, CA, USA)	AM2238
Tween 20 (10%)	Biorad (Hercules, CA, USA)	1610781
Universal Nuclease for Cell Lysis	Thermo Fisher scientific GmbH (Waltham, MA, USA)	88701
Urea, MB Grade	Merck (Darmstadt, Germany)	66122-500GM
Western Blocking Reagent, 100 ml	Sigma-Aldrich (Steinheim, Germany)	11921673001

TABLE 3.7: List of consumables

Name	Manufacturer	Catalog N
26-gauge needle	Becton Dickinson (Franklin Lakes, NJ, USA)	5518075
Alu-Stiel 150 mm	NeoLab Migge GmbH (Heidelberg, Germany)	21022
Biosphere Fil. Tip 1000 blau	Sarstedt (Numbrecht, Germany)	70.762.211
Biosphere Fil. Tip 20 farblos	Sarstedt (Numbrecht, Germany)	70.1114.210
Biosphere Fil. Tip 200 farblos	Sarstedt (Numbrecht, Germany)	70.760.211
PCR-tubes, 0.2 ml	Sigma-Aldrich (Steinheim, Germany)	BR781305-1000EA
Cell counter slides	Logos Biosystems (Anyang-si, South Korea)	872010
Coverslips 18 mm Nr. 1	NeoLab Migge GmbH (Heidelberg, Germany)	2637558
DNA/RNA LoBIND tubes, 1.5 ml	Eppendorf (Hamburg, Germany)	30108051
Holzstiel 150 x 2,5 mm	NeoLab Laborbedarf	290121021
Microseal 96-Well Skirted PCR Plates	BioRad (Hercules, CA, USA)	MSP-9601
Millicell Hanging Cell Culture Insert, P	Merck (Darmstadt, Germany)	MCSP06H48
Protein LoBIND tubes, 1.5 mL	Eppendorf (Hamburg, Germany)	300108116
Qubit Assay Tubes	Life Technologies (Carlsbad, CA, USA)	Q32856
Razors	Braun (Tuttlingen, Germany)	5518075
SafeSeal SurPhob Spitzen, 100 μl, steril	Biozym Scientific GmbH (Hessisch Oldendorf, Germany)	VT0230
SafeSeal SurPhob SpitzenJosé, 1250 μl, steril	Biozym Scientific GmbH (Hessisch Oldendorf, Germany)	VT0270
SafeSeal SurPhob Spitzen,10 μl	Biozym Scientific GmbH (Hessisch Oldendorf, Germany)	VT0200
SpinX column with 0.45 μm pore size	Costar (Washington, DC, USA)	CLS6162
Sterile Filter 0.22 μm 500ml	Life Technologies (Carlsbad, CA, USA)	TPP99505

TABLE 3.8: List of equipment

Instrument	Manufacturer
Agilent 2100 Bioanalyzer	Agilent Technologies (Santa Clara, CA, USA)
Alpha Imager HP	ProteinSimple (San Jose, CA, USA)
Binder CB incubator	Binder (Tuttlingen, Germany)
Bioruptor	Diagenode (Liege, Belgium)
Biospectrometer basic	Eppendorf (Hamburg, Germany)
C100 Touch Thermal cycler	BioRad (Hercules, CA, USA)
Centrifuge 5424	Eppendorf (Hamburg, Germany)
Centrifuge 5804	Eppendorf (Hamburg, Germany)
CFX96 Real-Time PCR system	BioRad (Hercules, CA, USA)
Cryostat CM1860	Leica (Welzlar, Germany)
DynaMag-2 Magnet	Thermo Fisher scientific GmbH (Waltham, MA, USA)
Electrophoresis apparatus	Carl Roth (Karlsruhe, Germany)
Fujifilm Luminescent Image Analyzer LAS4000	Fujifilm (Tokyo, Japan)
Ice Machine Scotsman AF10	Scotsman (Vernon Hills, USA)
Illustra Microspin S-400 HR Columns	GE Healthcare (Little Chalfont, UK)
ImageQuant LAS 4000	GE Healthcare (Little Chalfont, UK)
Incu-Line	VWR (Radnor, PA, USA)
Innova 42 incubator shaker	Eppendorf (Hamburg, Germany)
LAS-4000	GE Healthcare (Little Chalfont, UK)
Leica DMIL LED	Leica (Welzlar, Germany)
Luna automated cell counter	Logos Biosystems (Anyang-si, South Korea)
Mini Protean Tetra cell	BioRad (Hercules, CA, USA)
Mini Trans-Blot Power Supply	BioRad (Hercules, CA, USA)
Mini Trans-Blot Cell	BioRad (Hercules, CA, USA)
Nanodrop ND-1000 Spectrophotometer	Thermo Fisher scientific GmbH (Waltham, MA, USA)
NextSeq 500	Illumina (San Diego, CA, USA)
Qubit Fluorometer	Life Technologies (Carlsbad, CA, USA)
Qubit 2.0 Fluorometer	Thermo Fisher scientific GmbH (Waltham, MA, USA)
S1000 Thermal cycler	BioRad (Hercules, CA, USA)
Sorvall MTX 150 micro-ultracentrifuge	Thermo Fisher scientific GmbH (Waltham, MA, USA)
Sp5 confocal microscope	Leica (Welzlar, Germany)
Sp8 conocal microscope	Leica (Welzlar, Germany)
SpectraMax M2 Spectrophotometer	Molecular Devices (Sunnyvalle, CA, USA)
Table centrifuge 5415D	Eppendorf (Hamburg, Germany)
Thermocycler (PTC-200)	Biozym (Heidelberg, Germany)
Thermomixer 5436	Eppendorf (Hamburg, Germany)
Thermomixer compact	Eppendorf (Hamburg, Germany)
Trans Blot Turbo	BioRad (Hercules, CA, USA)

3.2 Methods

3.2.1 Cell culture work

mESC culturing, differentiation of Ascl1-induced neurons, and compartment separation

Ascl1-iNs were obtained by reprogramming of mouse embryonic stem cells (mESCs) through the induction of a TetOn doxycycline-inducible achaete-scute complex homolog-like 1 (*Ascl1*) cassette, as previously described (Zappulo*, Van Den Bruck*, Ciolli Mattioli*, Franke* et al., 2017). Briefly, mESC were kept in culture on gelatin-coated flasks in a medium composed of 80% mESC medium and 20% 2i medium (Table 3.2), and split when confluency reached 50-60% (every other day). To induce Ascl1-iNs formation, TrypLE was used to dissociate mESC colonies into single cells, which were plated in suspension on non-adherent dishes in AK medium (Table 3.2) at a density of 20,000 cells/cm^2 to induce the formation of embryoid bodies (EBs). After 2 days, EBs were collected and split 1:2 in fresh AK medium supplemented with 3 μg/ml doxycyxline (to induce *Ascl1* cassette). After 2 additional days, EBs were collected and plated on matrigel-coated filters (Millicell 6-well, Merck) at a density of $\sim$ 200,000 cells/cm^2 and cultured for 3 additional days in monolayer medium (Table 3.2) supplemented with 3 μg/ml doxycyxline. When microscopy experiments were carried out, EBs were split with TrypLE in order to allow the dissociation of EBs into single cells, which were plated on poly-L-ornithine (100 μg/ml)-coated coverslips at a density of 25,000 cells/cm^2. At day 5 from induction, cells were ready to be collected for further analysis. For isolation of subcellular compartments, the somatic fraction was collected by detaching it from the filter through harsh washes with PBS, spun and collected separately. After somatic collection, the filter - still carrying the neuritic compartment on the bottom side - was cleaned from the remaining somatic contaminants using cotton swabs, and after extensive cleaning it was cut out from the inlay and collected separately.

Stable isotope labelling by aminoacids

For stable isotope labeling with amino acids in cell culture (SILAC) experiments (Ong et al., 2002), mESCs were grown in light (L) or heavy (H) SILAC 80% 2i and 20% mESC medium. For L labelling, L-Lys monohydrochloride and L-Arg monohydrochloride were used. For H labelling, Lys-8 (L-lysine-$^{13}C_6$, $^{15}N_2$ monohydrochloride, + 8 Da) and Arg-10 (L-arginine-$^{13}C_6$, $^{15}N_4$ monohydrochloride, + 10 Da) were used. To ensure complete proteome

labelling, mESC were passaged six times and tested for incorporation efficiency (> 97%, data not shown). Labelled mESCs were further differentiated into neurons in SILAC-customized differentiation media (L or H).

Primary neurons culturing

Primary cortical neurons were isolated from P0 mouse pups by Mandy Terne and cultured as previously described (Kaech and Banker, 2006). For neurite/soma separation, neurons were plated at a density of 100,000 cells/cm^2 on double-coated (100 μg/ml poly-D-lysine and 5 μg/ml laminin) cell inserts (Millicell 6-well, Merck). At day *in vitro* 14 (DIV14) cells were used either for imaging or for neurites and soma isolation.

Generation of KD polyclonal cell lines

Viral titers were produced as in chapter 3.2.4, with transfer plasmids expressing shRNAs, purchased from sigma (see table 3.4). Titers were applied on mESC cells, and 72h after transduction mESC were selected with 1 μg/ml puromycin.

3.2.2 Microscopy assays

Immunofluorescence

For immunofluorescence (IF) staining, cells were fixed with 4% paraformaldehyde (PFA) for 10 min, permeabilized with 0.2% Triton X-100 in PBS for 10 min, and blocked with 1:5 dilution of the Western blocking reagent in PBS for 30 min. Cells were probed with primary antibodies (table 3.5) over night (ON) at 4°C, washed with PBS-tween 0.05%, and incubated with fluorophore-coupled secondary antibodies for 1 h at room temperature (RT). Slides were mounted with ProLong Gold with 4′,6-diamidino-2-phenylindole (DAPI). Images were acquired on SP5 or SP8 confocal microscope with a 40x or 63x oil objective and a pinhole of 90 μm as z-stacks, a z-step of 0.2 μm, and 1024 x 1024 pixels xy resolution.

smFISH

smFISH was performed with *Cdc42* isoform-specific Stellaris probes sets (Biosearch Technologies) on primary mouse cortical neurons (P0, DIV18) according to the manufacturer's instructions with few modifications. Instead of Vectashield

medium, coverslips were mounted with a home-made anti-fade mounting medium: GLOX buffer supplemented with 37 μg/ml glucose oxidase and 100 μg/ml catalase. *Cdc42* isoforms expression was examined with 125 nM Quasar-labeled probes: Q570 for *Cdc42E6* and Q670 for *Cdc42E7*. Images were acquired with a Keyence microscope using a 60x oil objective. Maximum projections were performed using Fiji (ImageJ) using 10 slices with a z-step of 0.3 μm. Images were further analyzed for signal quantification with StarSearch (rajlab).

puro-PLA and image analysis

Puro-PLA was performed as previously described (Tom Dieck et al., 2015). Briefly, Ascl-1iNs and primary neurons were incubated with 2 mM or 2 μM of puromycin respectively, for 5 minutes before fixation. After fixation in 4% PFA, cells were immunostained with mouse anti-puromycin 1:2,000 and rabbit anti-mCherry 1:500 antibodies (table 3.5) using Duolink FarRed reagent according to the manufacture's recommendations. For negative control, anti-IgG antibody was used instead of anti-mCherry, or untransduced cells. To visualize neurites, cells were immunostained with chicken anti-neurofilament 1:5,000 or chicken anti-Map2 1:200 antibody, in combination with anti-chicken Alexa Fluor 488 secondary antibody. Slides were mounted in Prolong gold antifade reagent with DAPI. Images were acquired with a Leica TCS SP8 confocal microscope using 63x oil objective. Puro-PLA signals were quantified using Fiji (ImageJ) function Analyze Particles. The function was applied to either soma (visualized by DAPI), or neurites (visualized by neurofilament staining) at a distance of at least 20 μm from DAPI signal. Each analyzed region corresponded to 150 μm^2 ($\sim$ cell body size). The results represent the average from 9 neurons expressing the wt reporter (E7 3′UTR) and 11 neurons expressing the swap reporter (E6 3′UTR). The data are presented as the ratios of signals detected in neurites versus soma.

3.2.3 Biochemical assays

Protein extraction

Soma and neurites from Ascl1- Ascl1-iNsor primary cells were isolated as described previously (chapter 3.2.1) and collected in protein low-binding tubes in protein extraction buffer (0.1 M Tris pH 8, 8 M urea). Samples were sonicated using a Bioruptor (15s ON, 45s OFF, high power, 4 cycles). Concentration was measured using Qubit protein kit.

Western blot

For western blotting, 5 μg of protein lysate mixed with 5xSDS loading buffer (50% glycerol, 300 mM Tris-HCl pH 6.8, 5% (v/v), 2-mercaptoethanol, 0.1% bromophenol blue, 1% SDS) from either neurites or soma was separated on a 12.5% Laemmli PAAG running at 80 V for the stacking gel ($\sim$ 15 minutes), increasing to 120 V for the rest of the gel ($\sim$ 2 h) in running buffer (25 mM Tris-base, 191 mM glycine, 0.1% SDS). Proteins were transferred to a methanol-activated PVDF membrane via semi-dry transfer for 30 min at 25 V on a Trans-Blot Turbo device or via wet transfer for 1 h at 100 V at 4°C in transfer buffer (25 mM Tris-base, 191 mM glycine, 20% or 10% MeOH for semi-dry or wet transfer respectively). The membrane was incubated in blocking solution (5% milk in PBS-Tween 0.05%) for 30 minutes at RT, and probed with the following primary antibodies ON at 4°C: rabbit anti-mCherry antibody 1:5000, rabbit anti-Tuj1/TUBB3 1:5000, rabbit anti-Histone H3F3a 1:5000, rabbit anti-Homer 1:1000 (table 3.5). Secondary antibody incubation was performed at RT 1h, before acquisition of the chemiluminescent signal in the ImageQuant Las 400 chemiluminescent analyzer after incubation in ECL reagent (100 mM Tris-HCl pH 8.5, 1.25 mM luminol, 225 μM coumaric acid, 0.01% H_2O_2). For western blot analysis mCherry-CDC42E7 levels were quantified with Fiji, normalized to the levels of TUBB3 and presented as the neurites/soma ratios.

RT and qPCR analysis

RNA from soma and neurites was extracted with Trifast following manufacturer's instructions. Isolated RNA was quantified with Qubit HS RNA kit, and equal amounts from different samples were treated with RQ1 DNase I to remove traces of genomic DNA (gDNA) and reverse-transcribed using the Maxima first strand cDNA synthesis kit. Quantitative reverse transcription polymerase chain reaction (RT-qPCR) was performed with sensiFAST SYBR No ROX qPCR kit using the primers in table 3.3. RT-qPCR reactions were carried out in technical duplicates and biological triplicates (soma) or duplicates (neurites), using a CFX96 Real-Time PCR system. Relative neurites/soma expression levels were calculated using $\Delta\Delta$Ct method, with *Thyn1* or *Gapdh* as a reference RNA.

Expression and purification of GST-λ protein

GST-λ protein was expressed in *E.coli* Rosetta BL21-DE3, which allows co-expression of rare tRNAs. 5 ml of ON culture of cells transformed with pGST-λ (from Czaplinski et al., 2005) was diluted in 1 L of Luria broth (LB), grown to an optical density (OD) of 0.4, and induced with 40 μM isopropyl β-D-1-thiogalactopyranoside (IPTG) ON at 18°C. Cell pellet was resuspended with 25 ml of resuspension buffer (50 mM HEPES pH 7.5, 300 mM NaCl, 2.5 mM DTT, 1 mg/ml lysozyme, 25 U/ml universal nuclease, 0.4 mM Pefabloc) by rotating for 20 min at 4°C, and lysed by sonication (10s ON, 30s OFF, high power, 10 cycles). Lysate was clarified at 12,000*xg* for 30 min at 4°C. The surnatant was added to 1 ml of glutathion sepharose beads (Amersham) equilibrated in equilibration buffer (50 mM HEPES pH 7.5, 150 mM NaCl, 2.5 mM DTT). After 1 hour of incubation at 4°C, beads were washed 3x with 25 ml of equilibration buffer, 25 ml of washing buffer (50 mM HEPES pH 7.5, 300 mM NaCl, 2.5 mM DTT), and 25 ml of equilibration buffer. Elution was performed 3x with 1 ml of equilibration buffer supplemented with 20 mM glutathion for 1 hour at 4°C. Aliquots were quantified and run on a gel to check for purification.

GRNA chromatography

boxB-Cdc42E7 and boxB-Cdc42E6 RNAs were generated using a T3 Megascript *in vitro* transcription kit according to the manufacturer's recommendations. The template plasmids were linearized with XmaI. Post-synthesis, plasmid DNA was removed with DNAse I and RNA purified using Agencourt RNA-Clean XP beads. GRNA chromatography (Czaplinski and Mattaj, 2006) was performed as described earlier (Chekulaeva, Hentze, and Ephrussi, 2006) with some modifications. Per 60 μg of GST-λ N fusion peptide, 20 μl of a 50% slurry of Glutathione-Sepharose 4B in binding buffer (BB, binding buffer (BB: 20 mM Tris-HCl pH 7.5, 200 mM NaCl, 1.5 mM $MgCl_2$, 9% Glycerol, 0.05% NP-40, 12 mg/ml heparin) were incubated on an orbital rocker for 30 min at RT. Glutathione-Sepharose beads were washed twice in 1 ml of BB to remove the unbound GST-λ N, and incubated with 18 pmol RNA (boxB-Cdc42E7 or boxB-Cdc42E6) in 200 μl for 1 hr at 4°C. The beads were washed twice with 1 ml of BB and incubated for 2 hr at 4°C with 2.9 mg of protein lysate prepared from H or L SILAC labelled Ascl1-iNs(lysis buffer: 50 mM TRIS-HCl pH 7.5, 150 mM KCl, 0.5% Triton, 0.4 mM Pefabloc). The beads were washed 3 times with 1 ml of BB, and bound proteins were eluted with 0.15 μg RNase A in 60 μl of BB for 30 min at 30°C on an orbital shaker. Eluates were supplemented with 70 μl 2.5 M NaOAC pH 5.0, 1 μl Glycoblue and absolute EtOH up to

2 ml and incubated at 4°C ON. Proteins were recovered by centrifugation at 18,000*xg* at 4°C for 30 min and subjected to liquid chromatography-tandem mass spectrometry (LC-MS/MS).

LC–MS/MS and SILAC-based protein quantification

LC-MS/MS and SILAC-based protein quantifications were done by Koshi Imami as previously described (Zappulo*, Van Den Bruck*, Ciolli Mattioli*, Franke* et al., 2017). In short, LC–MS/MS analysis was performed with in-solution digested protein samples on a Q Exactive plus mass spectrometer (Thermo Scientific) according to Sander et al., 2015, LFQ was done using MaxQuant Analysis Software. In SILAC experiments, the fw and rev experiments represent "label swap" replicates to eliminate biases introduced by the labelling procedure. The averages of H/L (fw) and L/H (rev) ratios were used to measure relative protein abundance in boxB-Cdc42E7 versus boxB-Cdc42E7 complexes.

3.2.4 Cloning and transduction

Cloning

Cdc42 CDS and 3′UTRs were PCR-amplified from cDNA prepared from Ascl1-iNs and fused with mCherry CDS at the C-terminus with overlap PCR (mCherry-Cdc42E7). For the 3′UTR swap experiment, mCherry-Cdc42E7 CDS was fused E6 3′UTR using overlap PCR (mCherry-Cdc42E7-E63′UTR). Next, mCherry-Cdc42 reporters were cloned into lentiviral vectors. For expression in Ascl1-iNs, we used S2F-IMCg lentiviral vector with doxycycline-inducible CMV promoter (Loew et al., 2006), to simultaneously induce neuronal differentiation and expression of the reporters with doxycycline. For expression in primary cortical cells, mCherry-Cdc42 fusions were cloned into lentiviral reporter with rat synapsin I promoter (Rusty Lansford, Addgene plasmid 51004). To generate RNA for GRNA chromatography (Cdc42E7 and E6 3′UTRs fused with boxB sites), the following plasmids were created to serve as templates in T3 *in vitro* transcription. E7 and E6 3′UTRs were PCR amplified and cloned into pBS-FLuc-5xboxB (Chekulaeva, Hentze, and Ephrussi, 2006) to substitute FLuc, resulting in pBS_Cdc42E7-boxB and pBS_Cdc42E6-boxB plasmids. All constructs (table 3.4) were confirmed by Sanger sequencing.

Lentivirus production and infection

To produce lentiviral particles, HEK293T cells were transfected in 10 cm dishes with 10 μg of the envelope (Addgene 12259), packaging (Addgene 12260) and transfer plasmid (table 3.4) in a 1:1:2 ratio, using polyethylenimine (PEI). The day after transfection the medium was exchanged to 10 ml of 2% FBS DMEM. Lentivirus-containing medium was harvested 72 hours post-transfection, and cleared from cell debris by centrifugation 5 min at 500xg. For transduction of Ascl1-iNs, 1 ml of supernatant was applied to 10^6 cells plated on the microporous filter. For primary neurons transduction, viral particles were concentrated using Lenti-X Concentrator as recommended by the supplier and resuspended in 100 μl PBS. 3 μl of the concentrated virus was applied to 0.5 x 10^6 of primary neurons on the day of plating after the cells have attached to the filter support, or to 0.5 x 10^6 mESC cells for polyclonal cell line generation.

3.2.5 Next generation sequencing

Ribosome profiling from Ascl1-iNs compartments

Ascl1-iNs grown on a Millicell filter were treated with cycloheximide (100 μg/ml), separated on neurites and soma as described earlier (chapter 3.2.1) and frozen in liquid nitrogen. Twenty-one inserts were pooled together for neurites isolation and three inserts for soma isolation. Ribo-seq libraries were generated as previously described (Ingolia et al., 2009) with some modifications. Each sample was lysed in 1 ml of polysome buffer (20 mM Tris pH 7.4, 150 mM NaCl, 5 mM $MgCl_2$, 1 mM dithiothreitol (DTT), 1% Triton X-100, 100 μg/ml cycloheximide, and 5 U/ml Turbo DNase) and digested with 70 U of RNaseI for 40 min at RT. As our analysis revealed that the quality and composition of the libraries generated with and without monosome recovery was comparable (chapter 4.2.1), we omitted the ribosome isolation step. After RNaseI digestion, RNA was isolated using Direct-zol RNA MiniPrep and 400 ng of the isolated footprinted RNA were depleted of rRNA using RiboZero Gold rRNA removal kit (Illumina). The sample was concentrated using RNA clean and concentrator-5 kit and phosphorylated with 10 U T4 polynucleotide kinase for 30 min at 37°C. The RNA was separated on a 15% Urea PAAG, 27–30 nt RNA fragments were eluted from the gel and used for library generation with Truseq small RNA library prep kit (Illumina) according to the manufacturer's instructions. Each Ribo-seq library was prepared in triplicate and sequenced on an Illumina NextSeq 500 sequencer with single-end 75 bp reads.

Ribosome profiling analysis

Ribosome profiling analysis was performed by Lorenzo Calviello and Vedran Franke. Raw reads were trimmed to remove adapters and low quality bases with the BBduk2 trimmer (https://sourceforge.net/projects/bbmap/): rref=$adapter_right.lref=$adapter_left k=10 ktrim=r qtrim=r minlength=10 minoverlap=5 trimq=25. Cleaned reads were subsequently aligned using the STAR aligner (Dobin et al., 2013) on the mm9 version of the mouse genome with the following parameters: –outFilterMultimapNmax 5–outFilterMismatchNoverLmax 0.05. To visualize the signal periodicity of the Ribo-seq data, we plotted the reads corresponding to the three translation frames, in a window of +/- 50-75 bp around the translation start site. If a transcript contained multiple translation start sites, the most upstream translation start site was chosen. Reads of width 28 and 29 nt were the most abundant. Reads were summarized over coding sequences. Differential expression analysis was done using DESeq2 as described in RNA sequence analysis. RPKM expression estimates were obtained by scaling the DESeq2 normalized counts by the corresponding CDS widths.

3′end-seq

3′end-seq was performed with QuantSeq 3′mRNA-Seq kit (Lexogen) according to the manufacturer's recommendations. 3′end-seq was done in biological triplicates (soma) or duplicates (neurites), using 260 ng of total RNA from neurites or soma of Ascl1-Ascl1-iNsper sample. Libraries were pooled and sequenced on Illumina NextSeq 500 system with a single-end 150-cycle run.

3′end-seq analysis

3′end-seq analysis was performed by Aviv Rom and Vedran Franke largely as previously described (Zappulo*, Van Den Bruck*, Ciolli Mattioli*, Franke* et al., 2017). Raw reads were trimmed to remove adapters and low quality bases with the BBduk2 trimmer (https://sourceforge.net/projects/bbmap/): k = 10 threads = 12 ktrim = r qtrim = r minlength = 100 minoverlap = 9 trimq = 25. Cleaned reads were subsequently aligned using the STAR aligner (Dobin et al., 2013) on the mm10 version of the mouse genome with the following parameters: –outFilterMultimapNmax 10 –outFilterMismatchNoverLmax 0.05. To define 3′end-seq clusters, all sequencing samples were merged. Genomic positions covered with 3′ most nucleotide of 3′end-seq reads were taken as

putative cluster seeds. Positions containing less than three reads were disregarded. Clusters were obtained by merging all seed position within 25 bp. 3′end-seq cluster end (putative alternative polyadenylation site) was set as the position within the cluster with the highest read coverage, and the cluster width was set to 25 bp. To remove the effects of internal priming, 3′end-seq clusters completely contained within introns were removed from the analysis, as so were the clusters within 10 bp of borders of internal exons. A region from -45 bp to -35 bp upstream of the 3′end-seq cluster 3′ end was searched for known alternative polyadenylation motifs. The following motifs were used in the analysis: AATAAA, ATTAAA, TATAAA, AAGAAA, AGTAAA, AATATA, AATACA, CATAAA, GATAAA, TTTAAA. Motif was considered as found if there was a perfect match. A region from -8 bp to +10 bp around the 3′end-seq cluster 3′ end was search for the known polyadenylation signal. The following motif was used: AAAAAAAA, with two allowed mismatches. All downstream analysis was done with 3′end-seq clusters containing a valid APA, and PolyA motifs, which were located in annotated 3′UTRs. Pairs of UTRs with the difference in usage between soma and neurites were then computed as in (Ulitsky et al., 2012). Briefly, for each gene we first counted the number of reads assigned to each 3′ end in each of the two samples (soma/neurites), and computed for each 3′ end its "relative usage" (number of reads mapping to the 3′ end/number of reads assigned to all the 3′ ends of that gene combined). Only 3′ ends with at least five reads in one of the libraries were considered. We then identified for each gene the 3′ end which showed the maximal "positive change" in relative usage (arbitrarily defining usage in soma as positive) and the one with maximal "negative change". Genes for which one of those changes was at least 20% were considered further, and the pair of UTRs with the maximal positive and negative changes were considered the "switching" isoforms.

PAR-CLIP

After one week of differentiation through doxycycline-dependent Acl1 induction, mESC differentiated into neurons where incubated with 200 uM 4sU (Cayman chemical) nucleoside analog for 8 hours, washed twice in ice-cold PBS, UV-crosslinked as previously described (Hafner et al., 2010a), frozen in liquid nitrogen and stored at -80°C. Cell pellets were lysed in 3 times the cell pellet volume of NP-40 lysis buffer (50 mM Tris pH 7.4, 100 mM NaCl, 1% (v/v) NP-40, 0.1% SDS, 0.5% (v/v) sodium deoxycholate, 0.2 mM pefabloc protease inhibitor), incubated 10 minutes on ice followed by RNaseI nuclease digestion, performed at 37°C for 5 minutes shaking at 1,100 rpm, at a final concentration of 100 units for 4 mg of protein lysate in 600 μl final volume.

Lysates were then clarified by centrifugation at max speed for 15 minutes at 4°C. IP was performed as previously described (Hafner et al., 2010a), with the following modifications. After 4 hours incubation with the lysate, anti-MOV10 (10 μg/sample, sigma PLA0195) coupled dynabeads were washed in the following high salt buffer: 50 mM tris pH 7.4, 1 M NaCl, 1 mM EDTA, 1% NP-40, 0.1% SDS. Dephosphrylation reaction was carried for 30 minutes. SDS-PAGE, nitrocellulose transfer and RNA isolation was performed as previously described (Huppertz et al., 2014), as well as RNA library (Hafner et al., 2010a) with the following modifications. Input was RNaseI-treated and processed as the CLIP sample in order to use it as control. Adapter ligation was performed in the presence of 10% PEG8000 without DMSO. cDNA synthesis was run for 30 min at 50°C. Libraries from biological duplicates were purified from a 5% novex TBE gel (Biorad) and sequenced on Nextseq500 platform.

RIP and IP for MS

mESC were differentiated for one week into neurons through doxycycline-dependent ASCL1 induction, and UV-crosslinked as previously described (Kenny et al., 2014). Cells were frozen in liquid nitrogen and stored at -80°C. Cell pellets were lysed in 3 times the cell pellet volume of lysis buffer (50 mM Tris pH 7.4, 150 mM NaCl, 0.5% (v/v) NP-40, 0.2 mM pefabloc protease inhibitor, 40 u/ml RNaseOUT), incubated 10 minutes on ice and cleared by centrifugation 15 min at 1,000xg at 4°C. After 4 hour incubation on anti-MOV10 or rabbit IgG (6 μg/sample, sigma PLA0195) coupled dynabeads, samples were washed 5x in wash buffer (50 mM Tris pH 7.4, 150 mM NaCl, 0.05% NP-40, 1 mM $MgCl_2$). Elution was performed 30 minutes at 55°C in 100 μl wash buffer supplemented with 30 μg proteinase K, and RNA isolated by adding three volumes of Trifast-FL (Peqgold) and Direct-zol extraction kit (Biozym), following manufacturer instructions. Libraries from biological triplicates were generated with Truseq stranded total RNA library prep kit (illumina) and sequenced on Nextseq500. The same procedure was applied for samples to be sent for mass-spectrometry analysis with the following modifications. Before clearing the lysates via centrifugation, half of them were RNaseI-treated for 5 min at 37°C with 200 units per 8 mg of lysate. Anti-MOV10 antibody and anti-rabbit IgG were cross-linked to the beads. Elution was performed in 3x 80 μl 0.2 M glycine buffer pH 3, neutralized in 45 μl of 1 M Tris, and pull-downs were ethanol-precipitated.

Data availability

Part of the NGS data reported in this thesis are deposited on Array Express with the accession numbers E-MTAB-7251 (3′end-seq), E-MTAB-4978 (RNA-seq), and E-MTAB-4979 (Ribo-seq). Mass spectrometry data are deposited on ProteomeXchange with the identifiers PXD004640 and PXD005059.

4 Results

Contributions from colleagues, when present, are stated for each figure in the caption section.

4.1 Separation of somatic and neuritic compartments is enabled by means of a microporous filter

This thesis aims to study how RNA metabolism can be regulated at the level of mRNA localization and local translation. I used a highly polarized cell system – induced neurons (iNs) - from which I analyzed the soma and the neurites as separate subcellular compartments. To highlight the suitability of the system and the necessary steps to assess its reliability, I first describe how the system works and all the controls introduced for handling the separation of the compartments.
iNs derived from mouse embryonic stem cells (mESCs) can be differentiated towards the neuronal fate through the formation of embryoid bodies (EBs), which are three-dimensional floating aggregates of pluripotent stem cells. EBs undergo differentiation and cell specification, spontaneously towards the ectoderm lineage (Behringer et al., 2016). With the additional induction of a pioneer transcription factor, ASCL1, it is possible to obtain a highly homogeneous population of excitatory neurons which possess all the basic neuronal properties: expression of mature neuronal markers, exhibition of passive and active intrinsic membrane properties, formation of functional synapses (Vierbuchen et al., 2010, Heinrich et al., 2011, Pang et al., 2011, Wapinski et al., 2013, Chanda et al., 2014, Liu et al., 2015, Raposo et al., 2015, Treutlein et al., 2016). This system is well-suited for genome-wide studies: it provides large amounts of material easily and relatively fast (7 days); it allows to grow functional neurons without the addition of neurotrophic factors, reducing both costs and handling times. Moreover, it ensures homogeneity of the culture, avoiding contamination from unrelated cell types affecting primary cultures, which often times is preparation-specific.

The differentiation protocol (described in depth in chapter 3.2.1) provides a useful tool for studying different cellular compartments, as the floating EBs can be transferred on a filter for the last step of neuronal differentiation. The filter allows the sprouting neurites to grow through the pores of the filter, on the opposite side of the somatic bodies. The separation is accomplished via size-selection: neurites can pass through the pores - which measure 3 μm in diameter (d) - thanks to their smaller size (d_{axons} = 0.3 μm, $d_{dendrites}$ = 0.9 μm) (Braitenberg and Schüz, 1998), whilst somatic bodies are too large and remain stuck on top (d = 20 μm) (Bannister and Larkman, 1995, Harris and Stevens, 1989). Moreover, the migration of the neurites to the bottom of the filter is ensured by the presence of an attractive coating agent - matrigel - obtained from the Engelbreth-Holm-Swarm (EHS) mouse sarcoma, containing several extracellular matrix molecules, approximately 60% laminin, 30% collagen IV, and 8% entactin (Zhang and Hu, 2013). The performance of this system was assessed by IF: DAPI and NF were used to mark nuclei and neurites, respectively (Fig. 4.1), and a complete z-stacks across the whole filter was acquired. Importantly, a precise separation of the upper and lower stacks was enabled by the filter's background signal in the DAPI channel (Fig. 4.1, right panel). This result confirms that the filter pores are big enough for the neurites to pass through, and small enough for the cell body to be trapped on top. Neurites are indeed able to grow through the pores on the bottom of the filter, whilst nuclei are present on the top only.

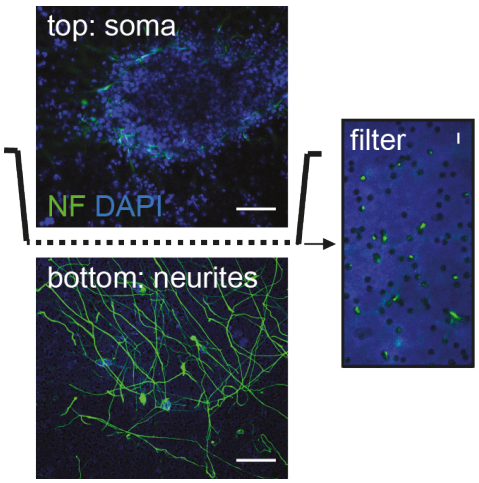

FIGURE 4.1: **Separation of iNs using a microporous filter device.** Efficiency of separation is confirmed with fluorescent micrographs of iNs above (top) and below the filter (bottom). NF: green, DAPI: blue. Size of each slice: 0.3 μm. Thickness of the filter: 9 μm. Scale bar: 50 μm. Neurites grow from the cell body (on top) through the pores of the filter to the bottom. IF by A. Zappulo.

4.1.1 Effective separation of somatic and neuritic compartments in iNs

Once the neurons are differentiated on the filter, soma and neurites are individually collected to be processed separately. Since the separation of the compartments is mechanical, accomplished by cleaning one or the other side of the filter, it might result in sample contamination. To assess the quality and purity of the two compartments I implemented several controls at RNA and protein levels.

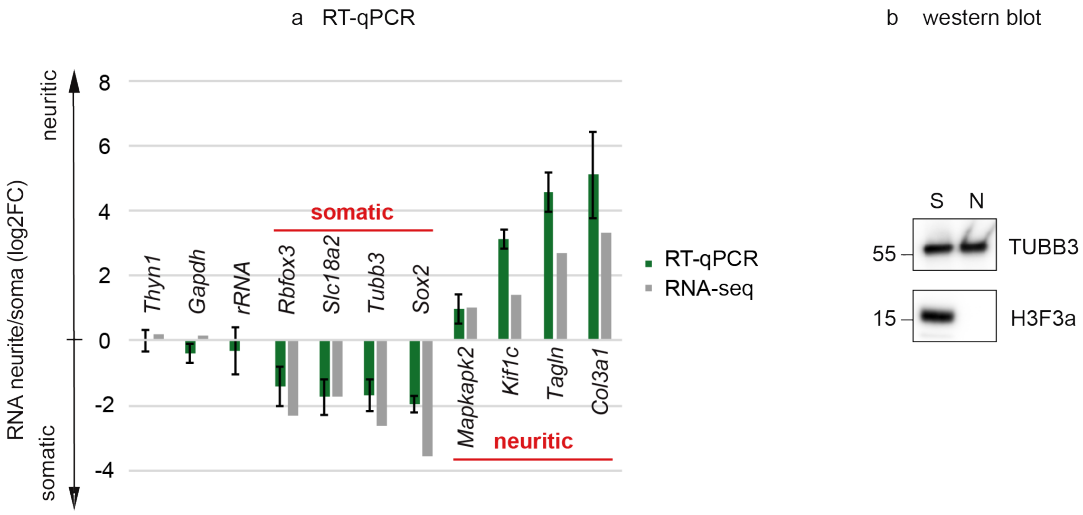

FIGURE 4.2: **Quality of compartment separation in Ascl1-iNs at protein and RNA levels.** a| qRT-PCR for selected controls for compartment separation: *Thyn1* (reference RNA, used for normalization), *Gapdh*, *rRNA* were used as unlocalized controls. *Rbfox3*, *Slc18a2*, *Tubb3* as soma-localized. *Mapkap2*, *Kif1c*, *Tagln*, *Col3a1* as neurite-localized controls. Error bars represent SD for two (neurites) to three (soma) biological replicates. Neurite/soma enrichment based on RNAseq data (in grey) is shown as reference next to RT-qPCR bars (in green). b| Protein lysates prepared from neurite and soma fractions were analyzed by western blotting. Histone H3F3a was used as a marker for soma, and TUBB3 is present in both soma and neurites.

At RNA level, I used RT-qPCR to evaluate the correct compartment enrichment of several marker genes (Fig. 4.2, panel a). For the somatic compartment I used *Rbfox3*, *Slc18a2*, *Tubb3*, and *Sox2*, which additionally to being soma-localized, are also markers for neuronal differentiation (Masserdotti, Gascón, and Götz, 2016). Specifically, *Rbfox3* encodes for the neuronal nuclei (NeuN) antigen that has been widely used as post-mitotic neuronal marker: it is mainly expressed in the central nervous system and plays a prominent role in neural tissue development and regulation of adult brain function (Gusel'nikova and Korzhevskiy, 2015). *Slc18a2* encodes for a transmembrane protein that transports amine neurotransmitters such as dopamine, norepinephrine, serotonin, and histamine into synaptic vesicles (Nirenberg et al.,

Gene name	**Ascl1-iNs**	**Cortical neurons**	**Dorsal root ganglia**	**Neuropil**
Slc18a2	-0.654	-	-2.07	-
Tubb3	-2.466	-	-1.859	-0.3542
Mapkapk2	1.218	1.731	1.244	1.759
Kif1c	1.66	1.555	3.471	-
Tagln	3.293	-	3.549	3.3367
Col3a1	3.523	-	2.231	1.3519
Syn1	-	-	-	-0.0668
Gria2	-	-	-	-0.5978
Grin1	-	-	-	-0.3359
Homer2	-	-	-	1.3378
Neurl1	-	-	-	1.8362
Dok6	-	-	-	1.7879
Jph3	-	-	-	0.9659
Psd95	-	-	-	0.9441

TABLE 4.1: Log2FC enrichment (neurites/soma) of localized transcripts in Ascl1-iNs (Zappulo*, Van Den Bruck*, Ciolli Mattioli*, Franke* et al., 2017), cortical neurons (Taliaferro et al., 2016), dorsal root ganglia (Minis et al., 2014), and neuropil (Tushev et al., 2018)

1995). Tubulin exists in different isotypes, alpha and beta, that heterodimerize and polymerize to form microtubules, and *Tubb3* is a classic neuronal marker as it encodes the only β-tubulin isoform constitutively expressed in all neurons (Ferreira and Caceres, 1992). *Sox2* characterizes neuronal progenitors, moreover small increases in its expression trigger differentiation of embryonic stem cells (ESCs) (Kopp et al., 2008). For the neuritic compartment I selected markers such as *Col3a1*, *Tagln* and *Mapkapk2* which are involved in cytoskeleton organization, shown to be critical for neurite outgrowth (Conde and Cáceres, 2009, Corrêa and Eales, 2012), and *Kif1c* involved in vesicle transport inside the cell (Schlager et al., 2010). Importantly, these markers were all found to be neurite-localized in compartment-specific datasets obtained from different types of primary neurons (cortical neurons, primary root ganglia, and neuropil, a region of the brain enriched in unmyelinated axons, dendrites and glia cell processes, containing a relatively small number of cell bodies) (Taliaferro et al., 2016, Minis et al., 2014, Tushev et al., 2018) (table 4.1).

As protein markers, I used H3F3a as somatic marker because of its nuclear localization, and TUBB3, commonly known as TUJ1, which is equally distributed between the compartments (Fig. 4.2, panel b). Noteworthy is the discrepancy of TUBB3 compartment enrichment at RNA and protein levels. This is explained by the fact that the protein is mainly synthesized in the somatic compartment and then transported: it has been previously shown in sympathetic neurons that less than 1% of the β-tubulin is axon-synthesized (Eng, Lund, and Campenot, 1999).

The enrichment of these markers was assessed in all the experiments where Ascl1-iNs were used.

4.1.2 Effective separation of somatic and neuritic compartments in primary neurons

I also applied compartment separation to primary neurons isolated from E16 mouse's cortex, used for validation experiments. I used primary neurons for biochemistry and microscopy experiments only, where non-neuronal contamination is irrelevant as I could discriminate visually or by means of neuron-specific promoter employed for reporter expression.

Primary cells were grown *in vitro* for 14 days, with some modifications: filters were double coated with poly-D-lysin and laminin instead of matrigel. As for Ascl1-iNs, the ability of growing through the pores of the filter device was assessed via IF, and the purity of compartment separation was evaluated by RT-qPCR and western blot (Fig. 4.3). Staining of the filter reveals an intricate bundle of neurites on the bottom, without nuclei contamination (Fig. 4.3, panel a).

For RNA quality controls, I chose *Syn1*, *Tubb3*, *Gria2* and *Grin1* as somatically-enriched neuronal markers, and *Homer2*, *CamkIIα*, *Neurl1*, *Dok6*, *Jph3*, and *Psd95* as neuritically-enriched neuronal markers. All markers showed the localization (Fig. 4.3, panel b) expected from a published dataset obtained from neuropil (a region of the brain enriched in unmyelinated axons, dendrites and glia cell processes, containing a relatively small number of cell bodies) (Tushev et al., 2018, table 4.1). When handling primary cells, it is particularly important to ensure the purity of the samples: often times during the dissection procedure, other cell types can be carried over, especially astrocytes and glia cells (Fig. 4.4).

For this reason in RT-qPCR, additionally to markers which stand for good separation of soma and neurites, I also used markers ensuring the purity of the preparation and compared them with cDNA obtained from a pure astrocytes culture (Fig. 4.3, panel b). In particular, synapsins represent 9% of the total amount of vesicle proteins in neurons, which make them the most abundant neuron-specific phospho-proteins regulating neurotransmitter release (Greengard et al., 1993). *Grin1* and *Gria2* encode for a subunit of the aspartate and glutamate receptor, respectively (Iida and Kozasa, 2004, Miller and Yeh, 2016). *Homer2* is a scaffold protein involved in intracellular calcium homeostasis and in regulation of glutamate receptor function (Foa and

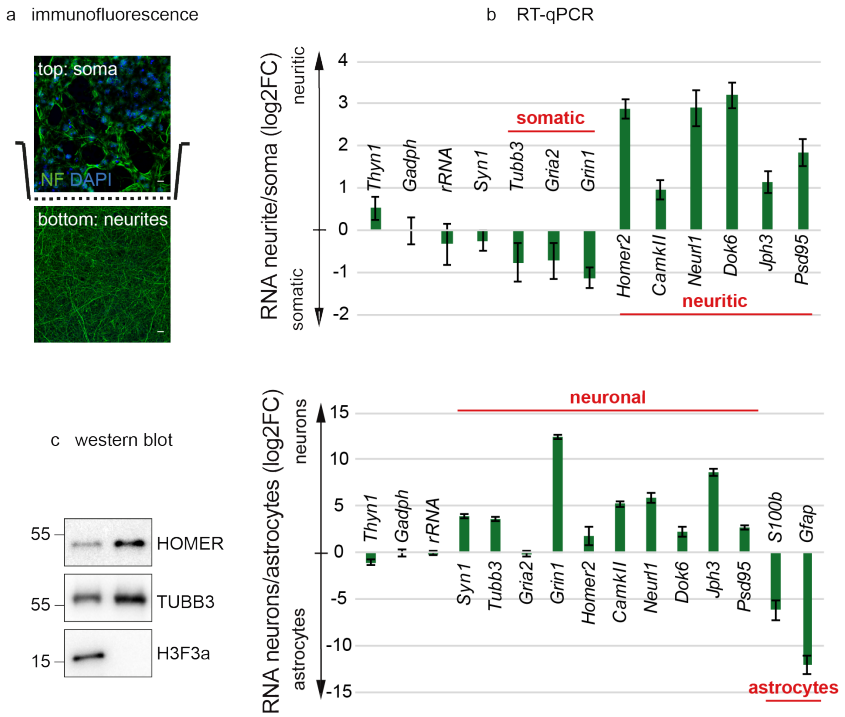

FIGURE 4.3: **Quality of compartment separation in primary neurons.** a | Efficiency of separation is confirmed with fluorescent micrographs of cortical neurons from E16 at DIV14 above (top) and below the membrane (bottom). NF: green, DAPI: blue. Size of each slice: 0.3 μm. Thickness of the filter: 9 μm. Scale bar: 10 μm.
b | In the upper part qRT-PCR for selected controls for compartment separation: *Thyn1*, *Gapdh* (reference RNA, used for normalization), *rRNA*, *Syn1* were used as unlocalized controls. *Tubb3*, *Gria2*, *Grin1* as soma-localized. *Homer2*, *CamkIIα*, *Neurl1*, *Dok6*, *Jph3*, *Psd95* as neurite-localized controls. In the lower part qRT-PCR for selected controls for primary cell contamination: *S100b* and *Gfap* were used as markers for astrocytes, the rest as markers for neurons. Error bars represent SD for two biological replicates. c | Protein lysates prepared from neurite and soma fractions were analyzed by western blotting. Histone H3F3a was used as a marker for soma, and HOMER as a marker for neurites. TUBB3 was used as loading control.

Gasperini, 2009). *CamkII* belongs to the Ca2+/calmodulin-dependent protein kinase subfamily, and regulates calcium signaling, crucial for plasticity at glutamatergic synapses (Soderling, 2000). *Dok6* belongs to the tyrosine kinase/docking protein adaptor protein family and it was shown to be involved in neurite outgrowth in mouse cortex neurons (Li et al., 2010). *Jph3* is a component of junctional complexes, common feature of all excitable cell types, present between the plasma membrane and the ER, and mediating cross talk between the cell surface and intracellular ion channels (Garbino et al., 2008). *Psd95* is a membrane-associated guanylate kinase, which is recruited into NMDA receptor and potassium channel clusters, and constitutes the major scaffolding protein in the excitatory postsynaptic density (Ziff,

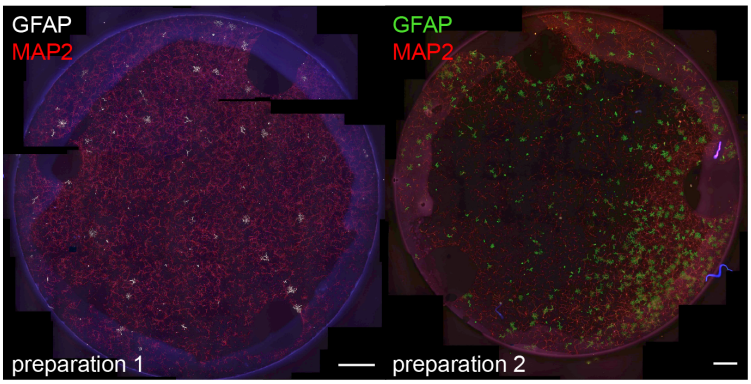

FIGURE 4.4: **Astrocytes contamination of primary culture is prep specific.** Contamination of primary neurons is shown with GFAP immunostaining on mouse cortical neurons from P0 at DIV7 in two different preparations. GFAP: white, MAP2: red. Scale bar: 1 mm. Images were stitched using ImageJ to reconstruct a 12-well coverslip.

1997). Moreover, *S100b* and *Gfap* were added as astrocytes markers, and all the markers show the correct enrichment showing a high degree of purity of the preparation, apart from *Gria2* which indeed is also expressed in astrocytes (Fan et al., 1999).

As protein markers, additionally to H3F3a and TUBB3 already used for Ascl1-iNs, I also performed HOMER immunoblot, confirming the neuritic enrichment (Fig. 4.3, panel c).

The enrichment of these markers was assessed in all the experiments where primary cells were used.

4.2 Ribosome profiling as a tool to study local translation in iNs

Neuronal homeostasis is sustained by local translation in both dendrites and axons (described in chapter 1.1.2). However, the extent of such a mechanism remains unclear and controversial. To investigate how much local translation defines the local neuritic proteome, I performed ribosome profiling on each of the compartments - soma and neurites - separately. I will first go through the optimization that was required to apply this technique to the isolated

subcellular compartments (chapter 4.2.1), and then I will describe the results that show the contribution of local translation in iNs (chapter 4.2.2).

4.2.1 A simplified version of ribosome profiling performs as well as the established method

Ribosome profiling is a technique which allows to quantitatively characterize the translational landscape by sequencing of ribosome protected footprints (RPFs) (Ingolia et al., 2009) (previously described in chapter 1.4.2). One of the biggest challenge to apply this technique to the study of local translation, is the amount of input required to perform the experiment, that is extremely large, around 30 - 50 μg of total RNA per sample (McGlincy and Ingolia, 2017). With our compartment separation approach, the average amount of total RNA obtained from the neuritic compartment accounts for $\sim$ 200 ng / filter, not compatible with ribosome profiling. Specifically, reaching the suggested input would require pulling together 150 filters. If one calculates a cleaning time of around 7 min / filter, this translates in a processing time of 17 hours per replicate. Because of this infeasibility, I evaluated different methods to adapt it to those cases where the input material is a limiting factor. Moreover, even though ribosome profiling is widely used, it lacks standardization. I optimized several steps of the protocol, resulting in a smaller loss of material, aiming to a simplification of a cumbersome procedure. In brief, the protocol comprises cell lysis, nuclease digestion, isolation of monosomes, rRNA depletion, gel-separation of RPFs, and library preparation (Fig. 4.5).

For the optimization, I tested different types of nucleases for the footprinting step, and different monosome isolation methods. I specifically focused on these two steps for the following reasons:

(i) footprinting is crucial for obtaining high quality data at single nucleotide resolution;

(ii) monosome isolation can be accomplished in several different ways, therefore amenable to standardization.

Starting with RNA footprinting, this step is achieved by the use of endoribonucleases, which hydrolyze unprotected single or double-stranded RNA. Different types of endonucleases exist, and depending on the test organism some are more suitable than others. In fact, RNases were shown to differently affect ribosome integrity in different organisms (Gerashchenko and Gladyshev, 2017). I tested RNaseI and micrococcal nucleases (MNases). RNaseI

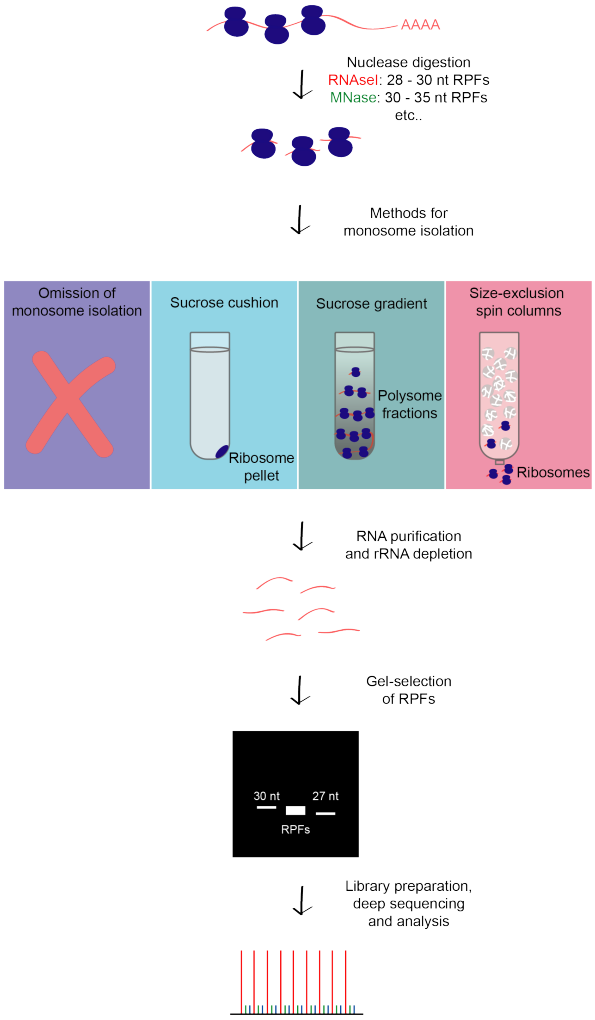

FIGURE 4.5: **Ribosome profiling workflow.** Ribosome footprints are generated by digesting the cellular lysate with a ribonuclease. Monosomes are isolated by ultracentrifugation or size-exclusion chromatography (optional). Following RNA purification and rRNA depletion, RPFs are separated on a gel, and converted into a DNA library for sequencing.

doesn't display any cutting preference, which is a valuable quality for ribosome profiling. In fact, one of the most important parameter to assess ribosome profiling performance is sub-codon phasing (or triplet periodicity), which goes hand in hand with obtaining RPFs of a specific length. MNase was shown to not damage the structural integrity of ribosomes, and this is an important feature, especially in model organisms such as *Drosophila*, where the unusual rRNA sequences and structures determine a hyper-sensitivity to RNaseI (Dunn et al., 2013, Hancock, Tautz, and Dover, 1988), leading to rRNA contamination of the libraries. MNase produces fragments of a longer size (35 nt) (Reid, Shenolikar, and Nicchitta, 2015), which arise from a strong 3′A/T cutting bias (Dingwall, Lomonossoff, and Laskey, 1981) that can affect peptidyl-site (P-site) mapping, mining sub-codon phasing.

Regarding monosome isolation, this step can be accomplished in several ways, i.e. via sucrose cushion, sucrose gradient, and via size-exclusion columns (Fig. 4.5). I tested size-exclusion columns and I compared them with a protocol where this step was omitted, relying on the very specific length of RPFs instead, readily separable through gel purification.

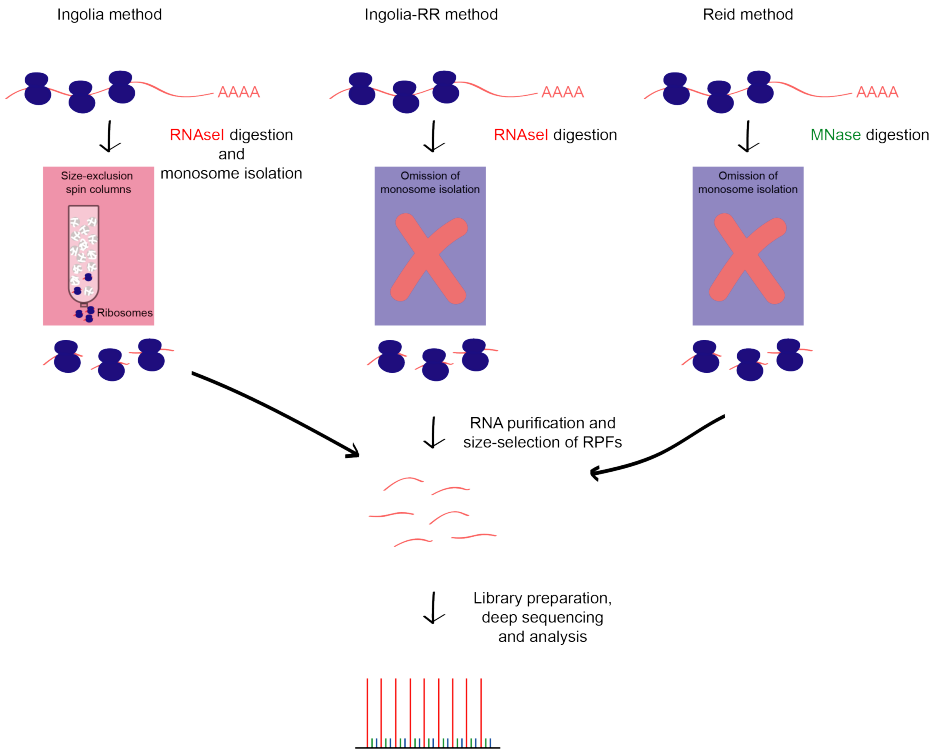

FIGURE 4.6: **Ribosome profiling methods' comparison.** Workflow of three different protocols tested in this thesis, where we compared different types of ribonucleases for the footprinting steps (RNaseI vs MNase), and different types of monosome recovery methods (size-exclusion chromatography vs omission of this step).

In summary, I compared three different protocols: in the first one (based on Ingolia et al., 2009) I used RNaseI for footprinting and size-exclusion columns for monosome isolation (Ingolia method); in the second one (based on Reid, Shenolikar, and Nicchitta, 2015) I used MNase for footprinting and omitted monosome isolation (Reid method); and a third mixed version where I used RNaseI for footprinting and omitted monosome isolation (Ingolia-RR method) (Fig. 4.6).

Computational analysis was performed by Lorenzo Calviello. Each library was assessed through several parameters: correlation heatmap (Fig. 4.7, panel a), mapping distribution (Fig. 4.7, panel b), length of RPFs (Fig. 4.8, panel a), % of read in frame (Fig. 4.8, panel b), and periodicity (Fig. 4.9). A very high correlation is observed between Ingolia and Ingolia-RR libraries,

whilst Reid libraries poorly correlate with the other two (Fig. 4.7, panel a). This might be due to the difference in mapping, as described below.

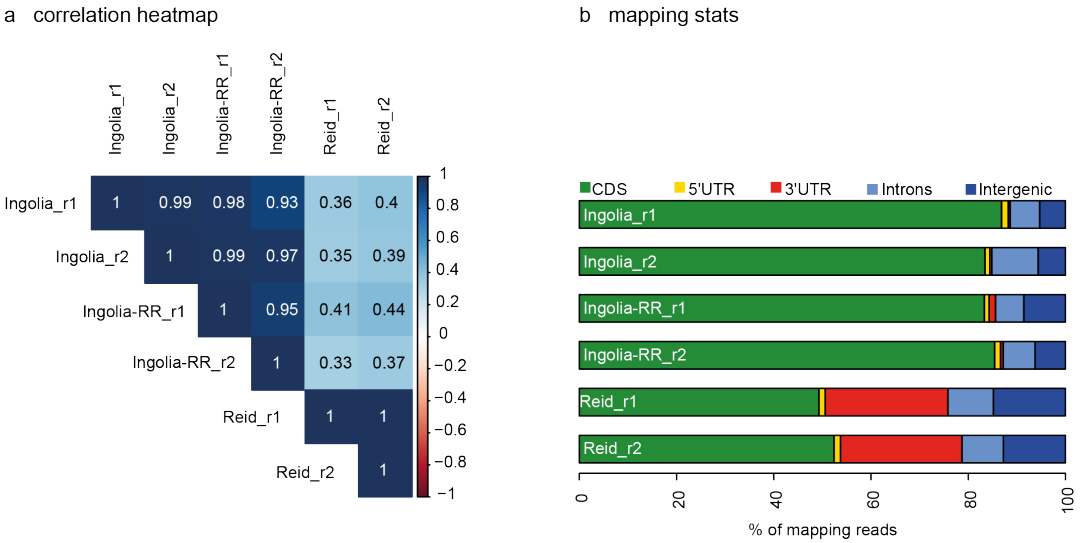

FIGURE 4.7: **Ribosome profiling mapping statistics.** a | Correlation heatmap of Ribo-seq libraries. b | Barplot depicting mapping statistics of Ribo-seq reads. CDS: green. 5′UTR: yellow. 3′UTR: red. Introns: light blue. Intergenic regions: blue. Analysis by L. Calviello.

Mapping distribution shows that most of the reads for Ingolia and Ingolia-RR libraries come from coding sequence (CDS), as expected from ribosome profiling data (Fig. 4.7, panel b). In Reid libraries instead, only 50% of the reads map to CDS, and around 30% to 3′UTR, with an increase in intergenic regions too. The presence of abundant reads mapping to 3′UTR in MNase-treated samples was consistent with previous studies where MNase was used instead of RNaseI. According to Reid and colleagues, RNaseI might damage the ribosomes resulting in loss of 3′UTR reads (Reid, Shenolikar, and Nicchitta, 2015). Miettinen et al. previously speculated that 3′UTR reads from ribosome profiling experiments might come from 3′UTRs interacting with ribosomes bound on the CDS (Miettinen and Bjorklund, 2015), idea supported by Eldad and colleagues (Eldad, Yosefzon, and Arava, 2008). In these studies, association of 3′UTRs and their ORFs was suggested to be intra-molecular or to happen through the binding of the 3′UTR to the ribosomes that are sitting on the CDS. To assess the nature of 3′UTR-ribosome binding, Eldad et al. used a range of salt concentrations, where the high concentration stabilizes interactions that are based on nucleotide base-pairing and minimizes weak ionic protein-RNA interaction (Eldad, Yosefzon, and Arava, 2008). In high salt condition, a disruption of co-precipitation of 3′UTRs with their cognate CDS was observed. On the other hand, Miettinen et al. observed the opposite effect in relation to salt concentration (Miettinen and Bjorklund, 2015),

making these results unclear and difficult to interpret. Alternatively, association of ribosomes with 3′UTRs may be due to ribosome migration through the stop codon (readthrough), a mechanism commonly exploited by viruses to complete their reproductive cycle (Cimino et al., 2011), and shown to be pervasive in *Drosophila* (Dunn et al., 2013). Ribosome readthrough might increase the complexity of the proteome by extending the protein C-terminus, as it was recently observed in cortical neurons, for 13 transcripts (Sapkota et al., 2019). Interestingly, in this study RNaseI was used, showing that readthrough events are possible to capture independently of the enzyme used in the footprinting step. Since readthrough events were also captured with RNaseI, the different content in reads mapping to 3′UTRs cannot be explained with the stronger harshness of RNaseI. On the contrary, MNase might be not harsh enough to digest all the non-protected mRNAs.

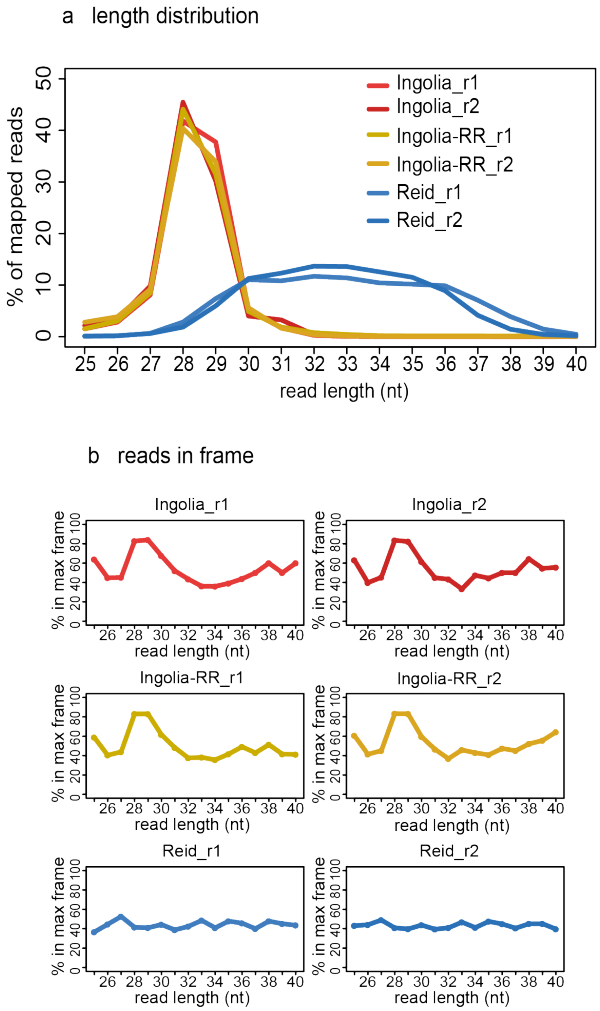

FIGURE 4.8: **Ribosome profiling reads distribution.** a| Metagene plots showing length distribution of mapped Ribo-seq reads. b| Metagene plots showing the percentage of reads in frame relative to the read length. Analysis by L. Calviello.

These experiments show that nucleases affected RPFs length: RNaseI produces fragments of 28 - 29 nt, corresponding exactly to the size of a translating eukaryotic ribosome on the mRNA (Wolin and Walter, 1988); MNase generates a range of fragments between 30 - 36 nt, with a wide distribution around the mean of 33 nt (Fig. 4.8, panel a). These results reflect the cutting properties of the nucleases: RNaseI is able to cut anywhere therefore produces precise RPFs, and MNase is biased towards 3′A/T cut therefore produces a range of RPFs of different lengths dependent on the sequence context.

The relationship between mapped reads' length and percentage of reads in frame show that 80% of the 28 - 29 nt RPFs obtained with RNaseI are in frame with the CDS, whilst for MNase-derived RPFs 40% only are in frame, independently of the length of the fragments (Fig. 4.8, panel b). These results suggest that triplet periodicity might lack in Reid libraries. In fact, the metagene aggregate plots - displaying the positions of the reads from the annotated start codon - show that sub-codon phasing is completely lost in Reid libraries, whereas it is present in Ingolia and Ingolia-RR libraries (Fig. 4.9).

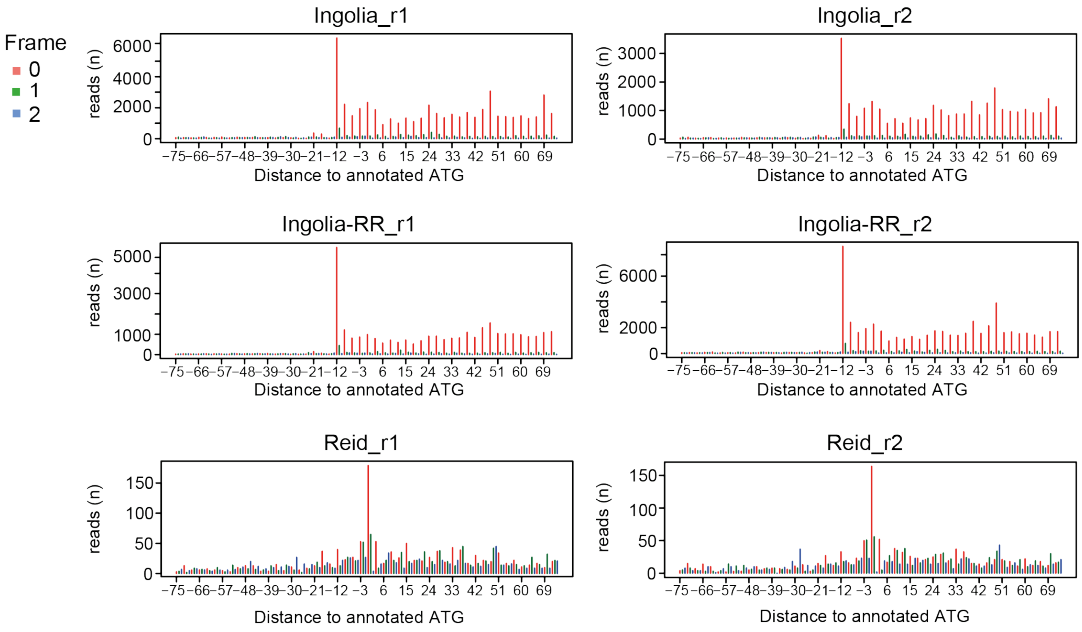

FIGURE 4.9: **Ribosome profiling reads periodicity.** Metagene aggregate plots displaying distance of 28-nt Ribo-seq reads from annotated start codon, each frame in a different color (see legend). The 5′-most peak (in position -12) in the metagene plots for Ingolia and Ingolia-RR libraries represents ribosomes with the start codon in the P-site and the second codon in the aminoacyl-site (A-site) Analysis by L. Calviello.

Based on this analysis, I concluded that Ingolia and Ingolia-RR protocols are the most reliable in terms of quality. Both show the hallmarks of *bona fide*

ribosome profiling data: CDS mapping reads, in-frame reads, and triplet periodicity. On the other hand, Reid libraries don't perform at the same extent in terms of sub-codon phasing. Moreover, there is not any gain in simplification when comparing Ingolia-RR and Reid protocols, and since the performance of Ingolia-RR resembles Ingolia's one, I concluded that Ingolia-RR version was the best option to proceed with. I gained in terms of amount of input material - with a 10x reduction - and in handling times, shortening the protocol from 5-7 days (Ingolia et al., 2012) to 2 days.

4.2.2 Local translation revealed by compartment-specific ribosome profiling

The successful optimization of the ribosome profiling protocol allowed me to combine it to the compartment-separation approach, in order to study local translation in the somatic and neuritic compartments of Ascl1-iNs. My interest was in understanding whether the local translatome would differ among different neuronal subcellular compartments. Through its simplification, I could use ribosome profiling to answer this question.

Computational analysis was performed by Vedran Franke. Mapping statistics relative to this experiment show high correlation between the replicates, majority of reads mapping to CDS (a relative high percentage of reads mapping to rRNA is to expect, not shown for the optimization libraries), and triplet periodicity assuring good quality of the data (Fig. 4.10).

From the enrichment analysis between soma and neurites, I could identify several transcripts differentially translated in either soma or neurites (Fig. 4.11). For instance, among the transcripts preferentially translated in the somatic compartment I found several transcription factors. *Neurog2* encodes for a proneural transcription factor which belongs to the family of the neural helix-loop-helix family, and controls neurogenesis at different levels (neuronal commitment, cell cycle exit, subtype specification, neuronal differentiation) (Bertrand, Castro, and Guillemot, 2002). *Nr0b1*, *Nr5a2*, and *Nr2e1* encode for members of the nuclear receptor superfamily. Specifically NR0B1 acts as a dominant-negative regulator of transcription mediated by the retinoic acid receptor, NR5A2 synchronizes induction of neurogenesis with cell-cycle exit (Stergiopoulos and Politis, 2016), NR2E1 is mainly expressed in developing brain and retina to maintain self-renewal capacity (Liu et al., 2008). *Rfx4* encodes for a winged helix transcription factor and it is crucial for brain development (Xu et al., 2018). On the other hand, some example of transcripts preferentially translated in the neurites are *Col3a1* and *Tagln* already

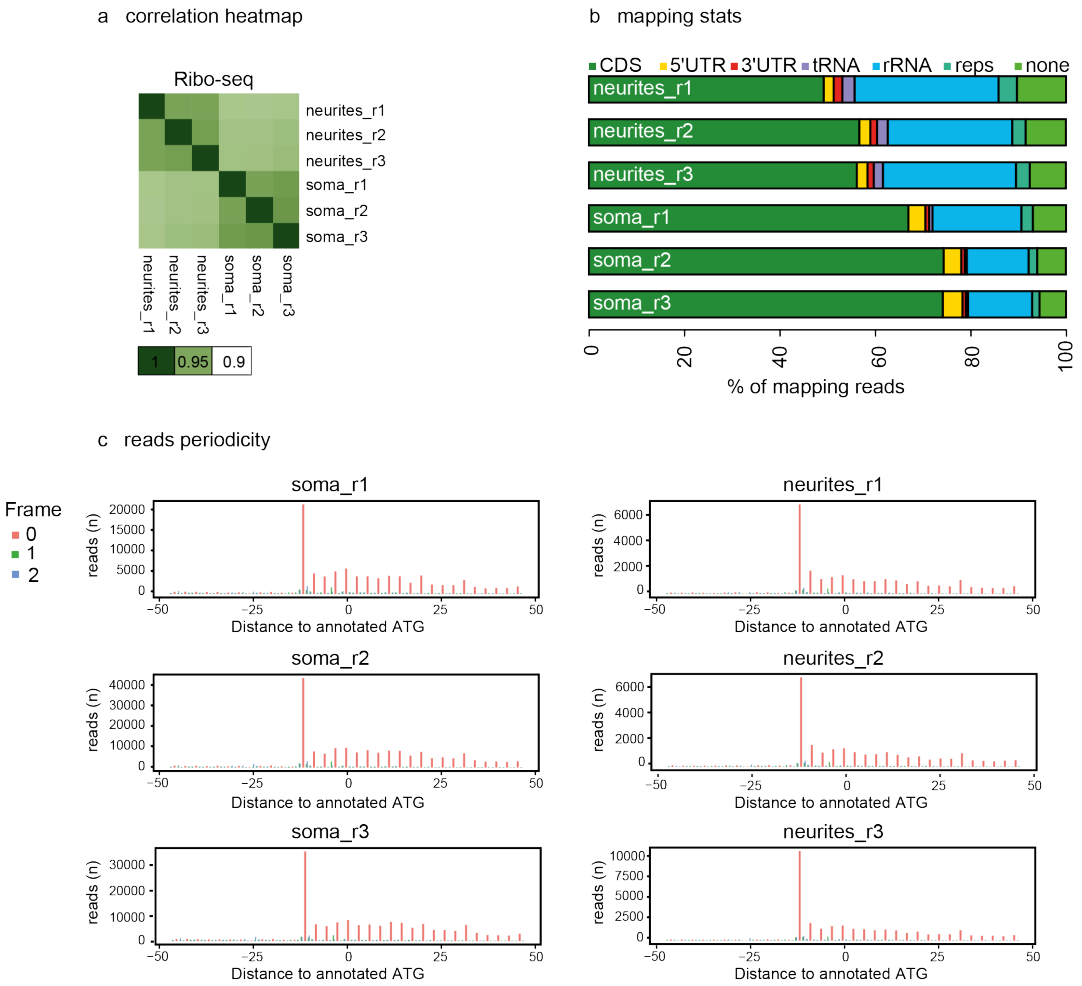

FIGURE 4.10: **Compartment-specific ribosome profiling statistics.** a | Correlation heatmap of Ribo-seq libraries obtained from the somatic or neuritic compartments. b | Barplot depicting mapping statistics of Ribo-seq reads. CDS: green. 5′UTR: yellow. 3′UTR: red. tRNA: violet. rRNA: light blue. Repetitive elements: cyan. None: green. c | Metagene aggregate plots displaying distance of 29-nt Ribo-seq reads from annotated start codon. Analysis by V. Franke.

introduced in chapter 4.1.1. *Mpz*, which encodes for myelin protein zero, an homophilic adhesion plasma-membrane protein, which is a major structural component of myelin in the peripheral nervous system (Roglio et al., 2008). *Fxyd1* encodes for a protein that maintains neuronal excitability by modulating Na^+, K^+-ATPase activity (Feschenko et al., 2003). *Plxnb3* encodes for a receptor of semaphorins, and promotes neuron projection outgrowth (Hartwig et al., 2005). *Clca2* encodes for a member of the calcium-activated chloride channel family and is widely expressed in brain (Piirsoo, Meijer, and Timmusk, 2009). GAS7 belongs to the Pombe Cdc15 homology protein family, and it has been shown to be involved in neurite outgrowth of hippocampal neurons (You and Lin-Chao, 2010). *Npy* encodes for neuropeptide Y which is a potent orexigenic neuropeptide widely expressed in the brain (Chee and

FIGURE 4.11: **Ribo-seq enrichment vs abundance.** Enrichment of Ribo-seq reads in neurite versus soma plotted against average abundance of Ribo-seq reads (RPKM mapped to CDS). Orange: transcripts preferentially translated in neurites (neurites/soma log2FC > 1, FDR (Benjamini Hochberg) < 0.05); blue: transcripts preferentially translated in soma (neurites/soma log2FC < -1, FDR (Benjamini Hochberg) < 0.05). Analysis by V. Franke.

Colmers, 2008). *Sema3g* encodes for an endothelium-secreted protein which regulates synaptic structure and plasticity in hippocampal neurons (Tan et al., 2019). It belongs to the semaphorin protein family, a large family of secreted and membrane-associated axon guidance molecules which function as attractants or repellents (Goodman et al., 1999). Among them, I also identified *Sema3b*, *Sema3d* and *Sema3c* as neurite-enriched.

Besides these specific examples, a GO analysis on neurite-enriched genes (log2FC > 2, false discovery rate (FDR) < 0.05), shows several interesting categories among the biological processes-enriched terms (Fig. 4.12), such as:

(i) regulation of cellular component organization;

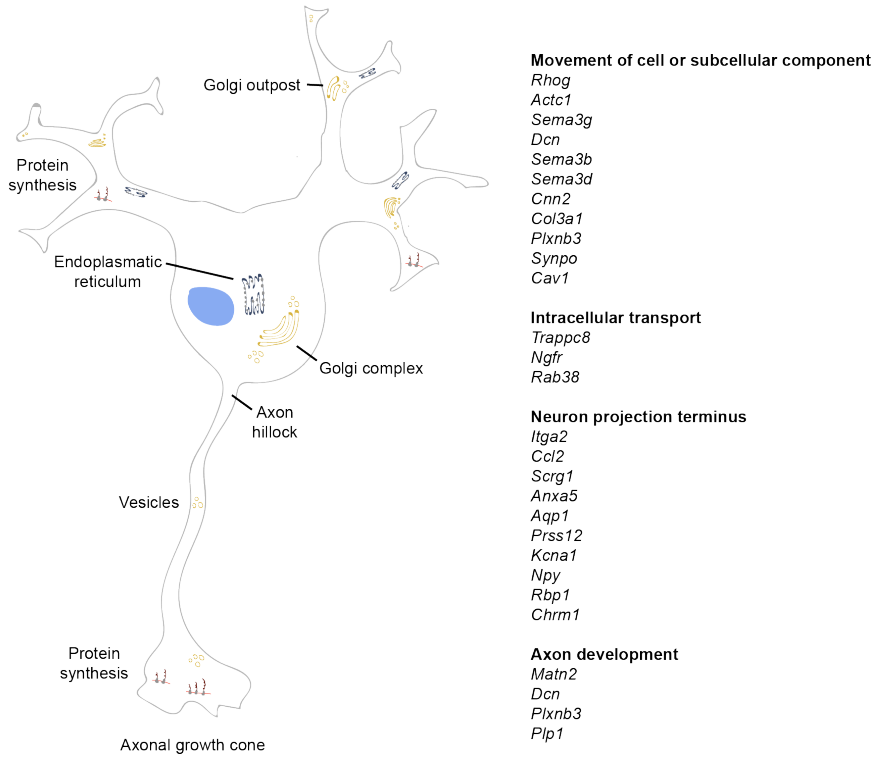

FIGURE 4.12: **Selection of GO terms of neurite-enriched translatome.** GO terms associated with neurite-enriched translatome (log2FC > 2, FDR (Benjamini Hochberg) < 0.05).

(ii) movement of subcellular component (to which cytoskeletal proteins belong);

(iii) intracellular transport;

(iv) axon development and myelination.

And among the cellular component-enriched terms:

(i) neuron projection terminus;

(ii) plasma membrane;

(iii) extracellular space.

In fact, in axonal growth cones synthesis of cytoskeletal proteins - which occurs on free ribosomes - seems to be prominent. It has been shown to regulate turning and advance (Lin and Holt, 2007), as well as growth cone regeneration after axotomy (Willis and Twiss, 2006). The presence of plasma membrane and extracellular proteins in neurite-enriched translatome is also not surprising: dendrites in fact can be considered as semi-autonomous regions of the neuron. They contain rough ER and Golgi outposts, which enable them to synthesize specific membrane proteins. On the other hand, axons

do not contain such organelles as the axon hillock prevents them from entering through a barrier involving the microtubule motor dynein (Zheng et al., 2008). Ribosomes and smooth ER are instead present (Bunge, 1973, Tennyson, 1970). Nevertheless, synthesis of membrane and lipid remodelling can also occur in axons: the modulation of responsiveness to guidance cues is supported by local translation of transmembrane and secreted proteins (Pfenninger, 2009), and it has been reported for at least two transmembrane proteins with established consensus glycosylation sites: the κ-opioid receptor and the guidance receptor EPHA2 (Bi et al., 2006, Tsai, 2006, Brittis, Lu, and Flanagan, 2002). Moreover, an immunolocalization study showed the presence of components belonging to the co-translational targeting machinery such as ER and Golgi proteins (Merianda et al., 2009) (see also chapter 1.1.2).

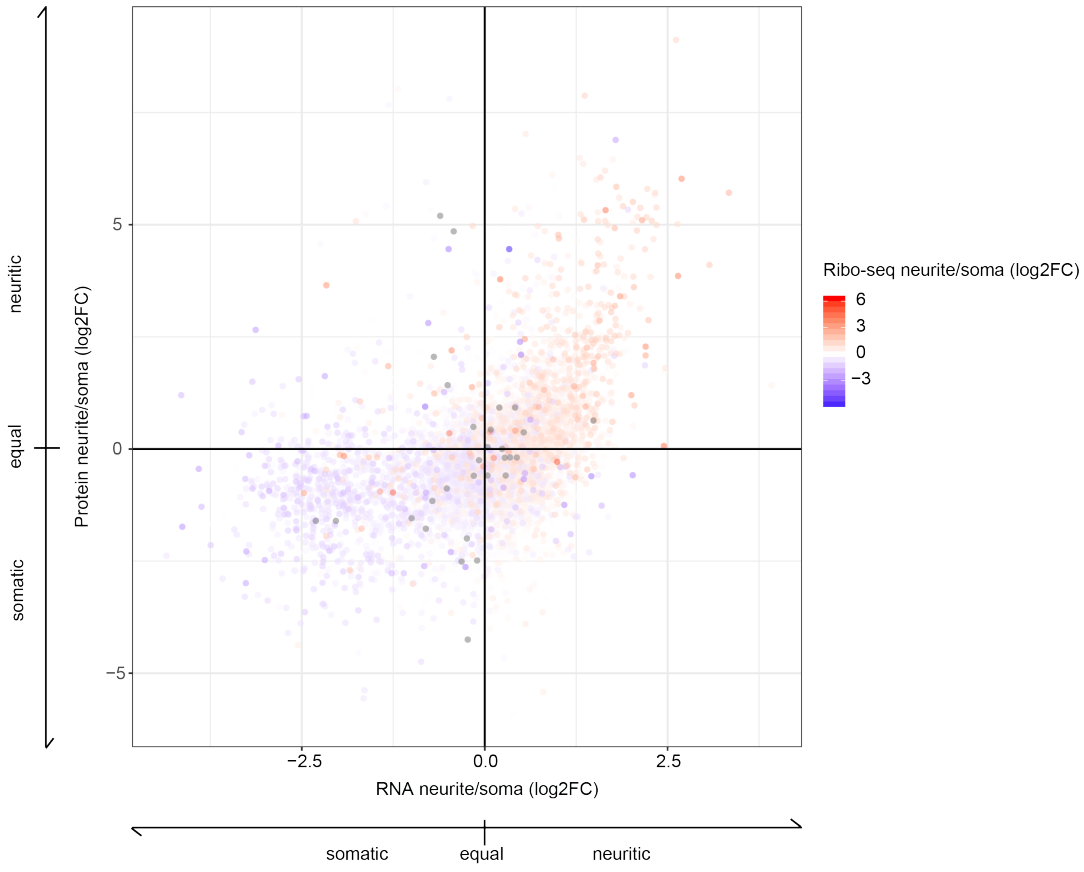

FIGURE 4.13: **Protein and RNA localization vs Ribo-seq.** RNA and protein enrichment in x- and y-axes respectively, color-coded for enrichment of Ribo-seq in neurite vs soma. Analysis by V. Franke and K. Imami. RNA-seq generated by D. van den Bruck. Proteins isolated by A. Zappulo.

To estimate how much of the local translation contributes to the formation of the local proteome, I overlayed the Ribo-seq data with the local transcriptome and proteome obtained through compartment-specific RNA-seq and

liquid chromatography-tandem mass spectrometry (LC-MS/MS) (produced by David van den Bruck and Alessandra Zappulo), and I observed a clear pattern of preferential translation for both of the compartments, in line with RNA and protein enrichment. In fact, in Fig. 4.13, the upper right quadrant contains proteins and mRNAs that are enriched in the neuritic compartment. Accordingly, these mRNAs are also preferentially translated there, as it is possible to appreciate from the color-coded positive log2FC values relative to Ribo-seq. The same is true for the somatic compartment, corresponding to the bottom left quadrant. This result shows that indeed RNA localization and local translation are the major determinants to the identity of local proteome.

Proteomics methods to study local translation

In order to acquire more evidence supporting the ribosome profiling results, where I observed extensive local translation happening in the neurites, pSILAC and QuaNCAT experiments were performed by David van den Bruck to compare novel synthesis with translation. pSILAC is a variation of SILAC where the labelling is only performed for a short period of time. QuaNCAT consists in quantitative noncanonical amino acid tagging. Both techniques allow to capture *de novo* synthesis (described in details in chapter 1.4.2). Even though the depth of proteomics analysis is much shallower compared to Ribo-seq (250 proteins, 450 proteins, 25,483 transcripts detected with pSILAC, QuaNCAT and Ribo-seq, respectively), a high correlation with both experiments was detected (0.51 and 0.56 with pSILAC and QuaNCAT, respectively), supporting the hypothesis that RNA localization and local translation are the main determinants for local proteome specification in Ascl1-iNs (Fig. 4.14).

Importantly, the correlation of pSILAC and QuaNCAT to Ribo-seq is higher than the correlation with mass-spectrometry (r=0.34). In fact, in the latter case, the presence of transported proteins negatively influences the correlation with Ribo-seq. Regarding this, it is important to consider that transported proteins might be present: even though the pulses were relatively short (2 hours for pSILAC and 30 min for QuaNCAT), I cannot exclude that proteins present in the neuritic pool could be localized there because of transport rather than local translation. In fact, considering a diffusion rate of noncanonical amino acids used for labelling of 1 mm/s (for a 10 nm plasma membrane to permeate) (Yang and Hinner, 2015, Heyden and Ortiz, 2017) and a translation speed of $\sim$ 5 amino acids per second (Chapter 1.1.2), an average protein of size $\sim$ 500 aa (like tubulin) could be translated in less than 2 minutes. Since the transport of cytoskeletal proteins follows a slow rate ($\sim$ 0.002 -

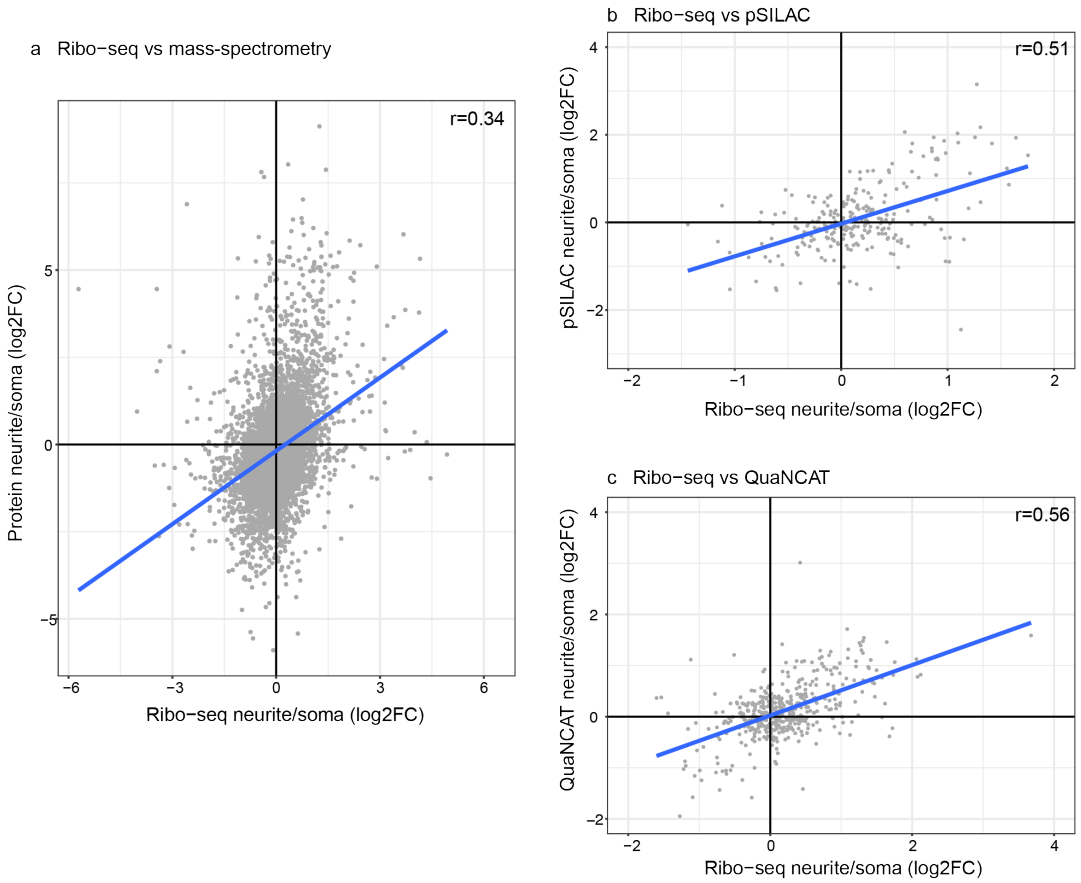

FIGURE 4.14: **Correlation of Ribo-seq with methods for quantification of protein synthesis.** a | Ribo-seq and pSILAC enrichment in x- and y-axes respectively. Pearson correlation = 0.51. b | Ribo-seq and QuaNCAT enrichment in x- and y-axes respectively. Pearson correlation = 0.56. Experiment by D. van den Bruck. Analysis by K. Imami and E. McShane.

0.011 μm/s) (Hirokawa, 1993, Grafstein and Forman, 1980, Roy, 2014), the remaining time after translation - when considering the 30 min pulse - would allow a movement of $\sim$ 3.36 - 18.5 μm (or 14 - 78 μm for a 2 hours pulse), enough to reach the neuritic compartment.

To conclude this chapter, I set up a protocol for ribosome profiling which gains in reduction of the input material and in processing times. With this optimized protocol I could perform ribosome profiling from subcellular compartments of iNs and identify several genes which are differentially translated between soma and neurites. By the comparison of Ribo-seq with transcriptomic and proteomic data, I can conclude that mRNA localization and local translation are the main determinants of the proteome identity in Ascl1-iNs.

4.3 Neurite-localized *trans*-acting elements: MOV10

From the previous experiments, I identified a strong degree of asymmetry between different cellular compartments, in terms of localized mRNAs, and I showed that local translation greatly contributes to the identity of the local proteome. Consequently, I decided to investigate which are the responsible factors for such a sectoral localization in Ascl1-iNs' neurites. In particular, I explored two directions of this topic, analyzing which *trans*-acting elements, namely RNA binding proteins (RBPs), could be responsible for RNA localization (this chapter), and whether different *cis*-elements might specify a specific address for a certain mRNA (chapter 4.4).

RBPs are important regulators of mRNA metabolism, including transport and translation (see chapter 1.1.2). In Ascl1-iNs, MOV10 is one of the neurite-localized RBPs (data not shown), which was chosen for further investigation. MOV10 is an RNA helicase belonging to the helicase superfamily 1 (SF1) (Fairman-Williams, Guenther, and Jankowsky, 2010), containing an N-terminal cysteine/histidine-rich domain (CH domain) and a C-terminal helicase core made of two RecA-like domains. RNA helicases are ATP-dependent enzymes, involved in RNA and RNA-protein complexes remodeling, through unwinding and RNPase activity. MOV10 is ortholog of the plant SDE-3 protein and of the *Drosophila melanogaster* Armitage protein, which are involved in RNA interference (RNAi) (Cook et al., 2004, Dalmay et al., 2001, Tomari et al., 2004). Consistently, MOV10 was found to coimmunoprecipitate with AGO2 (Meister et al., 2005, Chendrimada et al., 2007), and shown to be involved in translational regulation (Banerjee, Neveu, and Kosik, 2009, Kenny et al., 2014). Additionally to its association with the RISC complex and its role in translation regulation, MOV10 was shown to be implicated in antiviral defense, by inhibiting replication of human immunodeficiency virus type 1 virus (Burdick et al., 2010, Wang et al., 2010) and hepatitis C virus (Schoggins et al., 2011). Moreover, MOV10 was found to interact with UPF1, the main player in nonsense-mediated mRNA decay (NMD), and suggested to remodel secondary structures of mRNAs for UPF1-mediated degradation (Gregersen et al., 2014).

4.3.1 Identification of MOV10 targets by RIP and CLIP

First-of-all, I aimed at identifying MOV10 targets to verify its potential local function, given its neuritic localization. To identify MOV10 targets I used two different techniques: RIP and CLIP. Computational analysis was performed by Vedran Franke. Both techniques are antibody-based, and used to

map RNA-protein interactions. The RBP of interest is immunoprecipitated together with its associated RNAs for identification of bound transcripts. CLIP differs from RIP in the use of UV light to crosslink RNA to proteins, in the digestion of non-protected RNA, and in the isolation of RNA from protein-RNA complexes after SDS-PAGE separation and membrane transfer. In particular, photoactivatable ribonucleoside-enhanced crosslinking and immunoprecipitation (PAR-CLIP) relies on the incorporation of a ribonucleoside analog, 4-thiouridine (4sU), into nascent RNA transcripts. Cross-linking of 4sU at 365 nm results in thymidine to cytidine transitions, allowing the identification of the binding site with high accuracy (Hafner et al., 2010b).

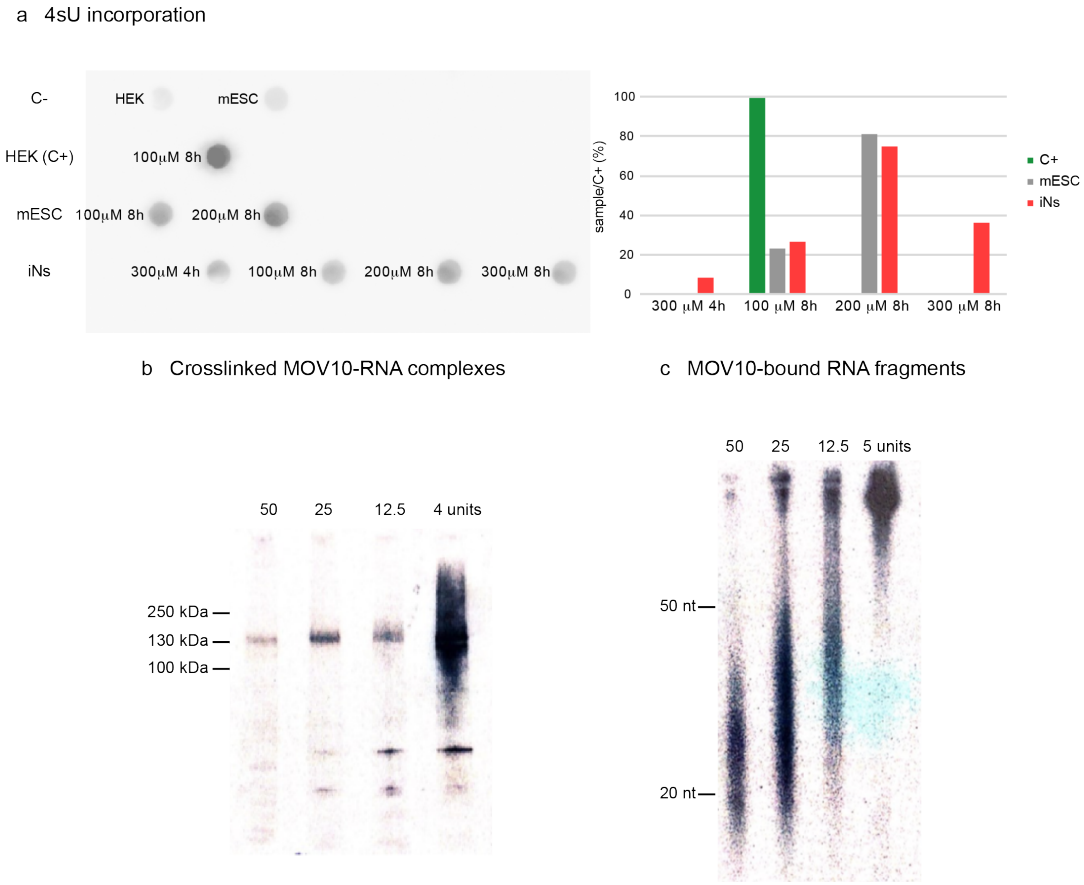

FIGURE 4.15: **Optimization of 4sU incorporation and RNase digestion.** a | 4sU incorporation was tested at different concentrations and at different incubation times. Cells used as negative controls were not incubated with 4sU. HEK were used as positive control. Both mESC and iNs were tested. Intensity of the 4sU signal was quantified and presented below the blot as fold enrichment versus the positive control. b | Autoradiograph showing MOV10 protein–RNA complexes that were treated with decreasing concentrations of RNaseI. c | Size separation of RNA fractions isolated from MOV10 protein–RNA complexes through proteinase K digestion. RNA was isolated from the region of the nitrocellulose membrane corresponding to MOV10.

I first tested 4sU incorporation to evaluate whether iNs would uptake 4sU

efficiently (Fig. 4.15, panel a). I tested different concentrations and incubation times, and by comparing to the positive control (HEK cells), iNs display a positive uptake, even though lower as compared to HEK (Fig. 4.15, panel a). Depending on the conditions tested, 4sU uptake ranged from 8 to 74% (setting the positive control to 100%). 200 μM for 8 hours was the best performing incubation.

Additionally, I tested several RNaseI digestion conditions (Fig. 4.15). It is important to evaluate fragment size after RNaseI digestion, to avoid over or under digestion and to select an optimal size for library preparation. When cell lysates were incubated RNaseI, and RNA was isolated after protein transfer on the membrane (Fig. 4.15, panel b), the fragments produced were in a range between 20 - 50 nucleotides to undigested, depending on the amount of RNaseI used (Fig. 4.15, panel c). PAR-CLIP libraries were obtained with the above selected conditions for 4sU incorporation (200 μM 8 hours) and RNaseI digestion (25 units per mg of lysate).

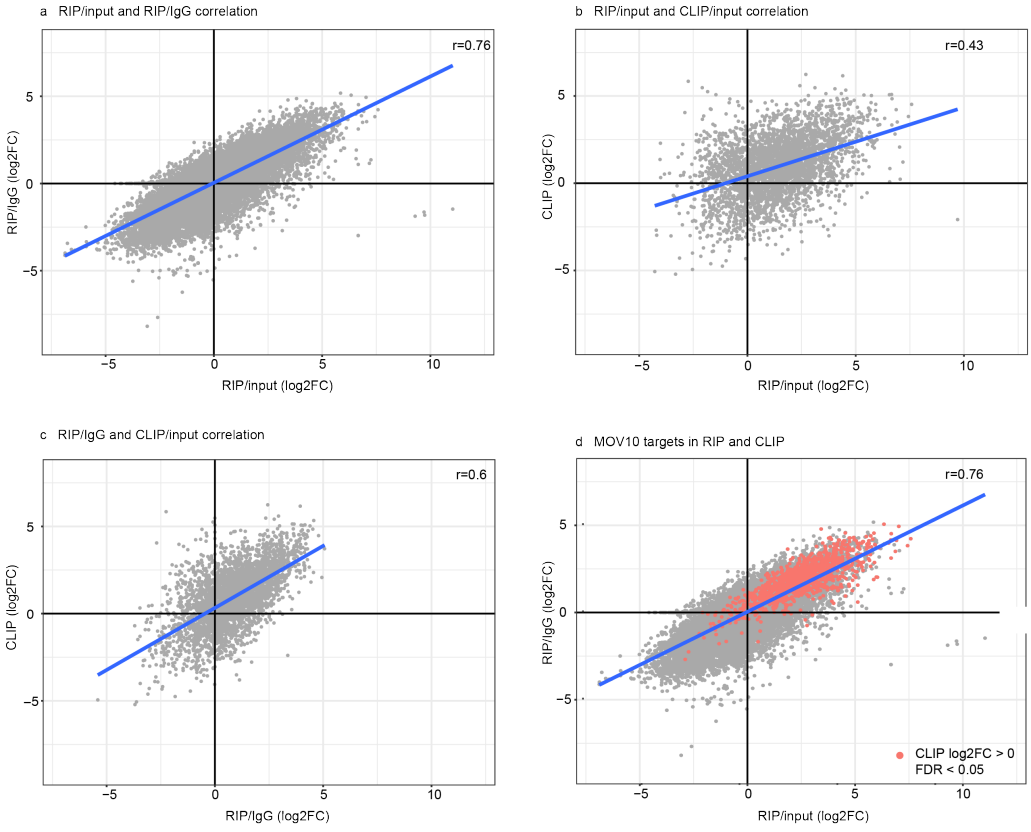

FIGURE 4.16: **MOV10-RIP and CLIP correlation.** a | Correlation among MOV10-RIP normalized against input or IgG controls. b and c | Correlation among MOV10-CLIP against RIP normalized to input (b) or IgG (c). r is the Pearson correlation coefficient. d | MOV10 targets identified with CLIP (MOV10-CLIP/input log2FC > 0, FDR (Benjamini Hochberg) < 0.05) are overlaid in red on RIP data. Analysis by V. Franke.

MOV10 targets were identified by calculating the enrichment in the pull-down compared to the input (total RNA) or to a control (IgG-pulldown). These two methods of selection were used for RIP, and showed a nice correlation (Pearson correlation = 0.76) (Fig. 4.16, panel a). In the case of PAR-CLIP, the IgG-pulldown did not allow to recover enough material to perform PAR-CLIP, therefore input only was used as control. PAR-CLIP also correlated with RIP (either RIP/input or RIP/IgG), however at a lower extent, with Pearson coefficients of 0.43 and 0.6, respectively (Fig. 4.16, panels b and c). What determines a lower correlation is not to be attributed to a contrasting detection of targets, but to the enrichment values. In other words, positive or negative enrichment is consistent among RIP and PAR-CLIP, what differs is the extent of the enrichment. In fact, MOV10 targets identified with PAR-CLIP, depicted in red in the panel d of Fig. 4.16, are also identified as targets in RIP, showing values above zero in the upper right quadrant of the plot.

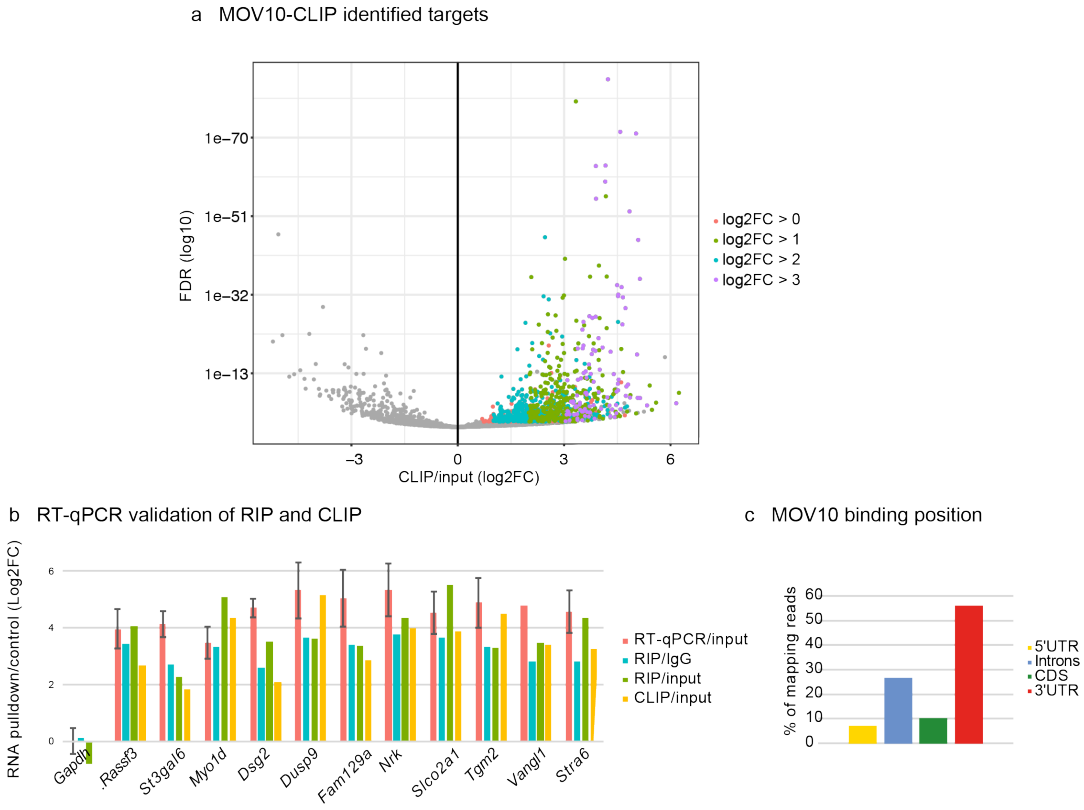

FIGURE 4.17: **Identification of MOV10 targets by RIP and CLIP.** a | MOV10 targets were identified via CLIP, and confirmed with RIP. Color-coded according to the extent of the enrichment (log2FC). b | RT-qPCR for validation of MOV10-targets identified with RIP and CLIP (in red). *Gapdh* (reference RNA) is used as control. As reference, enrichment values from RIP (in light blue and blue) and CLIP (in yellow) are shown next to the RT-qPCR. Error bars represent SD for three biological replicates. c | Mapping statistics of MOV10 PAR-CLIP reads in percentage. Yellow: 5′UTR. Blue: introns. Green: CDS. Red: 3′UTR. Analysis by V. Franke.

Among the 1081 CLIP-identified targets (with log2FC > 0 and FDR < 0.05), 89% are shared with the RIP experiment (log2FC > 0, FDR < 0.05): 959 candidates with log2FC values > 0, 803 with log2FC > 1, 396 with log2FC > 2, and 99 with log2FC > 3 (Fig. 4.17, panel a). Several candidates were validated by RT-qPCR (Fig. 4.17, panel b). Consistent with previous findings (Gregersen et al., 2014), I found MOV10 binding to the 3′UTR region of its targets (Fig. 4.17, panel c), however, a specific binding motif was not identified.

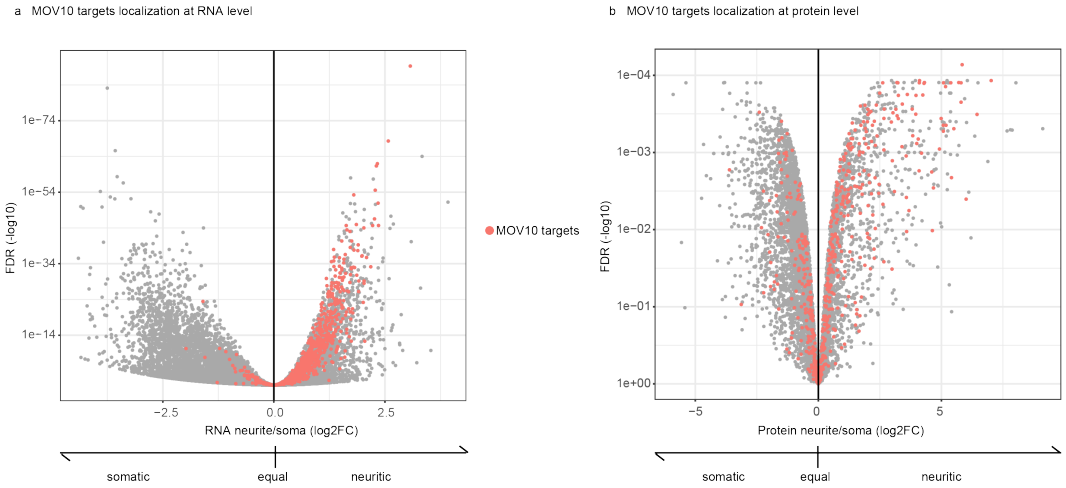

FIGURE 4.18: **RNA and protein localization of MOV10 targets.** MOV10 targets identified with CLIP and RIP (MOV10-CLIP/input, RIP/input, RIP/IgG log2FC > 0, FDR (Benjamini Hochberg) < 0.05) are overlaid in red on transcriptomic (a) and proteomic (b) data. Analysis by V. Franke and K. Imami. RNA-seq generated by D. van den Bruck. Proteins isolated by A. Zappulo.

TABLE 4.2: MOV10 targets in transcriptomic, translatomic, and proteomic data, selected via PAR-CLIP and RIP experiments

	Neurites	**Soma**	**Total**
RNA	675	36	771
Ribo-seq	278	75	353
Protein	237	88	325
RNA and Ribo-seq	247	17	264
RNA and protein	207	7	214
Ribo-seq and protein	116	75	191
All	110	4	114

Interestingly, MOV10 targets appear to be localized in the neuritic compartment. In fact, by selecting MOV10 targets and observing their localization on the local transcriptome and proteome, their enrichment in the neurites at RNA level is evident, with 87.5% of the targets localized in the neurites (Fig. 4.18, panel a in red). This result indirectly highlights the importance of the function of MOV10 in the neuritic compartment. On the other hand, at protein levels they are present in both compartments (Fig. 4.18, panel b in red).

Interestingly, when I add the information concerning local translation, it is noticeable that only a tiny fraction of targets present in the neuritic compartment are being translated, namely 36% (247 out of 675) (Table 4.2). This fact might hint towards an involvement of MOV10 in translation regulation.

4.3.2 MOV10 is not involved in localization of its targets

FIGURE 4.19: **MOV10 targets localization at RNA level in wt and MOV10-KO lines.** MOV10 targets identified with CLIP and RIP (MOV10-CLIP/input, RIP/input, RIP/IgG log2FC > 0, FDR (Benjamini Hochberg) < 0.05) are overlaid in red on transcriptomic data from wt and MOV10-KO lines. Analysis by V. Franke. MOV10-KO and RNA-seq generated by D. van den Bruck.

Because of the clear neuritic localization of MOV10 targets, I was interested in understanding its function in this compartment. One possibility is that MOV10 is responsible for the localization of its targets. Another possibility is that MOV10 localizes to the neuritic compartment to serve a precise function *in situ*, where its targets are localized by means independent of MOV10. One strategy to answer the first hypothesis is to produce a MOV10-KO cell line and analyze mRNA localization in absence of the RBP. CRISPR-Cas9 was

used to generate MOV10-KO cell line by David van den Bruck, who also generated the RNA-seq dataset from the compartments of this line. Through the comparison of local transcriptome between the wt and MOV10-KO lines, any role for MOV10 in RNA localization was excluded. In fact, MOV10 targets (depicted in red in Fig. 4.19), still localize to the neurites upon MOV10-KO, almost in the same number (675 in wt, 594 in MOV10-KO).

4.3.3 Identification of MOV10 co-interactors by MOV10-IP

Since localization of MOV10 targets was not affected by the depletion of the protein, the other hypothesis of MOV10 being involved in a specific function other than RNA localization needed to be tested. MOV10 has been implicated in different pathways, from NMD in combination with UPF1 (Gregersen et al., 2014), to translational repression via RNA-induced silencing complex (Banerjee, Neveu, and Kosik, 2009, Meister et al., 2005, Kenny et al., 2014) or translational activation, depending on the targets and the other RBPs in play (Kenny et al., 2014). Specifically in neurons, it has been linked to regulation of local protein synthesis: its degradation through the proteasome in a NMDA-receptor-mediated activity-dependent manner stimulates local translation (Banerjee, Neveu, and Kosik, 2009). I performed MOV10 immunoprecipitation to identify interaction partners, aimed at understanding the role of the protein in the neurites of Ascl1-iNs.

With this experiment I identified several candidates, some already known to be MOV10 interactors (Fig. 4.20, panel b). Specifically, among the RNA-dependent interactors I identified AGO2, in agreement with Meister et al., 2005, and FAM120A, UPF1, ZCCHC3 and PABPC1, identified also in Gregersen et al., 2014, as RNA-independent. This different result in terms of relationship to RNA could be explained by the conditions used for RNase digestion. However, since we used different nucleases (RNaseI or RNaseT1), a direct comparison is difficult. Among the RNA-independent interactors I identified FMR1, shown to interact with MOV10 in Kenny et al., 2014, and its homolog FXR1. Interestingly, I found TRIM71, an RBP involved in translational repression (Loedige et al., 2013).

In summary, to start dissecting the molecular mechanisms by which mRNAs get localized and locally translated, I focused on MOV10, an RNA helicase localized in the neurites of Ascl1-iNs. I identified its targets, which consistently with the neuritic localization of the protein, are also localized to the neurites. Among the possible functions that MOV10 could exert, its role in mRNA localization was excluded. Moreover, I identified its interactors, among which

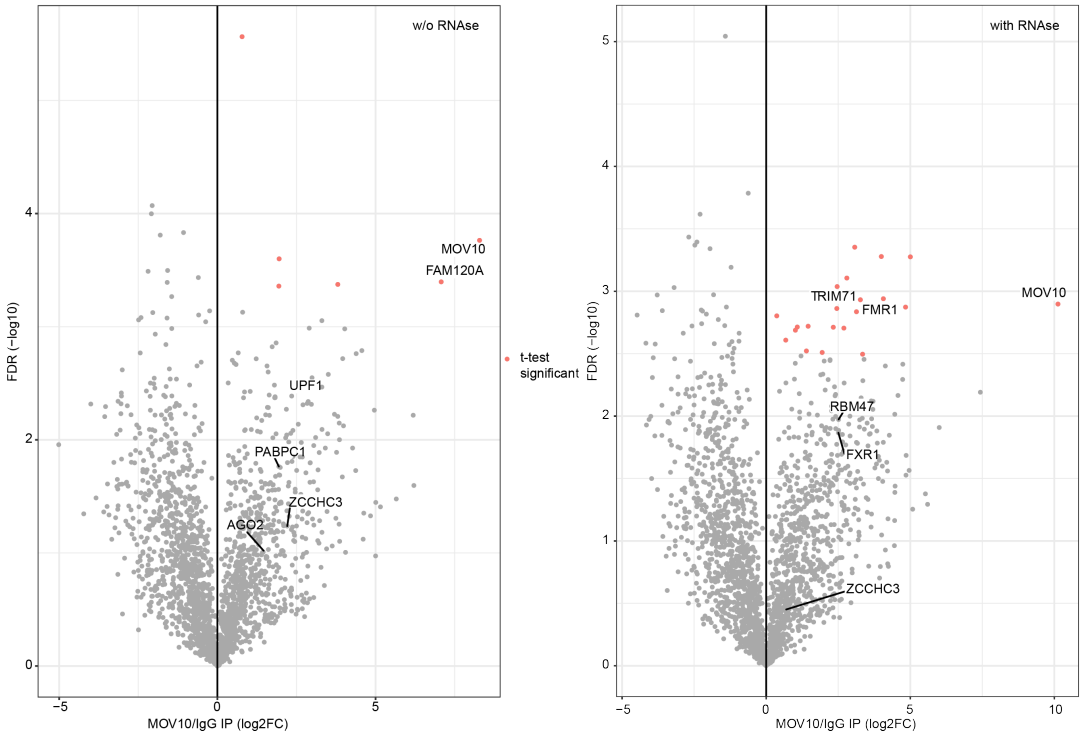

FIGURE 4.20: **Identification of MOV10 protein interactors.** MOV10 interactors identified by MOV10-pulldown, performed with or without RNase treatment, shown as volcano plot. In red t-test positive interactors. IgG-pulldown was used as negative control. Mass-spec by K. Imami.

several interesting candidates, some already known from literature. Further characterization of its specific function will be required.

4.4 Asymmetric distribution of mRNA isoforms in iNs

The results presented in chapter 4.2.2, showed that RNA localization and local translation are the main determinants of the local proteome. How is the mRNA localized though? I investigated two aspects of this question: on the perspective of the *trans*-acting elements (chapter 4.3), and on the perspective of the *cis*-element (this chapter). In fact, one important feature of mRNA determining its localization is its 3′UTR. This region contains the so-called *cis*-elements, important for RBP binding and RNA metabolism processes such as localization (see chapter 1.1.2). In the following chapter I will describe the results from a 3′end-seq experiment, aimed at understanding whether mRNA isoforms would localize differently due to different *cis*-elements present in their 3′UTRs. Then I will focus on a gene whose isoforms are differentially localized among the somatic and neuritic compartments, and I will go through

a set of experiments to show the role of the 3′UTR in RNA and ultimately in protein localization.

4.4.1 Alternative mRNA isoforms are differentially localized among the somatic and neuritic compartments

Using the compartment separation system introduced earlier (Chapter 4.1), I performed 3′end-seq to identify mRNA isoforms differentially distributed among the somatic and neuritic compartments. 3′end-seq is a technique which allows a precise mapping of the 3′end of the transcripts (Chen et al., 2017). It consists in enriching the 3′-termini of transcripts via reverse transcription with oligo(dT) primer to produce cDNA. 3′end-seq from the compartments of Ascl1-iNs allowed the identification of 19,175 different 3′UTRs corresponding to 10,868 genes. Computational analysis was performed by Vedran Franke and Aviv Rom.

Multiple 3′ ends were annotated for 4,149 genes. Among these, 3,675 genes encoded for tandem 3′UTR isoforms (UTR-APA or APA in short), and 474 for coding region-alternative polyadenylation (CR-APA), specifically for alternative last exon events (ALE in short). In fact, via 3′end-seq, APA and ALE events are both captured: these events produce alternative 3′UTR in terms of length or sequence, respectively (see chapter 1.2).

In neurons, a general interest around the length of 3′UTRs is widespread. Brain is characterized by longer 3′UTRs compared to other tissues (Miura et al., 2013), and this feature is generally associated with higher complexity in post-transcriptional regulation, thanks to the abundance of *cis*-elements. Several examples where localization is mediated by longer 3′UTRs are characterized in neurons: *BDNF* (An et al., 2008), *Ranbp1* (Yudin et al., 2008), *Impa1* (Andreassi et al., 2010), *MKK7* (Feltrin et al., 2012), *KPNB1* (Perry et al., 2012), *Bdnf* (An et al., 2008) and *CaMK4* (Harrison et al., 2014). Moreover, a recent genome-wide study identified distal APA isoforms enriched in neurites of rat neurons (Tushev et al., 2018).

To investigate the contribution of 3′UTR length to localization, for each transcript, the short and the long isoforms that showed the highest enrichment in soma or neurites were selected, and their relative enrichment plotted (Fig. 4.21). This analysis surprisingly revealed that often times the isoform enriched in the neurites was the short one. To be more stringent, 593 genes - 522 APA and 71 ALE - for which the relative change in usage for the most variable pair of alternative 3′UTRs was at least 20%, were selected. For 90% of those (534 genes) the more proximal cleavage and polyadenylation site

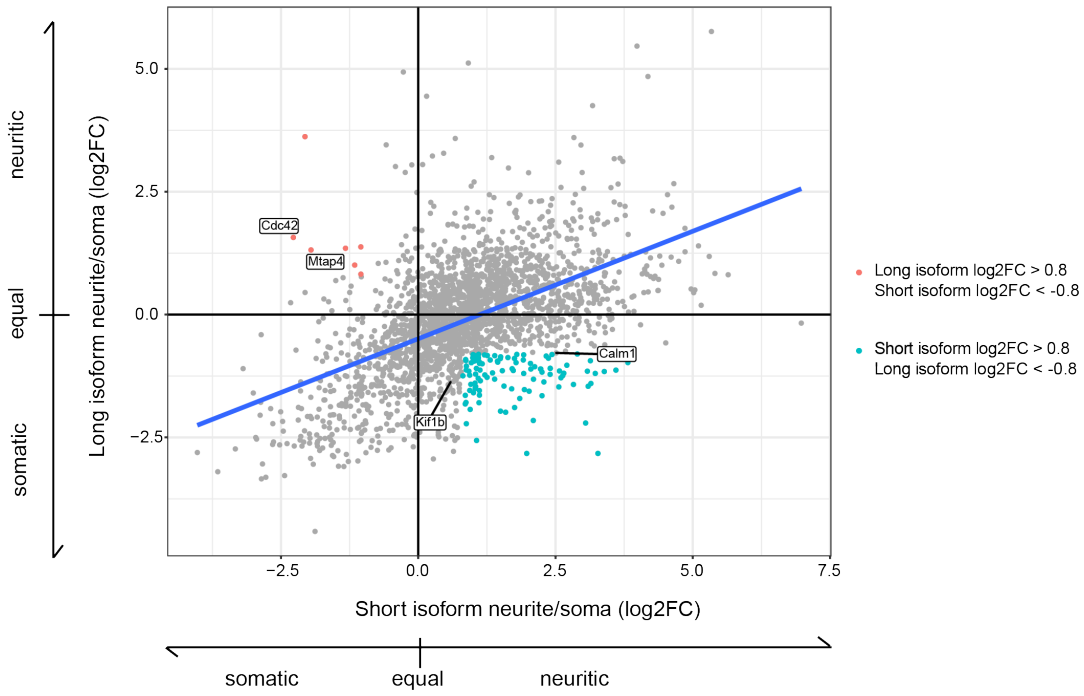

FIGURE 4.21: **Short vs long isoform enrichment in 3′end-seq.** Short and long isoform enrichment in x- and y-axes respectively. Orange: the long and the short isoforms are neurite and soma-enriched respectively (long isoform neurites/soma log2FC > 0.8, short isoform neurites/soma log2FC < -0.8); blue: the short and the long isoforms are neurite and soma-enriched respectively (short isoform neurites/soma log2FC > 0.8, long isoform neurites/soma log2FC < -0.8). Analysis by V. Franke.

was preferentially used in the neuritic pool of mRNAs. The 3′UTRs of the neurite-enriched isoforms were shortened in 59.2% of the ALE pairs, and 92.3% of the APA pairs. The difference in length is substantial: the average 3′UTR of the soma-enriched isoforms is 2,398 nt long compared to 1,080 nt for the neurite-enriched ones. This is especially surprising in the context of APA isoforms: as mentioned above, it is commonly perceived that the long isoform is synonymous with higher level of complexity and regulation. This concept relates to the fact that the long isoform contains extra sequence compared to the short one (that is completely embedded in the long one). Nevertheless different explanations of this phenomenon are possible (discussed further in chapter 5.3.2). On the other hand, ALE 3′UTRs differ in sequence and in length. Completely different sets of *cis*-elements can be present on each isoform, and a difference in length might be meaningless in the context of regulation.

I used RT-qPCR to validate the relative enrichment for 6 genes expressing multiple isoforms. To keep in mind is that by RT-qPCR, detection of different ALE isoforms is allowed by the difference in exon composition. On

the contrary, APA isoforms cannot be discerned by the sole sequence, as the short isoform is always contained in the long. As represented in Fig. 4.22 panel a), specific primer pairs are available only for the long 3′UTR APA isoform, whilst the other primer pair anneals on both long and short isoforms. I was able to validate several candidates, and found very good agreement (r= 0.86, Pearson correlation) with the sequencing data (Fig. 4.22, panel b and c). Specifically, *Calm1*, *Ascl1* and *Braf* of the APA class were validated, and *Kif1b*, *Mtap4*, and *Cdc42* of the ALE class.

Kif1b belongs to the kinesin-3 anterograde motor protein family, and I found *Kif1bβ* (transcript: 10,233 nt; protein: 1,816 aa) enriched in the somatic compartment, and *Kif1bα* (transcript: 6,991 nt; protein: 1,150 aa) in the neuritic one. The two alternatively spliced isoforms share several domains - the motor domain to mention one - but the shorter isoform lacks the kinesin-like Kif1-type, kinesin-like and the plekstrin homology domain. This latter domain is responsible for binding to phosphatidylinositol within membrane and proteins, and serves to recruit proteins to the appropriate cellular compartment or to enable the interaction with other components of the signal transduction pathway. In addition to the variation in the C-terminal region, *Kif1bβ* is also characterized by extra 40 amino acids in the hinge region, located in-between two stretches of α-helices, adjacent to the motor domain, and shown to enhance turnover rate of microtubule-dependent ATP-hydrolysis without affecting motility (Matsushita et al., 2009). In terms of cargo-binding, KIF1Bβ transports either synaptic vesicles or lysosomes in neuronal and non-neuronal cells, respectively (Zhao et al., 2001, Matsushita et al., 2004). Whereas KIF1Bα was shown to transport mitochondria, and cargos containing PSD95 proteins and synaptic scaffolding molecule (S-SCAM) (Nangaku et al., 1994, Mok et al., 2002), in line with the fact that I found it enriched in the neuritic compartment.

Mtap4 encodes for several isoforms of a microtubule-dependent protein 4, which possess different microtubule stabilization properties (Hasan et al., 2006). I found the so-called MAP4-LP (transcript: 6,091 nt; protein: 1125 aa) (Matsushima et al., 2005, Tokuraku et al., 2003) enriched in the neuritic fraction, and a much shorter isoform enriched in the somatic (transcript: 3,446 nt; protein: 99 aa). MAP4 proteins are composed of two domains: an N-terminal projection domain that suppresses microtubule bundling and maintains spacing between microtubules without binding to them (Iida et al., 2002); and a C-terminal domain responsible for microtubule binding. Each domain is also subdivided in sub-regions: the projection domain is composed of an N-terminal acidic region, a multiple KDM-repeated sequence,

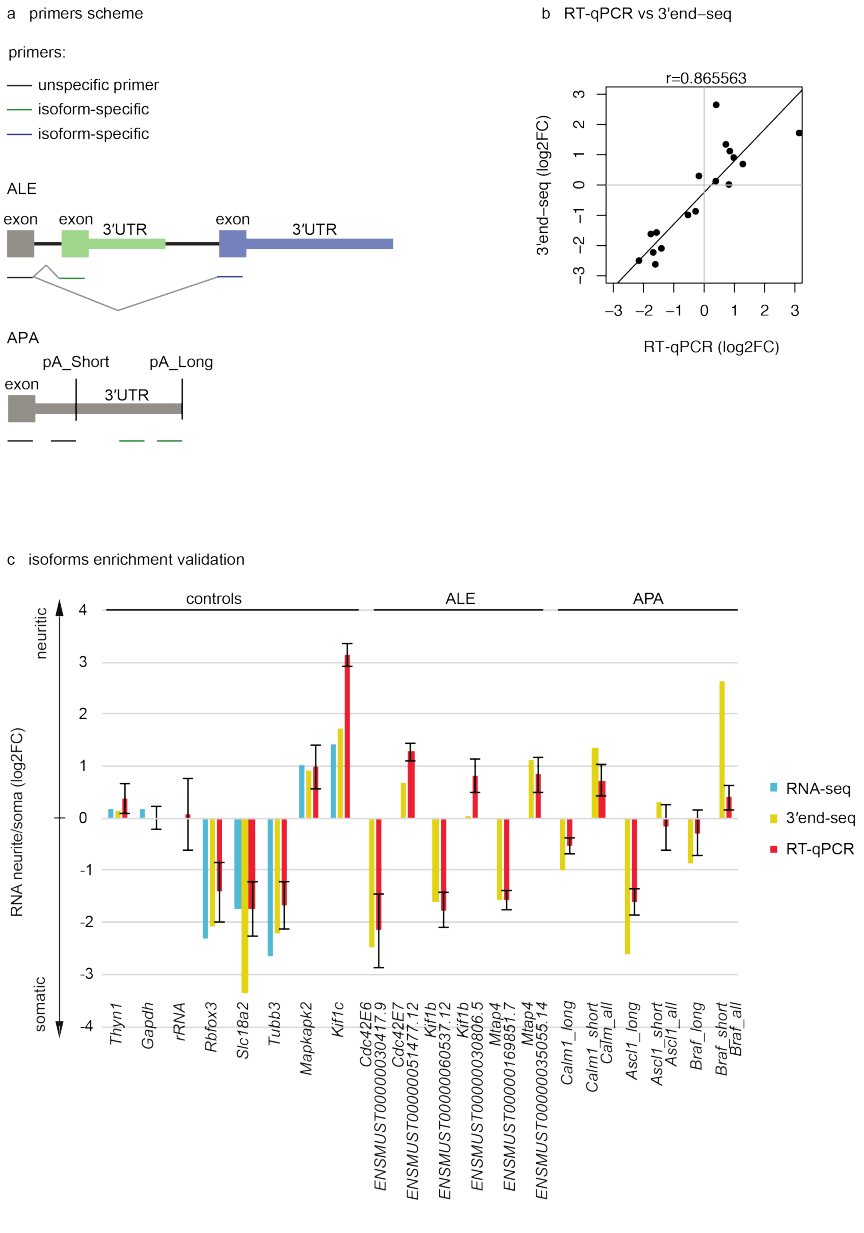

FIGURE 4.22: **RT-qPCR validation of sequencing data.** a | Scheme representing primer pairs. For ALE isoforms primers are designed in order to span an exon-exon junction: the same forward primer is used with different reverse pairs. For APA isoforms, the short isoform cannot be distinguished from the long one as the sequence is identical. b | Ratio of RNA levels in neurites versus soma (log2 fold change), measured by either RT-qPCR (X) or 3′end-seq (Y). The linear least squares fit between 3′end-seq and RT-qPCR data is shown. r is the Pearson correlation coefficient. c | qRT-PCR isoforms validation. Error bars represent SD for two (neurites) or three (soma) biological replicates. *Gapdh* (reference RNA), *Thyn1*, *rRNA* were used as unlocalized controls, *Rbfox3*, *Slc18a2*, *Tubb3* as soma-localized, *Mapkap2*, *Kif1c* as neurite-localized controls. ENSEMBL identifiers are used for ALE isoforms. For APA isoforms, the qRT-PCR data are shown for the long isoform and both isoforms combined (all), as the primers for the short isoform also anneal on the long isoform. As a reference, neurite/soma enrichment based on 3′end-seq (yellow) and RNA-seq data (blue bars, not isoform-specific) are shown next to the RT-qPCR data (red bars). RT-qPCR for *Kif1b* and *Mtap4* by G. Arrey.

and a b-region; the microtubule-binding domain is composed of a proline-rich region suggested to promote microtubule nucleation, a region with 3-to-5 imperfect repeats inducing tubulin polymerization, and a short hydrophobic C-terminal region (Tokuraku et al., 1999). MAP4-LP was suggested to contribute to long-range transport in neurons (Tokuraku et al., 2010), in line with my findings. To understand the function of the small isoform, soma-enriched, containing the N-terminal acidic region only, additional characterization is required.

Cdc42 was also validated, and it will be the focus of the following chapter (Chapter 4.4.2).

4.4.2 *Cdc42E7* isoform is enriched in the neurites at RNA and protein levels

As mentioned above (chapter 4.4.1), among the isoforms belonging to the ALE category I identified *Cdc42*, a gene which encodes for a small membrane-bound GTPase. CDC42 is a molecular switch that passes from a GTP-bound active state to a GDP-bound inactive one, involved in reshaping cellular morphology through a signalling cascade which leads to regulation of actin and microtubule cytoskeleton. CDC42 induces the formation of filipodia in a variety of cell types, and in neurons it was shown to promote neurite outgrowth, dendritic arborization, and spine formation (Egorov and Polishchuk, 2017, Nishimura, 2006, Negishi and Katoh, 2005, Choi, 2005, Nakazawa, 2003, Scott, Reuter, and Luo, 2003). It is a particularly interesting candidate, as it was shown to be an important regulator of neuronal morphology (Tahirovic and Bradke, 2009, Melendez, Grogg, and Zheng, 2011, Govek, Newey, and Van Aelst, 2005).

Cdc42 can be alternatively spliced to produce two transcripts almost identical in coding sequence, except for the last 10 amino acids, and unique in 3′UTR sequence and length, with *Cdc42E6* bearing a short 3′UTR (768 nt long), and *Cdc42E7* a longer one (1407 nt long). The two isoforms are expressed at different levels in different tissues: *Cdc42E6* is brain-specific and *Cdc42E7* is ubiquitous (Marks and Kwiatkowski, 1996, Hwang et al., 2017).

With 3′end-seq analysis, I found *Cdc42E6* enriched in the somatic compartment and *Cdc42E7* in the neuritic one (Fig. 4.23 (panel a), finding confirmed by RNA-seq (Fig. 4.23, panel a). To assess the consistency of the results obtained in Ascl1-iNs in a primary system, I tested the differential localization of *Cdc42* isoforms in primary neurons. I analyzed localization of *Cdc42E6* and *Cdc42E7* transcripts in mouse cortical neurons at DIV18 using smFISH

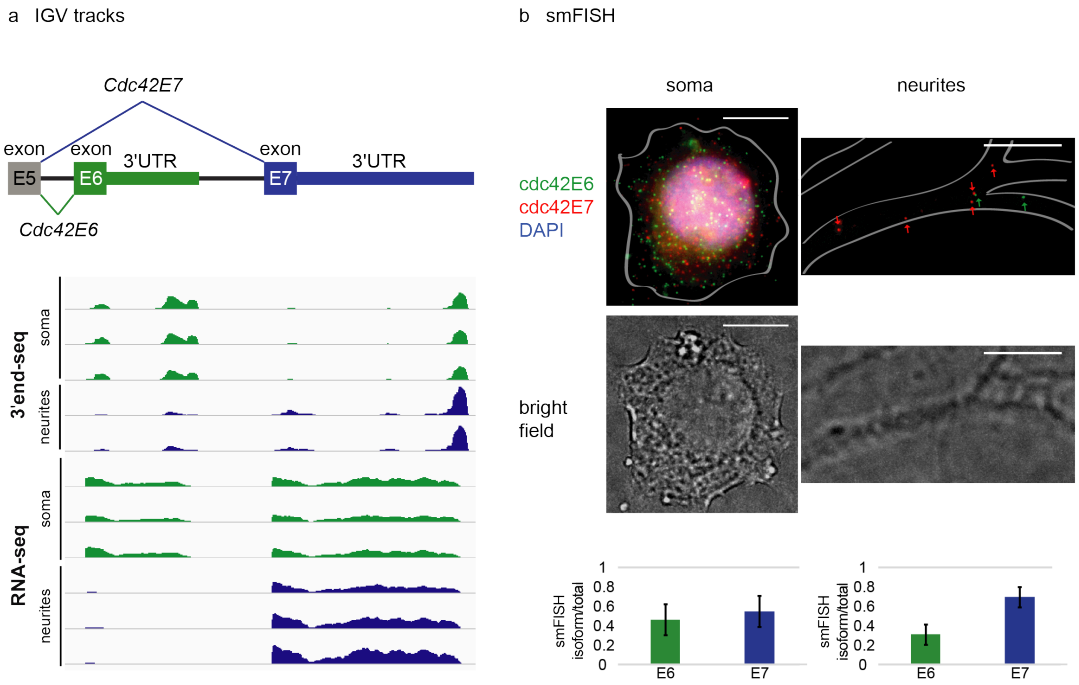

FIGURE 4.23: ***Cdc42* IGV tracks (3′end-seq and RNA-seq) and smFISH** a | Scheme of the last part of *Cdc42* gene locus. Below genome browser views of the sequence coverage for the two isoforms of *Cdc42* in 3′end-seq (upper panel) and total RNA-seq (bottom panel). Tracks' scales were set at the same threshold for soma and neurites. b | smFISH of *Cdc42* with isoform-specific Stellaris probes was performed in mouse cortical neurons from P0 at DIV18. *Cdc42E6*: green (Q570), *Cdc42E7*: red (Q670), DAPI: blue. Scale bar: 10 μm. Cell borders are outlined based on the brightfield image. Fluorescent spots corresponding to E6 and E7 isoforms were counted using StarSearch (Raj lab). Quantification plots are presented below the images (left: soma, right: neurites): Y-axis shows ratios of isoform-specific:total *Cdc42* signals in the analyzed subcellular compartment. The data represent averages of 13 neurons and the error bars are SD. RNA-seq by D. van den Bruck.

and isoform-specific Stellaris probes, designed on the 3′UTRs. Quantification of smFISH signal confirms that E7 isoform is indeed more abundant in outgrowths of cortical neurons compared to E6 isoform (Fig. 4.23, panel b), corroborating my findings in a primary cell system.

To fully characterize *Cdc42* isoforms distribution among the somatic and neuritic compartments, I used compartment-specific Ribo-seq data to assess whether translation was also localized. I observed a preferential neuritic translation of *Cdc42E7* isoform (Fig. 4.24, panel a), pointing to the fact that each isoform is probably localized at the mRNA level, and then locally translated.

Given the differential localization and local translation of *Cdc42* isoforms, I hypothesized that protein isoforms would also be differentially localized. Using compartment-specific LC-MS/MS data, I compared the intensities of

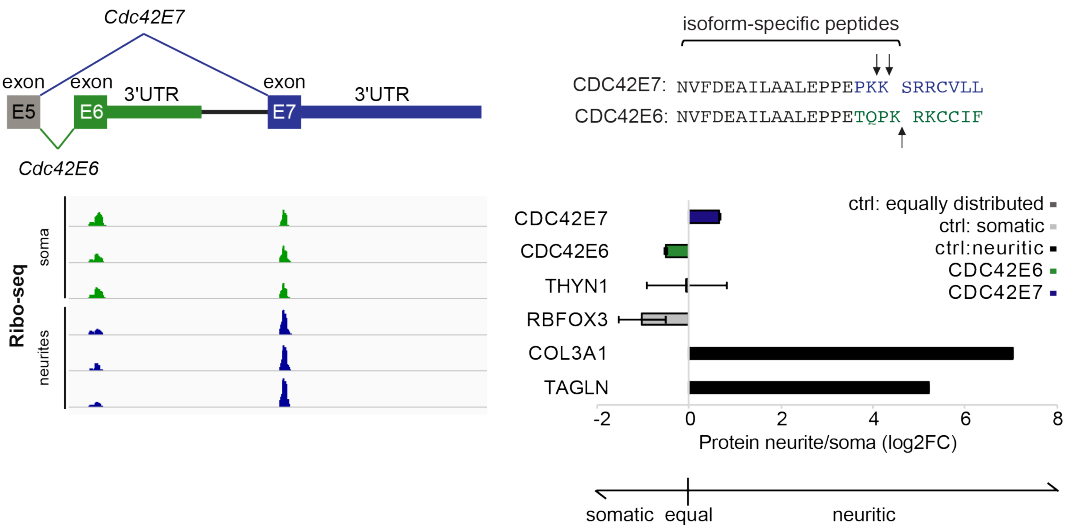

FIGURE 4.24: ***Cdc42* IGV tracks (Ribo-seq) and CDC42 protein isoforms distribution.** a | Scheme of the 3′ end of *Cdc42* gene locus. Genome browser views of the sequence coverage for the two isoforms of *Cdc42* in 3′end-seq (upper panel) and total RNA-seq (bottom panel). Tracks' height was set at the same threshold for soma and neurites. b | CDC42 isoform-specific peptides were extracted from the LC-MS/MS data and used to evaluate relative levels of E6 and E7 isoforms in neurites and soma of iNs. The sequences show 25 C-terminal amino acids from which isoform-specific peptides are derived, with arrows pointing at the positions of trypsin digest. Values were normalized to the intensities of peptides shared between E6 and E7 isoforms. THYN1 is used as unlocalized control, RBFOX3 as neuronal and somatic marker, TAGLN and COL3A1 as neuritic markers. Error bars represent FDR (Benjamini-Hochberg). Protein lysates were prepared by A. Zappulo.

the peptides specific to either E6 or E7 isoforms (identified by 10 amino acids difference at the C-terminus). Consistent with 3′end-seq and Ribo-seq results, CDC42E7 isoform is more abundant in neurites, and CDC42E6 in soma (Fig. 4.24, panel b). These results support the hypothesis of specific local translation for each isoform, leading to a different relative enrichment of the protein isoforms among the two compartments.

4.4.3 *Cdc42* 3′UTRs drive isoforms distribution

The results described so far show that *Cdc42E7* isoform is enriched in the neurites at RNA level, and that local translation contributes to the enrichment of CDC42E7 in this compartment. However, it remains still unclear

how *Cdc42* isoforms localize to different subcellular compartments. The results from 3′end-seq, total RNA-seq, and Ribo-seq data suggest a role for alternative 3′UTRs, mRNA transport and local translation. However, prior studies implied the role of post-translational modifications in the localization process of CDC42 proteins. To determine whether the 3′UTR is responsible for isoforms localization, I built a reporter system in which mCherry-tag is fused to *Cdc42E7* CDS, followed by either E7-3′UTR (wt reporter), or by E6-3′UTR (swap reporter) (Fig. 4.25, panel a). The reporters were tested for protein localization via western-blot, and for local translation via puro-PLA, in both Ascl1-iNs and primary neurons. In Ascl1-iNs, the reporter expression is driven by a TetOn doxycycline-inducible CMV promoter, to simultaneously induce expression of the reporter and neuronal differentiation (chapter 3.2.1). In primary neurons, the reporter expression is driven by synapsin promoter, a well-established promoter for primary cultures (Lesuisse and Martin, 2002).

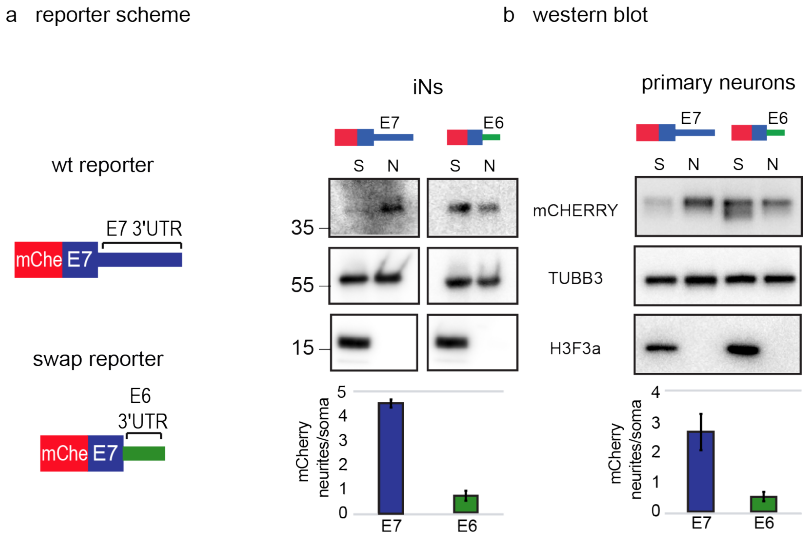

FIGURE 4.25: **Alternative 3′UTRs determine CDC42 protein localization.** a | Scheme of *Cdc42* reporters used: mCherry was fused to the CDS of *Cdc42E7* with either E7 3′UTR (wt reporter), or with E6 3′UTR (swap reporter). b | Western blotting showing localization of mCherry-CDC42E7 protein in Ascl1-iNs (left side) or primary neurons (right side) infected with either wt or swap reporter titer, and separated on neurites (N) and soma (S). Histone H3 was used as a soma marker and TUBB3 as a loading control. Intensity of the mCherry-CDC42E7 signal was quantified, normalized to TUBB3, and presented below the blot as fold enrichment in neurites versus soma. Error bars represent SD of three different blots.

As expected, the protein synthesized from mCherry-*Cdc42E7* reporter (wt reporter) shows preferential localization to the neurites (Fig. 4.25, panel b). To test whether the neurite-enriched localization is mediated by E7-3′UTR, I used the swap reporter, where E7-3′UTR is substituted with E6-3′UTR. Strikingly, mCherry-CDC42E7 protein produced from E6-3′UTR reporter shows

stronger localization to soma. These results point to the role of alternative 3′UTRs, rather than differences in protein modifications, as the defining factor in localization of CDC42 protein isoforms. I obtained similar results in primary neurons: when E7-3′UTR (wt reporter) is present, mCherry reporter localizes preferentially in the neuritic compartment, whilst when E6-3′UTR is present (swap reporter), mCherry localizes preferentially to the somatic compartment (Fig. 4.25, panel b). This result shows that the *Cdc42* 3′UTRs drive protein localization.

Ribo-seq data show that *Cdc42E7* isoform in not only localized to the neurites but also translated there (Fig. 4.24, panel a). Since this result is based on the last exon only, to acquire more evidence supporting local translation for *Cdc42E7*, I performed a microscopy experiment, and tested whether *Cdc42E7* neuritic translation is dependent on the 3′UTR. For that, I visualized *de novo* synthesis of mCherry-CDC42E7 protein, from either E7-3′UTR or E6-3′UTR reporters, using puro-PLA (Tom Dieck et al., 2015, described in Chapter 1.4.1) in both Ascl1-iNs and cortical neurons. I observed neuritic translation of the reporter when fused to E7-3′UTR, while when fused to E6-3′UTR translation is more abundant in soma. These observations are consistent with the results obtained by western blot (Fig. 4.26), corroborating the hypothesis that isoform-specific 3′UTRs mediate not only localization, but also local translation of *Cdc42*.

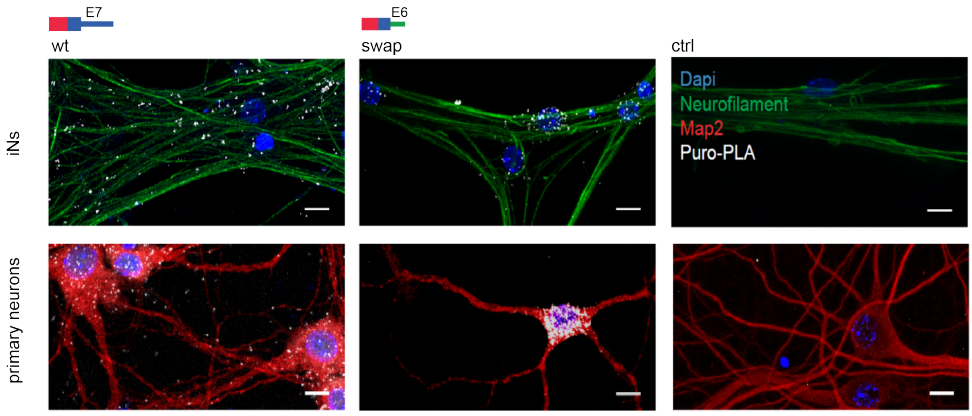

FIGURE 4.26: **puro-PLA on *Cdc42* isoforms.** Puro-PLA images showing localized translation of CDC42E7 from either E7 or E6 3′UTR reporter-infected Ascl1-iNs and primary neurons. For a negative control, puromycin treatment or titer were omitted. puro-PLA: red, NF: green, DAPI: blue. Scale bar: 10 μm.

4.4.4 Identification of the isoform-specific interactome of *Cdc42*-3′UTRs

The experiments described so far show that *Cdc42*-3′UTRs are the determinants of RNA localization and local translation, ultimately influencing protein distribution. I wanted to identify the factors mediating *Cdc42* RNA metabolism. Key regulators of mRNA metabolism are RBPs, that bind to mRNA and recruit i.e. components of transport machinery (Glock, Heumüller, and Schuman, 2017). Thus, to identify the RBPs involved in *Cdc42* regulation, I employed an RNA affinity capture approach, GRNA chromatography (Czaplinski and Mattaj, 2006), combined with SILAC.

The procedure is illustrated in Fig. 4.27. I tagged *Cdc42* E7 and E6 3′UTRs with five copies of boxB sequence, which binds λ N peptide, and I incubated the resulting E7-boxB and E6-boxB *in vitro* transcribed RNAs with neuronal lysates. Lysates were produced from neurons labelled with either H or L amino acid isotopes. The complexes formed on E7-boxB RNA and E6-boxB RNA were isolated by binding to a λ N-GST fusion protein immobilized on glutathione beads. Differentially labelled protein samples were pooled together (forward experiment: H E7-boxB + L E6-boxB; reverse experiment: H E6-boxB + L E7-boxB), and bound proteins were eluted with RNase A for further proteomic analysis. Using this approach I identified 17 RBPs enriched in E7-bound complexes (in blue) and and 6 in E6-bound complexes (in red), by at least 1.9-fold (Fig. 4.28, panel a). Focusing on E7 preferential binders, binding-motifs for 7 of the identified RBPs were available through RBPmap (Paz et al., 2014), and consistently they are present all across *Cdc42E7* 3′UTR (Fig. 4.28, panel b). Exact number of binding sites are listed in table 4.3, next to each RBP when available. I found RBPs belonging to different classes of RNA regulation: splicing factors, pre-mRNA binders, post-transcriptional regulators (table 4.3).

4.4.5 Exploring *Cdc42E7*-bound RBPs function

The identified RBPs are members of the spliceosome, general components found on mRNAs, or heterogeneous nuclear ribonucleoproteins (hnRNPs), common proteins involved in nucleus-cytoplasm transport. Depending on their reported function in literature, some candidates were selected and investigated in follow-up experiments. For instance, SNRPA, SNRPA1 and SNRPB2 are members of the spliceosome, which is a nuclear large complex, composed of small nuclear ribonucleoproteins (snRNPs) made of small nuclear RNAs and protein factors, and responsible of removing introns from pre-mRNAs. The major spliceosome is composed of U1, U2, U4, U5 and U6

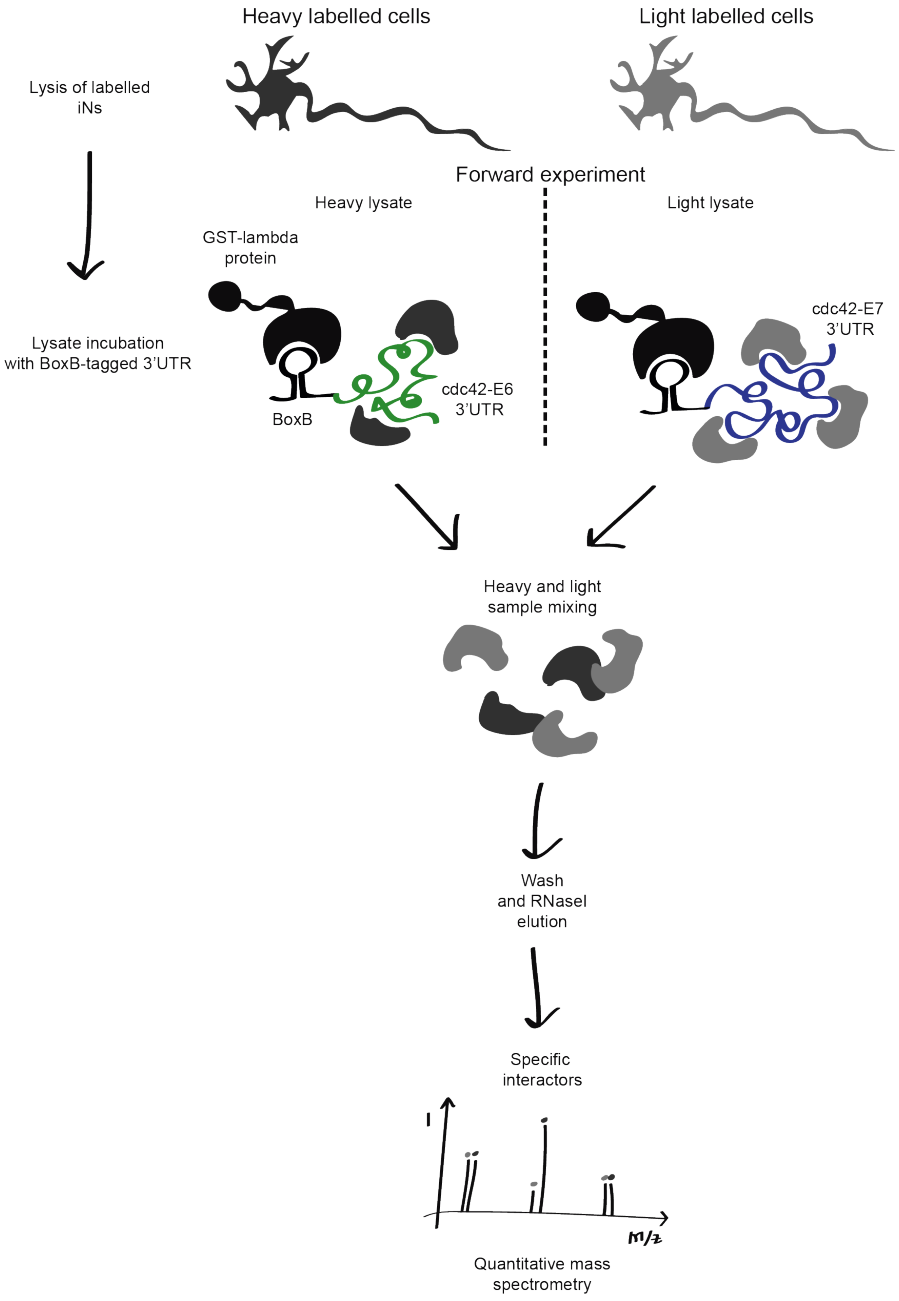

FIGURE 4.27: **3′UTR-bound proteome identification.** Schematic representation of GRNA chromatography combined with SILAC used to identify proteins bound to E6 or E7 3′UTRs of *Cdc42*. boxB-E7 3′UTR and boxB-E6 3′UTR RNAs are incubated with lysate prepared from either L or H Ascl1-iNs. Bound proteins are eluted with RNase A and combined as shown in the scheme (H E7 + L E6 in forward experiment and L E6 + H E7 in reverse experiment), and analyzed by mass spectrometry. The forward and reverse experiments represent "label swap" replicates standardly used in SILAC to account for biases of the labelling procedure. H/L (forward) and L/H (reverse) ratios for each protein represent fold of enrichment of a given protein in complexes formed on E7 versus E6 *Cdc42* 3′UTR.

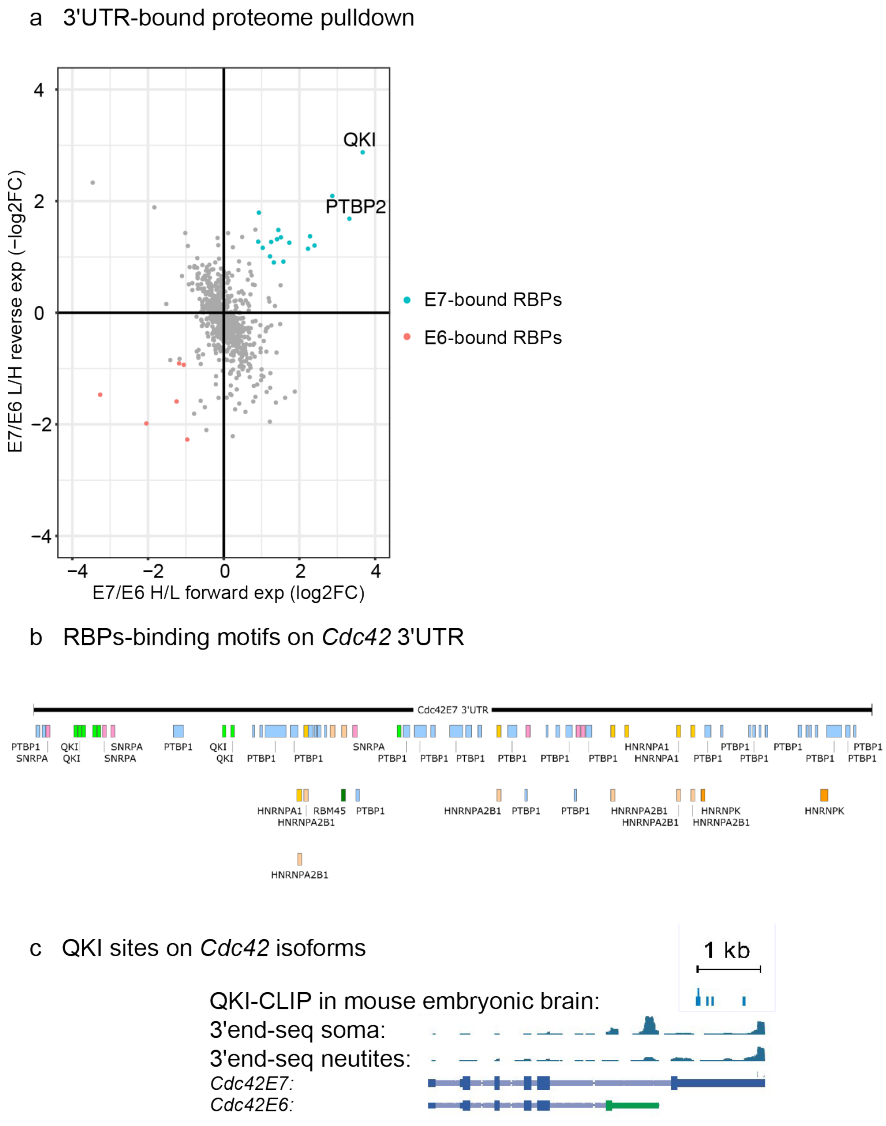

FIGURE 4.28: **3′UTR-bound proteome identification and validation.** a| Scatterplot of protein ratios pulled down with *Cdc42* E6 or E7 3′UTRs obtained in forward and reverse experiments. In blue, thirteen specific interactors showing at least 1.9-fold enrichment in E7 3′UTR pulldown. b| RBPs-binding sites from RBPmap if available (Paz et al., 2014) are mapped on *Cdc42E7* 3′UTR. c| QKI CLIP data from mouse embryonic brain (Hayakawa-Yano et al., 2017) were analyzed to visualize QKI sites on *Cdc42*. The snapshops from the genome browser showing distribution of *Cdc42* 3′end-seq reads between neurites and soma and position of QKI CLIP reads on *Cdc42*. Analysis of MS by K. Imami. CLIP analysis by A. Rom.

Splicing factors		**Pre-mRNA binders and RNP-forming particles**		**Post-transcriptional regulators**	
Name	Binding sites	Name	Binding sites	Name	Binding sites
PTBP2		hnRNP K	2	RC3H1	
PTBP1	36	hnRNP A2/B1	8	RC3H2	
SNRPA1		hnRNP A3		DIS3L	
SNRPA	7	hnRNP A1	7	ELAVL1	
SNRPB2				hnRNP A0	
hnRNP II				QKI	8
				RBM45	1

TABLE 4.3: E7-preferential binders, categorized according to their role in RNA metabolism, with the number of binding sites on *Cdc42E7* according to RBPmap (Paz et al., 2014)

snRNPs. SNRPA is a member of U1 snRNP, which binds to the 5′ splice site, whilst SNRPA1 and SNRPB2 are members of U2 snRNP, which binds to the branch point of the intermediate lariat-shaped intron. SNRPA and SNRPB2 share two regions of homology, which comprehend the RNA recognition motif, and they are structurally related (Nelissen et al., 1991). It was suggested that even if they are present in different particles of the spliceosome, they might exert the same function (Sillekens et al., 1987). These two proteins should not be present in the pulldown as they bind to intronic regions, and the reporter doesn't carry any. However, they share the same RNA recognition motif, therefore they might recognize unspecifically the same motif, on *Cdc42E7* only. Moreover, SNRPA1 is in complex with SNRPB2, therefore its presence in the pulldown might be attributed to this reason.

DIS3L is a component of the cytoplasmic exosome. It belongs to the RNase R family and it is responsible of degrading mRNAs through its 3′-5′ exonuclease activity (Wang and Kiledjian, 2001, Mukherjee et al., 2002). To be subject to exosome degradation, mRNAs that contain AU-rich elements (AREs) are targeted by specific ARE-binding proteins to the exosome (Chen et al., 2001, Gherzi et al., 2004). The presence of DIS3L in the pulldown is consistent with the presence of AU-rich elements in *Cdc42E7* 3′UTR, however it doesn't make DIS3L itself an interesting candidate since it is a general component of the exosome. What should be considered though, is a specific somatic-degradation of *Cdc42E7*, which might happen through the exosome pathway.

On the other hand, I also identified ELAVL1 (or HuR). The Hu protein family consists of the ubiquitous ELAVL1, and of the neuronal members ELAVL2,

3 and 4. Each protein contains of 3 RNA recognition motifs (RRMs), a basic hinge region important for nucleus-cytoplasm shuttling, and a divergent N-terminus (Okano and Darnell, 1997, Fan and Steitz, 1998). They are involved in several processes: in the cytoplasm they protect their target mRNAs from degradation by binding to AREs (Mobarak et al., 2013, Beckel-Mitchener et al., 2002, Peng et al., 1998, Levy et al., 1998, Atasoy et al., 2003, Bolognani et al., 2006); they can regulate translation (Jain et al., 1997, Antic, Lu, and Keene, 1999, Kullmann et al., 2002); in the nucleus they regulate polyadenylation and alternative splicing (Zhu et al., 2006, Zhu et al., 2007a, Zhu et al., 2007b, Bellavia et al., 2007).

The presence of both DIS3L and ELAVL1 is consistent with the presence of ARE elements within *Cdc42E7* 3′UTR. It is intriguing to speculate that AU-rich *Cdc42E7* might be subject to degradation in the somatic compartment via the exosome, but protected from degradation in the neurites via ELAVL1. However, the compartment-specific mass-spectrometry data shows the distribution of ELAVL proteins is not consistent with this hypothesis, since they are all enriched in the somatic compartment. Nevertheless, the somatic enrichment of ELAVL1 might be due to its nuclear localization, and not to the cytoplasmic fraction included in the somatic compartment. It might be worth analyzing the relative enrichment of ELAVL1 among the compartments, after nucleus removal.

Roquin proteins, RC3H1 and its paralog RC3H2, are also involved in degradation. They have been shown to induce degradation of mRNAs carrying in their 3′UTRs a stem-loop recognition motif called constitutive decay element (CDE), via the recruitment of the CCR4-CAF1-NOT deadenylation complex (Leppek et al., 2013, Schuetz et al., 2014). If their localization is confined to the soma, this would explain the enrichment of a set of mRNAs carrying the CDE element. *Cdc42E7*, and not *Cdc42E6*, carries a CDE-like element in its 3′UTR. This hypothesis is partially supported by the proteomics data, where RC3H1 appears to be slightly enriched in the somatic compartment (log2FC = -0.54), whilst RC3H2 was not detected.

Little is known regarding the function of RBM45. It's expression is predominant in the nervous system (Tamada et al., 2002). The protein localizes mostly in the nucleus (Li et al., 2015), even thought it is found in cytoplasmic inclusions containing TDP-43, in cells of patients affected by neurodegenerative disorders (Collins et al., 2012). Because of its prominent nuclear localization, I discarded it from further analysis.

In the nucleus, heterogeneous nuclear ribonucleoproteins (hnRNPs) are the most abundant proteins. They are associated with pre-mRNA, mostly able

A2RE	GCCAAGGAGCCAGAGAGCAUG
A2RE11	GCCAAGGAGCC
A2RE11* G1A	**A**CCAAGGAGCC
A2RE11* C2U	G**U**CAAGGAGCC
A2RE11* C3G	GC**G**AAGGAGCC
A2RE11* C10U	GCCAAGGAG**U**C
Nrgn	**C**CC**UGA**GAGC**A**
Arc	GC**UG**AGGAG**GA**
mouse CamKII	GCCA**GU**GAGCC
rat CamKII	G**G**CAAGGAG**AG**
Cdc42E7	**AGG**AAGGAG**UA**

FIGURE 4.29: **A2RE sequences.** Mutated sequences from Munro et al., 1999.

to shuttle between the nucleus and the cytoplasm, and involved in many aspects of mRNA metabolism (Geuens, Bouhy, and Timmerman, 2016). They are categorized accordingly to the domains contained (Dreyfuss, 1993). To the group A/B belong hnRNP A1, A2/B1, A3 and A0, and they are characterized by two tandemly arranged RRM domains that bind to RNA, and a C-terminal glycine-rich auxiliary domain. Little is known about hnRNP A3 and A0, while A1 and A2/B1 have been shown to regulate mRNA translation (Park et al., 2015) and splicing (Mayeda and Krainer, 1992). Interestingly, hnRNP A2/B1 has been shown to be responsible for the correct dendritic localization of mRNAs in oligodendrocytes and neurons (Shan et al., 2003). The mRNAs which are localized by hnRNP A2/B1 carry a A2 response element (A2RE) (Shan et al., 2000). This type of transport has been reported for *Mbp* (Makeyev and Liebhaber, 2002), and *CaMKII*, *Arc*, *Nrgn* (Gao et al., 2008). Moreover, it has been shown that the interaction of hnRNP A2/B1 with A2RE is stimulated upon increased levels of Ca^{2+} (Muslimov et al., 2014). Interestingly, *Cdc42E7* carries a A2RE-like element (Fig. 4.29). Mutational studies revealed that A2RE11 is the minimal region required for the binding by hnRNP A2/B1, and that nucleotide substitutions are tolerated in certain positions (Munro et al., 1999). For instance, in the case of C3G and C10U substitutions, that characterize *Cdc42E7* A2RE, binding of hnRNP A2/B1 is as strong as to the native element (Munro et al., 1999). On the

other hand, G1A substitution slightly decreases protein binding (Munro et al., 1999). Taking this information into account, it could be speculated that *Cdc42E7* might belong to the group of mRNAs localized via hnRNP A2/B1. hnRNP K is composed of three KH and two proline-rich domains, embedded in the K-interactive region. This region makes hnRNP K different from the rest of the hnRNPs by allowing interactions with many other proteins, which ultimately determines a high degree of functional versatility (Bomsztyk, Denisenko, and Ostrowski, 2004). In fact, hnRNP K has been linked to regulation of transcription (Stains et al., 2005), splicing (Cao et al., 2012), mRNA silencing (Fan et al., 2015), mRNA stability (Fukuda et al., 2009) and translation (Habelhah et al., 2001). The presence of hnRNP K in the pull-down might be due exactly to the fact that it interacts with many proteins, i.e. it was shown to interact with PTBP1 (Kim et al., 2000), a known *Cdc42* binder, which I also found among the bound RBPs.

PTBP1 (or hnRNPI) and its neuronal paralog PTBP2 (Licatalosi et al., 2012, Keppetipola et al., 2012) are splicing factors, previously characterized as regulators of *Cdc42* splicing (Yap et al., 2016). PTBP1 regulates *Ptbp2* mRNA levels, by inducing exon skipping, an event that determines *Ptbp2* mRNA degradation via nonsense-mediated mRNA decay (Ni et al., 2007, Makeyev et al., 2007). During neuronal differentiation, PTBP1 and PTBP2' protein levels change, with a decrease in PTBP1 driven by miR-124 silencing and a subsequent increase in PTBP2 (Polydorides et al., 2000, Boutz et al., 2007, Li et al., 2014). The change in PTBP1/2 ratio affects alternative splicing, leading to a general transition towards splicing patterns specific of the nervous system. Relative to *Cdc42E7*, PTBP2 has been shown to facilitate E7 exon inclusion by promoting E6 exon skipping (Hwang et al., 2017). In fact, high-throughput sequencing of RNA isolated by crosslinking immunoprecipitation (HITS-CLIP) data from brain confirmed binding sites for PTBP2 between intron 5 and exon 6, and downstream exon 6 of *Cdc42* (Licatalosi et al., 2012). Mutations in these sequences were previously shown to promote E6 inclusion (Yap et al., 2016), supporting the role of PTBP2 in promoting E6 exon skipping.
Interestingly, recent HITS-CLIP data from spermatogenic cells identified additional PTBP2-binding sites in the 3′UTR of *Cdc42E7* (Hannigan, Zagore, and Licatalosi, 2017). This is in line with my result where I identified PTBP2 binding to *Cdc42E7* 3′UTR, and might suggest that after *Cdc42* splicing, PTBP2 remains bound to the 3′UTR of *Cdc42E7*, possibly regulating functions other than splicing.

Finally, QKI has been previously suggested to play a role in RNA localization and translation in perisynaptic astrocytes processes (Sakers et al., 2017),

therefore particularly interesting in the context of *Cdc42* localization. Analysis of QKI-CLIP data from mouse brain (Hayakawa-Yano et al., 2017) confirmed the presence of QKI binding sites in the 3′UTR of *Cdc42E7* (Fig. 4.28, panel c), but not of E6 isoform, corroborating the possibility that QKI is a specific regulator of E7 isoform only.

Among all the candidates, PTBP2 and QKI were chosen to start dissecting their function. I generated cell lines depleted in PTBP2 or QKI, by expressing shRNAs, and upon knock-down I screened for splicing impairment and defects in localization. Knock-down efficiency for PTBP2, performed with two different sets of shRNAs (see table 3.4), and QKI reached 80% depletion (data not shown). Upon PTBP2-KD I observed an impairment in splicing: *Cdc42* RNA levels are reduced, namely because of a decrease in *Cdc42E7* (Fig. 4.30, panel a). This result confirms the role of PTBP2 in *Cdc42*-splicing regulation by promoting E7 exon usage, in agreement with previous published work (Yap et al., 2016, Hwang et al., 2017). On the other hand, QKI and PTBP2 failed in influencing *Cdc42E7* mRNA localization. I did not observe any difference in the relative enrichment upon RBP-KD compared to the control (scramble shRNA) (Fig. 4.30, panel b). This result suggests that these RBPs might accomplish different functions in *Cdc42E7* RNA metabolism. In particular, QKI has been shown to play a role in translational repression of mRNAs containing a QKI RBP response element (QRE) motif (Sakers et al., 2017), and therefore might be involved in translational repression of *Cdc42E7* during transport.

To summarize this part, I identified several genes expressing isoforms that are differentially distributed among the somatic and neuritic compartments. Among the different features that could be responsible for the different localization of the isoforms I looked at the length of the 3′UTRs. The fraction of isoforms enriched in the neurites is surprisingly characterized by shorter 3′UTRs. Among the isoforms showing a different localization I focused on *Cdc42*. I showed that *Cdc42E7* isoform localizes at RNA level in the neuritic compartment thanks to its 3′UTR, and that this ultimately determines its protein localization. To find regulators of *Cdc42* RNA metabolism, I identified the specific RBPs binding to *Cdc42* 3′UTRs. I confirmed the role of PTBP2 in *Cdc42* splicing, but failed in identifying factors responsible in its localization. Further characterization of the identified *Cdc42E7*-RBPome will be required to fully understand the mechanism which is responsible for mRNA localization and local translation of *Cdc42*, and potentially of other localized isoforms.

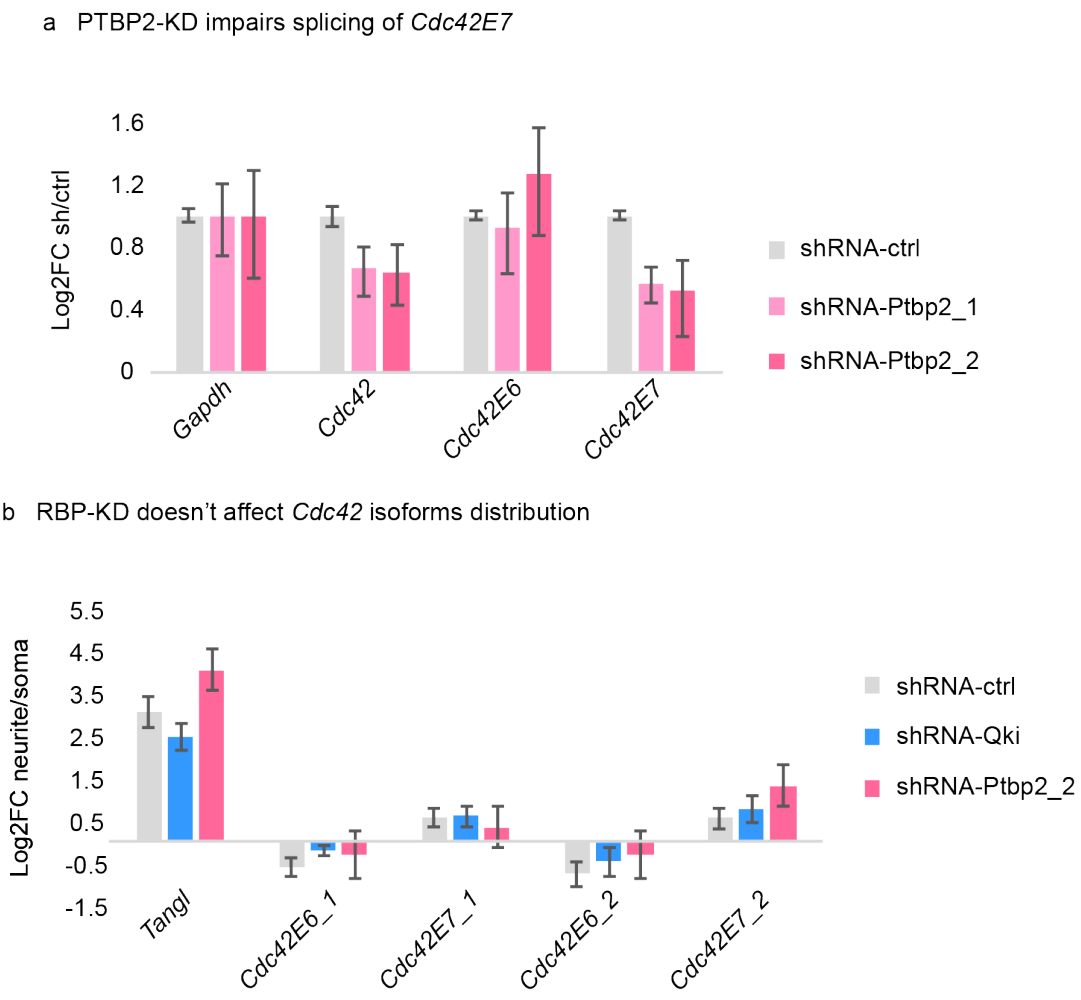

FIGURE 4.30: **RBPs-KD and their effect on splicing and localization of *Cdc42* isoforms.** a | qRT-PCR to assess splicing of *Cdc42* upon PTBP2-KD, performed with two different shRNAs. Histogram colors stand for the different shRNA-treated samples: control shRNA (in grey), shRNA-Ptbp2_1 (in pink), shRNA-Ptbp2_2 (in fucsia). Data are normalized to the control sample (shRNA-ctrl). Error bars represent SD for three biological replicates. b | qRT-PCR to assess localization of *Cdc42* upon PTBP2-KD and QKI-KD, performed with two different set of primer pairs for each *Cdc42* isoform (1 and 2). Histogram colors stand for the different shRNA-treated samples: control shRNA (in grey), shRNA-Qki (in blue), shRNA-Ptbp2_2 (in fucsia). *Tangl* is used as control for the proper neuritic enrichment of the samples. Error bars represent SD for three biological replicates.

5 Discussion and perspectives

5.1 The study of asymmetry in neuronal subcellular compartments

Neurons are a very interesting class of highly polarized cells. Many fundamental processes where gene expression is spatially and temporally controlled, such as neuronal polarity, axonal growth, axonal arbor architecture, dendrite morphology, plasticity and memory formation, are ruled by mRNA and protein localization. Consequently, understanding how asymmetry is established is crucial to understand how neurons work. Cellular asymmetric distribution is regulated by a combination of processes, spanning from mRNA localization, local translation, local degradation, local protection from degradation. Extensive literature covers the topic of mRNA localization in neurons (Cajigas et al., 2012, Gumy et al., 2011, Taylor et al., 2009, Minis et al., 2014, Taliaferro et al., 2016, Rotem et al., 2017, Briese et al., 2015, Tushev et al., 2018). The extent of agreement (Pearson correlation) of the local transcriptome among different datasets varies (Fig. 5.1), and depends on several factors:

(i) different neuronal types should be intuitively equipped with different pools of localized mRNAs;

(ii) contaminating cell types, especially relevant for primary cell cultures, will affect the correct identification of the localized mRNAs;

(iii) the technique/device used for compartment separation will affect the composition of the local mRNA pool.

Therefore it is crucial to take into account the experiment's parameters. For instance, when filters or microfluidic chambers are used for separation, the neuritic fraction will contain either axons and dendrites or axons only, respectively. This difference, which is dependant on the device used, results in a relatively low correlation between two datasets (from Briese et al., 2015, Rotem et al., 2017), both obtained from motoneurons (r = 0.49) (Fig. 5.1). This consideration underlines how the local transcriptome changes greatly not only between soma and neurites, but also between axons and dendrites.

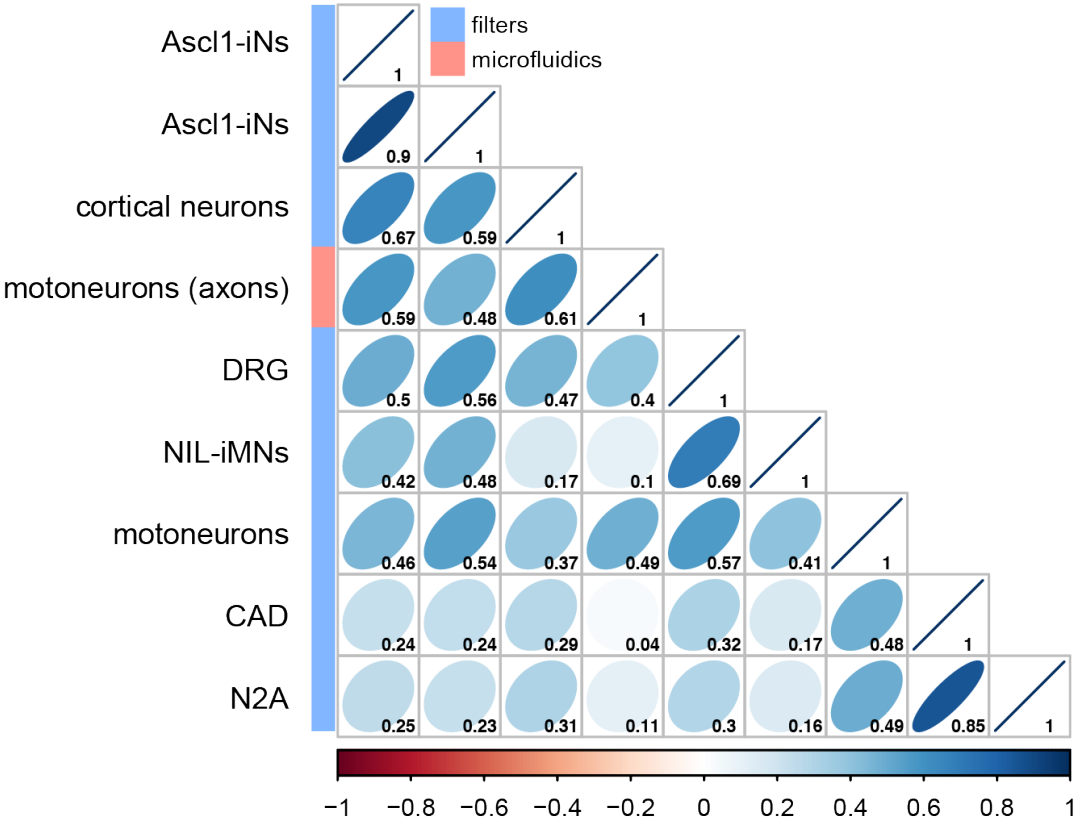

FIGURE 5.1: **Comparison of neuritic transcriptome among several published datasets.** Pairwise correlation plot comparing different datasets of local transcriptome. Colors and numbers correspond to Pearson correlation coefficients. Ascl1-iNs from Zappulo*, Van Den Bruck*, Ciolli Mattioli*, Franke* et al., 2017, cortical neurons, CAD and N2A from Taliaferro et al., 2016, motorneurons (axons only) from Briese et al., 2015, DRG from Minis et al., 2014, NIL-iMNs (unpublished), motoneurons from Rotem et al., 2017. Analysis by N. von Kügelgen.

Since different pools of mRNAs localize to different subcellular compartments, I was interested in understanding whether mRNA localization and local translation would be the main determinants of local proteome. Moreover, I aimed at studying the mechanisms that establish such an asymmetric distribution of mRNAs.

The system chosen to address such topics was obtained through the differentiation of mESC into neurons thanks to the induction of the transcription factor ASCL1 (Ascl1-iNs). Ascl1-iNs were grown on a microporous filter, which allowed the mechanical separation of the somatic and neuritic compartments. Using an *in vitro* system allows to work with an homogeneous population of cells, whereas the neuronal population isolated *in vivo*, i.e. from the cortex, is a mixed population of different types of neuronal and non-neuronal cells. Contamination of non-neuronal cell types - astrocytes,

oligodendrocytes, microglia, endothelial cells, fibroblasts, erythrocytes - is very common in primary cell preparations, and many of these also extend neurite-like protrusions. Since I aimed at comparing subcellular compartments with genome-wide techniques, by performing a relative enrichment analysis among the somatic and neuritic compartments, the presence of different cell types would be very harmful for the outcome of this analysis. In fact any enrichment would be unbalanced depending on the cells present in the preparation, resulting in a meaningless average of relative enrichment. I used primary neurons for microscopy and biochemistry experiments only, where non-neuronal contamination was irrelevant as I could discriminate visually or by means of neuron-specific promoter employed for reporter expression.

A suitable system to study separately subcellular compartments of Ascl1-iNs was implemented by the use of a filter device, which allowed to physically separate soma and neurites, where the latter comprehends both axons and dendrites. Different methods exist to perform the same task of separation, for instance microfluidic chambers, where two wells are separated by a set of microgrooves in which the axons grow. Here the separation is enabled by the maintenance of a fluidic gradient of chemoattractants in the two chambers, which is possible thanks to the hydrostatic pressure formed by the difference in volumes. This system allows a higher resolution of separation: if the microgrooves are sufficiently long, only axons can enter the distal department of the chamber, effectively separating from dendrites. I opted for higher amount but lower resolution, in order to apply genome-wide techniques which require more input than what is possible to obtain with microfluidic devices.

The filter separation method allowed to obtain a still humble but sufficient amount of RNA and protein from the neuritic fraction (200 ng for RNA, 5 μg for protein for iNs). Importantly, for each experiment I set up several controls to assess the quality of separation via immunofluorescence, RT-qPCR and western-blot. In all the assays, somatic and neuritic markers showed the correct relative enrichment, confirming the good performance of this system.

5.2 Modification of ribosome profiling enables the study of local translation

To understand how the local proteome is defined in Ascl1-iNs and how much can be explained by RNA localization and local translation rather than protein transport, I identified the local translatome.

Classic techniques that enable the study of translation are polysome profiling and ribosome profiling. Due to their laborious and cumbersome procedure, they cannot be applied to the study of subcellular compartments as they require quite a large amount of input material.

The compartment separation approach to study separately the somatic and neuritic compartments of Ascl1-iNs allows to recover only a small amount of RNA, not sufficient to perform ribosome profiling. With the aim of applying this technique to small samples, I compared three different protocols. The purpose was a simplification which would result in a smaller loss of the input material, allowing to start with a limited amount. The methods compared involved the use of different RNases for the footprinting step (RNaseI or MNase), and different types of monosome recovery (size-exclusion columns or omission of monosome recovery). These two steps were chosen for the following reasons: footprinting is crucial to obtain high quality data, as it impacts subcodon phasing, *ad hoc* feature of ribosome profiling. On the other hand, standardization is lacking concerning monosome isolation, and i.e. sucrose cushion does not guarantee the isolation of ribosomes only (large RNPs can also co-sediment with ribosomes). Moreover, Reid and colleagues suggested the possibility of omitting this step as ribosome protected footprints (RPFs) can be easily purified by size-selection thanks to their very specific length (Reid, Shenolikar, and Nicchitta, 2015). Through this experiment, where I compared RNaseI vs MNase, and column-based monosome isolation vs omission of the step, I obtained high quality of sub-codon phasing only when RNaseI was used. Most importantly, I observed a very high correlation (r = 0.96) between libraries where monosome isolation was carried out, and libraries where monosome isolation was omitted. Moreover, reads were in frame, and mapped to CDS as expected. In addition, I also changed the timing of dephosphorylation of the RPFs, required for library preparation. Instead of performing this step after gel separation, I anticipated it right before, shortening the protocol even further and avoiding additional loss of RNA. Thanks to these modifications, I was able to perform ribosome profiling with a starting material of 5 μg of total RNA, obtaining a $\sim$ 10-fold reduction compared to the classic protocol, and shortening it in time from 5-7 to 2 days (Fig. 5.2).

A different way to obtain the local translatome information could be achieved by modifying and adapting the proximity-ribosome profiling method developed by Jan and colleagues (Jan, Williams, and Weissman, 2014). In this case, ribosomes are modified to contain a biotin acceptor peptide (AVI-tag), available for biotinylation. By localizing the BirA enzyme to a specific subcellular compartment, it is possible to tag with biotin only those ribosomes which are

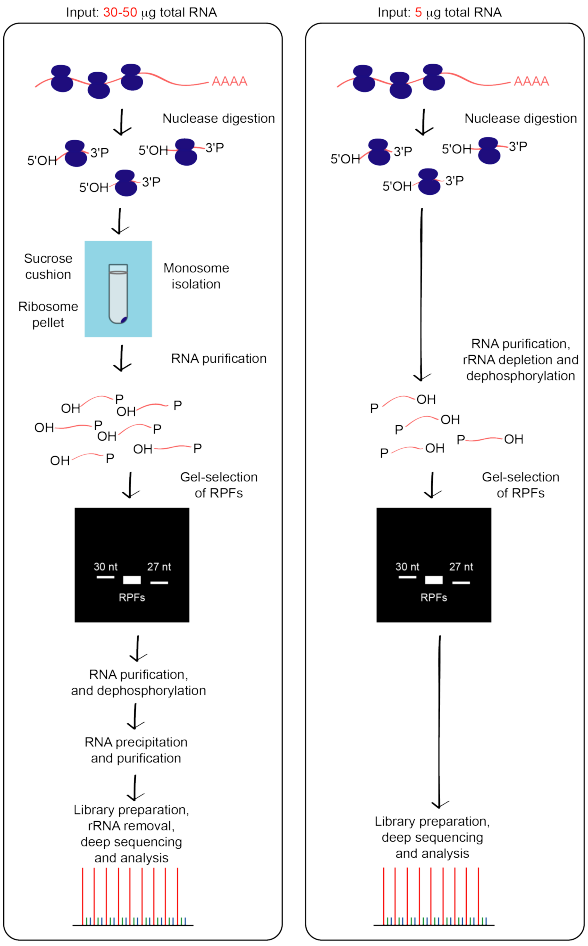

FIGURE 5.2: **Comparison of the classical ribosome profiling method to the optimized and shortened version.** The protocols differ in several steps. The monosome isolation step is achieved by sucrose cushion in the classical protocol, and is omitted in the shortened protocol. In the shortened protocol, phosphorylation is anticipated before gel separation.

in proximity of the enzyme. Biotinylation allows the pulldown with streptavidin, to isolate the tagged ribosomes only. This method was employed to study local translation at the ER and mitochondria, by fusing BirA with SEC61β or OM45, respectively (Jan, Williams, and Weissman, 2014). One possibility would be the fusion of BirA to a neurite-localized protein, or to a 3′UTR known to be able to localize to axons or dendrites. However, a clear-cut distribution is rare. By testing several 3′UTRs fusions to BirA, I was never able to observe a sharply outlined localization of BirA in neurites only (data not shown). Several might have been the problems:

(i) the 3′UTR used;

(ii) the neuronal system employed;

(iii) the time of analysis;

(iv) the fact that translation can already start during transport (Wang et al., 2016);

(v) the diffusion of the protein after translation.

One way of troubleshooting could be through the use of specific 3′UTRs known to mediate translational repression during transport, e.g. the 3′UTR of *β-actin*. A more complex, but likely more successful approach, could be the BirA fusion to a neurite-localized membrane protein, which would undergo the ER-Golgi processing, and importantly, transport via vesicles. This would protect from ectopic biotinylation as the protein would be released from the vesicle upon destination arrival only. In conjunction with such an approach, the biotin pulse could be synchronized with another stimulus which would induce translation of a certain subset of mRNAs depending on the signal. This would allow the analysis of local translation in relation to stimuli (i.e. guidance cues, growth factors), and determine the stimulus-dependent translatome.

5.2.1 Local proteome is determined by the combination of mRNA localization and local translation

So far, ribosome profiling has not been applied to subcellular compartments, with the exception of the proximity-ribosome profiling protocol, which was used for analyzing the ER- and mitochondria-translatome (Jan, Williams, and Weissman, 2014). Using a simplified and optimized version, I was able to study local translation from neuronal subcellular compartments. The overlay of compartment-specific transcriptome and proteome data, shows that $\sim$ half of the local proteome can be explained by mRNA localization and local translation (Zappulo*, Van Den Bruck*, Ciolli Mattioli*, Franke* et al., 2017). Among the locally translated mRNAs I found several cytoskeletal, secreted and membrane proteins. In fact, in growth cones, translation of cytoskeletal proteins is prominent, as it is involved in regulation of axonal turning and advance (Lin and Holt, 2007), as well as growth cone regeneration after axotomy (Willis and Twiss, 2006). Membrane and secreted proteins, which require processing via rough ER and Golgi, are also part of the local translated proteome. This is not surprising in dendrites, where both organelles are present. On the other hand, rough ER and Golgi outposts are prevented from accessing the axons because of the axon hillock (Zheng et al., 2008). However, ER and Golgi proteins were identified in axons (Merianda et al., 2009), and axonal translation of membrane proteins has been reported for the κ-opioid receptor and the guidance receptor EPHA2 (Bi et al., 2006, Tsai, 2006, Brittis, Lu, and Flanagan, 2002). This shows that axonal translation of

transmembrane and secreted proteins might also occurs in axons.
In summary, the dataset resulting from local ribosome profiling shows a high degree of asymmetry in terms of locally translated mRNAs, between the somatic and neuritic compartments. Interestingly, the combination of compartment-specific translatome, with other omics datasets such as transcriptome and proteome (mass-spectrometry, pSILAC and QuaNCAT), shows that $\sim$ half of the local proteome can be explained by mRNA localization and local translation (Zappulo*, Van Den Bruck*, Ciolli Mattioli*, Franke* et al., 2017). This result highlights how different subcellular compartments require a different pool of localized mRNAs and proteins, and that local translation plays a prominent role in defining the local proteome.

A couple of more studies analyzes local translation at a genome-wide level: one in axons of retinal ganglion cells (RGCs) based on RNA-seq (Shigeoka et al., 2016), and one in protrusion of a cancer cell line based on mass-spectrometry (Mardakheh et al., 2015). Shigeoka and colleagues combined the use of RiboTag knock-in mouse line (Sanz et al., 2009) to dissection (Shigeoka et al., 2016). Using this system, they isolate ribosomes from retinal axons, from which the ribosome-bound mRNAs can be sequenced (chapter 1.4.2). In this study, Shigeoka and colleagues were not interested in a comparison of the axonal translatome with the somatic one, but in analyzing the translation in axons at different developmental stages. With this comparison, they identified two sets of mRNAs, one that is constitutively translated independently of the developmental stage, and one that is stage-specific, confirming the importance of the localized translation machinery for the maintenance of general homeostasis and for stage-specific contribution.
Mardakheh and colleagues used puromycinylation (10 min pulse) to assess the amount of newly synthesized proteins and pSILAC (2 hours pulse) to identify the locally synthesized proteome from the protrusions of an epithelial cancer cell line in comparison with the cell body (Mardakheh et al., 2015). From the pSILAC experiment, Mardakheh and colleagues derive translational rates, and compare them to the local transcriptome and proteome (Mardakheh et al., 2015). From this comparison they found a poor correlation with mRNAs (0.02 Pearson correlation), whilst a significant correlation with proteins (0.3 Pearson correlation). These results partially agree with mine, where ribosome profiling significantly correlates with proteome (0.34 Pearson correlation), and partially disagree, as in my case ribosome profiling also correlates with transcriptome (0.33 Pearson correlation).

It is important to mention that the translational rates calculated by Mardakheh and colleagues are based on pSILAC, where the pulse was 2 hours

long. With such a long pulse, protein transport to protrusion cannot be excluded, especially in a system where protrusions are relatively short, 15 μm on average. In fact, as mentioned in chapter 4.2.2, a protein like tubulin is synthesized in less than two minutes (translation speed of 5 aa per second for a 500 aa protein). By considering a slow rate of diffusion, typical for cytoskeletal proteins ($\sim$ 0.002 - 0.011 μm/s), a 2 hours pulse would allow a movement of 14 - 78 μm, more than sufficient to reach the protrusions from the cell body.
That said, our results overlap for the main message of identifying local translation as the main driver of local proteome.

Here, I identified the specific identity of the local pools of translated mRNAs in the somatic and neuritic compartments of iNs. Since dendrites and axons are specialized subcompartments, one interesting venue would be the separate analysis of their specific translatome. In a context where translation can be induced upon certain stimuli, it would be interesting to expand the question of RNA localization and local translation in a broader functional perspective, by playing with several factors influencing these mechanisms, and ruling out the specific stimulus-translatome relationship.

5.3 *Trans*- and *cis*-elements and their role in localization

Localization can be achieved by the synergistic activity of *trans*- and *cis*-acting elements, where the latter are elements present in the 3′UTR of mRNAs, which serve as docking points for RNA binding proteins (*trans*-acting elements). RBPs are important regulators of mRNA metabolism, acting at different layers such as mRNA localization, translational regulation, mRNA stability and degradation. I investigated in both these directions, specifically, MOV10 was the *trans*-acting factor chosen for dissection, and alternative polyadenylation as the mechanism generating diversity in *cis*-elements. Precisely, 3′end-seq was used to identify which alternative isoforms were transcribed, and among those, the differentially localized ones.

5.3.1 MOV10 is neurite-localized and its function might be related to regulation of local translation

One way to dissect how the mechanisms of mRNA localization and local translation are regulated, is to identify the *trans*-acting factors, namely RBPs, involved in these processes. To investigate in this direction, I chose one of the 29 neurite-localized RBP identified in Zappulo*, Van Den Bruck*, Ciolli

Mattioli*, Franke* et al., 2017 to dissect further. MOV10 is an RNA helicase which participates in many aspects of RNA metabolism. It was shown to be involved in translational repression through the interaction with the RNA-induced silencing complex (Banerjee, Neveu, and Kosik, 2009, Meister et al., 2005, Kenny et al., 2014), but also in translational activation in combination with FMR1 (Kenny et al., 2014). Moreover, its degradation via the NMDA-stimulated proteasome was shown to stimulate translation at the synapses (Banerjee, Neveu, and Kosik, 2009). Additionally, MOV10 has been shown to interact with UPF1, the main player in nonsense-mediated mRNA decay (NMD), to remove secondary structure from NMD-targeted mRNAs.
Because of the importance of MOV10 in mRNA metabolism, I first identified its mRNA targets by means of two techniques, RIP and PAR-CLIP. Consistent with MOV10-neuritic localization, also MOV10 targets are localized in the neurites. However, MOV10 is not involved in localization of its targets. In fact, the knock-out of the protein does not affect mRNA localization. By looking at local transcriptome, translatome and proteome, MOV10 targets appear to be localized at mRNA level in the neurites, but only a small fraction is locally translated (36%). This hints to a possible role of MOV10 in translational repression, in agreement with previous published data (Banerjee, Neveu, and Kosik, 2009, Kenny et al., 2014, Meister et al., 2005). Consistently, in the pulldown of MOV10 interactors, I identified several proteins involved in translational repression, among which AGO2, FMR1, and TRIM71. AGO2 and FMR1 are known interactors of MOV10 (Meister et al., 2005, Kenny et al., 2014), whilst TRIM71 is a new potential candidate which might work together with MOV10 for mRNA translational repression. Further characterization will be required to investigate further this hypothesis.

5.3.2 Alternative 3′UTR isoforms localize in different subcellular compartments

The study of alternative isoforms is usually framed in the context of tissue expression, in order to identify tissue-specific isoforms. On the other hand, the idea that isoforms might be expressed in one cell, in order to be differentially localized thanks to the differences in their 3′UTRs, is very intriguing. In order to investigate this idea, I performed 3′end-seq from the somatic and neuritic compartments of Ascl1-iNs. In agreement with a recent study (Tushev et al., 2018), this experiment revealed that there are indeed several of such cases, where different isoforms localize to different compartments. To understand whether any particular feature would be associated to a specific localization, first I looked at the length of the 3′UTR. Unexpectedly, I found that the short isoform is usually enriched in neurites. This is particularly

surprising in the context of APA isoforms, since the sequence of the short isoform is completely embedded within the long one, and it is generally believed that short isoforms cannot be more complex than the long ones in terms of regulation. However, this result can be explained in several ways:

(i) extra sequences present in the long APA isoforms mediate their anchoring in soma or degradation in neurites via localized *trans*-acting factors, e.g. RBPs and miRNAs;

(ii) sequences within shorter isoforms required for localization are hidden within secondary structures formed by long APA isoforms;

(iii) long APA isoforms undergo 3′UTR shortening in neurites (Andreassi et al., 2019).

Notably, prior studies obtained conflicting results on localization of short and long APA isoforms. Taliaferro and colleagues reported similar numbers of short and long APA isoforms localized to neurites of CAD and N2A neuroblastoma cell lines (Taliaferro et al., 2016). Analysis of rat brain slices detected a slightly higher number of long APA isoforms in neuropil than in soma (Tushev et al., 2018). Also, longer isoforms were reported in axons of cultured rat sympathetic neurons (Andreassi et al., 2019). Moreover, Taliaferro et al. analyzed mRNA decay rates and didn't detect any difference between the neuritic and somatic pool of mRNAs (Taliaferro et al., 2016). On the other hand, Tushev and colleagues reported that neuropil enriched 3′UTRs have longer half lives (Tushev et al., 2018). A possible explanation for this discrepancy is usage of different test systems. In addition, brain slices contain not only neurons, but also glia, and computational subtraction of glial transcripts might bias the analysis.

A mechanism that might explain the presence of short isoforms in the neurites, and that recently gained more evidence, is post-transcriptional cleavage in the cytosol, a mechanism producing shorter isoforms and 3′UTR tail fragments (Malka et al., 2017, Kocabas et al., 2015). This has been shown for *Impa1* in sympathetic axons, and suggested to be a widespread event (Andreassi et al., 2019). Since I observed an enrichment of shorter isoforms in neurites, it would be important to investigate such possibility. For example, by building a library of lenti-plasmids, containing a reporter gene, followed by a pool of long APA tandem 3′UTRs. After compartment separation and targeted amplicon sequencing (to recover the library only, and not endogenous mRNAs), the identification of post-transcriptional cleavage events - if they arise - would be possible (since the library initially contains long isoforms only).

Additional work will be required to understand why short isoforms are enriched in the neurites, whether post-transcriptional cleavage applies to my data, and what would be the biological function of such a process.

Disregarding of which isoforms are localized and focusing on the common ground of asymmetric localization of isoforms, one factor that could be important to consider is mRNA stability and translation efficiency. A global assessment showed that alternative 3′UTRs have little effect on either mRNA stability or translation (Spies, Burge, and Bartel, 2013). However, this observation might change if one looks into subcellular compartments, where the availability and abundance of the translation machinery might vary. In fact, Tushev and colleagues showed that longer 3′UTR neurite-localized isoforms are characterized by longer half-lives (Tushev et al., 2018), in contrast to what reported globally in Spies, Burge, and Bartel, 2013. It might be important to have a higher mRNA stability or translation efficiency in distal neurites, where the translation machinery is probably present in lower amounts than in soma. In light of this hypothesis, it would be interesting to analyze translation efficiency of 3′UTR tandem APA isoforms in relation to their localization and to their 3′UTR length, to test whether there is a difference in translation efficiency.
Regarding the ALE class, a tool was recently developed for the study of alternative spliced isoforms in ribosome profiling data (Reixachs-Sole et al., 2019). It would be very interesting to analyze the translation levels for the ALE category, which can be differentiated thanks to the difference in exons.

Cdc42 3′UTR is the determinant of protein localization

Among the isoforms that showed different localization between the somatic and neuritic compartments, I found *Cdc42*, belonging to the ALE category. The two isoforms of *Cdc42* differ in the last exon, meaning in the last part of the CDS and in the 3′UTR sequence. Both isoforms are characterized by two signals for targeting to the plasma membrane: a stretch of polybasic amino acids (Johnson, Erickson, and Cerione, 2012), and a CaaX motif (CCIF in CDC42E6, CVLL in CDC42E7) both in the C-terminal hypervariable region. These motifs are target of post-translational modification consisting of prenylation (geranylgeranylation/farnesylation) at the first cysteine, proteolysis of the aaX peptide, and carboxymethylation. CDC42E6 can also undergo a dual lipidation pathway with prenylation at the first cysteine, and palmitoylation at the second, omitting the proteolysis of the aaX peptide (Nishimura and Linder, 2013). This alternative pathway accounts for 5-20% of palmitoylated

CDC42E6 in neonatal mouse brain (Nishimura and Linder, 2013). The reversible nature of palmitoylation allows a dynamic tethering of proteins to the membrane or specific lipid micro-domains (Linder and Deschenes, 2007, Smotrys and Linder, 2004), providing an important tool in modulation of neuronal protein trafficking.

The reasons to choose this particular candidate to investigate further reside in the fact that some inconsistencies exist in literature: the two isoforms of *Cdc42* have been related to different functions in neurons, with *Cdc42E6* involved in spine morphogenesis and *Cdc42E7* in axon specification (Yap et al., 2016), implying a different localization (dendritic or axonal, respectively) for the two protein isoforms, and addressing post-translational modification (palmitoylation or prenylation) as the potential responsible factor for the different subcellular localization. However, a different localization for the two protein isoforms has not been shown. On the contrary, both isoforms have been shown to localize to dendrites (Kang et al., 2008), and CDC42E6 has been shown to localize to the axon tip (Mukai et al., 2015). More discrepancies arise in Yap et al., 2016 and Mukai et al., 2015, where in the first case CDC42E7, and in the second case CDC42E6, were suggested to be involved in axogenesis or axonal length and branching (Fig. 5.3).

The hypothesis of post-translational modification-dependent localization that these previous studies suggested presents some flaws: since both isoforms can be prenylated, why this modification would favour the axonal localization of one isoform only? Moreover, the extent of palmitoylation for CDC42E6 has been estimated to be around 5-20%, while in the remaining cases CDC42E6 gets prenylated as CDC42E7 (Nishimura and Linder, 2013), raising more doubts on the localization being dependent on different post-translational modifications only.

Interestingly, the comprehensive combination of datasets, including 3′end-seq, total RNA-seq, Ribo-seq and mass spectrometry from neurites and soma, allowed me to investigate local expression of *Cdc42* at different levels. I found that *Cdc42* mRNA isoforms are differentially localized and their alternative 3′UTRs are required for proper localization of the protein isoforms. Thus, these data point to the role of 3′UTRs and mRNA localization in generating differential localization of CDC42 protein isoforms. I showed that the protein modification motif is not sufficient to localize CDC42E7 protein, although it likely contributes to maintain protein localization by anchoring the protein to the membrane and preventing diffusion. Importantly, this mechanism is functional not only in Ascl1-iNs but also in primary cortical neurons. Consistently, differential localization of *Cdc42* isoforms was detected in previously reported 3′-seq from rat somata and neuropil (Tushev et al., 2018).

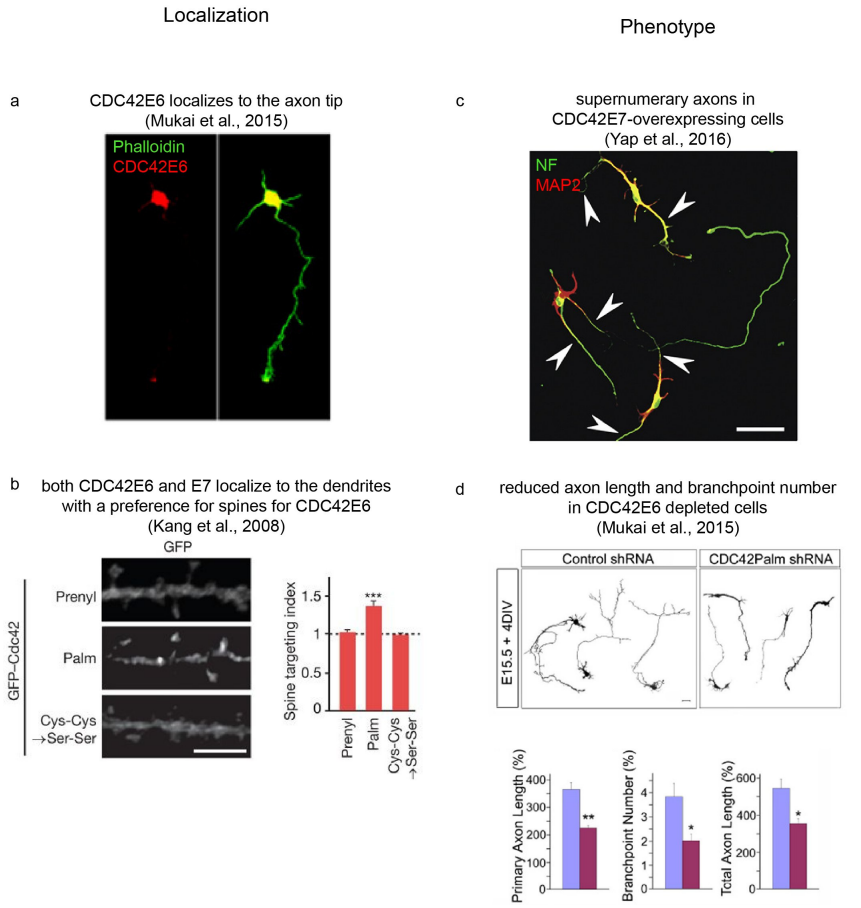

FIGURE 5.3: **Data available on *Cdc42* isoforms gathered from published literature.** a | CDC42E6 localizes to the tip of the axon (Mukai et al., 2015). b | Both isoforms of CDC42 localize to the dendrites, with an increase in spine localization for CDC42E6 (Kang et al., 2008). c | CDC42E7 overexpression induces supernumerary axons (Yap et al., 2016). d | CDC42E6 depletion causes a reduction in axon length and branchpoint number (Mukai et al., 2015).

Moreover, I identified 17 *Cdc42E7* 3′UTRs-bound RBPs. Among them, QKI and PTBP2′ function was further dissected. QKI belongs to the STAR (signal transduction and activation of RNA) family of K homology (KH) domain-containing RBP with multiple functions in RNA metabolism, and reported to contribute to RNA localization and translation regulation in perisynaptic astrocyte processes (Sakers et al., 2017). Available QKI high-throughput sequencing of RNA isolated by crosslinking immunoprecipitation (HITS-CLIP) data indeed suggest the presence of QKI-binding sites in the 3′UTRs of *Cdc42E7*, but not of *Cdc42E6* (Hayakawa-Yano et al., 2017).
PTBP2 is a neuronal protein that regulates *Cdc42* alternative splicing during neuronal development, stimulating the inclusion of exon 7. I could confirm the role of PTBP2 in *Cdc42* splicing, however I could not show any involvement in *Cdc42E7* mRNA localization for neither of these RBPs.

Many other candidates are still to be tested (Fig. 5.4). For example, hnRNP A2/B1 is responsible for the neuritic localization of several transcripts carrying a A2RE element. *Cdc42E7* possesses a A2RE-like element (Fig. 4.29), which makes this venue very interesting. Otherwise *Cdc42E7* enrichment in the neurites could result from a specific degradation of the isoform in the somatic compartment, or from neuritic protection from degradation. Some interesting candidates to test for this hypothesis are Roquin proteins, and ELAVL1. Roquin proteins degrade mRNAs carrying a constitutive decay element (CDE). If Roquin proteins are confined in the somatic compartment and they indeed degrade *Cdc42E7*, this would explain *Cdc42E7* enrichment in the neurites. The local proteome data supports this hypothesis, as RC3H1 shows a slight somatic enrichment.
ELAVL1 protects mRNAs carrying AU-rich elements. If ELAVL1 is neuritically localized, it would protect *Cdc42E7* from degradation, specifically in the neuritic compartment. This hypothesis is not supported by the local proteome data, where ELAVL1 is enriched in the somatic compartment. However ELAVL proteins also possess a nuclear function. Therefore, the somatic enrichment shown in the local proteome dataset might be attributed to the nuclear fraction of the protein, leaving the door open for ELAVL1 involvement in neuritic protection from degradation.

Finally, it remains to be understood why different *Cdc42* isoforms are required in different subcellular compartments. From a preliminary experiment were I depleted either *Cdc42E6* or *Cdc42E7* from primary neurons, I observed a overnumerary number of axon growth cones when E6 was depleted (data not shown). This result supports the hypothesis that the ratio between the two isoforms is necessary for the neurons to establish the proper polarity. When CDC42E7 only is present, the polarization fails to recognize one neurite as the future axon. This observation agrees with results by Yap and colleagues, where they observed overnumerary axons in response to *Cdc42E7* overexpression (Yap et al., 2016).

To conclude, in this work I explored how neurons organize their subcellular compartments in terms of localized pools of mRNAs and proteins. Interestingly, mRNA localization and local translation define $\sim$ half of the localized proteome, giving local homeostasis a prominent role compared to protein transport. I investigated how mRNA asymmetry can be established, by analyzing *trans*-acting elements and *cis*-elements. Among the *trans*-acting elements, I showed that the RBP MOV10 binds to mRNAs that are localized in the neurites, and that it might be involved in translational repression. Consistently, I identified several potential MOV10 protein interactors, known to

be translational repressors, corroborating this hypothesis. On the side of *cis*-elements, I investigated whether neurons express alternative isoforms that differ in their 3′UTR, and whether alternative 3′UTRs are mediating localization. I showed that alternative polyadenylation is extensively used in neurons, and that surprisingly short 3′UTR isoforms are enriched in neurites. It remains to be elucidated whether these are localized as such, or if they are a product of post-transcriptional cleavage. Among the isoforms that showed different localization, I focused on *Cdc42*, belonging to the alternative last exon class, particularly interesting for its role in neurons and for the contrasting evidence coming from published work. I showed that the two isoforms of *Cdc42* are differentially localized already at mRNA levels, and that the 3′UTR determines mRNA and, ultimately, protein localization. I identified the RBPome of each *Cdc42* isoform, including several potential regulator of *Cdc42* localization. It remains to be elucidated which of these RBPs is the responsible for *Cdc42* localization, and why these isoforms are needed at different subcellular locations in neurons.

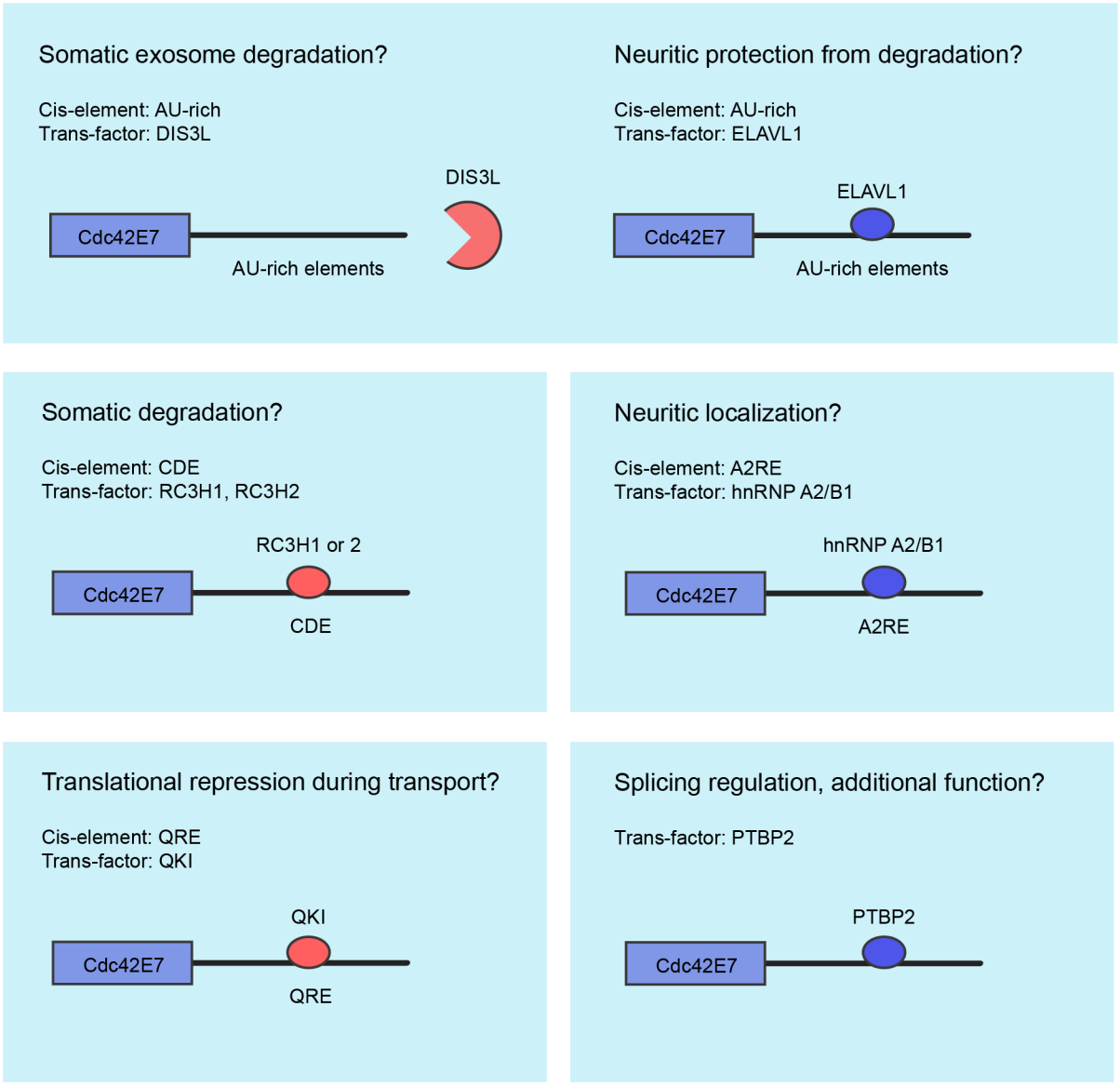

FIGURE 5.4: **Potential *cis*-elements and *trans*-acting factors involved in *Cdc42E7* localization.** Depending on the *cis*-elements and *trans*-acting factors considered, different hypotheses could explain *Cdc42E7* localization to the neuritic compartment.

Bibliography

Amack, Jeffrey D., Aileen P. Paguio, and Mani S. Mahadevan (1999). "Cis and trans effects of the myotonic dystrophy (DM) mutation in a cell culture model". In: *Human Molecular Genetics*. DOI: 10.1093/hmg/8.11.1975.

An, Juan Ji et al. (2008). "Distinct Role of Long 3′ UTR BDNF mRNA in Spine Morphology and Synaptic Plasticity in Hippocampal Neurons". In: *Cell*. DOI: 10.1016/j.cell.2008.05.045.

Andreassi, Catia et al. (2010). "An NGF-responsive element targets myo-inositol monophosphatase-1 mRNA to sympathetic neuron axons". In: *Nature Neuroscience*. DOI: 10.1038/nn.2486.

Andreassi, Catia et al. (2019). "3′UTR cleavage of transcripts localized in axons of sympathetic neurons". In: *bioRxiv*, p. 170100. DOI: 10.1101/170100.

Antic, Dragana, Ning Lu, and Jack D. Keene (1999). "ELAV tumor antigen, Hel-N1, increases translation of neurofilament M mRNA and induces formation of neurites in human teratocarcinoma cells". In: *Genes and Development*. DOI: 10.1101/gad.13.4.449.

Aslemarz, Azam, Paul Lasko, and Francois Fagotto (2018). "Limited significance of the in situ proximity ligation assay". In: *bioRxiv*, p. 411355. DOI: 10.1101/411355. URL: https://www.biorxiv.org/content/early/2018/09/09/411355.

Atasoy, U. et al. (2003). "Regulation of Eotaxin Gene Expression by TNF-α and IL-4 Through mRNA Stabilization: Involvement of the RNA-Binding Protein HuR". In: *The Journal of Immunology*. DOI: 10.4049/jimmunol.171.8.4369.

Banerjee, Sourav, Pierre Neveu, and Kenneth S. Kosik (2009). "A Coordinated Local Translational Control Point at the Synapse Involving Relief from Silencing and MOV10 Degradation". In: *Neuron*. DOI: 10.1016/j.neuron.2009.11.023.

Bannister, N. J. and A. U. Larkman (1995). "Dendritic morphology of CA1 pyramidal neurones from the rat hippocampus: I. Branching patterns". In: *Journal of Comparative Neurology*. DOI: 10.1002/cne.903600111.

Bartel, David P. (2009). "MicroRNAs: Target Recognition and Regulatory Functions". In: DOI: 10.1016/j.cell.2009.01.002. arXiv: 0208024 [gr-qc].

Batista, Andreia F.R., José C. Martínez, and Ulrich Hengst (2017). "Intra-axonal Synthesis of SNAP25 Is Required for the Formation of Presynaptic Terminals". In: *Cell Reports*. DOI: 10.1016/j.celrep.2017.08.097.

Beaudoing, Emmanuel et al. (2000). "Patterns of variant polyadenylation signal usage in human genes". In: *Genome Research*. DOI: 10.1101/gr.10.7.1001.

Beckel-Mitchener, Andrea C. et al. (2002). "Poly(A) tail length-dependent stabilization of GAP-43 mRNA by the RNA-binding protein HuD". In: *Journal of Biological Chemistry*. DOI: 10.1074/jbc.M201982200.

Behringer, Richard et al. (2016). "Differentiating mouse embryonic stem cells into embryoid bodies by hanging-drop cultures". In: *Cold Spring Harbor Protocols*. DOI: 10.1101/pdb.prot092429.

Bellavia, Diana et al. (2007). "Notch3 and the Notch3-upregulated RNA-binding protein HuD regulate Ikaros alternative splicing". In: *EMBO Journal*. DOI: 10.1038/sj.emboj.7601626.

Berkovits, Binyamin D. and Christine Mayr (2015). "Alternative 3′UTRs act as scaffolds to regulate membrane protein localization". In: *Nature*. DOI: 10.1038nature/14321. arXiv: 15334406.

Bertrand, Nicolas, Diogo S. Castro, and François Guillemot (2002). "Proneural genes and the specification of neural cell types". In: DOI: 10.1038/nrn874.

Besse, Florence and Anne Ephrussi (2008). "Translational control of localized mRNAs: Restricting protein synthesis in space and time". In: DOI: 10.1038/nrm2548. arXiv: NIHMS150003.

Betticher, DC. et al. (1995). "Alternate splicing produces a novel cyclin D1 transcript". In: *Oncogene*.

Bi, J. et al. (2006). "Axonal mRNA transport and localized translational regulation of κ-opioid receptor in primary neurons of dorsal root ganglia". In: *Proceedings of the National Academy of Sciences*. DOI: 10.1073/pnas.0607394104.

Bicker, Silvia et al. (2013). "The DEAH-box helicase DHX36 mediates dendritic localization of the neuronal precursor-microRNA-134". In: *Genes and Development*. DOI: 10.1101/gad.211243.112.

Birsoy, B. (2006). "Vg1 is an essential signaling molecule in Xenopus development". In: *Development*. DOI: 10.1242/dev.02144.

Black, Douglas L. and S. Lawrence Zipursky (2008). *To Cross or Not to Cross: Alternatively Spliced Forms of the Robo3 Receptor Regulate Discrete Steps in Axonal Midline Crossing*. DOI: 10.1016/j.neuron.2008.04.019.

Blobel, G. (1985). "Gene gating: a hypothesis." In: *Proceedings of the National Academy of Sciences*. DOI: 10.1073/pnas.82.24.8527.

Böckers, Tobias M. et al. (2004). "Differential expression and dendritic transcript localization of Shank family members: Identification of a dendritic targeting element in the 3′ untranslated region of Shank1 mRNA". In: *Molecular and Cellular Neuroscience*. DOI: 10.1016/j.mcn.2004.01.009.

Boersma, Sanne et al. (2019). "Multi-Color Single-Molecule Imaging Uncovers Extensive Heterogeneity in mRNA Decoding". In: *Cell*. DOI: 10.1016/J.CELL.2019.05.001.

Bohl, F. (2000). "She2p, a novel RNA-binding protein tethers ASH1 mRNA to the Myo4p myosin motor via She3p". In: *The EMBO Journal*. DOI: 10.1093/emboj/19.20.5514.

Bolognani, Federico et al. (2006). "In vivo post-transcriptional regulation of GAP-43 mRNA by overexpression of the RNA-binding protein HuD". In: *Journal of Neurochemistry*. DOI: 10.1111/j.1471-4159.2005.03607.x.

Bomsztyk, Karol, Oleg Denisenko, and Jerzy Ostrowski (2004). "hnRNP K: One protein multiple processes". In: *BioEssays*. DOI: 10.1002/bies.20048.

Boutz, Paul L. et al. (2007). "A post-transcriptional regulatory switch in polypyrimidine tract-binding proteins reprograms alternative splicing in developing neurons". In: *Genes and Development*. DOI: 10.1101/gad.1558107.

Braitenberg, Valentino and Almut Schüz (1998). *Cortex: Statistics and Geometry of Neuronal Connectivity*. Berlin, Heidelberg. DOI: 10.1007/978-3-662-03733-1.

Bramham, Clive R. and David G. Wells (2007). "Dendritic mRNA: Transport, translation and function". In: DOI: 10.1038/nrn2150. arXiv: NIHMS150003.

Briese, Michael et al. (2015). "Whole transcriptome profiling reveals the RNA content of motor axons". In: *Nucleic Acids Research*. DOI: 10.1093/nar/gkv1027.

Brittis, Perry A., Qiang Lu, and John G. Flanagan (2002). "Axonal protein synthesis provides a mechanism for localized regulation at an intermediate target". In: *Cell*. DOI: 10.1016/S0092-8674(02)00813-9.

Brunet, Jean François et al. (1991). "Identification of a peptide specific for Aplysia sensory neurons by PCR-based differential screening". In: *Science*. DOI: 10.1126/science.1840700.

Bullock, S. L. (2004). "Differential cytoplasmic mRNA localisation adjusts pair-rule transcription factor activity to cytoarchitecture in dipteran evolution". In: *Development*. DOI: 10.1242/dev.01289.

Bunge, Mary Bartlett (1973). "Fine structure of nerve fibers and growth cones of isolated sympathetic neurons in culture". In: *Journal of Cell Biology*. DOI: 10.1083/jcb.56.3.713.

Burdick, R. et al. (2010). "P Body-Associated Protein Mov10 Inhibits HIV-1 Replication at Multiple Stages". In: *Journal of Virology*. DOI: 10.1128/jvi.00585-10.

Burgin, K E et al. (1990). "In situ hybridization histochemistry of Ca^{2+}/calmodulin-dependent protein kinase in developing rat brain." In: *The Journal of neuroscience : the official journal of the Society for Neuroscience*.

Buxbaum, Adina R., Gal Haimovich, and Robert H. Singer (2015). "In the right place at the right time: Visualizing and understanding mRNA localization". In: DOI: 10.1038/nrm3918.

Cajigas, Iván J. et al. (2012). "The Local Transcriptome in the Synaptic Neuropil Revealed by Deep Sequencing and High-Resolution Imaging". In: *Neuron*. DOI: 10.1016/j.neuron.2012.02.036.

Calarco, John A., Mei Zhen, and Benjamin J. Blencowe (2011). *Networking in a global world: Establishing functional connections between neural splicing regulators and their target transcripts*. DOI: 10.1261/rna.2603911.

Calviello, Lorenzo et al. (2016). "Detecting actively translated open reading frames in ribosome profiling data". In: *Nature Methods*. DOI: 10.1038/nmeth.3688.

Campbell, Douglas S. and Christine E. Holt (2001). "Chemotropic responses of retinal growth cones mediated by rapid local protein synthesis and degradation". In: *Neuron*. DOI: 10.1016/S0896-6273(01)00551-7.

Cao, Wenguang et al. (2012). "Control of alternative splicing by forskolin through hnRNP K during neuronal differentiation". In: *Nucleic Acids Research*. DOI: 10.1093/nar/gks504.

Chanda, Soham et al. (2014). "Generation of induced neuronal cells by the single reprogramming factor ASCL1". In: *Stem Cell Reports*. DOI: 10.1016/j.stemcr.2014.05.020.

Chang, P. (2004). "Localization of RNAs to the Mitochondrial Cloud in Xenopus Oocytes through Entrapment and Association with Endoplasmic Reticulum". In: *Molecular Biology of the Cell*. DOI: 10.1091/mbc.e04-03-0265.

Chang, Yao-Fu, J. Saadi Imam, and Miles F. Wilkinson (2007). "The Nonsense-Mediated Decay RNA Surveillance Pathway". In: *Annual Review of Biochemistry*. DOI: 10.1146/annurev.biochem.76.050106.093909.

Chapman, Erich G. et al. (2014). "The structural basis of pathogenic subgenomic flavivirus RNA (sfRNA) production". In: *Science*. DOI: 10.1126/science.1250897.

Chartron, Justin W., Katherine C.L. Hunt, and Judith Frydman (2016). "Cotranslational signal-independent SRP preloading during membrane targeting". In: *Nature*. DOI: 10.1038/nature19309. arXiv: NIHMS150003.

Chee, Melissa J.S. and William F. Colmers (2008). "Y eat?" In: *Nutrition* 24.9, pp. 869–877. DOI: 10.1016/J.NUT.2008.06.007.

Chekulaeva, Marina, Matthias W. Hentze, and Anne Ephrussi (2006). "Bruno acts as a dual repressor of oskar translation, promoting mRNA oligomerization and formation of silencing particles". In: *Cell*. DOI: 10.1016/j.cell.2006.01.031.

Chen, Ching Yi et al. (2001). "AU binding proteins recruit the exosome to degrade ARE-containing mRNAs". In: *Cell*. DOI: 10.1016/S0092-8674(01)00578-5.

Chen, Wei et al. (2017). "Alternative Polyadenylation: Methods, Findings, and Impacts". In: *Genomics, Proteomics & Bioinformatics*. DOI: 10.1016/j.gpb.2017.06.001.

Chen, Zhe et al. (2008). "Alternative Splicing of the Robo3 Axon Guidance Receptor Governs the Midline Switch from Attraction to Repulsion". In: *Neuron*. DOI: 10.1016/j.neuron.2008.02.016.

Chendrimada, Thimmaiah P. et al. (2007). "MicroRNA silencing through RISC recruitment of eIF6". In: *Nature*. DOI: 10.1038/nature05841.

Choi, J. (2005). "Regulation of Dendritic Spine Morphogenesis by Insulin Receptor Substrate 53, a Downstream Effector of Rac1 and Cdc42 Small GTPases". In: *Journal of Neuroscience*. DOI: 10.1523/jneurosci.3212-04.2005.

Cimino, Peter A. et al. (2011). "Multifaceted regulation of translational readthrough by RNA replication elements in a tombusvirus". In: *PLoS Pathogens*. DOI: 10.1371/journal.ppat.1002423.

Ciolli Mattioli, Camilla et al. (2018). "Alternative 3′ UTRs direct localization of functionally diverse protein isoforms in neuronal compartments." In: *Nucleic acids research*. DOI: 10.1093/nar/gky1270.

Colak, Dilek et al. (2013). "Regulation of axon guidance by compartmentalized nonsense-mediated mRNA decay". In: *Cell*. DOI: 10.1016/j.cell.2013.04.056.

Collins, Mahlon et al. (2012). "The RNA-binding motif 45 (RBM45) protein accumulates in inclusion bodies in amyotrophic lateral sclerosis (ALS) and frontotemporal lobar degeneration with TDP-43 inclusions (FTLD-TDP) patients". In: *Acta Neuropathologica*. DOI: 10.1007/s00401-012-1045-x.

Colón-Ramos, Daniel A. et al. (2003). "Asymmetric distribution of nuclear pore complexes and the cytoplasmic localization of β2-tubulin mRNA in Chlamydomonas reinhardtii". In: *Developmental Cell*. DOI: 10.1016/S1534-5807(03)00163-1.

Comstock, Clay E.S. et al. (2009). "Cyclin D1 splice variants: Polymorphism, risk, and isoform-specific regulation in prostate cancer". In: *Clinical Cancer Research*. DOI: 10.1158/1078-0432.CCR-08-2865.

Conde, Cecilia and Alfredo Cáceres (2009). *Microtubule assembly, organization and dynamics in axons and dendrites*. DOI: 10.1038/nrn2631. arXiv: NIHMS150003.

Cook, Heather A. et al. (2004). "The Drosophila SDE3 homolog armitage is required for oskar mRNA silencing and embryonic axis specification". In: *Cell*. DOI: 10.1016/S0092-8674(04)00250-8.

Corrêa, Sônia A. L. and Katherine L. Eales (2012). "The Role of p38 MAPK and Its Substrates in Neuronal Plasticity and Neurodegenerative Disease". In: *Journal of Signal Transduction*. DOI: 10.1155/2012/649079.

Court, F. A. et al. (2008). "Schwann Cell to Axon Transfer of Ribosomes: Toward a Novel Understanding of the Role of Glia in the Nervous System". In: *Journal of Neuroscience*. DOI: 10.1523/jneurosci.2429-08.2008.

Court, Felipe A. et al. (2011). "Morphological evidence for a transport of ribosomes from Schwann cells to regenerating axons". In: *GLIA*. DOI: 10.1002/glia.21196.

Czaplinski, Kevin and Iain W. Mattaj (2006). "40LoVe interacts with Vg1RBP/Vera and hnRNP I in binding the Vg1-localization element". In: *RNA*. DOI: 10.1261/rna.2820106.

Czaplinski, Kevin et al. (2005). "Identification of 40LoVe, a xenopus hnRNP D family protein involved in localizing a TGF-β-related mRNA during oogenesis". In: *Developmental Cell*. DOI: 10.1016/j.devcel.2005.01.012.

Dalmay, Tamas et al. (2001). "SDE3 encodes an RNA helicase required for post-transcriptional gene silencing in Arabidopsis". In: *EMBO Journal*. DOI: 10.1093/emboj/20.8.2069.

Dass, Brinda et al. (2002). "The gene CSTF2T, encoding the human variant CSTF-64 polyadenylation protein τCstF-64, lacks introns and may be associated with male sterility". In: *Genomics*. DOI: 10.1016/S0888-7543(02)96862-X.

Davis, Hasker P. and Larry R. Squire (1984). "Protein synthesis and memory: A review". In: *Psychological Bulletin*. DOI: 10.1037/0033-2909.96.3.518.

Dent, Erik W. and Frank B. Gertler (2003). *Cytoskeletal dynamics and transport in growth cone motility and guidance*. DOI: 10.1016/S0896-6273(03)00633-0.

Derti, Adnan et al. (2012). "A quantitative atlas of polyadenylation in five mammals". In: *Genome Research*. DOI: 10.1101/gr.132563.111.

Dienstbier, Martin et al. (2009). "Egalitarian is a selective RNA-binding protein linking mRNA localization signals to the dynein motor". In: *Genes and Development*. DOI: 10.1101/gad.531009.

Dieterich, Daniela C. et al. (2007). "Labeling, detection and identification of newly synthesized proteomes with bioorthogonal non-canonical amino-acid tagging". In: *Nature Protocols*. DOI: 10.1038/nprot.2007.52.

Ding, Dali et al. (1993). "Dynamic Hsp83 RNA localization during Drosophila oogenesis and embryogenesis." In: *Molecular and cellular biology*. DOI: 10.1128/MCB.13.6.3773.Updated.

Dingwall, Colin, George P. Lomonossoff, and Ronald A. Laskey (1981). "High sequence specificity of micrococcal nuclease". In: *Nucleic Acids Research*. DOI: 10.1093/nar/9.12.2659.

Dobin, Alexander et al. (2013). "STAR: Ultrafast universal RNA-seq aligner". In: *Bioinformatics*. DOI: 10.1093/bioinformatics/bts635. arXiv: 1201.0052.

Doma, Meenakshi K. and Roy Parker (2007). *RNA Quality Control in Eukaryotes*. DOI: 10.1016/j.cell.2007.10.041.

Dostie, Josée and Gideon Dreyfuss (2002). "Translation is required to remove Y14 from mRNAs in the cytoplasm". In: *Current Biology*. DOI: 10.1016/S0960-9822(02)00902-8.

Dotti, C G, C A Sullivan, and G A Banker (1988). "The establishment of polarity by hippocampal neurons in culture." In: *The Journal of neuroscience : the official journal of the Society for Neuroscience*. DOI: 10.1523/JNEUROSCI.08-04-01454.1988.

Doyle, Michael and Michael A. Kiebler (2011). "Mechanisms of dendritic mRNA transport and its role in synaptic tagging". In: DOI: 10.1038/emboj.2011.278.

Dreyfuss, G (1993). "hnRNP Proteins and the Biogenesis of mRNA". In: *Annual Review of Biochemistry*. DOI: 10.1146/annurev.biochem.62.1.289.

Dunn, Joshua G. et al. (2013). "Ribosome profiling reveals pervasive and regulated stop codon readthrough in Drosophila melanogaster". In: *eLife*. DOI: 10.7554/eLife.01179.

Egorov, M. V. and R. S. Polishchuk (2017). "Emerging role of Cdc42-specific guanine nucleotide exchange factors as regulators of membrane trafficking in health and disease". In: DOI: 10.1016/j.tice.2016.10.002.

Eldad, Naama, Yahav Yosefzon, and Yoav Arava (2008). "Identification and characterization of extensive intra-molecular associations between 3′-UTRs and their ORFs". In: *Nucleic Acids Research*. DOI: 10.1093/nar/gkn754.

Eng, Chee-Huat Linus et al. (2017). "Profiling the transcriptome with RNA SPOTs". In: *Nature Methods* 14.12, pp. 1153–1155. DOI: 10.1038/nmeth.4500.

Eng, H, K Lund, and R B Campenot (1999). "Synthesis of beta-tubulin, actin, and other proteins in axons of sympathetic neurons in compartmented cultures." In: *The Journal of neuroscience : the official journal of the Society for Neuroscience*. DOI: 10.1242/JCS.00745.

Fabian, Marc R. and Nahum Sonenberg (2012). "The mechanics of miRNA-mediated gene silencing: A look under the hood of miRISC". In: DOI: 10.1038/nsmb.2296.

Fairman-Williams, Margaret E., Ulf Peter Guenther, and Eckhard Jankowsky (2010). *SF1 and SF2 helicases: Family matters*. DOI: 10.1016/j.sbi.2010.03.011.

Fan, Dali et al. (1999). "AMPA receptor protein expression and function in astrocytes cultured from hippocampus". In: *Journal of Neuroscience Research*. DOI: 10.1002/(SICI)1097-4547(19990815)57:4<557::AID-JNR16>3.0.CO;2-I.

Fan, Huizhou et al. (1996). "Suppression of malignancy by the 3′ untranslated regions of ribonucleotide reductase R1 and R2 messenger RNAs". In: *Cancer Research*.

Fan, X C and J A Steitz (1998). "HNS, a nuclear-cytoplasmic shuttling sequence in HuR." In: *Proceedings of the National Academy of Sciences of the United States of America*.

Fan, Xiaoqin et al. (2015). "Cytoplasmic hnRNPK interacts with GSK3β and is essential for the osteoclast differentiation". In: *Scientific Reports*. DOI: 10.1038/srep17732.

Fazeli, Amin et al. (1997). "Phenotype of mice lacking functional Deleted in colorectal cancer (Dcc) gene". In: *Nature*. DOI: 10.1038/386796a0.

Feig, S and P Lipton (1993). "Pairing the cholinergic agonist carbachol with patterned Schaffer collateral stimulation initiates protein synthesis in hippocampal CA1 pyramidal cell dendrites via a muscarinic, NMDA-dependent mechanism". In: *The Journal of Neuroscience*. DOI: 10.1523/jneurosci.13-03-01010.1993.

Feltrin, Daniel et al. (2012). "Growth Cone MKK7 mRNA Targeting Regulates MAP1b-Dependent Microtubule Bundling to Control Neurite Elongation". In: *PLoS Biology*. DOI: 10.1371/journal.pbio.1001439.

Femino, Andrea M. et al. (1998). "Visualization of single RNA transcripts in situ". In: *Science*. DOI: 10.1126/science.280.5363.585.

Ferreira, A and A Caceres (1992). "Expression of the class III beta-tubulin isotype in developing neurons in culture." In: *Journal of neuroscience research*. DOI: 10.1002/jnr.490320407.

Feschenko, Marina S et al. (2003). "Phospholemman, a single-span membrane protein, is an accessory protein of Na,K-ATPase in cerebellum and choroid plexus". In: *Journal of Neuroscience*. DOI: 10.1523/JNEUROSCI.23-06-02161.2003.

Flavell, Steven W. et al. (2008). "Genome-Wide Analysis of MEF2 Transcriptional Program Reveals Synaptic Target Genes and Neuronal Activity-Dependent Polyadenylation Site Selection". In: *Neuron*. DOI: 10.1016/j.neuron.2008.11.029.

Fletcher, Daniel A. and Julie A. Theriot (2004). *An introduction to cell motility for the physical scientist*. DOI: 10.1088/1478-3967/1/1/T01.

Foa, Lisa and Robert Gasperini (2009). *Developmental roles for Homer: More than just a pretty scaffold*. DOI: 10.1111/j.1471-4159.2008.05726.x.

Forrest, Kevin M. and Elizabeth R. Gavis (2003). "Live imaging of endogenous RNA reveals a diffusion and entrapment mechanism for nanos mRNA localization in Drosophila". In: *Current Biology*. DOI: 10.1016/S0960-9822(03)00451-2. arXiv: arXiv:1011.1669v3.

Fu, Xiang Dong and Manuel Ares (2014). "Context-dependent control of alternative splicing by RNA-binding proteins". In: DOI: 10.1038/nrg3778.

Fu, Yonggui et al. (2011). "Differential genome-wide profiling of tandem 3′ UTRs among human breast cancer and normal cells by high-throughput sequencing". In: *Genome Research*. DOI: 10.1101/gr.115295.110.

Fukuda, Toshiyuki et al. (2009). "hnRNP K interacts with RNA binding motif protein 42 and functions in the maintenance of cellular ATP level during stress conditions". In: *Genes to Cells*. DOI: 10.1111/j.1365-2443.2008.01256.x.

Gagnon, James A. and Kimberly L. Mowry (2011). "Molecular motors: Directing traffic during RNA localization". In: DOI: 10.3109/10409238.2011.572861.

Gao, Yuanzheng et al. (2008). "Multiplexed dendritic targeting of alpha calcium calmodulin-dependent protein kinase II, neurogranin, and activity-regulated cytoskeleton-associated protein RNAs by the A2 pathway." In: *Molecular biology of the cell*. DOI: 10.1091/mbc.E07-09-0914.

Garalde, Daniel R et al. (2018). "Highly parallel direct RNA sequencing on an array of nanopores". In: *Nature Methods* 15.3, pp. 201–206. DOI: 10.1038/nmeth.4577.

Garbino, Alejandro et al. (2008). "Molecular evolution of the junctophilin gene family." In: *Physiological Genomics*. DOI: 10.1152/physiolgenomics.00017.2009.

Gáspár, Imre et al. (2017). "An RNA-binding atypical tropomyosin recruits kinesin-1 dynamically to oskar mRNPs". In: *The EMBO Journal*. DOI: 10.15252/embj.201696038.

Gerashchenko, Maxim V. and Vadim N. Gladyshev (2017). "Ribonuclease selection for ribosome profiling". In: *Nucleic Acids Research*. DOI: 10.1093/nar/gkw822.

Geuens, Thomas, Delphine Bouhy, and Vincent Timmerman (2016). *The hnRNP family: insights into their role in health and disease*. DOI: 10.1007/s00439-016-1683-5.

Gherzi, Roberto et al. (2004). "A KH domain RNA binding protein, KSRP, promotes ARE-directed mRNA turnover by recruiting the degradation machinery". In: *Molecular Cell*. DOI: 10.1016/j.molcel.2004.05.002.

Giraldez, Antonio J. et al. (2006). "Zebrafish MiR-430 promotes deadenylation and clearance of maternal mRNAs". In: *Science*. DOI: 10.1126/science.1122689. arXiv: arXiv:1011.1669v3.

Giuditta, A., W. D. Dettbarn, and M. Brzin (1968). "Protein synthesis in the isolated giant axon of the squid." In: *Proceedings of the National Academy of Sciences*. DOI: 10.1073/pnas.59.4.1284.

Glock, Caspar, Maximilian Heumüller, and Erin M. Schuman (2017). "mRNA transport & local translation in neurons". In: DOI: 10.1016/j.conb.2017.05.005.

Gonsalvez, Graydon B, Carl R Urbinati, and Roy M Long (2005). "RNA localization in yeast: moving towards a mechanism". In: *Biol. Cell*. DOI: 10.1042/BC20040066.

Goodman, C.S et al. (1999). "Unified Nomenclature for the Semaphorins/Collapsins". In: *Cell* 97.5, pp. 551–552. DOI: 10.1016/S0092-8674(00)80766-7.

Govek, Eve Ellen, Sarah E. Newey, and Linda Van Aelst (2005). "The role of the Rho GTPases in neuronal development". In: DOI: 10.1101/gad.1256405.

Grafstein, B and D S Forman (1980). "Intracellular transport in neurons." In: *Physiological reviews* 60.4, pp. 1167–283. DOI: 10.1152/physrev.1980.60.4.1167.

Greengard, P et al. (1993). "Synaptic vesicle phosphoproteins and regulation of synaptic function." In: *Science*. DOI: 10.1126/science.8430330.

Gregersen, Lea H. et al. (2014). "MOV10 Is a 5′ to 3′ RNA Helicase Contributing to UPF1 mRNA Target Degradation by Translocation along 3′ UTRs". In: *Molecular Cell*. DOI: 10.1016/j.molcel.2014.03.017.

Gumy, Laura F. et al. (2011). "Transcriptome analysis of embryonic and adult sensory axons reveals changes in mRNA repertoire localization". In: *RNA*. DOI: 10.1261/rna.2386111.

Gusel'nikova, V. V. and D. E. Korzhevskiy (2015). "NeuN as a neuronal nuclear antigen and neuron differentiation marker". In:

Guydosh, Nicholas R. and Rachel Green (2014). "Dom34 rescues ribosomes in 3′ untranslated regions". In: *Cell*. DOI: 10.1016/j.cell.2014.02.006. arXiv: NIHMS150003.

Habelhah, Hasem et al. (2001). "ERK phosphorylation drives cytoplasmic accumulation of hnRNP-K and inhibition of mRNA translation". In: *Nature Cell Biology*. DOI: 10.1038/35060131.

Hafner, Markus et al. (2010a). "PAR-CliP - A Method to Identify Transcriptome-wide the Binding Sites of RNA Binding Proteins". In: *Journal of Visualized Experiments*. DOI: 10.3791/2034.

– (2010b). "Transcriptome-wide Identification of RNA-Binding Protein and MicroRNA Target Sites by PAR-CLIP". In: *Cell*. DOI: 10.1016/j.cell.2010.03.009.

Halstead, James M. et al. (2015). "An RNA biosensor for imaging the first round of translation from single cells to living animals". In: *Science*. DOI: 10.1126/science.aaa3380. arXiv: 15334406.

Hancock, J M, D Tautz, and G a Dover (1988). "Evolution of the secondary structures and compensatory mutations of the ribosomal RNAs of Drosophila melanogaster." In: *Molecular biology and evolution*. DOI: 10.1093/oxfordjournals.molbev.a040501.

Hannigan, Molly M., Leah L. Zagore, and Donny D. Licatalosi (2017). "Ptbp2 Controls an Alternative Splicing Network Required for Cell Communication during Spermatogenesis". In: *Cell Reports*. DOI: 10.1016/j.celrep.2017.05.089.

Harris, KM and JK Stevens (1989). "Dendritic spines of CA 1 pyramidal cells in the rat hippocampus: serial electron microscopy with reference to their biophysical characteristics". In: *The Journal of Neuroscience*. DOI: 10.1523/JNEUROSCI.09-08-02982.1989.

Harrison, Benjamin J. et al. (2014). "IB4-binding sensory neurons in the adult rat express a novel 3′UTR-extended isoform of CaMK4 that is associated with its localization to axons". In: *Journal of Comparative Neurology*. DOI: 10.1002/cne.23398.

Hartwig, Christine et al. (2005). "Plexin B3 promotes neurite outgrowth, interacts homophilically, and interacts with Rin". In: *BMC Neuroscience*. DOI: 10.1186/1471-2202-6-53.

Hasan, Mohammad Rubayet et al. (2006). "Differences in the regulation of microtubule stability by the pro-rich region variants of microtubule-associated protein 4". In: *FEBS Letters*. DOI: 10.1016/j.febslet.2006.05.028.

Hayakawa-Yano, Yoshika et al. (2017). "An RNA-binding protein, Qki5, regulates embryonic neural stem cells through pre-mRNA processing in cell adhesion signaling". In: *Genes and Development*. DOI: 10.1101/gad.300822.117.

Heinrich, Christophe et al. (2011). "Generation of subtype-specific neurons from postnatal astroglia of the mouse cerebral cortex". In: *Nature Protocols*. DOI: 10.1038/nprot.2010.188.

Heyden, S. and M. Ortiz (2017). "Investigation of the influence of viscoelasticity on oncotripsy". In: *Computer Methods in Applied Mechanics and Engineering*. DOI: 10.1016/j.cma.2016.08.026.

Hirokawa, Nobutaka (1993). "Axonal transport and the cytoskeleton". In: *Current Opinion in Neurobiology*. DOI: 10.1016/0959-4388(93)90144-N.

Hirokawa, Nobutaka et al. (1989). "Submolecular domains of bovine brain kinesin identified by electron microscopy and monoclonal antibody decoration". In: *Cell*. DOI: 10.1016/0092-8674(89)90691-0.

Hoek, Tim A. et al. (2019). "Single-Molecule Imaging Uncovers Rules Governing Nonsense-Mediated mRNA Decay". In: *Molecular Cell* 0.0. DOI: 10.1016/j.molcel.2019.05.008.

Hoffman, Yonit et al. (2016). "3′UTR Shortening Potentiates MicroRNA-Based Repression of Pro-differentiation Genes in Proliferating Human Cells". In: *PLoS Genetics*. DOI: 10.1371/journal.pgen.1005879.

Holt, Christine E. and Erin M. Schuman (2013). "The central dogma decentralized: New perspectives on RNA function and local translation in neurons". In: DOI: 10.1016/j.neuron.2013.10.036.

Honnappa, Srinivas et al. (2009). "An EB1-Binding Motif Acts as a Microtubule Tip Localization Signal". In: *Cell*. DOI: 10.1016/j.cell.2009.04.065.

Hoque, Mainul et al. (2013). "Analysis of alternative cleavage and polyadenylation by 3′ region extraction and deep sequencing". In: *Nature methods*. DOI: 10.1038/nmeth.2288. arXiv: 15334406.

Howard, J. (2002). "Mechanics of motor proteins". In: *Physics of bio-molecules and cells. Physique des biomolécules et des cellules*. Springer Berlin Heidelberg, pp. 69–94. DOI: 10.1007/3-540-45701-1_2.

Howden, Andrew J.M. et al. (2013). "QuaNCAT: Quantitating proteome dynamics in primary cells". In: *Nature Methods*. DOI: 10.1038/nmeth.2401.

Hu, J.-Y. (2004). "Target-Dependent Release of a Presynaptic Neuropeptide Regulates the Formation and Maturation of Specific Synapses in Aplysia". In: *Journal of Neuroscience*. DOI: 10.1523/jneurosci.3329-04.2004.

Huang, Yan You et al. (1996). *Long-lasting forms of synaptic potentiation in the mammalian hippocampus*. DOI: 10.1101/lm.3.2-3.74.

Huang, Yi Shuian et al. (2002). "N-methyl-D-aspartate receptor signaling results in Aurora kinase-catalyzed CPEB phosphorylation and αCaMKII mRNA polyadenylation at synapses". In: *EMBO Journal*. DOI: 10.1093/emboj/21.9.2139.

Huppertz, Ina et al. (2014). "iCLIP: Protein-RNA interactions at nucleotide resolution". In: *Methods*. DOI: 10.1016/j.ymeth.2013.10.011.

Hüttelmaier, Stefan et al. (2005). "Spatial regulation of β-actin translation by Src-dependent phosphorylation of ZBP1". In: *Nature*. DOI: 10.1038/nature04115.

Hwang, Hun Way et al. (2017). "cTag-PAPERCLIP Reveals Alternative Polyadenylation Promotes Cell-Type Specific Protein Diversity and Shifts Araf Isoforms with Microglia Activation". In: *Neuron*. DOI: 10.1016/j.neuron.2017.08.024.

Iida, Junko et al. (2002). "The projection domain of MAP4 suppresses the microtubule-bundling activity of the microtubule-binding domain". In: *Journal of Molecular Biology*. DOI: 10.1016/S0022-2836(02)00402-3.

Iida, Naoyuki and Tohru Kozasa (2004). "Identification and biochemical analysis of GRIN1 and GRIN2". In: *Methods in Enzymology*. DOI: 10.1016/S0076-6879(04)90029-8.

Inagaki, Naoyuki et al. (2001). "CRMP-2 induces axons in cultured hippocampal neurons". In: *Nature Neuroscience*. DOI: 10.1038/90476.

Ingolia, Nicholas T., Liana F. Lareau, and Jonathan S. Weissman (2011). "Ribosome profiling of mouse embryonic stem cells reveals the complexity and dynamics of mammalian proteomes". In: *Cell*. DOI: 10.1016/j.cell.2011.10.002.

Ingolia, Nicholas T. et al. (2009). "Genome-wide analysis in vivo of translation with nucleotide resolution using ribosome profiling". In: *Science*. DOI: 10.1126/science.1168978. arXiv: arXiv:1408.1149.

Ingolia, Nicholas T et al. (2012). "The ribosome profiling strategy for monitoring translation in vivo by deep sequencing of ribosome-protected mRNA fragments". In: *Nature Protocols* 7.8, pp. 1534–1550. DOI: 10.1038/nprot.2012.086.

Ishigaki, Yasuhito et al. (2001). "Evidence for a pioneer round of mRNA translation: mRNAs subject to nonsense-mediated decay in mammalian cells are bound by CBP80 and CBP20". In: *Cell*. DOI: 10.1016/S0092-8674(01)00475-5.

Jain, R G et al. (1997). "Ectopic expression of Hel-N1, an RNA-binding protein, increases glucose transporter (GLUT1) expression in 3T3-L1 adipocytes." In: *Molecular and Cellular Biology*. DOI: 10.1128/mcb.17.2.954.

Jan, Calvin H., Christopher C. Williams, and Jonathan S. Weissman (2014). "Principles of ER cotranslational translocation revealed by proximity-specific ribosome profiling". In: *Science*. DOI: 10.1126/science.1257521. arXiv: NIHMS150003.

Jenal, Mathias et al. (2012). "The poly(A)-binding protein nuclear 1 suppresses alternative cleavage and polyadenylation sites." In: *Cell* 149.3, pp. 538–53. DOI: 10.1016/j.cell.2012.03.022.

Jenny, A. (2006). "A translation-independent role of oskar RNA in early Drosophila oogenesis". In: *Development*. DOI: 10.1242/dev.02456.

Ji, Z. et al. (2009). "Progressive lengthening of 3′ untranslated regions of mRNAs by alternative polyadenylation during mouse embryonic development". In: *Proceedings of the National Academy of Sciences*. DOI: 10.1073/pnas.0900028106.

Jiang, Hui et al. (2005). "Both the establishment and the maintenance of neuronal polarity require active mechanisms: Critical roles of GSK-3β and its upstream regulators". In: *Cell*. DOI: 10.1016/j.cell.2004.12.033.

Johnson, Jared L., Jon W. Erickson, and Richard A. Cerione (2012). "C-terminal Di-arginine motif of Cdc42 protein is essential for binding to phosphatidylinositol 4,5-bisphosphate-containing membranes and inducing cellular transformation". In: *Journal of Biological Chemistry*. DOI: 10.1074/jbc.M111.336487.

Johnston, Daniel St and Christiane Nüsslein-Volhard (1992). *The origin of pattern and polarity in the Drosophila embryo*. DOI: 10.1016/0092-8674(92)90466-P.

Jupe, E. R. et al. (1996). "The 3′ untranslated region of prohibitin and cellular immortalization". In: *Experimental Cell Research*. DOI: 10.1006/excr.1996.0120.

Kaech, Stefanie and Gary Banker (2006). "Culturing hippocampal neurons". In: *Nature Protocols*. DOI: 10.1038/nprot.2006.356.

Kalil, Katherine and Erik W. Dent (2014). *Branch management: Mechanisms of axon branching in the developing vertebrate CNS*. DOI: 10.1038/nrn3650.

Kalsotra, Auinash and Thomas A. Cooper (2011). *Functional consequences of developmentally regulated alternative splicing*. DOI: 10.1038/nrg3052.

Kang, Rujun et al. (2008). "Neural palmitoyl-proteomics reveals dynamic synaptic palmitoylation". In: DOI: 10.1038/nature07605.

Karginov, Fedor V. et al. (2010). "Diverse Endonucleolytic Cleavage Sites in the Mammalian Transcriptome Depend upon MicroRNAs, Drosha, and Additional Nucleases". In: *Molecular Cell*. DOI: 10.1016/j.molcel.2010.06.001.

Kasteren, Sander I van et al. (2007). "Site-selective glycosylation of proteins: creating synthetic glycoproteins". In: *Nature Protocols*. DOI: 10.1038/nprot.2007.430.

Keino-Masu, Kazuko et al. (1996). "Deleted in Colorectal Cancer (DCC) encodes a netrin receptor". In: *Cell*. DOI: 10.1016/S0092-8674(00)81336-7.

Keller, Matthew W et al. (2018). "Complete genome direct RNA sequencing of influenza A virus". In: *bioRxiv*, p. 300384. DOI: 10.1101/300384. URL: https://www.biorxiv.org/content/early/2018/04/12/300384.

Kenny, Phillip J. et al. (2014). "MOV10 and FMRP Regulate AGO2 Association with MicroRNA Recognition Elements". In: *Cell Reports*. DOI: 10.1016/j.celrep.2014.10.054.

Keppetipola, Niroshika et al. (2012). "Neuronal regulation of pre-mRNA splicing by polypyrimidine tract binding proteins, PTBP1 and PTBP2". In: DOI: 10.3109/10409238.2012.691456.

Ketteler, Robin (2012). "On programmed ribosomal frameshifting: The alternative proteomes". In: DOI: 10.3389/fgene.2012.00242.

Kim, Jong Heon et al. (2000). "Protein-protein interaction among hnRNPs shuttling between nucleus and cytoplasm". In: *Journal of Molecular Biology*. DOI: 10.1006/jmbi.2000.3687.

Kimura, Toshihide et al. (2005). "Tubulin and CRMP-2 complex is transported via Kinesin-1". In: *Journal of Neurochemistry*. DOI: 10.1111/j.1471-4159.2005.03063.x.

Kocabas, Arif et al. (2015). "Widespread Differential Expression of Coding Region and 3′ UTR Sequences in Neurons and Other Tissues". In: *Neuron*. DOI: 10.1016/j.neuron.2015.10.048.

Koenig, E and R Martin (1996). "Cortical plaque-like structures identify ribosome-containing domains in the Mauthner cell axon". In: *The Journal of Neuroscience*. DOI: 10.1523/jneurosci.16-04-01400.1996.

Koenig, E et al. (2000). "Cryptic peripheral ribosomal domains distributed intermittently along mammalian myelinated axons." In: *The Journal of neuroscience : the official journal of the Society for Neuroscience*. DOI: 10.1523/JNEUROSCI.20-22-08390.2000.

Koenig, Edward (1967). "Synthetic mechanisms in the axon. IV. In vitro incorporation of [3H] precursors into axonal protein and RNA". In: *Journal of Neurochemistry*. DOI: 10.1111/j.1471-4159.1967.tb09542.x.

Kondrashov, Nadya et al. (2011). "Ribosome-mediated specificity in Hox mRNA translation and vertebrate tissue patterning". In: *Cell*. DOI: 10.1016/j.cell.2011.03.028.

Kopp, Janel L. et al. (2008). "Small Increases in the Level of Sox2 Trigger the Differentiation of Mouse Embryonic Stem Cells". In: *Stem Cells*. DOI: 10.1634/stemcells.2007-0951. arXiv: NIHMS150003.

Kosik, Kenneth S. (2006). *The neuronal microRNA system*. DOI: 10.1038/nrn2037.

Krijnse-Locker, J. et al. (1995). "The organization of the endoplasmic reticulum and the intermediate compartment in cultured rat hippocampal neurons." In: *Molecular Biology of the Cell*. DOI: 10.1091/mbc.6.10.1315.

Kullmann, Michael et al. (2002). "ELAV/Hu proteins inhibit p27 translation via an IRES element in the p27 5′UTR". In: *Genes and Development*. DOI: 10.1101/gad.248902.

Kun, Alejandra et al. (2007). "Ribosomal distributions in axons of mammalian myelinated fibers". In: *Journal of Neuroscience Research*. DOI: 10.1002/jnr.21340. arXiv: NIHMS150003.

Kye, Min Jeong et al. (2007). "Somatodendritic microRNAs identified by laser capture and multiplex RT-PCR". In: *RNA*. DOI: 10.1261/rna.480407.

Langford, George M. (1999). "ER transport on actin filaments in squid giant axon: implications for signal transduction at synapse". In: *The FASEB Journal*. DOI: 10.1096/fasebj.13.9002.s248.

Lareau, Liana F. et al. (2014). "Distinct stages of the translation elongation cycle revealed by sequencing ribosome-protected mRNA fragments". In: *eLife*. DOI: 10.7554/eLife.01257. arXiv: arXiv:1011.1669v3.

Lee, Shih-Han and Christine Mayr (2019). "Gain of Additional BIRC3 Protein Functions through 3′-UTR-Mediated Protein Complex Formation". In: *Molecular Cell*. DOI: 10.1016/j.molcel.2019.03.006.

Lejeune, Fabrice and Lynne E. Maquat (2005). *Mechanistic links between nonsense-mediated mRNA decay and pre-mRNA splicing in mammalian cells*. DOI: 10.1016/j.ceb.2005.03.002.

Leppek, Kathrin et al. (2013). "Roquin promotes constitutive mrna decay via a conserved class of stem-loop recognition motifs". In: *Cell*. DOI: 10.1016/j.cell.2013.04.016.

Lesuisse, Christian and Lee J. Martin (2002). "Long-term culture of mouse cortical neurons as a model for neuronal development, aging, and death". In: *Journal of Neurobiology*. DOI: 10.1002/neu.10037.

Leung, Kin Mei et al. (2006). "Asymmetrical β-actin mRNA translation in growth cones mediates attractive turning to netrin-1". In: *Nature Neuroscience*. DOI: 10.1038/nn1775.

Levy, Nina S. et al. (1998). "Hypoxic stabilization of vascular endothelial growth factor mRNA by the RNA-binding protein HuR". In: *Journal of Biological Chemistry*. DOI: 10.1074/jbc.273.11.6417.

Li, Qin et al. (2014). "The splicing regulator PTBP2 controls a program of embryonic splicing required for neuronal maturation". In: *eLife*. DOI: 10.7554/eLife.01201.001.

Li, Wei qi et al. (2010). "Downstream of tyrosine kinase/docking protein 6, as a novel substrate of tropomyosin-related kinase C receptor, is involved in neurotrophin 3-mediated neurite outgrowth in mouse cortex neurons." In: *BMC biology* 8, p. 86. DOI: 10.1186/1741-7007-8-86.

Li, Wencheng et al. (2016). "Alternative cleavage and polyadenylation in spermatogenesis connects chromatin regulation with post-transcriptional control". In: *BMC Biology*. DOI: 10.1186/s12915-016-0229-6.

Li, Xiu Qing and Donglei Du (2013). "RNA polyadenylation sites on the genomes of microorganisms, animals, and plants". In: *PLoS ONE*. DOI: 10.1371/journal.pone.0079511.

Li, Yang et al. (2015). "RBM45 homo-oligomerization mediates association with ALS-linked proteins and stress granules". In: *Scientific Reports*. DOI: 10.1038/srep14262.

Lianoglou, Steve et al. (2013). "Ubiquitously transcribed genes use alternative polyadenylation to achieve tissue-specific expression". In: *Genes and Development*. DOI: 10.1101/gad.229328.113.

Liao, Guoning et al. (2015). *Control of cell migration through mRNA localization and local translation*. DOI: 10.1002/wrna.1265.

Licatalosi, Donny D. et al. (2012). "Ptbp2 represses adult-specific splicing to regulate the generation of neuronal precursors in the embryonic brain". In: *Genes and Development*. DOI: 10.1101/gad.191338.112.

Lin, Andrew C. and Christine E. Holt (2007). "Local translation and directional steering in axons". In: DOI: 10.1038/sj.emboj.7601808.

Lin, Yuefeng et al. (2012). "An in-depth map of polyadenylation sites in cancer". In: *Nucleic Acids Research*. DOI: 10.1093/nar/gks637.

Linder, Maurine E. and Robert J. Deschenes (2007). *Palmitoylation: Policing protein stability and traffic*. DOI: 10.1038/nrm2084.

Liu, Donglin et al. (2007). "Systematic variation in mRNA 3′-processing signals during mouse spermatogenesis". In: *Nucleic Acids Research*. DOI: 10.1093/nar/gkl919.

Liu, Gang et al. (2002). "Interactions of Elongation Factor 1alpha with F-Actin and beta-Actin mRNA: Implications for Anchoring mRNA in Cell Protrusions". In: *Molecular Biology of the Cell*. DOI: 10.1091/mbc.01-03-0140.

Liu, Hai Kun et al. (2008). "The nuclear receptor tailless is required for neurogenesis in the adult subventricular zone". In: *Genes and Development*. DOI: 10.1101/gad.479308.

Liu, Y. et al. (2015). "Ascl1 Converts Dorsal Midbrain Astrocytes into Functional Neurons In Vivo". In: *Journal of Neuroscience*. DOI: 10.1523/JNEUROSCI.3975-14.2015.

Liu, Yang et al. (2018). "Enhanced mRNA FISH with compact quantum dots". In: *Nature Communications*. DOI: 10.1038/s41467-018-06740-x.

Loedige, Inga et al. (2013). "The mammalian TRIM-NHL protein TRIM71/LIN-41 is a repressor of mRNA function". In: *Nucleic Acids Research*. DOI: 10.1093/nar/gks1032.

Loew, R et al. (2006). "Retroviral vectors containing Tet-controlled bidirectional transcription units for simultaneous regulation of two gene activities". In: *J Mol Genet Med*.

Long, Hua et al. (2004). "Conserved roles for Slit and Robo proteins in midline commissural axon guidance". In: *Neuron*. DOI: 10.1016/S0896-6273(04)00179-5.

Lowery, Laura Anne and David Van Vactor (2009). *The trip of the tip: Understanding the growth cone machinery*. DOI: 10.1038/nrm2679.

Lu, Fengmin, Andrew B. Gladden, and J. Alan Diehl (2003). "An Alternatively Spliced Cyclin D1 Isoform, Cyclin D1b, Is a Nuclear Oncogene". In: *Cancer Research*. DOI: 10.1105/tpc.113.251013.

Lubeck, Eric et al. (2014). "Single-cell in situ RNA profiling by sequential hybridization". In: DOI: 10.1038/nmeth.2892. arXiv: NIHMS150003.

Lyles, Vlasta, Yali Zhao, and Kelsey C. Martin (2006). "Synapse formation and mRNA localization in cultured Aplysia neurons". In: *Neuron*. DOI: 10.1016/j.neuron.2005.12.029.

Ma, Weirui and Christine Mayr (2018). "A Membraneless Organelle Associated with the Endoplasmic Reticulum Enables 3′UTR-Mediated Protein-Protein Interactions". In: *Cell*. DOI: 10.1016/j.cell.2018.10.007.

MacDonald, Clinton C. and K. Wyatt McMahon (2010). *Tissue-specific mechanisms of alternative polyadenylation: Testis, brain, and beyond*. DOI: 10.1002/wrna.29.

Makeyev, Aleksandr V. and Stephen A. Liebhaber (2002). *The poly(C)-binding proteins: A multiplicity of functions and a search for mechanisms*. DOI: 10.1017/S1355838202024627.

Makeyev, Eugene V. et al. (2007). "The MicroRNA miR-124 Promotes Neuronal Differentiation by Triggering Brain-Specific Alternative Pre-mRNA Splicing". In: *Molecular Cell*. DOI: 10.1016/j.molcel.2007.07.015.

Malka, Yuval et al. (2017). "Post-transcriptional 3′-UTR cleavage of mRNA transcripts generates thousands of stable uncapped autonomous RNA fragments". In: *Nature Communications* 8.1, p. 2029. DOI: 10.1038/s41467-017-02099-7.

Maquat, Lynne E. (2004). *Nonsense-mediated mRNA decay: Splicing, translation and mRNP dynamics*. DOI: 10.1038/nrm1310.

Marchand, Virginie, Imre Gaspar, and Anne Ephrussi (2012). "An Intracellular Transmission Control Protocol: Assembly and transport of ribonucleoprotein complexes". In: DOI: 10.1016/j.ceb.2011.12.014.

Mardakheh, Faraz K. et al. (2015). "Global Analysis of mRNA, Translation, and Protein Localization: Local Translation Is a Key Regulator of Cell Protrusions". In: *Developmental Cell*. DOI: 10.1016/j.devcel.2015.10.005.

Marks, Peter W. and David J. Kwiatkowski (1996). "Genomic organization and chromosomal location of murine CDC42". In: *Genomics*. DOI: 10.1006/geno.1996.0586.

Marquardt, Till et al. (2001). "Pax6 is required for the multipotent state of retinal progenitor cells". In: *Cell*. DOI: 10.1016/S0092-8674(01)00295-1.

Martin, Kelsey C. and Anne Ephrussi (2009). "mRNA Localization: Gene Expression in the Spatial Dimension". In: DOI: 10.1016/j.cell.2009.01.044.

Martin, Rainer, Wolfgang Fritz, and Antonio Giuditta (1989). "Visualization of polyribosomes in the postsynaptic area of the squid giant synapse by electron spectroscopic imaging". In: *Journal of Neurocytology*. DOI: 10.1007/BF01188419.

Masserdotti, Giacomo, Sergio Gascón, and Magdalena Götz (2016). "Direct neuronal reprogramming: learning from and for development". In: *Development*. DOI: 10.1242/dev.092163.

Matsushima, Kazuyuki et al. (2005). "Identification of a Neural Cell Specific Variant of Microtubule-Associated Protein 4". In: *Cell Structure and Function* 29.5,6, pp. 111–124. DOI: 10.1247/csf.29.111.

Matsushita, Masafumi et al. (2004). "A novel kinesin-like protein, KIF1Bβ3 is involved in the movement of lysosomes ot the cell periphery in non-neuronal cells". In: *Traffic*. DOI: 10.1111/j.1600-0854.2003.00165.x.

Matsushita, Masafumi et al. (2009). "Altered motor activity of alternative splice variants of the mammalian kinesin-3 protein KIF1B". In: *Traffic*. DOI: 10.1111/j.1600-0854.2009.00975.x.

Mayeda, Akila and Adrian R. Krainer (1992). "Regulation of alternative pre-mRNA splicing by hnRNP A1 and splicing factor SF2". In: *Cell*. DOI: 10.1016/0092-8674(92)90477-T.

Mayford, M. et al. (2002). "The 3′-untranslated region of CaMKII alpha is a cis-acting signal for the localization and translation of mRNA in dendrites". In: *Proceedings of the National Academy of Sciences*. DOI: 10.1073/pnas.93.23.13250.

Mayr, Christine (2017). "Regulation by 3′ Untranslated Regions". In: *Annual Review of Genetics*. DOI: 10.1146/annurev-genet-120116-024704.

Mayr, Christine and David P. Bartel (2009). "Widespread Shortening of 3′UTRs by Alternative Cleavage and Polyadenylation Activates Oncogenes in Cancer Cells". In: *Cell*. DOI: 10.1016/j.cell.2009.06.016.

McGlincy, Nicholas J. and Nicholas T. Ingolia (2017). "Transcriptome-wide measurement of translation by ribosome profiling". In: *Methods* 126, pp. 112–129. DOI: 10.1016/J.YMETH.2017.05.028.

Meister, Gunter et al. (2005). "Identification of novel argonaute-associated proteins". In: *Current Biology*. DOI: 10.1016/j.cub.2005.10.048.

Melendez, Jaime, Matthew Grogg, and Yi Zheng (2011). "Signaling role of Cdc42 in regulating mammalian physiology". In: DOI: 10.1074/jbc.R110.200329.

Mercer, Tim R. et al. (2011). "Expression of distinct RNAs from 3′ untranslated regions". In: *Nucleic Acids Research*. DOI: 10.1093/nar/gkq1158.

Merianda, Tanuja T. et al. (2009). "A functional equivalent of endoplasmic reticulum and Golgi in axons for secretion of locally synthesized proteins". In: *Molecular and Cellular Neuroscience*. DOI: 10.1016/j.mcn.2008.09.008.

Messitt, Timothy J. et al. (2008). "Multiple Kinesin Motors Coordinate Cytoplasmic RNA Transport on a Subpopulation of Microtubules in Xenopus Oocytes". In: *Developmental Cell*. DOI: 10.1016/j.devcel.2008.06.014. arXiv: NIHMS150003.

Miettinen, Teemu P. and Mikael Bjorklund (2015). "Modified ribosome profiling reveals high abundance of ribosome protected mRNA fragments derived from 3′ untranslated regions". In: *Nucleic Acids Research*. DOI: 10.1093/nar/gku1310.

Miller, S. L. and H. H. Yeh (2016). "Neurotransmitters and Neurotransmission in the Developing and Adult Nervous System". In: *Conn's Translational Neuroscience*. DOI: 10.1016/B978-0-12-802381-5.00004-X.

Millevoi, Stefania and Stéphan Vagner (2009). "Molecular mechanisms of eukaryotic pre-mRNA 3′ end processing regulation". In: *Nucleic Acids Research*. DOI: 10.1093/nar/gkp1176.

Minis, Adi et al. (2014). "Subcellular transcriptomics-Dissection of the mRNA composition in the axonal compartment of sensory neurons". In: *Developmental Neurobiology*. DOI: 10.1002/dneu.22140.

Miura, Pedro et al. (2013). "Widespread and extensive lengthening of 39 UTRs in the mammalian brain". In: *Genome Research*. DOI: 10.1101/gr.146886.112.

Mobarak, C. D. et al. (2013). "The RNA-binding Protein HuD Is Required for GAP-43 mRNA Stability, GAP-43 Gene Expression, and PKC-dependent Neurite Outgrowth in PC12 Cells". In: *Molecular Biology of the Cell*. DOI: 10.1091/mbc.11.9.3191.

Mok, Hyejung et al. (2002). "Association of the Kinesin Superfamily Motor Protein KIF1Ba with Postsynaptic Density-95 (PSD-95), Synapse-Associated Protein-97, and Synaptic Scaffolding Molecule PSD-95/Discs Large/Zona Occludens-1 Proteins". In: *The Journal of Neuroscience*. DOI: 20026553.

Monné, Ludwik (1948). "Functioning of the Cytoplasm". In: John Wiley & Sons, Ltd, pp. 1–69. DOI: 10.1002/9780470122532.ch1.

Morisaki, Tatsuya et al. (2016). "Real-time quantification of single RNA translation dynamics in living cells". In: *Science*. DOI: 10.1126/science.aaf0899.

Moroz, Leonid L. et al. (2006). "Neuronal Transcriptome of Aplysia: Neuronal Compartments and Circuitry". In: *Cell*. DOI: 10.1016/j.cell.2006.09.052.

Muddashetty, Ravi S. et al. (2011). "Reversible Inhibition of PSD-95 mRNA Translation by miR-125a, FMRP Phosphorylation, and mGluR Signaling". In: *Molecular Cell*. DOI: 10.1016/j.molcel.2011.05.006. arXiv: NIHMS150003.

Mukai, Jun et al. (2015). "Molecular Substrates of Altered Axonal Growth and Brain Connectivity in a Mouse Model of Schizophrenia". In: *Neuron*. DOI: 10.1016/j.neuron.2015.04.003.

Mukherjee, Chandrama, Baskar Bakthavachalu, and Daniel R. Schoenberg (2014). "The Cytoplasmic Capping Complex Assembles on Adapter Protein Nck1 Bound to the Proline-Rich C-Terminus of Mammalian Capping Enzyme". In: *PLoS Biology*. DOI: 10.1371/journal.pbio.1001933.

Mukherjee, Devi et al. (2002). "The mammalian exosome mediates the efficient degradation of mRNAs that contain AU-rich elements". In: *EMBO Journal*. DOI: 10.1093/emboj/21.1.165.

Munro, Trent P. et al. (1999). "Mutational analysis of a heterogeneous nuclear ribonucleoprotein A2 response element for RNA trafficking". In: *Journal of Biological Chemistry*. DOI: 10.1074/jbc.274.48.34389.

Muslimov, Ilham A. et al. (2014). "Interactions of noncanonical motifs with hnRNP A2 promote activity-dependent RNA transport in neurons". In: *Journal of Cell Biology*. DOI: 10.1083/jcb.201310045.

Nakazawa, T. (2003). "p250GAP, a Novel Brain-enriched GTPase-activating Protein for Rho Family GTPases, Is Involved in the N-Methyl-D-aspartate Receptor Signaling". In: *Molecular Biology of the Cell*. DOI: 10.1091/mbc.e02-09-0623.

Nangaku, Masaomi et al. (1994). "KIF1B, a novel microtubule plus end-directed monomeric motor protein for transport of mitochondria". In: *Cell*. DOI: 10.1016/0092-8674(94)90012-4.

Negishi, Manabu and Hironori Katoh (2005). *Rho family GTPases and dendrite plasticity*. DOI: 10.1177/1073858404268768.

Nelissen, Rob L.H. et al. (1991). "Structure, chromosomal localization and evolutionary conservation of the gene encoding human U1 snRNP-specific A protein". In: *Gene*. DOI: 10.1016/0378-1119(91)90077-O.

Ni, Julie Z. et al. (2007). "Ultraconserved elements are associated with homeostatic control of splicing regulators by alternative splicing and nonsense-mediated decay". In: *Genes and Development*. DOI: 10.1101/gad.1525507.

Nirenberg, M J et al. (1995). "The vesicular monoamine transporter 2 is present in small synaptic vesicles and preferentially localizes to large dense core vesicles in rat solitary tract nuclei." In: *Proceedings of the National Academy of Sciences of the United States of America*. DOI: 10.1073/pnas.92.19.8773.

Nishimura, A. and M. E. Linder (2013). "Identification of a Novel Prenyl and Palmitoyl Modification at the CaaX Motif of Cdc42 That Regulates RhoGDI Binding". In: *Molecular and Cellular Biology*. DOI: 10.1128/MCB.01398-12. arXiv: 0209403v1 [arXiv:cond-mat].

Nishimura, T. (2006). "Role of Numb in Dendritic Spine Development with a Cdc42 GEF Intersectin and EphB2". In: *Molecular Biology of the Cell*. DOI: 10.1091/mbc.e05-07-0700.

Oinuma, Izumi, Hironori Katoh, and Manabu Negishi (2007). "R-Ras controls axon specification upstream of glycogen synthase kinase-3β through integrin-linked kinase". In: *Journal of Biological Chemistry*. DOI: 10.1074/jbc.M607979200.

Okano, H J and R B Darnell (1997). "A hierarchy of Hu RNA binding proteins in developing and adult neurons." In: *The Journal of neuroscience : the official journal of the Society for Neuroscience*.

Ong, Shao-En et al. (2002). "Stable Isotope Labeling by Amino Acids in Cell Culture, SILAC, as a Simple and Accurate Approach to Expression Proteomics". In: *Molecular & Cellular Proteomics*. DOI: 10.1074/mcp.M200025-MCP200. arXiv: NIHMS150003.

Ostroff, Linnaea E. et al. (2002). "Polyribosomes redistribute from dendritic shafts into spines with enlarged synapses during LTP in developing rat hippocampal slices". In: *Neuron*. DOI: 10.1016/S0896-6273(02)00785-7.

Otsuka, Y., N. L. Kedersha, and D. R. Schoenberg (2009). "Identification of a Cytoplasmic Complex That Adds a Cap onto 5'-Monophosphate RNA". In: *Molecular and Cellular Biology*. DOI: 10.1128/MCB.01325-08.

Pan, Luyuan et al. (2004). "The Drosophila fragile X gene negatively regulates neuronal elaboration and synaptic differentiation". In: *Current Biology*. DOI: 10.1016/j.cub.2004.09.085.

Pang, Z P et al. (2011). "Induction of human neuronal cells by defined transcription factors". In: *Nature*. DOI: 10.1038/nature10202.

Pannese, E and M Ledda (1991). "Ribosomes in myelinated axons of the rabbit spinal ganglion neurons". In: *J Submicrosc Cytol Pathol*.

Park, Hye Yoon et al. (2012). "An Unbiased Analysis Method to Quantify mRNA Localization Reveals Its Correlation with Cell Motility". In: *Cell Reports*. DOI: 10.1016/j.celrep.2011.12.009.

Park, Hye Yoon et al. (2014). "Visualization of dynamics of single endogenous mRNA labeled in live mouse". In: *Science*. DOI: 10.1126/science.1239200.

Park, So Jung et al. (2015). "Heterogeneous nuclear ribonucleoprotein A1 post- transcriptionally regulates Drp1 expression in neuroblastoma cells". In: *Biochimica et Biophysica Acta - Gene Regulatory Mechanisms*. DOI: 10.1016/j.bbagrm.2015.10.017.

Paz, Inbal et al. (2014). "RBPmap: A web server for mapping binding sites of RNA-binding proteins". In: *Nucleic Acids Research*. DOI: 10.1093/nar/gku406.

Peng, Sheila S.Y. et al. (1998). "RNA stabilization by the AU-rich element binding protein, HuR, an ELAV protein". In: *EMBO Journal*. DOI: 10.1093/emboj/17.12.3461.

Perry, Rotem Ben Tov et al. (2012). "Subcellular Knockout of Importin β1 Perturbs Axonal Retrograde Signaling". In: *Neuron*. DOI: 10.1016/j.neuron.2012.05.033.

Pfenninger, Karl H. (2009). *Plasma membrane expansion: A neuron's Herculean task*. DOI: 10.1038/nrn2593.

Piirsoo, Marko, Dies Meijer, and Tõnis Timmusk (2009). "Expression analysis of the CLCA gene family in mouse and human with emphasis on the nervous system". In: *BMC Developmental Biology* 9.1, p. 10. DOI: 10.1186/1471-213X-9-10.

Piper, Michael et al. (2006). "Signaling mechanisms underlying Slit2-induced collapse of Xenopus retinal growth cones". In: *Neuron*. DOI: 10.1016/j.neuron.2005.12.008.

Polydorides, Alexandros D. et al. (2000). "A brain-enriched polypyrimidine tract-binding protein antagonizes the ability of Nova to regulate neuron-specific alternative splicing". In: *Proceedings of the National Academy of Sciences*. DOI: 10.1073/pnas.110128397.

Raj, Arjun et al. (2008). "Imaging individual mRNA molecules using multiple singly labeled probes". In: *Nature Methods*. DOI: 10.1038/nmeth.1253. arXiv: NIHMS150003.

Raj, Bushra and Benjamin J. Blencowe (2015). "Alternative Splicing in the Mammalian Nervous System: Recent Insights into Mechanisms and Functional Roles". In: DOI: 10.1016/j.neuron.2015.05.004.

Raposo, Alexandre A.S.F. et al. (2015). "Ascl1 coordinately regulates gene expression and the chromatin landscape during neurogenesis". In: *Cell Reports*. DOI: 10.1016/j.celrep.2015.02.025.

Rastinejad, Farzan and Helen M. Blau (1993). "Genetic complementation reveals a novel regulatory role for 3′ untranslated regions in growth and differentiation". In: *Cell*. DOI: 10.1016/0092-8674(93)90579-F.

Rastinejad, Farzan et al. (1993). "Tumor suppression by RNA from the 3′ untranslated region of α-tropomyosin". In: *Cell*. DOI: 10.1016/0092-8674(93)90320-P.

Reid, David W., Shirish Shenolikar, and Christopher V. Nicchitta (2015). "Simple and inexpensive ribosome profiling analysis of mRNA translation". In: *Methods*. DOI: 10.1016/j.ymeth.2015.07.003.

Reixachs-Sole, Marina et al. (2019). "Ribosome profiling at isoform level reveals an evolutionary conserved impact of differential splicing on the proteome". In: *bioRxiv*, p. 582031. DOI: 10.1101/582031.

Richter, Joel D. (2007). *CPEB: a life in translation*. DOI: 10.1016/j.tibs.2007.04.004.

Roglio, Ilaria et al. (2008). "Neuroactive steroids and peripheral neuropathy". In: DOI: 10.1016/j.brainresrev.2007.04.010.

Rosenwasser, L. J. (2001). "A rare polyadenylation signal mutation of the FOXP3 gene (AAUAAA → AAUGAA) leads to the IPEX syndrome". In: *Immunogenetics*. DOI: 10.1007/s002510100358.

Rotem, Nimrod et al. (2017). "ALS along the Axons - Expression of coding and non-coding RNA differs in axons of ALS models". In: *Scientific Reports*. DOI: 10.1038/srep44500.

Roy, Subhojit (2014). *Seeing the unseen: The hidden world of slow axonal transport*. DOI: 10.1177/1073858413498306.

Ruthazer, E. S. (2006). "Stabilization of Axon Branch Dynamics by Synaptic Maturation". In: *Journal of Neuroscience*. DOI: 10.1523/jneurosci.0069-06.2006.

Sakers, Kristina et al. (2017). "Astrocytes locally translate transcripts in their peripheral processes". In: *Proceedings of the National Academy of Sciences*. DOI: 10.1073/pnas.1617782114.

Sambandan, Sivakumar et al. (2017). "Activity-dependent spatially localized miRNA maturation in neuronal dendrites". In: *Science*. DOI: 10.1126/science.aaf8995. arXiv: 1504.00980.

Sandberg, Rickard et al. (2008). "Proliferating cells express mRNAs with shortened 3′ untranslated regions and fewer microRNA target sites". In: *Science*. DOI: 10.1126/science.1155390.

Sander, Sandrine et al. (2015). "PI3 Kinase and FOXO1 Transcription Factor Activity Differentially Control B Cells in the Germinal Center Light and Dark Zones". In: *Immunity*. DOI: 10.1016/j.immuni.2015.10.021. arXiv: 15334406.

Sanz, E. et al. (2009). "Cell-type-specific isolation of ribosome-associated mRNA from complex tissues". In: *Proceedings of the National Academy of Sciences*. DOI: 10.1073/pnas.0907143106. arXiv: 1408.1149.

Sapkota, Darshan et al. (2019). "Cell-Type-Specific Profiling of Alternative Translation Identifies Regulated Protein Isoform Variation in the Mouse Brain." In: *Cell reports* 26.3, 594–607.e7. DOI: 10.1016/j.celrep.2018.12.077.

Schlager, Max A. et al. (2010). "Pericentrosomal targeting of Rab6 secretory vesicles by Bicaudal-D-related protein 1 (BICDR-1) regulates neuritogenesis". In: *EMBO Journal*. DOI: 10.1038/emboj.2010.51.

Schoenberg, Daniel R. (2011). "Mechanisms of endonuclease-mediated mRNA decay". In: DOI: 10.1002/wrna.78. arXiv: NIHMS150003.

Schoggins, John W. et al. (2011). "A diverse range of gene products are effectors of the type i interferon antiviral response". In: *Nature*. DOI: 10.1038/nature09907.

Schratt, Gerhard M. et al. (2006). "A brain-specific microRNA regulates dendritic spine development". In: *Nature*. DOI: 10.1038/nature04367.

Schroer, T. A. (2013). "Dynactin". In: *Encyclopedia of Biological Chemistry: Second Edition*. DOI: 10.1016/B978-0-12-378630-2.00423-0.

Schuetz, Anja et al. (2014). "Roquin binding to target mRNAs involves a winged helix-turn-helix motif". In: *Nature Communications*. DOI: 10.1038/ncomms6701.

Schwamborn, Jens C. and Andreas W. Püschel (2004). "The sequential activity of the GTPases Rap1B and Cdc42 determines neuronal polarity". In: *Nature Neuroscience*. DOI: 10.1038/nn1295.

Schwanhäusser, Björn et al. (2009). "Global analysis of cellular protein translation by pulsed SILAC". In: *Proteomics*. DOI: 10.1002/pmic.200800275.

Schwanhüusser, Björn et al. (2011). "Global quantification of mammalian gene expression control". In: *Nature*. DOI: 10.1038/nature10098.

Scott, Ethan K., John E. Reuter, and Liqun Luo (2003). "Small GTPase Cdc42 Is Required for Multiple Aspects of Dendritic Morphogenesis". In: *The Journal of Neuroscience*. DOI: 10.1523/jneurosci.23-08-03118.2003.

Semotok, Jennifer L. et al. (2005). "Smaug recruits the CCR4/POP2/NOT deadenylase complex to trigger maternal transcript localization in the early Drosophila embryo". In: *Current Biology*. DOI: 10.1016/j.cub.2005.01.048. arXiv: /linkinghub.elsevier.com/retrieve/pii/S0960982205000989 [http:].

Shan, J. et al. (2000). "Binding of an RNA trafficking response element to heterogeneous nuclear ribonucleoproteins A1 and A2". In: *Journal of Biological Chemistry*. DOI: 10.1074/jbc.M007642200.

Shan, Jianguo et al. (2003). "A molecular mechanism for mRNA trafficking in neuronal dendrites." In: *The Journal of neuroscience*.

Shi, Song Hai, Lily Yeh Jan, and Yuh Nung Jan (2003). "Hippocampal neuronal polarity specified by spatially localized mPar3/mPar6 and PI 3-kinase activity". In: DOI: 10.1016/S0092-8674(02)01249-7.

Shi, Zhen et al. (2017). "Heterogeneous Ribosomes Preferentially Translate Distinct Subpools of mRNAs Genome-wide". In: *Molecular Cell*. DOI: 10.1016/j.molcel.2017.05.021. arXiv: 15334406.

Shigeoka, Toshiaki et al. (2016). "Dynamic Axonal Translation in Developing and Mature Visual Circuits". In: *Cell*. DOI: 10.1016/j.cell.2016.05.029.

Shigeoka, Toshiaki et al. (2018). "On-site ribosome remodeling by locally synthesized ribosomal proteins in axons". In: *bioRxiv*, p. 500033. DOI: 10.1101/500033. URL: https://www.biorxiv.org/content/early/2018/12/19/500033.

Sillekens, P. T. et al. (1987). "cDNA cloning of the human U1 snRNA-associated A protein: extensive homology between U1 and U2 snRNP-specific proteins." In: *The EMBO Journal*. DOI: 10.1002/j.1460-2075.1987.tb02721.x.

Singh, Priyam et al. (2009). "Global changes in processing of mRNA 3′ untranslated regions characterize clinically distinct cancer subtypes". In: *Cancer Research*. DOI: 10.1158/0008-5472.CAN-09-2236.

Sinsimer, Kristina S. et al. (2011). " A late phase of germ plasm accumulation during Drosophila oogenesis requires Lost and Rumpelstiltskin ". In: *Development*. DOI: 10.1242/dev.065029.

Slavov, Nikolai et al. (2015). "Differential Stoichiometry among Core Ribosomal Proteins". In: *Cell Reports*. DOI: 10.1016/j.celrep.2015.09.056. arXiv: 1406.0399.

Smibert, Peter et al. (2012). "Global Patterns of Tissue-Specific Alternative Polyadenylation in Drosophila". In: *Cell Reports*. DOI: 10.1016/j.celrep.2012.01.001.

Smotrys, Jessica E. and Maurine E. Linder (2004). "Palmitoylation of Intracellular Signaling Proteins: Regulation and Function". In: *Annual Review of Biochemistry*. DOI: 10.1146/annurev.biochem.73.011303.073954.

Soderling, Thomas R. (2000). *CaM-kinases: Modulators of synaptic plasticity*. DOI: 10.1016/S0959-4388(00)00090-8.

Solomon, David A. et al. (2003). "Cyclin D1 splice variants: Differential effects on localization, RB phosphorylation, and cellular transformation". In: *Journal of Biological Chemistry*. DOI: 10.1074/jbc.M303969200.

Sotelo-Silveira, José R. et al. (2004). "Myosin Va and kinesin II motor proteins are concentrated in ribosomal domains (periaxoplasmic ribosomal plaques) of myelinated axons". In: *Journal of Neurobiology*. DOI: 10.1002/neu.20015.

Spencer, G. E. et al. (2000). "Synthesis and functional integration of a neurotransmitter receptor in isolated invertebrate axons". In: *Journal of Neurobiology*. DOI: 10.1002/1097-4695(200007)44:1<72::AID-NEU7>3.0.CO;2-#.

Spies, Noah, Christopher B. Burge, and David P. Bartel (2013). "3′ UTR-Isoform choice has limited influence on the stability and translational efficiency of most mRNAs in mouse fibroblasts". In: *Genome Research*. DOI: 10.1101/gr.156919.113.

Stains, Joseph P. et al. (2005). "Heterogeneous nuclear ribonucleoprotein K represses transcription from a cytosine/thymidine-rich element in the osteocalcin promoter". In: *Biochemical Journal*. DOI: 10.1042/bj20040680.

Stergiopoulos, Athanasios and Panagiotis K. Politis (2016). "Nuclear receptor NR5A2 controls neural stem cell fate decisions during development". In: *Nature Communications*. DOI: 10.1038/ncomms12230.

Steward, O. (2007). "Protein synthesis at synaptic sites on dendrites". In: *Handbook of Neurochemistry and Molecular Neurobiology: Neural Protein Metabolism and Function*. DOI: 10.1007/978-0-387-30379-6_4.

Steward, Oswald and W B Levy (1982). "Preferential localization of polyribosomes under the base of dendritic spines in granule cells of the dentate gyrus." In: *The Journal of neuroscience : the official journal of the Society for Neuroscience*. DOI: 0270-6474/82/0203-0284.

Sudmant, Peter H. et al. (2018). "Widespread Accumulation of Ribosome-Associated Isolated 3′ UTRs in Neuronal Cell Populations of the Aging Brain". In: *Cell Reports*. DOI: 10.1016/j.celrep.2018.10.094.

Sundell, Cynthia L. and Robert H. Singer (1991). "Requirement of microfilaments in sorting of actin messenger RNA". In: *Science*. DOI: 10.1126/science.1891715.

Tabb, J et al. (1998). "Transport of ER vesicles on actin filaments in neurons by myosin V". In: *Journal of Cell Science*.

Tahirovic, Sabina and Frank Bradke (2009). "Neuronal polarity." In: DOI: 10.1101/cshperspect.a001644.

Taliaferro, J. Matthew et al. (2016). "Distal Alternative Last Exons Localize mRNAs to Neural Projections". In: *Molecular Cell*. DOI: 10.1016/j.molcel.2016.01.020.

Tamada, Hiroshi et al. (2002). "cDNA cloning and characterization of Drb1, a new member of RRM-type neural RNA-binding protein". In: *Biochemical and Biophysical Research Communications*. DOI: 10.1016/S0006-291X(02)02132-0.

Tan, Chao et al. (2019). "Endothelium-Derived Semaphorin 3G Regulates Hippocampal Synaptic Structure and Plasticity via Neuropilin-2/PlexinA4." In: *Neuron* 0.0. DOI: 10.1016/j.neuron.2018.12.036.

Tanenbaum, Marvin E. et al. (2014). "A protein tagging system for signal amplification in gene expression and fluorescence imaging". In: *Cell*. DOI: 10.1016/j.cell.2014.09.039.

Taylor, A M et al. (2009). "Axonal mRNA in uninjured and regenerating cortical mammalian axons". In: *Journal of Neuroscience*. DOI: 10.1523/jneurosci.6130-08.2009.

Tcherkezian, Joseph et al. (2010). "Transmembrane Receptor DCC Associates with Protein Synthesis Machinery and Regulates Translation". In: *Cell*. DOI: 10.1016/j.cell.2010.04.008.

Tennyson, Virginia M. (1970). "The fine structure of the axon and growth cone of the dorsal root neuroblast of the rabbit embryo". In: *Journal of Cell Biology*. DOI: 10.1083/jcb.44.1.62.

Tian, Bin et al. (2005). "A large-scale analysis of mRNA polyadenylation of human and mouse genes". In: *Nucleic Acids Research*. DOI: 10.1093/nar/gki158.

Tokuraku, Kiyotaka et al. (1999). "A new model for microtubule-associated protein (MAP)-induced microtubule assembly". In: *European Journal of Biochemistry* 259.1-2, pp. 158–166. DOI: 10.1046/j.1432-1327.1999.00019.x.

Tokuraku, Kiyotaka et al. (2003). "The number of repeat sequences in microtubule-associated protein 4 affects the microtubule surface properties". In: *Journal of Biological Chemistry*. DOI: 10.1074/jbc.M302186200.

Tokuraku, Kiyotaka et al. (2010). "Distinct neuronal localization of microtubule-associated protein 4 in the mammalian brain". In: *Neuroscience Letters*. DOI: 10.1016/j.neulet.2010.08.038.

Tom Dieck, Susanne et al. (2015). "Direct visualization of newly synthesized target proteins in situ". In: *Nature Methods*. DOI: 10.1038/nmeth.3319. arXiv: arXiv:1011.1669v3.

Tomari, Yukihide et al. (2004). "RISC assembly defects in the Drosophila RNAi mutant armitage". In: *Cell*. DOI: 10.1016/S0092-8674(04)00218-1.

Torre, ER and O Steward (1992). "Demonstration of local protein synthesis within dendrites using a new cell culture system that permits the isolation of living axons and dendrites from their cell bodies". In: *The Journal of Neuroscience*. DOI: 10.1523/jneurosci.12-03-00762.1992.

Treutlein, Barbara et al. (2016). "Dissecting direct reprogramming from fibroblast to neuron using single-cell RNA-seq". In: *Nature*. DOI: 10.1038/nature18323. arXiv: 15334406.

Tsai, N.-P. (2006). "Netrin-1 Signaling Regulates De Novo Protein Synthesis of kappa Opioid Receptor by Facilitating Polysomal Partition of Its mRNA". In: *Journal of Neuroscience*. DOI: 10.1523/jneurosci.3014-06.2006.

Tsukita, Shoichiro and Harunori Ishikawa (1976). "Three-dimensional distribution of smooth endoplasmatic reticulum in myelinated axons". In: *Journal of Electron Microscopy*. DOI: 10.1093/oxfordjournals.jmicro.a050013.

– (1979). "Morphological evidence for the involvement of the smooth endoplasmic reticulum in axonal transport". In: *Brain Research*. DOI: 10.1016/0006-8993(79)90853-9.

Tucker, Ben, Robert I. Richards, and Michael Lardelli (2006). "Contribution of mGluR and Fmr1 functional pathways to neurite morphogenesis, craniofacial development and fragile X syndrome". In: *Human Molecular Genetics*. DOI: 10.1093/hmg/ddl422.

Tushev, Georgi et al. (2018). "Alternative 3′ UTRs Modify the Localization, Regulatory Potential, Stability, and Plasticity of mRNAs in Neuronal Compartments". In: *Neuron*. DOI: 10.1016/j.neuron.2018.03.030.

Udagawa, Tsuyoshi et al. (2012). "Bidirectional Control of mRNA Translation and Synaptic Plasticity by the Cytoplasmic Polyadenylation Complex". In: *Molecular Cell*. DOI: 10.1016/j.molcel.2012.05.016.

Ule, Jernej et al. (2006). "An RNA map predicting Nova-dependent splicing regulation". In: *Nature*. DOI: 10.1038/nature05304.

Ulitsky, Igor et al. (2012). "Extensive alternative polyadenylation during zebrafish development". In: *Genome Research*. DOI: 10.1101/gr.139733.112. arXiv: 11.

van Kasteren, Sander I. et al. (2007). "Expanding the diversity of chemical protein modification allows post-translational mimicry". In: *Nature*. DOI: 10.1038/nature05757.

Van Roey, Kim, Toby J. Gibson, and Norman E. Davey (2012). "Motif switches: Decision-making in cell regulation". In: DOI: 10.1016/j.sbi.2012.03.004.

Van Roey, Kim et al. (2013). "The switches.ELM resource: A compendium of conditional regulatory interaction interfaces". In: *Science Signaling*. DOI: 10.1126/scisignal.2003345. arXiv: arXiv:1011.1669v3.

Vierbuchen, Thomas et al. (2010). "Direct conversion of fibroblasts to functional neurons by defined factors". In: *Nature*. DOI: 10.1038/nature08797.

Wang, Chong et al. (2016). "Real-Time Imaging of Translation on Single mRNA Transcripts in Live Cells". In: *Cell*. DOI: 10.1016/j.cell.2016.04.040. arXiv: 15334406.

Wang, Eric T et al. (2008). "Alternative isoform regulation in human tissue transcriptomes." In: *Nature*. DOI: 10.1038/nature07509.

Wang, Xiaojun et al. (2010). "Moloney leukemia virus 10 (MOV10) protein inhibits retrovirus replication". In: *Journal of Biological Chemistry*. DOI: 10.1074/jbc.M110.109314.

Wang, Zefeng and Christopher B. Burge (2008). *Splicing regulation: From a parts list of regulatory elements to an integrated splicing code*. DOI: 10.1261/rna.876308.

Wang, Zuoren and Megerditch Kiledjian (2001). "Functional link between the mammalian exosome and mRNA decapping". In: *Cell*. DOI: 10.1016/S0092-8674(01)00592-X.

Wapinski, Orly L. et al. (2013). "Hierarchical mechanisms for direct reprogramming of fibroblasts to neurons". In: *Cell*. DOI: 10.1016/j.cell.2013.09.028.

Weatheritt, Robert J., Toby J. Gibson, and M. Madan Babu (2014). "Asymmetric mRNA localization contributes to fidelity and sensitivity of spatially localized systems". In: *Nature Structural and Molecular Biology*. DOI: 10.1038/nsmb.2876.

Weclewicz, Katarzyna, Lennart Svensson, and Krister Kristensson (1998). "Targeting of endoplasmic reticulum-associated proteins to axons and dendrites in rotavirus-infected neurons". In: *Brain Research Bulletin*. DOI: 10.1016/S0361-9230(98)00013-6.

Weil, Timothy T., Kevin M. Forrest, and Elizabeth R. Gavis (2006). "Localization of bicoid mRNA in Late Oocytes Is Maintained by Continual Active Transport". In: *Developmental Cell*. DOI: 10.1016/j.devcel.2006.06.006.

Willis, D. (2005). "Differential Transport and Local Translation of Cytoskeletal, Injury-Response, and Neurodegeneration Protein mRNAs in Axons". In: *Journal of Neuroscience*. DOI: 10.1523/jneurosci.4235-04.2005.

Willis, Dianna E. and Jeffery L. Twiss (2006). *The evolving roles of axonally synthesized proteins in regeneration*. DOI: 10.1016/j.conb.2006.01.002.

Wolin, Sandra L and Peter Walter (1988). "Ribosome pausing and stacking during translation of a eukaryotic mRNA." In: *The EMBO journal*. DOI: 10.1002/J.1460-2075.1988.TB03233.X.

Wong, Hovy Ho Wai et al. (2017). "RNA Docking and Local Translation Regulate Site-Specific Axon Remodeling In Vivo". In: *Neuron*. DOI: 10.1016/j.neuron.2017.07.016.

Wu, Bin et al. (2016). "Translation dynamics of single mRNAs in live cells and neurons". In: *Science*. DOI: 10.1126/science.aaf1084. arXiv: 15334406.

Wu, Colin Chih-Chien et al. (2019). "High-Resolution Ribosome Profiling Defines Discrete Ribosome Elongation States and Translational Regulation during Cellular Stress". In: *Molecular Cell* 0.0. DOI: 10.1016/J.MOLCEL.2018.12.009.

Wu, Karen Y. et al. (2005). "Local translation of RhoA regulates growth cone collapse". In: *Nature*. DOI: 10.1038/nature03885. arXiv: NIHMS150003.

Wu, Lin et al. (1998). "CPEB-mediated cytoplasmic polyadenylation and the regulation of experience-dependent translation of α-CaMKII mRNA at synapses". In: *Neuron*. DOI: 10.1016/S0896-6273(00)80630-3.

Xia, Zheng et al. (2014). "Dynamic analyses of alternative polyadenylation from RNA-seq reveal a 3′-UTR landscape across seven tumour types". In: *Nature Communications*. DOI: 10.1038/ncomms6274.

Xu, Ping et al. (2018). "Conditional ablation of the RFX4 isoform 1 transcription factor: Allele dosage effects on brain phenotype". In: *PLoS ONE*. DOI: 10.1371/journal.pone.0190561.

Xue, Shifeng and Maria Barna (2012). "Specialized ribosomes: A new frontier in gene regulation and organismal biology". In: DOI: 10.1038/nrm3359. arXiv: NIHMS150003.

Yamagishi, Mai et al. (2009). "Single-molecule imaging of β-actin mRNAs in the cytoplasm of a living cell". In: *Experimental Cell Research*. DOI: 10.1016/j.yexcr.2009.02.009.

Yan, Dong, Li Guo, and Yizheng Wang (2006). "Requirement of dendritic Akt degradation by the ubiquitin-proteasome system for neuronal polarity". In: *Journal of Cell Biology*. DOI: 10.1083/jcb.200511028.

Yan, Xiaowei et al. (2016). "Dynamics of Translation of Single mRNA Molecules in Vivo". In: *Cell*. DOI: 10.1016/j.cell.2016.04.034. arXiv: 15334406.

Yang, Joy T., Robert A. Laymon, and L S Goldstein (1989). "A three-domain structure of kinesin heavy chain revealed by DNA sequence and microtubule binding analyses." In: *Cell*. DOI: 10.1016/0092-8674(89)90692-2.

Yang, Nicole J. and Marlon J. Hinner (2015). "Getting across the cell membrane: An overview for small molecules, peptides, and proteins". In: *Site-Specific Protein Labeling: Methods and Protocols*. DOI: 10.1007/978-1-4939-2272-7_3.

Yao, Jiaqi et al. (2006). "An essential role for β-actin mRNA localization and translation in Ca2+-dependent growth cone guidance". In: *Nature Neuroscience*. DOI: 10.1038/nn1773.

Yap, Karen et al. (2016). "Polarizing the Neuron through Sustained Co-expression of Alternatively Spliced Isoforms". In: *Cell Reports*. DOI: 10.1016/j.celrep.2016.04.012.

You, Jhong Jhe and Sue Lin-Chao (2010). "Gas7 functions with N-WASP to regulate the neurite outgrowth of hippocampal neurons". In: *Journal of Biological Chemistry*. DOI: 10.1074/jbc.M109.051094.

Yu, P. C. et al. (2006). "Microtubule affinity-regulating kinase 2 functions downstream of the PAR-3/PAR-6/atypical PKC complex in regulating hippocampal

neuronal polarity". In: *Proceedings of the National Academy of Sciences*. DOI: 10.1073/pnas.0509955103.

Yudin, Dmitry et al. (2008). "Localized Regulation of Axonal RanGTPase Controls Retrograde Injury Signaling in Peripheral Nerve". In: *Neuron*. DOI: 10.1016/j.neuron.2008.05.029.

Zaessinger, S., I. Busseau, and M. Simonelig (2006). "Oskar allows nanos mRNA translation in Drosophila embryos by preventing its deadenylation by Smaug/CCR4". In: *Development*. DOI: 10.1242/dev.02649.

Zappulo*, Van Den Bruck*, Ciolli Mattioli*, Franke* et al. (2017). "RNA localization is a key determinant of neurite-enriched proteome". In: *Nature Communications*. DOI: 10.1038/s41467-017-00690-6.

Zelená, Jiřina (1972). "Ribosomes in myelinated axons of dorsal root ganglia". In: *Zeitschrift für Zellforschung und Mikroskopische Anatomie*. DOI: 10.1007/BF00335680.

Zhang, Haibo, Ju Youn Lee, and Bin Tian (2005). "Biased alternative polyadenylation in human tissues." In: *Genome biology*. DOI: 10.1186/gb-2005-6-12-r100.

Zhang, Yonggang and Wenhui Hu (2013). "Mouse enteric neuronal cell culture". In: *Methods in Molecular Biology*. DOI: 10.1007/978-1-62703-640-5_6.

Zhao, Chunjie et al. (2001). "Charcot-Marie-Tooth disease type 2A caused by mutation in a microtubule motor KIF1Bβ". In: *Cell*. DOI: 10.1016/S0092-8674(01)00363-4.

Zheng, Yi et al. (2008). "Dynein is required for polarized dendritic transport and uniform microtubule orientation in axons". In: *Nature Cell Biology*. DOI: 10.1038/ncb1777.

Zhu, H. et al. (2006). "A Nuclear Function of Hu Proteins as Neuron-specific Alternative RNA Processing Regulators". In: *Molecular Biology of the Cell*. DOI: 10.1091/mbc.e06-02-0099.

Zhu, H. et al. (2007a). "Regulation of Neuron-Specific Alternative Splicing of Neurofibromatosis Type 1 Pre-mRNA". In: *Molecular and Cellular Biology*. DOI: 10.1128/mcb.01509-07.

Zhu, Hui et al. (2007b). "Hu proteins regulate polyadenylation by blocking sites containing U-rich sequences". In: *Journal of Biological Chemistry*. DOI: 10.1074/jbc.M609349200.

Ziff, Edward B. (1997). "Enlightening the postsynaptic density". In: DOI: 10.1016/S0896-6273(00)80409-2.

Zimyanin, Vitaly L. et al. (2008). "In Vivo Imaging of oskar mRNA Transport Reveals the Mechanism of Posterior Localization". In: *Cell*. DOI: 10.1016/j.cell.2008.06.053.